Contents

Plenary Talks

Proceedings of the International School-seminar
"New Physics and Quantum Chromodynamics at External Conditions", pp. 6 – 11,
May 22-24, 2013, Dnipropetrovsk, Ukraine

Z-Z' MIXING AND ITS DETERMINATION AT THE LHC AND ILC

V. V. Andreev[a,1], A. A. Pankov[b,2], I. A. Serenkova[c,2], A. V. Tsytrinov[d,2]

[1]Gomel State University, Gomel, Belarus

[2]Abdus Salam ICTP Affiliated Centre at Gomel State Technical University, Gomel, Belarus

New heavy neutral gauge bosons Z' are predicted by many models of physics beyond the Standard Model. The potential for measuring the $Z'W^+W^-$ coupling in W^+W^- pair production at the LHC is investigated. Also, we discuss the foreseeable sensitivity to Z's of $W^\pm$-pair production cross sections at the e^+e^- ILC. We show that the sensitivity of the ILC for probing the Z-Z' mixing is substantially enhanced when the polarization of the initial beams and the produced $W^\pm$ bosons are considered.

1 Introduction

interactions describes nearly all experimental data available today [1], it is widely believed that it is not the ultimate theory. Grand Unified Theories (GUTs), eventually supplemented by Supersymmetry to achieve a successful unification of the three gauge coupling constants at the high scale, are prime candidates for the physics beyond the SM. Many of these GUTs, including superstring and left-right-symmetric models, predict the existence of new neutral gauge bosons, which might be light enough to be accessible at current and/or future colliders [2–4].

The search for these Z' particles is an important aspect of the experimental physics program of current and future high-energy colliders. Present limits from direct production at the LHC and Tevatron, and virtual effects at LEP, through interference or mixing with the Z boson, imply that new Z' bosons are rather heavy and mix very little with the Z boson. Depending on the considered theoretical models, Z' masses of the order of 2.4–2.9 TeV (LHC) [5,6] and Z–Z' mixing angles at the level of a few per-mile are excluded [7]. A Z' boson, if lighter than about 5 TeV, could be discovered at the LHC with $\sqrt{s} = 14$ TeV in the Drell-Yan process

$$pp \to Z' \to \ell^+\ell^- \tag{1}$$

with $\ell = e, \mu$. Future e^+e^- International linear collider (ILC) with high c.m. energies and longitudinally polarized beams could indicate the existence of Z' bosons via its interference effects, with masses up to about $6 \times \sqrt{s}$. After the discovery of a Z' boson at the LHC, some diagnosis of its coupling and $Z - Z'$ mixing needs to be done in order to identify the correct theoretical frame.

The $W^\pm$ boson pair production processes

$$e^+ + e^- \to W^+ + W^- \tag{2}$$

and

$$p + p \to W^+W^- + X \tag{3}$$

are a crucial ones for studying the electroweak gauge symmetry in the ILC and LHC, respectively. Properties of the weak gauge bosons are closely related to electroweak symmetry breaking and the structure of the gauge sector in general. Thus, detailed examination of (2) at the ILC and (3) at the LHC will both test this sector of the standard model with the highest accuracy and throw light on New Physics (NP) that may appear beyond the SM. We shall here focus on the phenomenological effects in reactions (1)-(3) of the so-called $Z'_{\rm SSM}$ and Z'_{E_6} models. Actually, in some sense, we may consider these Z' models as representative of this NP sector.

The discovery of the Z' boson would constrain models of electroweak symmetry breaking. The Drell-Yan process (1) is sensitive to the Z' mass, while decay rate $Z' \longrightarrow W^+W^-$ is sensitive to the $Z - Z'$ mixing angle. In the present paper, we examine the feasibility of detecting the Z' boson via the decay rate $Z' \longrightarrow W^+W^-$ at the LHC, which is not the principal discovery channels as Drell-Yan process, but can help to understand the origin of the new gauge bosons. Also, we study the indirect effects evidencing the mentioned extra Z' gauge bosons in $W^\pm$ pair production (2) at ILC, with a center of mass energy $\sqrt{s} = 0.5 - 1$ TeV and typical time-integrated luminosities of $\mathcal{L}_{\rm int} \sim 0.5 - 1$ ab^{-1}. At the foreseen, really high luminosity this process should

e-mail: [a]selfdenied@tut.by, [b]pankov@ictp.it, [c]inna.serenkova@cern.ch, [b]tsytrin@rambler.ru

be quite sensitive to the indirect NP effects at a collider with $M_Z \ll \sqrt{s} \ll M_{Z'}$, the deviations of cross sections from the SM predictions being expected to increase with $\sqrt{s}$ due to the violation of the SM gauge cancellation among the different contributions.

2 Z' models

The Z' models that will be considered in our analysis are the following [8–10]:

(i) The four possible $U(1)$ Z' scenarios originating from the spontaneous breaking of the exceptional group E_6. In this case, two extra, heavy neutral gauge bosons appear as consequence of the symmetry breaking and, generally, only the lightest is assumed to be within reach of the collider. It is defined, in terms of a new mixing angle β, by the linear combination

$$Z' = Z'_\chi \cos\beta + Z'_\psi \sin\beta. \tag{4}$$

Specific choices of β: $\beta = 0$; $\beta = \pi/2$; $\beta = -\arctan\sqrt{5/3}$ and $\beta = \arctan\sqrt{3/5}$, corresponding to different E_6 breaking patterns, define the popular scenarios Z'_χ, Z'_ψ, Z'_η and Z'_I, respectively.

(ii) The $Z'_{\rm ALR}$ predicted by the so-called 'alternative' left-right scenario. For the LR model we need not introduce additional fermions to cancel anomalies. However, in the E_6 case a variant of this model (called the Alternative LR model) can be constructed by altering the embeddings of the SM and introducing exotic fermions into the ordinary 10 and 5 representations.

(iii) The so-called sequential $Z'_{\rm SSM}$, where the couplings to fermions are the same as those of the SM Z.

In the extended gauge theories predicting the existence of an extra neutral Z' gauge boson, the mass-squared matrix of the Z and Z' can have non-diagonal entries δM^2, which are related to the vacuum expectation values of the fields of an extended Higgs sector:

$$M^2_{ZZ'} = \begin{pmatrix} M_Z^2 & \delta M^2 \\ \delta M^2 & M_{Z'}^2 \end{pmatrix}. \tag{5}$$

Here, Z and Z' denote the weak gauge boson eigenstates of $SU(2)_L \times U(1)_Y$ and of the extra $U(1)'$, respectively. The mass eigenstates, Z_1 and Z_2, diagonalizing the matrix (5), are then obtained by the rotation of the fields Z and Z' by a mixing angle ϕ:

$$Z_1 = Z\cos\phi + Z'\sin\phi\,, \tag{6}$$

$$Z_2 = -Z\sin\phi + Z'\cos\phi\,. \tag{7}$$

Here, the mixing angle ϕ is expressed in terms of masses as:

$$\tan^2\phi = \frac{M_Z^2 - M_1^2}{M_2^2 - M_Z^2} \simeq \frac{2M_Z\Delta M}{M_2^2}\,, \tag{8}$$

where $\Delta M = M_Z - M_1 > 0$, M_Z is the mass of the Z_1-boson in the absence of mixing, i.e., for $\phi = 0$. Once we assume the mass M_1 to be determined experimentally, the mixing depends on two free parameters, which we identify as ϕ and M_2.

The mixing angle ϕ will play an important role in our analysis. In general, such mixing effects reflect the underlying gauge symmetry and/or the Higgs sector of the model. To a good approximation, for $M_1 \ll M_2$, in specific "minimal-Higgs models",

$$\phi \simeq -s_{\rm W}^2\,\frac{\sum_i \langle\Phi_i\rangle^2 I^i_{3L} Q'_i}{\sum_i \langle\Phi_i\rangle^2 (I^i_{3L})^2} = \mathcal{C}\;\frac{M_1^2}{M_2^2}. \tag{9}$$

Here $\langle\Phi_i\rangle$ are the Higgs vacuum expectation values spontaneously breaking the symmetry, and Q'_i are their charges with respect to the additional $U(1)'$. In addition, in these models the same Higgs multiplets are responsible for both generation of mass M_1 and for the strength of the Z-Z' mixing. Thus $\mathcal{C}$ is a model-dependent constant. For example, in the case of E_6 superstring-inspired models $\mathcal{C}$ can be expressed as [11]

$$\mathcal{C} = 4 s_{\rm W}\left(A - \frac{\sigma-1}{\sigma+1}B\right), \tag{10}$$

where σ is the ratio of vacuum expectation values squared, and the constants A and B are determined by the mixing angle β: $A = \cos\beta/2\sqrt{6}$, $B = \sqrt{10}/12\sin\beta$.

An important property of the models under consideration is that the gauge eigenstate Z' does not couple to the W^+W^- pair since it is neutral under $SU(2)_L$. Therefore the process (1), and the searched-for deviations

of the cross sections from the SM, are sensitive to a Z' only in the case of a non-zero Z-Z' mixing. The mixing angle is rather highly constrained, to an upper limit of afew $\times 10^{-3}$, mainly from LEP measurements at the Z [7,12]. The high statistics on W-pair production expected at the ILC might in principle allow to probe such small mixing angles effectively.

From (6) and (7), one obtains the vector and axial-vector couplings of the Z_1 and Z_2 bosons to fermions:

$$v_{1f} = v_f \cos\phi + v'_f \sin\phi\,, \quad a_{1f} = a_f \cos\phi + a'_f \sin\phi\,, \tag{11}$$

$$v_{2f} = -v_f \sin\phi + v'_f \cos\phi\,, \quad a_{2f} = -a_f \sin\phi + a'_f \cos\phi, \tag{12}$$

with $(v_f, a_f) = (g_L^f \pm g_R^f)/2$, and (v'_f, a'_f) similarly defined in terms of the Z' couplings. The fermionic Z' couplings can be found in [8,9].

Analogously, one obtains according to the remarks above:

$$g_{WWZ_1} = \cos\phi\, g_{WWZ}\,, \tag{13}$$

$$g_{WWZ_2} = -\sin\phi\, g_{WWZ}\,, \tag{14}$$

where $g_{WWZ} = \cot\theta_W$.

3 Discovery reach on Z' in lepton pair production at LHC

The cross section of process (1) for inclusive production of a dilepton with invariant mass M can be written as $(R = Z')$ [13]

$$\frac{\mathrm{d}\sigma(R_{ll})}{\mathrm{d}M\,\mathrm{d}y\,\mathrm{d}z} = K\frac{2M}{s}\sum_{ij} f_i(\xi_1, M) f_j(\xi_2, M)\frac{\mathrm{d}\hat{\sigma}}{\mathrm{d}z}(i + j \to l^+ + l^-). \tag{15}$$

Here, s is the proton-proton center-of-mass energy squared; $z = \cos\theta_{\mathrm{c.m.}}$ with $\theta_{\mathrm{c.m.}}$ the lepton-quark angle in the dilepton center-of-mass frame; y is the dilepton rapidity; $f_{i,j}(\xi_{1,2}, M)$ are parton distribution functions in the protons P_1 and P_2, respectively, with $\xi_{1,2} = (M/\sqrt{s})\exp(\pm y)$ the parton fractional momenta; finally, $\mathrm{d}\hat{\sigma}_{ij}$ are the partonic differential cross sections. The color-averaged differential cross section for the relevant, leading order, partonic subprocess $q\bar{q} \to Z' \to l^+ l^-$ can be expressed as:

$$\left.\frac{\mathrm{d}\hat{\sigma}^{Z'}_{\mathrm{q\bar{q}}}}{\mathrm{dz}}\right|_{z-\mathrm{even}} = \frac{1}{N_c}\,\frac{\pi\alpha^2_{\mathrm{em}}}{2M^2}\,[S_q^{Z'}\,(1+z^2)], \tag{16}$$

with

$$S_q^{Z'} = \frac{1}{4}\,(g_L^{q\,\prime 2} + g_R^{q\,\prime 2})\,(g_L^{l\,\prime 2} + g_R^{l\,\prime 2})|\chi_{Z'}|^2, \qquad \chi_{Z'} = \frac{M^2}{M^2 - M^2_{Z'} + i\,M_{Z'}\Gamma_{Z'}}. \tag{17}$$

In (15), the factor K accounts for next-to-leading order QCD contributions [14]. For simplicity, and to make our procedure more transparent, we will use as an approximation a global flat value $K = 1.3$.

Since we are interested in a (narrow) peak production and subsequent decay into the DY pair, $pp \to R \to l^+l^-$, we consider the lepton differential angular distribution, integrated over an interval of M around M_R:

$$\frac{\mathrm{d}\sigma(\mathrm{R_{ll}})}{\mathrm{dz}} = \int_{M_R - \Delta M/2}^{M_R + \Delta M/2} \mathrm{dM} \int_{-\mathrm{Y}}^{\mathrm{Y}} \frac{\mathrm{d}\sigma}{\mathrm{dM\,dy\,dz}}\,\mathrm{dy}. \tag{18}$$

The number of events under the peak, that determines the statistics, is therefore given by:

$$\sigma(R_{ll}) \equiv \sigma(pp \to R)\cdot \mathrm{BR}(R \to l^+l^-) = \int_{-z_{\mathrm{cut}}}^{z_{\mathrm{cut}}} \mathrm{dz} \int_{\mathrm{M_R}-\Delta\mathrm{M}/2}^{\mathrm{M_R}+\Delta\mathrm{M}/2} \mathrm{dM} \int_{-\mathrm{Y}}^{\mathrm{Y}} \mathrm{dy}\frac{\mathrm{d}\sigma}{\mathrm{dM\,dy\,dz}}. \tag{19}$$

For the full final phase space, $z_{\mathrm{cut}} = 1$ and $Y = \log(\sqrt{s}/M)$. However, if the finite detector angular acceptance is accounted for, $z_{\mathrm{cut}} < 1$ and Y in Eqs. (18) and (19) must be replaced by a maximum value $y_{\max}(z, M)$. Concerning the size of the bin ΔM, it should include a number (at least one) of peak widths to enhance the probability to pick up the resonance. In the models we will consider, widths are predicted to be small, typically of the order of a percent (or less) of the mass M_R, so that the integral under the peak should practically be insensitive to the actual value of ΔM. Conversely, the SM 'background' is expected to depend on ΔM. We denote by N_B and N_S the number of 'background' and 'signal' events in the bin, the criterion $N_S = 5\sqrt{N_B}$ or 10 events, whichever is larger, as the minimum signal for the peak discovery.

To evaluate the statistics, we shall use in Eqs. (18) and (19) the CTEQ6.5 parton distributions [15], and impose cuts relevant to the LHC detectors, namely: pseudorapidity $|\eta| < 2.5$ for both leptons assumed massless (this leads to a boost-dependent cut on z; lepton transverse momentum $p_\perp > 20\,\mathrm{GeV}$. Moreover, the reconstruction efficiency is taken to be 90% for both electrons and muons and throughout this paper a time-integrated LHC luminosity $\mathcal{L}_{\mathrm{int}} = 100\,\mathrm{fb}^{-1}$.

For the proton-proton initiated process $pp \to l^+l^- + X$, only the z-even parts of the partonic differential cross sections contribute to the right-side of Eq. (18), z-odd terms do not contribute after the y-integration. Also, due to $M_Z \ll M_R$ and the narrow width peak, the resonant amplitude interference with the SM is expected to give negligible contributions to the right-hand sides of (18) and (19) after the symmetric M-integration around M_R needed there. Thus, we can retain in these equations just the SM and the resonance pole contributions.

In Fig.1 we show the predicted number of resonance (signal) events N_S in the Drell-Yan process at LHC, *vs.* M_R, where $R = Z'$. The assumed integrated luminosity is $\mathcal{L}_{\rm int} = 100\,{\rm fb}^{-1}$, the cuts in phase space relevant to the foreseen detector acceptance specified above have been imposed, and the channels $l = e, \mu$ have been combined.

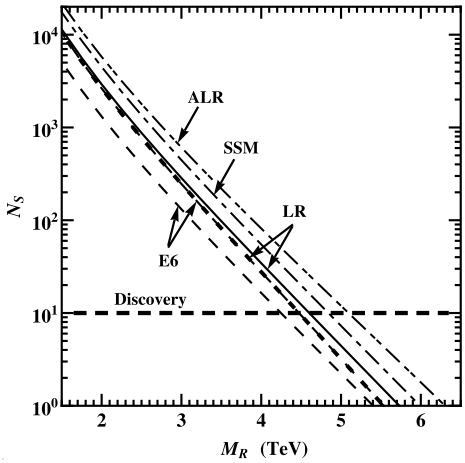

Figure 1. Number of resonance events N_S, as a function of the Z'-resonance mass M_R ($R = Z'$) at $\mathcal{L}_{\rm int} = 100\ {\rm fb}^{-1}$ in the production of Z' bosons that is followed by their decay to dileptons ($l^+l^- = e^+e^-, \mu^+, \mu^-$).

As regards the discovery of Z' we are interested in, the signature spaces in Fig. 1 reduce to the lines labeled by the different models, because the event rates are fixed, once M'_Z is given. In Fig. 1 shows that, with the assumed luminosity of $100\,{\rm fb}^{-1}$, Z' gauge boson masses up to 4–5 TeV are in principle within the 5-σ reach of the LHC.

4 Z-Z' mixing at the ILC and LHC

The general expression for the cross section of process (2) with longitudinally polarized electron and positron beams can be expressed as [2]

$$\frac{d\sigma}{d\cos\theta} = \frac{1}{4}\left[(1+P_L)\left(1-\bar{P}_L\right)\frac{d\sigma^+}{d\cos\theta} + (1-P_L)\left(1+\bar{P}_L\right)\frac{d\sigma^-}{d\cos\theta}\right], \tag{20}$$

where P_L and $\bar{P}_L$ are the actual degrees of electron and positron longitudinal polarization, respectively, and $\sigma^\pm$ are the cross sections for purely right-handed ($\lambda = 1/2$) and left-handed ($\lambda = -1/2$) electrons.

The polarized cross sections can generally be written as follows:

$$\frac{d\sigma^\pm}{d\cos\theta} = \frac{|\mathbf{p}|}{4\pi s\sqrt{s}}\sum_{\tau,\tau'}|F_{\lambda\tau\tau'}(s,\cos\theta)|^2. \tag{21}$$

Here, the helicities of the W^- and W^+ are denoted by $\tau, \tau' = \pm 1, 0$, the helicity amplitudes $F_{\lambda\tau\tau'}(s,\cos\theta)$, $p = |\boldsymbol{p}|$ the c.m. momentum of the W^-. Furthermore, s and t are the Mandelstam variables, and θ the c.m. scattering angle, with $t = M_W^2 - s(1-\beta\cos\theta)/2$.

The sensitivity of the polarized differential cross sections to Z' is assessed numerically by dividing the angular range $|\cos\theta| \le 0.98$ into 10 equal bins, and defining a χ^2 function in terms of the expected number of events $N(i)$ in each bin for a given combination of beam polarizations:

$$\chi^2 = \sum_{\{P_L,\,\bar{P}_L\}}\sum_{i}^{\rm bins}\left[\frac{N_{{\rm SM}+Z'}(i) - N_{\rm SM}(i)}{\delta N_{\rm SM}(i)}\right]^2, \tag{22}$$

where $N(i) = \mathcal{L}_{\rm int}\,\sigma_i\,\varepsilon_W$ with $\mathcal{L}_{\rm int}$ the time-integrated luminosity. Furthermore,

$$\sigma_i = \sigma(z_i, z_{i+1}) = \int\limits_{z_i}^{z_{i+1}} \left(\frac{d\sigma}{dz}\right) dz, \tag{23}$$

where $z = \cos\theta$ and polarization indices have been suppressed. Also, ε_W is the efficiency for W^+W^- reconstruction, for which we take the channel of lepton pairs ($e\nu + \mu\nu$) plus two hadronic jets, giving $\varepsilon_W \simeq 0.3$ basically from the relevant branching ratios. The procedure outlined above is followed to evaluate both $N_{\rm SM}(i)$ and $N_{\rm SM+Z'}(i)$.

The uncertainty on the number of events $\delta N_{\rm SM}(i)$ combines both statistical and systematic errors where the statistical component is determined by $\delta N^{\rm stat}_{\rm SM}(i) = \sqrt{N_{\rm SM}(i)}$. Concerning systematic uncertainties, an important source is represented by the uncertainty on beam polarizations, for which we assume $\delta P_L/P_L = \delta\bar{P}_L/\bar{P}_L = 0.5\%$ with the "standard" envisaged values $|P_L| = 0.8$ and $|\bar{P}_L| = 0.5$ [16, 17]. As for the time-integrated luminosity, for simplicity we assume it to be equally distributed between the different polarization configurations. Another source of systematic uncertainty originates from the efficiency of reconstruction of $W^\pm$ pairs which we assume to be $\delta\varepsilon_W/\varepsilon_W = 0.5\%$. Also, in our numerical analysis to evaluate the sensitivity of the differential distribution to model parameters we include initial-state QED corrections to on-shell $W^\pm$ pair production in the flux function approach that assures a good approximation within the expected accuracy of the data.

As a criterion to derive the constraints on the coupling constants in the case where no deviations from the SM were observed within the foreseeable uncertainties on the measurable cross sections, we impose that

$$\chi^2 \leq \chi^2_{\rm min} + \chi^2_{\rm CL}, \tag{24}$$

where $\chi^2_{\rm CL}$ is a number that specifies the chosen confidence level, $\chi^2_{\rm min}$ is the minimal value of the χ^2 function. With two independent parameters the 95% CL is obtained by choosing $\chi^2_{\rm CL} = 5.99$.

Fig. 2 shows the discovery reach (at a 95% C.L.) in the plane spanned by the $Z - Z'$ mixing angle and the Z_2-boson mass for the Z'_{SSM} and Z'_ψ models, respectively, from an analysis of the polarized cross sections for $P_L = \pm 0.8$ and $\overline{P}_L = \pm 0.5$. Two options of energy and time integrated luminosity have been chosen, namely, $\sqrt{s}$ =0.5 TeV and L_{int} =0.5 ab^{-1} (thin dot-dashed lines) and $\sqrt{s}$ =1.0 TeV and L_{int} =1 ab^{-1} (dashed lines). The ILC with energy of 0.5 TeV is able to place the limits on the $Z - Z'$ mixing angle at the level of few$\times 10^{-3}$ that comparable with the current ones obtained from the global analysis electroweak data and shown in the figures as thick dot-dashed lines with attached label of "EW data" . It turns out that doubling energy and luminosity leads to further improvement of the limit on $Z - Z'$ mixing angle up to $|\phi| \sim 10^{-4}$.

One can perform a similar analysis of $Z - Z'$ mixing effects at the LHC in process (3) taking into account the pure leptonic decay channels of $W^\pm$ bosons, $pp \to W^+W^+ \to l\nu l'\nu' + X$. The result of this analysis shown in Fig. 2 where corresponding limits indicated by solid lines. These figures demonstrate a high ability of the LHC to study the $Z - Z'$ mixing effects that comparable with those obtained at the ILC operating in high energy and luminosity option.

Also, the Z' mass limits obtained from the Drell-Yan process (1) in the current experiments at the LHC at $\sqrt{s} = 8$ TeV and $\mathcal{L}_{\rm int} = 20$ fb^{-1} as well as at nominal energy and luminosity, $\sqrt{s} = 14$ TeV and $\mathcal{L}_{\rm int} = 100$ fb^{-1}, are depicted in Fig. 2 by horizontal lines. The resulting area on (ϕ, M_2) parameter space lays above of those horizontal lines and constrained by the forceable data on process (3). From those figures one can conclude that LHC and ILC would provide a complementary information on $Z - Z'$ mixing angle.

In conclusion, the possibility to observe a new Z' boson in the $Z' \to W^+W^-$ channel at the LHC was examined. We demonstrated that even if the Z' boson is first observed via purely leptonic decay mode in process (1), the measurement of the $Z'W^+W^-$ vertex would give independent information on the new physics. We also show that LHC and ILC will be able to provide a complementary information on $Z - Z'$ mixing angle and Z' mass.

Acknowledgements. This research has been partially supported by the Abdus Salam ICTP under the TRIL and Associates Scheme and the Belarusian Republican Foundation for Fundamental Research.

References

[1] J. Beringer *et. al.* (Particle Data Group), Phys. Rev. D **86**, 010001 (2012).
[2] V. V. Andreev, G. Moortgat-Pick, P. Osland, A. A. Pankov and N. Paver, Eur. Phys. J. C **72**, 2147 (2012) [arXiv:1205.0866 [hep-ph]].
[3] A. V. Gulov, A. A. Kozhushko, V. V. Skalozub, A. A. Pankov and A. V. Tsytrinov, Prob. Atomic Sci. Technol. **2012N1**, 48 (2012).
[4] A. Gulov and V. Skalozub, Int. J. Mod. Phys. A **25**, 5787 (2010) [arXiv:1009.2320 [hep-ph]].

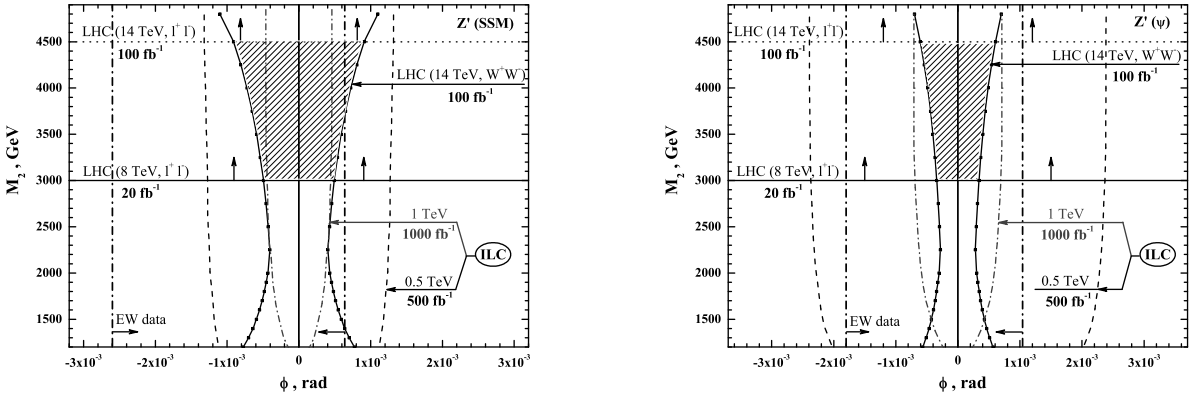

a b

Figure 2. a) Discovery reach (at 95% C.L.) in the plane spanned by the $Z-Z'$ mixing angle and the Z_2-boson mass for SSM model obtained from an analysis of the polarized cross sections of process $e^+e^- \to W^+W^-$ with $P_L = \pm 0.8$ and $\overline{P}_L = \pm 0.5$ at the ILC. Two options of energy and time integrated luminosity have been taken as follows: $\sqrt{s}$ =0.5 TeV and L_{int} =0.5 ab^{-1} (thin dot-dashed lines) and $\sqrt{s}$ =1.0 TeV and L_{int} =1 ab^{-1} (dashed lines). Current limits obtained from the global analysis of electroweak data are also shown and indicated by label "EW data" (thick dot-dashed lines). Also, limits derived at the LHC from process $pp \to W^+W^+ \to l\nu l'\nu' + X$ (thick solid lines) and from the Drell-Yan process (1) at $\sqrt{s} = 8$ TeV and $\mathcal{L}_{\rm int} = 20$ fb^{-1} (thin solid line) as well as at nominal energy and luminosity, $\sqrt{s} = 14$ TeV and $\mathcal{L}_{\rm int} = 100$ fb^{-1} (dotted line), are displayed; b) Same as in a), but for ψ model.

[5] S. Chatrchyan *et al.* [CMS Collaboration], Phys. Lett. **B714**, 158-179 (2012) [arXiv:1206.1849 [hep-ex]].
[6] G. Aad *et al.* [ATLAS Collaboration], JHEP **1211**, 138 (2012) [arXiv:1209.2535 [hep-ex]].
[7] J. Erler, P. Langacker, S. Munir, E. Rojas, JHEP **0908**, 017 (2009) [arXiv:0906.2435 [hep-ph]].
[8] P. Langacker, Rev. Mod. Phys. **81**, 1199-1228 (2009) [arXiv:0801.1345 [hep-ph]].
[9] A. Leike, Phys. Rept. **317**, 143-250 (1999) [hep-ph/9805494].
[10] J. L. Hewett, T. G. Rizzo, Phys. Rept. **183**, 193 (1989).
[11] P. Langacker and M. -x. Luo, Phys. Rev. D **45**, 278 (1992).
[12] P. Langacker, [arXiv:0911.4294 [hep-ph]].
[13] P. Osland, A. A. Pankov, A. V. Tsytrinov and N. Paver, Phys. Rev. D **79**, 115021 (2009) [arXiv:0904.4857 [hep-ph]].
[14] M. S. Carena, A. Daleo, B. A. Dobrescu and T. M. P. Tait, Phys. Rev. D **70**, 093009 (2004) [arXiv:hep-ph/0408098].
[15] J. Pumplin, D. R. Stump, J. Huston, H. L. Lai, P. Nadolsky and W. K. Tung, JHEP **0207**, 012 (2002) [arXiv:hep-ph/0201195].
[16] J. Brau *et al.* [ILC Collaboration], "ILC Reference Design Report Volume 1 - Executive Summary," arXiv:0712.1950 [physics.acc-ph].
[17] G. Aarons *et al.* [ILC Collaboration], "International Linear Collider Reference Design Report Volume 2: PHYSICS AT THE ILC," arXiv:0709.1893 [hep-ph].

Proceedings of the International School-seminar
"New Physics and Quantum Chromodynamics at External Conditions", pp. 12 – 19,
May 22-24, 2013, Dnipropetrovsk, Ukraine

HIGGS BOSON DECAY TO γZ AND TEST OF CP AND CPT SYMMETRIES

A. Yu. Korchin[1,2,a], V. A. Kovalchuk[1,b]

[1] National Science Center 'Kharkov Institute of Physics and Technology', 61108 Kharkiv, Ukraine
[2]V.N. Karazin Kharkiv National University, 61022 Kharkiv, Ukraine

Polarization characteristics of $\gamma\gamma$ and γZ states in the Higgs boson decays $h \to \gamma\gamma$ and $h \to \gamma Z$ are discussed. Based on effective Lagrangian, describing $h\gamma\gamma$ and $h\gamma Z$ interactions with CP-even and CP-odd parts, we calculate polarization parameters ξ_1, ξ_2, ξ_3. A nonzero value of the photon circular polarization, defined by parameter ξ_2, arises due to presence of both parts in effective Lagrangian and its non-Hermiticity. The circular polarization is proportional to the forward-backward asymmetry of fermions in the decay $h \to \gamma Z \to \gamma f \bar{f}$. Measurement of this observable will allow one to search for deviation from the standard model and possible violation of CPT symmetry. We discuss also a possibility to measure parameters ξ_1, ξ_3, describing correlation of linear polarizations of photon and Z boson, in the decay $h \to \gamma^* Z \to \ell^+\ell^- Z$ via distribution over the azimuthal angle between the decay planes of $\gamma^* \to \ell^+\ell^-$ and $Z \to \bar{f} f$. Deviation of the measured value of ξ_1 from zero will indicate CP violation in the Higgs sector.

1 Introduction

The ATLAS and CMS collaborations at the LHC have recently observed [1, 2] a boson h with mass around 126 GeV with statistical significance of about five standard deviations. The experimental evidence of this new particle is the strongest in the two-photon and four-lepton final channels, where the detectors give the best mass resolution.

Although the decay pattern of h is mainly consistent with the predictions of the standard model (SM), the clarification of the nature of this particle still needs more data and time. The spin of this boson is known to be zero or two, while the CP properties are not yet ascertained. Recent data are more consistent with the pure scalar boson hypothesis than the pure pseudoscalar one [3]. Though in the SM the Higgs boson has $J^{PC} = 0^{++}$, there are many extensions of the SM with a more complicated Higgs sector, in which some of the Higgs bosons may not have definite CP parity [4–6].

This aspect of the Higgs study is also related to the origin of the CP violation. In the SM the source of the CP violation is the complex irreducible phase in the Cabibbo-Kobayashi-Maskawa (CKM) matrix [7], however this effect is not sufficient to explain the observed matter-antimatter asymmetry in the Universe [8]. There may be other mechanisms of the CP violation beyond the CKM matrix, for example, in the Higgs sector. From this point of view, the elucidation of the CP properties of the observed h boson would be an important step towards clarification of the mechanisms giving rise to the masses of particles, their mixing and CP violation.

Recently the CP properties of the Higgs boson in the two-photon decay channel $h \to \gamma\,\gamma$ have been addressed in Ref. [9]. In this channel the branching fraction, measured by the ATLAS collaboration, is larger than the value predicted in the SM by a factor of 1.60 ± 0.30 for $m_h = 125.2 \pm 0.26\,(\text{stat})^{+0.5}_{-0.6}\,(\text{syst})\,\text{GeV}$ [10], while the CMS collaboration obtained for this factor 0.77 ± 0.27 for $m_h = 125.7 \pm 0.3(\text{stat}) \pm 0.3\,(\text{syst})\,\text{GeV}$ [11]. The author of [9], in framework of a model with vectorlike fermions, showed that the CP violation in the $h \to \gamma\,\gamma$ decay results in the dependence of the differential decay rate on the angle between linear polarization vectors of the photons. Experimentally, this angular distribution can be measured after both photons are converted into the e^+, e^- pairs via the azimuthal angle distribution between the planes spanned by the two e^+, e^- pairs. In Ref. [12] a model-independent analysis of the CP violation effects in the Higgs boson into a pair of the gauge bosons W^+, W^- or Z, Z has been presented. The author has studied the angular distributions of the fermions $f = \ell$, q in the cascade processes $h \to V_1\,V_2 \to (f_1\,\bar{f}_2)\,(f_3\,\bar{f}_4)$ and analyzed possibilities of observation of the CP violation in these decays to various final lepton and quark pairs.

Here we would like to address the decay of the Higgs boson to the photon and Z boson, $h \to \gamma\,Z$, pointing out to a possibility of studying in this decay not only the CP properties of the newly discovered boson, but also the validity of the CPT symmetry [13]. In this connection one can recall Ref. [14] in which the author showed that an observation of the circular polarization of the photon in the neutral pion decay $\pi^0 \to \gamma\,\gamma$ (or $\eta \to \gamma\,\gamma$) would signal violation of the CPT symmetry. Indeed, the product $\vec{s}\,\vec{k}$ (where $\vec{s}$ is the photon spin and $\vec{k}$ is its momentum) is P odd and T even. Such a correlation in the π^0 decay arises due to interference of the two

e-mail: [a]korchin@kipt.kharkov.ua, [b]koval@kipt.kharkov.ua

terms in the interaction Lagrangian: a scalar $\tilde{c}\,\pi^0\,\epsilon^{\mu\nu\rho\sigma}\,F_{\mu\nu}\,F_{\rho\sigma}$ and a pseudoscalar $c\,\pi^0\,F_{\mu\nu}\,F^{\mu\nu}$, with $\tilde{c}$ and c being couplings constants and $F_{\mu\nu}=\partial_\mu A_\nu-\partial_\nu A_\mu$. The analysis of [14] demonstrated that a nonzero value of $\vec{s}\vec{k}$ correlation may appear due to a non-Hermiticity of the tree-level amplitude, i.e. Im$\tilde{c}\neq 0$ or/and Im$c\neq 0$, and/or higher-order loop corrections to the amplitude inducing imaginary part of $\tilde{c}$.

Note that such a correlation in the Higgs boson decay to two transversally polarized Z bosons in connection with possible violation of CPT symmetry has been discussed in [12].

Generally, similar arguments can be applied to the two-photon decay of the Higgs boson with an analogous conclusion. However measurement of the photon circular polarization in the $h\to\gamma\,\gamma$ decay is a rather difficult task. Here we suggest to study CP and possible CPT violation in the decay

$$h\to\gamma\,Z\;\to\gamma\,f\,\bar{f}\,, \tag{1}$$

with $f=\ell$, q. It turns out that the decay distribution over the angle θ between the momentum of the fermion f (in the rest frame of the Z) and momentum of the Z (in the rest frame of the h) gives information on the photon circular polarization. Namely, a nonzero photon circular polarization induces a term $\sim\cos\theta$ in this distribution which can be measured through the forward-backward asymmetry $A_{\rm FB}$.

In the SM the $h\to\gamma\,Z$ decay amplitude in the lowest order is determined by the loop contributions [15,16] which have a small but nonzero imaginary part arising due to rescattering effects $h\to f\bar{f}\to\gamma\,Z$ for the fermions f with masses $m_f\leq m_h/2$. The corresponding effective Lagrangian $\mathcal{L}_{\rm eff}^{h\gamma Z}$, describing interaction of h, γ and Z, is thus non-Hermitian. Non-Hermiticity of effective Lagrangian leads to a nonzero value of the net photon helicity once we assume a mixture of CP violating term in $\mathcal{L}_{\rm eff}^{h\gamma Z}$. Note that in the SM and theories beyond the SM which are CPT symmetric, there are no sources of non-Hermiticity of $\mathcal{L}_{\rm eff}^{h\gamma Z}$ apart from rescattering effects.

The CPT theorem is one of the most profound results of quantum field theory [17]. It is a consequence of Lorentz invariance, locality, connection between spin and statistics, and a Hermitian Hamiltonian. However there are many extensions of the SM in which CPT violation appears due to nonlocality in the string theory, or violation of Lorentz symmetry in the extra dimensional models (see, for example, [18]). One can also mention possible deviations from the standard quantum mechanical evolution of states in some models of quantum gravity, and the corresponding breakdown of the CPT symmetry is investigated in the neutral-meson system, where novel CPT-violating observables for the ϕ-factories and B-factories are proposed [19]. The CPT violating effects in some of these underlying theories, in principle, can be additional sources of non-Hermiticity of effective Lagrangian $\mathcal{L}_{\rm eff}^{h\gamma Z}$ and hence contribute to photon circular polarization.

As for experimental results on the SM Higgs boson decay to the Z boson and photon, we mention recent ATLAS and CMS results [20,21]. The Higgs production cross section times the $h\to\gamma\,Z$ branching fraction limits are about an order of magnitude larger than the SM expectation for $m_h=125$ GeV.

2 Formalism

The effective Lagrangian for the $h\,\gamma\,\gamma$ and $h\,\gamma\,Z$ interactions can be written, as

$$\mathcal{L}_{\rm eff}^{h\gamma\gamma}=\frac{e^2}{32\,\pi^2\,v}\left(c_\gamma\,F_{\mu\nu}F^{\mu\nu}h-\tilde{c}_\gamma\,F_{\mu\nu}\widetilde{F}^{\mu\nu}h\right)\,, \tag{2}$$

$$\mathcal{L}_{\rm eff}^{h\gamma Z}=\frac{e\,g}{16\,\pi^2\,v}\Big(c_{1Z}\,Z_{\mu\nu}F^{\mu\nu}h-c_{2Z}\,(\partial_\mu h\,Z_\nu-\partial_\nu h\,Z_\mu)\,F^{\mu\nu}-\tilde{c}_Z\,Z_{\mu\nu}\widetilde{F}^{\mu\nu}h\Big)\,, \tag{3}$$

where e is the positron electric charge, g is the $SU(2)_L$ coupling constant and $v=\left(\sqrt{2}G_{\rm F}\right)^{-1/2}\approx 246$ GeV is the vacuum expectation value of the Higgs field. Here $F_{\mu\nu}$ and $Z_{\mu\nu}$ are the standard field strengths for the electromagnetic and Z field and $\widetilde{F}_{\mu\nu}=\varepsilon_{\mu\nu\alpha\beta}F^{\alpha\beta}/2$, with convention $\varepsilon_{0123}=+1$. Dimensionless parameters c_γ, c_{1Z}, c_{2Z}, $\tilde{c}_\gamma$, and $\tilde{c}_Z$ are effective coupling constants[1]. As these coupling constants are, in general, complex-valued, the operators (2) and (3) are non-Hermitian, while being local and Lorentz invariant.

It is convenient to write the couplings c_γ and c_{1Z} as the sums of terms in the SM and new physics (NP) beyond the SM: $c_\gamma=c_\gamma^{\rm SM}+c_\gamma^{\rm NP}$, $c_{1Z}=c_Z^{\rm SM}+c_{1Z}^{\rm NP}$. In the SM, $\tilde{c}_\gamma=c_{2Z}=\tilde{c}_Z=0$ and their nonzero values come from effects of NP. The couplings $c_\gamma^{\rm SM}$ and $c_Z^{\rm SM}$ have small imaginary parts which arise due to the intermediate on mass shell $\ell^+\,\ell^-$ and $q\bar{q}$ states in the one-loop contributions [where $\ell=e$, μ, τ denote leptons and $q=u$, d, s, c, b denote quarks (excluding t quark)]. We calculate couplings $c_\gamma^{\rm SM}$ and $c_Z^{\rm SM}$ in the one-loop order [16,23,24] and obtain [13]

$$c_\gamma^{\rm SM}=-6.60+0.08i\,,\qquad\qquad c_Z^{\rm SM}=-5.540+0.005i\,, \tag{4}$$

where for $m_h=126$ GeV the SM parameters are taken from [25] and the quark masses - from [26].

[1] Note that the $h\gamma Z$ effective interaction in the form (3) was discussed in [22].

The terms c_γ, c_{1Z}, and c_{2Z} above correspond to a CP-even scalar h, while the terms $\tilde{c}_\gamma$ and $\tilde{c}_Z$ indicate a CP-odd pseudoscalar h. The presence of both sets of terms means that h is not a CP eigenstate. Interference of these terms lead to CP violating effects which reveal in polarization states of the photon. Generally, the couplings $c_\gamma^{\rm NP}$, $c_{1Z}^{\rm NP}$, $\tilde{c}_\gamma$, c_{2Z}, $\tilde{c}_Z$ may be complex.

Values of coupling constants $c_\gamma^{\rm NP}$, $c_{1Z}^{\rm NP}$, $\tilde{c}_\gamma$, c_{2Z}, $\tilde{c}_Z$ can be calculated in various models. In particular, there are models with more than one Higgs doublet which induce CP violation due to the specific coupling of neutral Higgs bosons to fermions. We calculate $c_\gamma^{\rm NP}$, $c_{1Z}^{\rm NP}$, $\tilde{c}_\gamma$, c_{2Z}, $\tilde{c}_Z$ assuming that the couplings of h boson to the fermion fields, ψ_f, are given by the Lagrangian including both scalar and pseudoscalar parts

$$\mathcal{L}^{hff} = -\sum_f \frac{m_f}{v}\, h\, \bar{\psi}_f\, (1 + s_f + i\, p_f \gamma_5)\, \psi_f\,, \tag{5}$$

where m_f is the fermion mass, s_f, p_f are real parameters and $s_f = p_f = 0$ corresponds to the SM.

Evaluating the fermion contribution to the one-loop $h \to \gamma\,\gamma$ and $h \to \gamma\, Z$ amplitudes we obtain (see details in Ref. [13])

$$c_\gamma^{\rm NP} \approx 1.84 s_t - (3s_b + 2s_c + 2s_\tau) \times 10^{-2} + i\, 2\, (2s_b + s_c + s_\tau) \times 10^{-2}\,, \tag{6}$$

$$\tilde{c}_\gamma \approx 2.79 p_t + (3p_b + 2p_c + 2p_\tau) \times 10^{-2} - i\, 2\, (2p_b + p_c + p_\tau) \times 10^{-2}\,, \tag{7}$$

$$c_{1Z}^{\rm NP} \approx 0.3253 s_t - (8.2 s_b + 1.2 s_c + 0.2 s_\tau) \times 10^{-3} + i\, (4.8 s_b + 0.5 s_c + 0.1 s_\tau) \times 10^{-3}\,, \tag{8}$$

$$\tilde{c}_Z \approx -0.4939 p_t + (9.6 p_b + 1.3 p_c + 0.3 p_\tau) \times 10^{-3} - i\, (4.9 p_b + 0.5 p_c + 0.1 p_\tau) \times 10^{-3}\,. \tag{9}$$

In obtaining numerical values in (6)–(9) we have taken into account dominant contributions from the charm, bottom, top quarks and τ lepton, in particularly, the charm, bottom quarks and τ lepton give rise to the imaginary parts of the couplings in (6)–(9).

In terms of the parameters s_f and p_f the width of the decay $h \to f\bar{f}$ is written as

$$\Gamma(h \to f\bar{f}) \;=\; \frac{N_f G_F}{4\sqrt{2}\pi}\, m_f^2\, m_h\, \beta_f\, \left((1 + s_f)^2 \beta_f^2 \;+\; p_f^2\right)\,, \tag{10}$$

where m_h is the mass of h boson, $\beta_f = \sqrt{1 - 4m_f^2/m_h^2}$ is velocity of fermion $f = (\ell, q)$ in the rest frame of h. With a good accuracy one can put $\beta_f = 1$. Note that if one chooses $(1 + s_f)^2 + p_f^2 = 1$, then the width in Eq. (10) coincides with the decay width of the SM Higgs boson.

3 Amplitudes and angular distributions

Let us consider the decay of the zero-spin Higgs h boson into a pair of photons

$$h(p) \to \gamma(k_1, \epsilon_1)\, \gamma(k_2, \epsilon_2)\,, \tag{11}$$

where p is the four-momentum of h boson, k_1, k_2 are the four-momenta of photons and ϵ_1, ϵ_2 are the corresponding polarization four-vectors. In the rest frame of h, the amplitude of this decay can be written in the form

$$\mathcal{A}(h \to 2\,\gamma) = \frac{e^2 m_h^2}{16\,\pi^2\, v} \left(c_\gamma (\vec{e}_1^{\,*}\, \vec{e}_2^{\,*}) + \tilde{c}_\gamma (\hat{\vec{k}}\, [\vec{e}_1^{\,*} \times \vec{e}_2^{\,*}])\right)\,. \tag{12}$$

The polarization vectors are chosen in the form $\epsilon_1 = (0,\, \vec{e}_1)$, $\epsilon_2 = (0,\, \vec{e}_2)$, where $\vec{e}_1\, \vec{k} = \vec{e}_2\, \vec{k} = 0$, $\vec{k}$ is the three-momentum of one of the photons and $\hat{\vec{k}} \equiv \vec{k}/|\vec{k}|$.

The helicity amplitudes for decay (11) are equal to

$$H_\pm = -\frac{e^2 m_h^2}{16\,\pi^2\, v}\, (c_\gamma \pm i\, \tilde{c}_\gamma) \tag{13}$$

and the decay width is

$$\Gamma(h \to 2\gamma) = \frac{1}{32\,\pi m_h} \left(|H_+|^2 + |H_-|^2\right). \tag{14}$$

The polarization states of a single photon are usually described through the density matrix $\rho^{(\gamma)}$. For the process (11), one can write the two-photon density matrix following Ref. [27] as follows:

$$\rho^{(\gamma\gamma)} = \frac{1}{4}\, [1 \otimes 1 - \sigma_3 \otimes \sigma_3 + \xi_1\, (\sigma_1 \otimes \sigma_2 - \sigma_2 \otimes \sigma_1) + \xi_2\, (\sigma_3 \otimes 1 - 1 \otimes \sigma_3) - \xi_3\, (\sigma_1 \otimes \sigma_1 + \sigma_2 \otimes \sigma_2)]\,, \tag{15}$$

where $\vec{\sigma} = (\sigma_1,\, \sigma_2,\, \sigma_3)$ are the Pauli matrices, 1 is 2×2 unit matrix, and $\otimes$ means the direct product of two matrices. The reference frame is chosen with the OZ axis along $\hat{\vec{k}}$, and matrices on the left (right) from symbol $\otimes$ refer to the photon with momentum $\vec{k}$ $(-\vec{k})$.

In (15) the following parameters are introduced

$$\begin{aligned}
\xi_1 &= \frac{2\,\mathrm{Im}\left(H_+ H_-^*\right)}{|H_+|^2+|H_-|^2} = \frac{2\,\mathrm{Re}(c_\gamma \tilde{c}_\gamma^*)}{|c_\gamma|^2+|\tilde{c}_\gamma|^2}\,,\\
\xi_2 &= \frac{|H_+|^2-|H_-|^2}{|H_+|^2+|H_-|^2} = \frac{2\,\mathrm{Im}(c_\gamma \tilde{c}_\gamma^*)}{|c_\gamma|^2+|\tilde{c}_\gamma|^2}\,,\\
\xi_3 &= -\frac{2\,\mathrm{Re}\left(H_+ H_-^*\right)}{|H_+|^2+|H_-|^2} = \frac{|\tilde{c}_\gamma|^2-|c_\gamma|^2}{|c_\gamma|^2+|\tilde{c}_\gamma|^2}\,.
\end{aligned} \tag{16}$$

The Stokes parameter ξ_2 defines degree of the circular polarization of the photon with momentum $\vec{k}$, it has the meaning of average photon helicity. Parameters ξ_1, ξ_3 define correlation of linear polarizations of two photons (in particular, for $\xi_1 = 0, \xi_3 = -1$ the linear polarizations are parallel, while for $\xi_1 = 0, \xi_3 = 1$ they are orthogonal).

Next we come to the decay of h to γ and Z boson

$$h(p) \to \gamma(k_1,\epsilon_1)\, Z(k_2,\epsilon_2)\,, \tag{17}$$

where k_1, (k_2) is the four-momentum of photon (Z boson), ϵ_1, (ϵ_2) is polarization vector of the photon (Z boson).

The helicity amplitudes for the decay (17) are

$$H_\pm = -\frac{e g m_h^2}{16\,\pi^2\, v}\left(1-\frac{m_Z^2}{m_h^2}\right)(c_{1Z}+c_{2Z} \pm i\,\tilde{c}_Z)\,, \tag{18}$$

with the decay width

$$\Gamma(h\to\gamma Z) = \frac{1}{16\,\pi m_h}\left(1-\frac{m_Z^2}{m_h^2}\right)\left(|H_+|^2+|H_-|^2\right)\,, \tag{19}$$

where m_Z is the Z boson mass.

From definitions (16) we find the polarization parameters

$$\begin{aligned}
\xi_1 &= -\frac{2\,\mathrm{Im}(A_\parallel\, A_\perp^*)}{|A_\parallel|^2+|A_\perp|^2} = \frac{2\,\mathrm{Re}((c_{1Z}+c_{2Z})\tilde{c}_Z^*)}{|c_{1Z}+c_{2Z}|^2+|\tilde{c}_Z|^2}\,,\\
\xi_2 &= \frac{2\,\mathrm{Re}(A_\parallel\, A_\perp^*)}{|A_\parallel|^2+|A_\perp|^2} = \frac{2\,\mathrm{Im}((c_{1Z}+c_{2Z})\tilde{c}_Z^*)}{|c_{1Z}+c_{2Z}|^2+|\tilde{c}_Z|^2}\,,\\
\xi_3 &= \frac{|A_\perp|^2-|A_\parallel|^2}{|A_\parallel|^2+|A_\perp|^2} = \frac{|\tilde{c}_Z|^2-|c_{1Z}+c_{2Z}|^2}{|c_{1Z}+c_{2Z}|^2+|\tilde{c}_Z|^2}\,,
\end{aligned} \tag{20}$$

where $H_\pm$ from Eq. (18) for further convenience are replaced by the amplitudes $A_\parallel = (H_+ + H_-)/\sqrt{2}$ and $A_\perp = (H_+ - H_-)/\sqrt{2}$ corresponding to linearly polarized final states.

Numerical values of parameters ξ_1, ξ_2, ξ_3 will be discussed in Sec. 4.

In the decay (17), due to the zero-spin nature of the Higgs boson, the photon and Z boson have equal helicities[2]. This allows for measurement of the photon circular polarization through the decay $h \to \gamma\, Z \to \gamma\, f\bar{f}$. Indeed, we derive the following angular distribution of the process in the polar angle θ between the momentum of the fermion f in the Z boson rest frame and the direction of the Z boson motion in the h boson rest frame,

$$\frac{1}{\Gamma}\frac{d\Gamma(h\to\gamma\, Z\to\gamma\, f\bar{f})}{d\cos\theta} = \frac{3}{8}\Big(1+\cos^2\theta - 2\,A^{(f)}\,\xi_2\,\cos\theta\Big)\,, \tag{21}$$

where

$$A^{(f)} \equiv \frac{2\, g_V^f g_A^f}{(g_V^f)^2+(g_A^f)^2}\,. \tag{22}$$

The vector g_V^f and axial-vector g_A^f constants are

$$g_V^f \equiv t_{3L,\,f} - 2\,Q_f \sin^2\theta_W\,, \qquad g_A^f \equiv t_{3L,\,f}\,, \tag{23}$$

where θ_W is the weak angle, $t_{3L,\,f}$ is the projection of the weak isospin and Q_f is the charge (in units of the electric charge of the positron) of the fermion f.

[2]Of course for background processes the photon and Z boson helicities can differ.

Measurement of the forward-backward asymmetry $A_{\rm FB}$ relative to the direction of Z boson motion in the h boson rest frame for the f fermions produced in decay (1),

$$A_{\rm FB} \equiv \frac{F-B}{F+B}\,, \tag{24}$$

where

$$F \equiv \int_0^1 \frac{1}{\Gamma}\frac{d\Gamma}{d\cos\theta}\,d\cos\theta\,, \qquad B \equiv \int_{-1}^0 \frac{1}{\Gamma}\frac{d\Gamma}{d\cos\theta}\,d\cos\theta\,, \tag{25}$$

which is

$$A_{\rm FB} = -\frac{3}{4}\,A^{(f)}\,\xi_2\,, \tag{26}$$

allows one to find ξ_2.

Note that $A^{(\mu)}$ for the decay

$$h \to \gamma\, Z \to \gamma\, \mu^-\mu^+ \tag{27}$$

is 0.142 ± 0.015 [25], therefore in view of the condition $|\xi_2| \le 1$, the absolute value of the asymmetry for this decay is not larger than 0.11. At the same time for the decay channel

$$h \to \gamma\, Z \to \gamma\, b\,\bar b \tag{28}$$

($A^{(b)} = 0.923 \pm 0.020$ [25]), the absolute value of $A_{\rm FB}$ can be much larger, namely, as large as 0.69.

Consider now feasibility to measure the distribution (21) at the LHC after its upgrade to higher luminosity and energy $\sqrt{s} = 14$ TeV. Taking into account various mechanisms of Higgs boson production in pp collisions, the inclusive cross section is $\sigma = 57.0163$ pb [26]. Then the cross section for the process $p\,p \to h\,X \to \gamma\,Z\,X \to \gamma\,\ell^+\ell^-\,X$ in the SM is

$$\sigma \times {\rm BR}(h \to \gamma Z)\,{\rm BR}(Z \to \ell^+\ell^-) = 6.24\ {\rm fb}\,, \tag{29}$$

where $\ell = e,\,\mu$ and the branching fractions are taken from Refs. [25, 28]. In order to observe the forward-backward asymmetry $A_{\rm FB}$ for maximal value $|\xi_2| = 1$ at a $3\,\sigma$ level, the number of events should be bigger than 734. This number of events can be obtained, with ideal detector, with integrated luminosity about 120 fb^{-1}.

Let us discuss a possibility to determine the polarization parameters ξ_1 and ξ_3. For this one can study the process

$$h \to \gamma^*\, Z\ \to \ell^+\ell^-\, Z \tag{30}$$

with the decay $Z \to \bar f f$ on mass shell. For the process (30) we obtain the distribution over the dilepton invariant mass squared $q^2 \equiv m^2_{\ell\ell}$ and azimuthal angle ϕ between the decay planes of $\gamma^* \to \ell^+\ell^-$ and $Z \to \bar f f$ in the h rest frame:

$$\frac{d\Gamma(h \to \ell^+\ell^- Z)}{dq^2\,d\phi}\Big/\frac{d\Gamma}{dq^2} = \frac{1}{2\,\pi}\Big[1 - \frac{1}{4}\left(1 - F_L(q^2)\right)\,\left(\xi_3(q^2)\cos 2\phi + \xi_1(q^2)\sin 2\phi\right)\Big]\,. \tag{31}$$

Here

$$F_L(q^2) \equiv \frac{|A_0(q^2)|^2}{|A_0(q^2)|^2 + |A_\parallel(q^2)|^2 + |A_\perp(q^2)|^2} \tag{32}$$

is the fraction of longitudinal polarization of virtual photon, and the amplitudes are defined as

$$A_0(q^2) = \frac{e\,g}{16\,\pi^2\,v}\sqrt{\frac{q^2}{m_Z^2}}\Big(2\,c_{1Z}\,m_Z^2 + c_{2Z}\left(m_h^2 - q^2 + m_Z^2\right)\Big)\,, \tag{33}$$

$$A_\parallel(q^2) = -\frac{e\,g}{8\,\sqrt{2}\,\pi^2\,v}\Big(c_{1Z}\left(m_h^2 - q^2 - m_Z^2\right) + c_{2Z}\left(m_h^2 + q^2 - m_Z^2\right)\Big)\,, \tag{34}$$

$$A_\perp(q^2) = -i\frac{e\,g}{8\,\sqrt{2}\,\pi^2\,v}\tilde c_Z\sqrt{\lambda(m_h^2, q^2, m_Z^2)}\,, \tag{35}$$

with $\lambda(a,b,c) \equiv a^2 + b^2 + c^2 - 2\,(ab + ac + bc)$ and the distribution over the invariant mass squared reads

$$\frac{d\Gamma}{dq^2} = \frac{\alpha_{\rm em}\,\sqrt{\lambda(m_h^2, q^2, m_Z^2)}}{48\,\pi^2\,m_h^3\,q^2}\Big(\left|A_0(q^2)\right|^2 + \left|A_\parallel(q^2)\right|^2 + \left|A_\perp(q^2)\right|^2\Big)\,, \tag{36}$$

where $\alpha_{\rm em} = e^2/(4\pi)$ is the electromagnetic fine-structure constant. The q^2-dependent quantities $\xi_1(q^2)$ and $\xi_3(q^2)$ can be obtained from Eqs. (20) in which the amplitudes $A_\parallel\,(A_\perp)$ are substituted by the q^2-dependent amplitudes $A_\parallel(q^2)\,(A_\perp(q^2))$. In derivation of (31) we assumed that leptons are massless.

In expressions (33)–(35) we did not take into account the process $h \to Z^* Z \to \ell^+\ell^- Z$ and additional two-fermion current operators of dimension 6 in the effective Hamiltonian approach [29,30]. Both these mechanisms contribute at tree level to the decay $h \to \ell^+\ell^- Z$.

From (31) one can approximately find ξ_1 and ξ_3 in the decay $h \to \gamma Z$. Neglecting the amplitude (33) for longitudinally polarized photon $|A_0(q^2)|^2 \sim q^2$, and q^2-dependence of the transverse amplitudes, i.e. substituting $A_\parallel(q^2) \approx A_\parallel(0)$ and $A_\perp(q^2) \approx A_\perp(0)$, we obtain the distribution over the azimuthal angle

$$\frac{d\Gamma(h \to \ell^+\ell^- Z)}{d\phi} \approx \left(\frac{\alpha_{\rm em}}{3\,\pi} \log\frac{q^2_{\rm max}}{q^2_{\rm min}}\right) \Gamma(h \to \gamma\, Z)\, \frac{1}{2\,\pi} \left[1 - \frac{1}{4}\left(\xi_3 \cos 2\phi + \xi_1 \sin 2\phi\right)\right] . \tag{37}$$

The lower integration limit $q^2_{\rm min}$ is determined by possibilities of detectors, in particular, to provide sufficient ϕ resolution to separate $\sin 2\phi$ and $\cos 2\phi$ terms in the distribution (37). In this connection we should mention recent measurements of the $B^0 \to K^{*0}\, e^+e^-$ branching fraction [31], in which the LHCb detector allowed selection of the lower value of dilepton invariant mass equal to 30 MeV.

Theoretical accuracy of Eq. (37) improves with the decreasing value of $q^2_{\rm max}$, since contribution of the competing mechanism $h \to Z^* Z \to \ell^+\ell^- Z$ diminishes for $q^2_{\rm max} \ll m_Z^2$. Consider for example production of the e^+e^- pair in the process $h \to e^+e^- Z$ with dilepton invariant mass from 30 MeV to 1000 MeV. Our calculation including both $h \to \gamma^* Z \to e^+e^- Z$ and $h \to Z^* Z \to e^+e^- Z$ amplitudes shows that theoretical error in ξ_1, ξ_3, which arises when neglecting the $h \to Z^* Z \to e^+e^- Z$ mechanism, can be 10–20% [13].

Of course, the process $h \to \gamma^* Z \to e^+e^- Z$ is rare. Let us make an estimate of its observability at the LHC energy $\sqrt{s} = 14$ TeV. Using (37) and choosing the Higgs production inclusive cross section $\sigma = 57.0163$ pb [26] we calculate the SM cross section for the $p\,p \to h\,X \to \gamma^*\,Z\,X \to e^+e^-\,Z\,X$ in the interval of dilepton invariant mass from 30 MeV to 1000 MeV,

$$\sigma \times \frac{\Gamma(h \to e^+e^- Z)|_{30\ {\rm MeV} < m_{ee} < 1000\ {\rm MeV}}}{\Gamma(h \to {\rm all})} = 0.5\ {\rm fb}\,. \tag{38}$$

When detecting Z boson via $Z \to e^+e^-$ and $Z \to \mu^+\mu^-$ channels the cross section (38) is reduced by factor 0.067, and for the integrated luminosity of 100 fb^{-1} we can expect about 3 events. This number is too small and a higher integrated luminosity will be needed to observe the decay $h \to \gamma^* Z \to \ell^+\ell^- Z$ and analyze its angular distribution.

4 Results of calculation and discussion

First we note that in the SM the polarization parameters are $\xi_1^{SM} = \xi_2^{SM} = 0$ and $\xi_3^{SM} = -1$. Any deviations of the measured values of ξ_i from ξ_i^{SM} $(i = 1, 2, 3)$ will indicate presence of effects beyond the SM.

In order to estimate magnitude of effects of NP, we consider the model (5) with the scalar and pseudoscalar couplings of fermions to the Higgs boson. We choose the parameters

$$p_t = p_b = p_c = p_\tau = \pm\, 1/\sqrt{2}\,, \qquad\qquad s_t = s_b = s_c = s_\tau = 1/\sqrt{2} - 1 \tag{39}$$

satisfying normalization $(1 + s_f)^2 + p_f^2 = 1$ discussed in Sec. 2.

As a result, for the decay $h \to \gamma\,\gamma$ we find

$$\begin{aligned} \xi_1 &= \mp 0.528, \qquad \xi_2 = \mp 0.010, \qquad \xi_3 = -0.849, \\ \mu_{\gamma\gamma} &\equiv \frac{\Gamma(h \to \gamma\,\gamma)}{\Gamma^{\rm SM}(h \to \gamma\,\gamma)} = 1.26 \end{aligned} \tag{40}$$

while for decay $h \to \gamma\, Z$

$$\begin{aligned} \xi_1 &= \pm 0.121, \qquad \xi_2 = \mp 0.001, \qquad \xi_3 = -0.993, \\ \mu_{\gamma Z} &\equiv \frac{\Gamma(h \to \gamma\, Z)}{\Gamma^{\rm SM}(h \to \gamma\, Z)} = 1.04. \end{aligned} \tag{41}$$

In addition, the $h \to f\bar f$ decay width calculated with s_f, p_f in (39) coincides with the SM decay width and agrees with the CMS data [11] for $h \to \tau^+\tau^-$ and $h \to b\,\bar b$ decays,

$$\begin{aligned} \mu_{\tau\tau} &\equiv \frac{\Gamma(h \to \tau^+\,\tau^-)}{\Gamma^{\rm SM}(h \to \tau^+\,\tau^-)} = 1.10 \pm 0.41\,, \\ \mu_{b\,b} &\equiv \frac{\Gamma(h \to b\,\bar b)}{\Gamma^{\rm SM}(h \to b\,\bar b)} = 1.15 \pm 0.62\,. \end{aligned} \tag{42}$$

At the same time the channel $h \to c\,\bar c$ is not measured yet. Thus the $h \to c\,\bar c$ width, in general, may differ from the SM prediction, and consequently the constraint $(1 + s_c)^2 + p_c^2 = 1$ for the charm quark may not hold.

We can make an assumption that $\Gamma(h \to c\,\bar{c}) \le \Gamma(h \to b\,\bar{b})$. Combining this inequality with Eqs. (10) and (42) we find

$$(1+s_c)^2 + p_c^2 \le \mu_{bb} \times \frac{\Gamma^{\rm SM}(h \to b\,\bar{b})}{\Gamma^{\rm SM}(h \to c\,\bar{c})}\,. \tag{43}$$

Taking the central values of μ_{bb} and the widths from [28] (Table 1 therein) we obtain the following constraint for the $h\,c\,\bar{c}$ couplings: $(1+s_c)^2 + p_c^2 \le 22.8$.

To estimate maximal values of polarization parameter ξ_2 in the channel $h \to \gamma\,Z$ let us take s_c, p_c satisfying $(1+s_c)^2 + p_c^2 = 22.8$, although the latter equality does not fix s_c, p_c uniquely. In addition, put $s_f = p_f = 0$ for $f \neq c$. Then calculation using (8) and (9) gives values of ξ_2 which do not exceed 8.6×10^{-4}. It is seen that even for such a radical modification of the Higgs couplings to the charm quarks, the parameter ξ_2 remains very small.

Thus the existing data on the Higgs boson decay to the $\tau^+\tau^-$ and $b\,\bar{b}$ pairs and a reasonable assumption on the upper bound of the decay width to the charm quarks lead to conclusion that the rescattering effects on the one-loop level result in values of ξ_2 in the $h \to \gamma Z$ decay about 10^{-3} or smaller.

It would be of interest to check in the experimental analysis of the distribution (21) whether the parameter ξ_2 is very small indeed. If the analysis yielded sizable values of ξ_2, this would mean the presence of additional sources of non-Hermiticity of effective Lagrangian. The latter may arise, for example, due to the breaking of Hermiticity in an underlying (fundamental) theory at very small distances. Note, that similar aspects have been discussed in [32] for the process $\gamma\gamma \to h$, where the authors calculated various asymmetries as functions of complex coefficients c_γ, $\tilde{c}_\gamma$ in Eq. (2). Since the requirement of Hermiticity is one of the conditions in the proof of the CPT theorem [17], measurement of the photon circular polarization in the decay $h \to \gamma Z \to \gamma \bar{f} f$ through the forward-backward asymmetry $A_{\rm FB}$ can be useful for testing CPT symmetry.

The parameters ξ_1 and ξ_3 carry information on the CP properties of the Higgs boson. Besides, ξ_1 is CP-odd and T-odd observable and, in the absence of final-state interaction between the leptons and fermions, a nonzero value of ξ_1 will point to the violation of T invariance.

5 Conclusions

The polarization properties of the $\gamma\gamma$ and γZ states in the decays $h \to \gamma\gamma$ and $h \to \gamma Z$ of recently discovered scalar boson have been considered [13]. We have chosen effective Lagrangian, describing $h\gamma\gamma$ and $h\gamma Z$ interactions with CP-even and CP-odd parts. This allowed for calculation of polarization parameters ξ_1, ξ_2, ξ_3. In the SM these parameters take on values $\xi_1^{SM} = \xi_2^{SM} = 0$, $\xi_3^{SM} = -1$ and deviations of the measured values of ξ_i from ξ_i^{SM} $(i = 1, 2, 3)$ will point to effects of NP.

The parameter ξ_2, which defines the circular polarization of the photon, can be measured in the $h \to \gamma\,Z \to \gamma\,f\,\bar{f}$ decay through the forward-backward asymmetry $A_{\rm FB} \sim \xi_2$ of the fermion f. The parameters ξ_1, ξ_3, which define correlation of linear polarizations of γ and Z, can be extracted from the azimuthal angle distribution in the process $h \to \gamma^*\,Z \to \ell^+\ell^-\,Z$ with decay $Z \to \bar{f} f$ on the mass shell.

In numerical estimates of these parameters we included the one-loop contribution from the SM, and models beyond the SM. Namely, we used the model (5) with scalar and pseudoscalar couplings of fermions to the Higgs boson on the one-loop level. In addition, in Ref. [13] we applied effective field-theory approach [24,29,30,33–35] in which NP is described by gauge invariant dimension-6 operators in the fields of the SM.

The value of photon circular polarization turns out to be very small, of the order 10^{-3}. In general, nonzero value of ξ_2 arises due to presence of the CP-even and CP-odd parts in effective Lagrangian $\mathcal{L}_{\rm eff}^{h\gamma Z}$ and absorptive parts of one-loop diagrams, or rescattering effects of the type $h \to a\bar{a} \to \gamma\,Z$, where a are charged particles with masses $m_a \le m_h/2$. Only leptons and quarks u, d, s, c, b satisfy this condition and hence contribute to absorptive parts of one-loop diagrams. Contributions from leptons e, μ and light quarks u, d, s are negligibly small. The couplings of h to the τ lepton and bottom quark are constrained by recent CMS data on the $h \to \tau^+\tau^-$ and $h \to b\,\bar{b}$ decays, and couplings to the charm quark are constrained from an assumption on the upper bound of the $h \to c\,\bar{c}$ decay width.

Apart from rescattering effects, in framework of CPT symmetric models, there are no sources of non-Hermiticity of $\mathcal{L}_{\rm eff}^{h\gamma Z}$ which could contribute to parameter ξ_2. If there is a violation of CPT symmetry in an underlying theory at small distances, then this may give rise to additional non-Hermiticity effects in $\mathcal{L}_{\rm eff}^{h\gamma Z}$ which will change the value of ξ_2. Therefore measurement of this parameter in the $h \to \gamma\,Z \to \gamma\,f\,\bar{f}$ process would allow one to test the prediction of the SM, and to search for deviations from the SM, and even possible effects of CPT violation in an underlying theory.

Nonzero values of parameter ξ_1 point to violation of CP symmetry in the $h \to \gamma\gamma$ and $h \to \gamma Z$ decays. In the chosen models of NP, for the $h \to \gamma Z$ decay, ξ_1 appears to be 0.1-0.2. Its experimental determination can put constraints on models describing physics beyond the SM.

We also estimated in the SM a feasibility of measurement of the discussed processes in the pp collisions at the LHC, after its upgrade to energy $\sqrt{s} = 14$ TeV and higher luminosity. The cross section for the process

$p\,p \to h\,X \to \gamma\,Z\,X \to \gamma\,\ell^+\ell^-\,X$ $(\ell = e,\,\mu)$ turns out to be 6.24 fb. With integrated luminosity about 120 fb^{-1} and ideal detector it may be possible to observe the forward-backward asymmetry A_{FB} for $|\xi_2| = 1$ at a $3\,\sigma$ level.

Here we should mention papers [36,37], where possibilities of studying at the LHC the $h \to \gamma\,\ell^+\ell^-$ decay via $\gamma\,Z$ channel are considered. Although observation of the Higgs is difficult in view of the background which is a few orders of magnitude larger than the signal and unfavorable kinematics of this decay [37], in these papers optimistic conclusions are made as for measurement of the branching ratio of the SM Higgs decay to $\gamma\,Z$ at the 14 TeV LHC with integrated luminosity of 100 fb^{-1} [36].

The reaction $p\,p \to h\,X \to \gamma^*\,Z\,X \to e^+e^-\,Z\,X$ is a more rare process, and our estimate of its observability is less optimistic. One can expect about 3 events in the interval of e^+e^- invariant mass from 30 MeV to 1000 MeV if Z boson is detected through the $Z \to e^+e^-$, $\mu^+\mu^-$ channels. Clearly an integrated luminosity higher than 100 fb^{-1} will be needed to study the $h \to \gamma^*\,Z \to e^+e^-\,Z$ process.

In conclusion, we hope that with increasing the integrated luminosity at the LHC investigation of the angular distributions discussed above will become possible.

Acknowledgements. A.Yu. K. thanks the Organizers of the International School-Seminar NPQCD-2013 for invitation to present a talk and kind hospitality in Dnipropetrovsk.

References

[1] G. Aad *et al.* (ATLAS Collaboration), Phys. Lett. B **716**, 1 (2012).
[2] S. Chatrchyan *et al.* (CMS Collaboration), Phys. Lett. B **716**, 30 (2012).
[3] S. Chatrchyan *et al.* (CMS Collaboration), Phys. Rev. Lett. **110**, 081803 (2013).
[4] A. Pilaftsis and C.E.M. Wagner, Nucl. Phys. **B553**, 3 (1999).
[5] V. Barger, P. Langacker, M. McCaskey *et al.*, Phys. Rev. D **79**, 015018 (2009).
[6] G.C. Branco, P.M. Ferreira, L. Lavoura *et al.*, Phys. Rep. **516**, 1 (2012).
[7] N. Cabibbo, Phys. Rev. Lett. **10**, 531 (1963); M. Kobayashi and T. Maskawa, Prog. Theor. Phys. **49**, 652 (1973).
[8] D. Bailin and A. Love, *Cosmology in Gauge Field Theory and String Theory* (Institute of Physics Publishing, Bristol-Philadelphia, 2004).
[9] M.B. Voloshin, Phys. Rev. D **86**, 093016 (2012).
[10] ATLAS Collaboration, Report No. ATLAS-CONF-2013-034, 2013.
[11] CMS Collaboration, Report No. CMS-PAS-HIG-13-005.
[12] V.A. Kovalchuk, Zh. Eksp. Theor. Fiz. **134**, 907 (2008) [J. Exp. Theor. Phys. **107**, 774 (2008)].
[13] A.Yu. Korchin and V.A. Kovalchuk, Phys. Rev. D **88**, 036009 (2013).
[14] L.B. Okun, arXiv:hep-ph/0210052.
[15] R. Cahn, M.S. Chanowitz, and N. Fleishon, Phys. Lett. B **82**, 113 (1979).
[16] L. Bergström and G. Hulth, Nucl. Phys. **B259**, 137 (1985); **B276**, 744(E) (1986).
[17] R.F. Streater and A.S. Wightman, *PCT, Spin and Statistics and All That* (W.A. Benjamin, Inc. New York-Amsterdam, 1964).
[18] A. Kostelecky, arXiv:0802.0581v1.
[19] J. Bernabeu, N.E. Mavromatos and J. Papavassiliou, Phys. Rev. Lett. **92**, 131601 (2004).
[20] ATLAS Collaboration, Report No. ATLAS-CONF-2013-009, 2013.
[21] CMS Collaboration, arXiv:1307.5515v1.
[22] K. Hagiwara and M.L. Stong, Z. Phys. C **62**, 99 (1994).
[23] M. Spira, Fortsch. Phys. **46**, 203 (1998).
[24] A.V. Manohar and M.B. Wise, Phys. Lett. B **636**, 107 (2006).
[25] J. Beringer *et al.* (Particle Data Group), Phys. Rev. D **86**, 010001 (2012).
[26] LHC Higgs Cross Section Working Group, arXiv:1101.0593v3.
[27] J. Bernstein and L. Michel, Phys. Rev. **118**, 871 (1960).
[28] LHC Higgs Cross Section Working Group, arXiv:1307.1347v1.
[29] W. Buchmüller and D. Wyller, Nucl. Phys. **B268**, 621 (1986).
[30] B. Grzadkowski, M. Iskrzynski, M. Misiak, and J. Rosiek, J. High Energy Phys. 10 (2010) 085.
[31] R. Aaij *et al.* (LHCb Collaboration), J. High Energy Phys. 05 (2013) 159.
[32] I.F. Ginzburg and I.P. Ivanov, Eur. Phys. J. C **22**, 411 (2001).
[33] K. Hagiwara, R. Szalapski, and D. Zeppenfeld, Phys. Lett. B **318**, 155 (1993).
[34] K. Hagiwara, S. Ishihara, R. Szalapski, and D. Zeppenfeld, Phys. Rev. D **48**, 2182 (1993).
[35] C. Grojean, E.E. Jenkins, A.V. Manohar, and M. Trott, J. High Energy Phys. 04 (2013) 016.
[36] J.S. Gainer, W.-Y. Keung, I. Low, and P. Schwaller, Phys. Rev. D **86**, 033010 (2012).
[37] J.M. Campbell, R.K. Ellis, W.T. Giele, and C. Williams, Phys. Rev. D **87**, 073005 (2013).

Proceedings of the International School-seminar
"New Physics and Quantum Chromodynamics at External Conditions", pp. 20 – 24,
May 22-24, 2013, Dnipropetrovsk, Ukraine

RANDALL-SUNDRUM SCENARIO WITH SMALL CURVATURE AND DILEPTON PRODUCTION AT LHC

A.V. Kisselev

Institute for High Energy Physics, 142281, Protvino, Russia

The brief review of the recent results obtained in the Randall-Sundrum scenario with the small curvature of the five-dimensional space-time is presented.

1 RSSC model

In the recent papers [1], [2] the dilepton (dimuon and dielectron) production at the LHC was studied in the framework of the *RSSC model* (Randall-Sundrum-like model with the small curvature) [3]- [5].

The classical action of the model is

$$\begin{aligned} S &= \int d^4x \int_{-\pi r_c}^{\pi r_c} dy \, \sqrt{G} \, (2\bar{M}_5^3 \mathcal{R} - \Lambda) \\ &+ \int d^4x \sqrt{|g^{(1)}|} \, (\mathcal{L}_1 - \Lambda_1) + \int d^4x \sqrt{|g^{(2)}|} \, (\mathcal{L}_2 - \Lambda_2) \, , \end{aligned} \tag{1}$$

where $G_{MN}(x,y)$ is the 5-dimensional metric, with $M,N = 0,1,2,3,4$, $\mu = 0,1,2,3$, and y is the 5-th dimension coordinate of the size r_c. The quantities

$$g_{\mu\nu}^{(1)}(x) = G_{\mu\nu}(x, y=0) \, , \quad g_{\mu\nu}^{(2)}(x) = G_{\mu\nu}(x, y=\pi r_c) \tag{2}$$

are induced metrics on the branes, $\mathcal{L}_1$ and $\mathcal{L}_2$ are brane Lagrangians, $G = \det(G_{MN})$, $g^{(i)} = \det(g_{\mu\nu}^{(i)})$.

As in the original RS model [6], the periodicity $y = y + 2\pi r_c$ is imposed and the points (x_μ, y) and $(x_\mu, -y)$ are identified. Thus, we get the orbifold S^1/Z_2. There are two 3D branes located at the fixed points $y = 0$ (Plank brane) and $y = \pi r_c$ (TeV brane). The SM fields are constrained to the TeV brane, while the gravity propagates in all spatial dimensions.

In order to solve Einstein-Hilbert's equations which follow from the action (1), it is assumed that the background metric respects 4-dimensional Poincare invariance

$$ds^2 = e^{-2\sigma(y)} \, \eta_{\mu\nu} \, dx^\mu \, dx^\nu - dy^2 \, , \tag{3}$$

Thus, the 5-dimensional metric tensor has the form

$$G_{MN} = \begin{pmatrix} g_{\mu\nu} & 0 \\ 0 & -1 \end{pmatrix} \, , \tag{4}$$

where

$$g_{\mu\nu} = e^{-2\sigma(y)} \, \eta_{\mu\nu} \, , \tag{5}$$

and $\eta_{\mu\nu}$ is the Minkowski tensor $(1,-1,-1,-1)$.

The background metric was found to be [2]

$$\sigma(y) = \frac{\kappa}{2} \, (|y| - |\pi r_c - y|) - \frac{\kappa \pi r_c}{2} \, , \tag{6}$$

with the fine tuning

$$\begin{aligned} \Lambda &= -6\bar{M}_5^3 \kappa^2 [\varepsilon(y) + \varepsilon(\pi r_c - y)]^2 \, , \\ \Lambda_1 &= -\Lambda_2 = 12 \bar{M}_5^3 \kappa \, . \end{aligned} \tag{7}$$

The quantity κ defines the curvature of the 5-dimensional space-time.

e-mail: alexandre.kisselev@ihep.ru

In the RSSC model the hierarchy relation looks like

$$\bar{M}_{\rm Pl}^2 = \frac{\bar{M}_5^3}{\kappa}\left(e^{2\pi\kappa r_c} - 1\right) \ , \tag{8}$$

where $\bar{M}_{\rm Pl} = M_{\rm Pl}/\sqrt{8\pi}$ is the reduced Planck scale, and $\bar{M}_5$ is the *reduced* fundamental gravity scale. $\bar{M}_5$ is related to the 5-dimensional Planck scale as

$$\bar{M}_5 = (2\pi)^{-1/3} M_5 \ . \tag{9}$$

The masses of the Kaluza-Klein (KK) graviton excitations $h_{\mu\nu}^{(n)}$ are proportional to κ,

$$m_n = x_n \kappa \ , \quad n = 1, 2, \dots \ . \tag{10}$$

The interaction Lagrangian of gravitons is given by [3], [4]

$$\begin{aligned} \mathcal{L}_{\rm int} &= -\frac{1}{\bar{M}_5^{3/2}} \sum_{n=1}^{\infty} \int dy \, \sqrt{G} \, h_{\mu\nu}^{(n)}(x,y) \, T_{\alpha\beta}(x) \, g^{\mu\alpha} g^{\nu\beta} \delta(y - \pi\kappa r_c) \\ &= -\frac{1}{\Lambda_\pi} T_{\alpha\beta}(x) \sum_{n=1}^{\infty} h_{\mu\nu}^{(n)}(x) \, \eta^{\mu\alpha} \eta^{\nu\beta} \ , \end{aligned} \tag{11}$$

where $T_{\alpha\beta}(x)$ is the energy-momentum tensor of the SM fields on the TeV brane, and

$$\Lambda_\pi = \bar{M}_{\rm Pl} \, e^{-\pi\kappa r_c} \ . \tag{12}$$

Note that in the RSSC model the mass spectrum (10) and experimental signature are similar to those in the ADD model with one flat extra dimension [7]. Let us remember that the original RS model predicts heavy graviton resonances.

2 Graviton contribution to dilepton production at the LHC

In the framework of the RSSC model [4], [5], gravity effects can be searched for in the dilepton production ($l = \mu$ or e),

$$p\,p \to l^+ l^- + X \ . \tag{13}$$

In particular, the $p_\perp$-distribution of the final leptons in the process (13) is given by the formula

$$\begin{aligned} \frac{d\sigma}{dp_\perp}(pp \to l^+ l^- + X) &= 2p_\perp \sum_{a,b=q,\bar{q},g} \int \frac{d\tau\sqrt{\tau}}{\sqrt{\tau - x_\perp^2}} \int \frac{dx_1}{x_1} f_{a/p}(\mu^2, x_1) \\ &\times \ f_{b/p}(\mu, \tau/x_1) \, \frac{d\hat{\sigma}}{d\hat{t}}(ab \to l^+ l^-) \ , \end{aligned} \tag{14}$$

Here $f_{c/p}(\mu^2, x)$ is the distribution of the parton of the type c in momentum fraction x inside the proton taken at the scale μ. $d\hat{\sigma}/d\hat{t}$ is the differential cross section of the subprocess $ab \to l^+ l^-$. In eq. (14) two dimensionless variables are introduced

$$x_\perp = \frac{2p_\perp}{\sqrt{s}} \ , \quad \tau = x_1 x_2 \ , \tag{15}$$

where x_2 is the momentum fraction of the parton b inside the proton.

The contribution of the virtual gravitons to lepton pair production comes from the quark-antiquark annihilation and gluon-gluon fusion,

$$\begin{aligned} \frac{d\hat{\sigma}}{d\hat{t}}(q\bar{q} \to l^+ l^-) &= \frac{\hat{s}^4 + 10\hat{s}^3\hat{t} + 42\,\hat{s}^2\hat{t}^2 + 64\hat{s}\,\hat{t}^3 + 32\,\hat{t}^4}{1536\,\pi\hat{s}^2} \left|\mathcal{S}(\hat{s})\right|^2 \ , \\ \frac{d\hat{\sigma}}{d\hat{t}}(gg \to l^+ l^-) &= -\frac{\hat{t}(\hat{s} + \hat{t})(\hat{s}^2 + 2\hat{s}\,\hat{t} + 2\,\hat{t}^2)}{256\,\pi\hat{s}^2} \left|\mathcal{S}(\hat{s})\right|^2 \ , \end{aligned} \tag{16}$$

where $\hat{s}$ and $\hat{t}$ are Mandelstam variables of the subprocess. The sum

$$\mathcal{S}(s) = \frac{1}{\Lambda_\pi^2} \sum_{n=1}^{\infty} \frac{1}{s - m_n^2 + i\, m_n \Gamma_n} \tag{17}$$

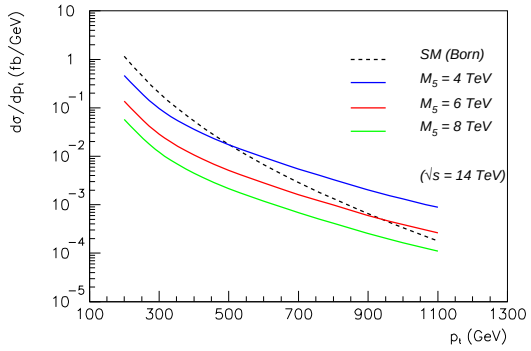

Figure 1. The KK graviton contribution to the dimuon production at the LHC for several values of 5-dimensional reduced Planck scale (solid curves) vs. SM contribution (dashed curve) at $\sqrt{s} = 14$ TeV.

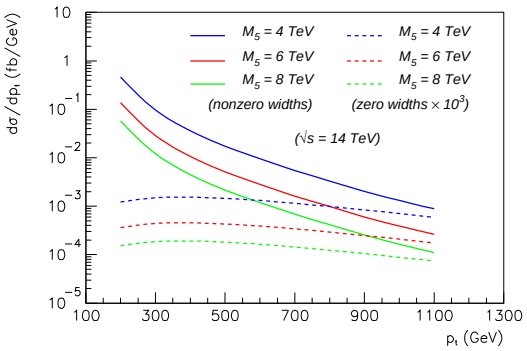

Figure 2. The contributions to the dimuon events from the KK gravitons with nonzero widths (solid curves) vs. contributions from zero width gravitons (multiplied by 10^3, dashed curves).

is the invariant part of the partonic matrix elements, with Γ_n being total width of the graviton with the KK number n and mass m_n [5]

$$\Gamma_n = \eta\, m_n \left(\frac{m_n}{\Lambda_\pi}\right)^2 , \quad \eta \simeq 0.09 . \tag{18}$$

Note that the function $\mathcal{S}(s)$ is universal for all processes mediated by s-channel virtual gravitons.

In the RSSC model [5] the explicit expression was obtained for $\mathcal{S}(s)$ (17) at $s \sim \bar{M}_5 \gg \kappa$

$$\mathcal{S}(s) = -\frac{1}{4\bar{M}_5^3\sqrt{s}}\, \frac{\sin 2A + i \sinh 2\varepsilon}{\cos^2 A + \sinh^2 \varepsilon} , \tag{19}$$

where

$$A = \frac{\sqrt{s}}{\kappa} , \qquad \varepsilon = \frac{\eta}{2}\Big(\frac{\sqrt{s}}{\bar{M}_5}\Big)^3 . \tag{20}$$

In papers [1], [2] contributions from s-channel gravitons to the $p_\perp$-distributions of the final leptons were calculated in the RSSC model by using eqs. (14)- (20). The calculations were made for different values of 5-dimensional Planck scale $\bar{M}_5$. The MSTW 2008 NNLO parton distributions [8] were used. The PDF scale μ was taken to be equal to the invariant mass of the lepton pair, $\mu = M_{l^+l^-} = \sqrt{\hat{s}}$.

The CMS cuts on the lepton pseudorapidities were imposed. For the dimuon events the cut looks like

$$|\eta| < 2.4 , \tag{21}$$

while for the dielectron events the cuts are the following

$$|\eta| < 1.44 , \quad 1.57 < |\eta| < 2.50 . \tag{22}$$

The reconstruction efficiency of 85% was assumed for the dilepton events [9].

In Fig. 1 the gravity cross sections for the dimuon production at the LHC are presented. The gravity mediated contributions to the cross sections do not include the SM contribution. Fig. 2 demonstrates that an ignorance of the graviton widths would be a rough approximation since it results in very large suppression of the gravity contributions. The $p_\perp$-distributions for the dielectron production are shown in Fig. 3 and Fig. 4, for $\sqrt{s} = 8$ TeV and $\sqrt{s} = 13$ TeV, respectively.

Let $N_S(N_B)$ be a number of signal (background) dilepton events with $p_\perp > p_\perp^{\rm cut}$,

$$N_B = \int\limits_{p_\perp > p_\perp^{\rm cut}} \frac{d\sigma({\rm SM})}{dp_\perp} dp_\perp , \quad N_S = \int\limits_{p_\perp > p_\perp^{\rm cut}} \frac{d\sigma({\rm grav})}{dp_\perp} dp_\perp . \tag{23}$$

Then one can define the statistical significance

$$\mathcal{S} = \frac{N_S}{\sqrt{N_B + N_S}} , \tag{24}$$

and require a 5σ effect. In Fig. 5 the statistical significance is shown for $\sqrt{s} = 7$ TeV as a function of the transverse momentum cut $p_\perp^{\rm cut}$ and reduced 5-dimensional Planck scale $\bar{M}_5$. Fig. 6 represents the statistical

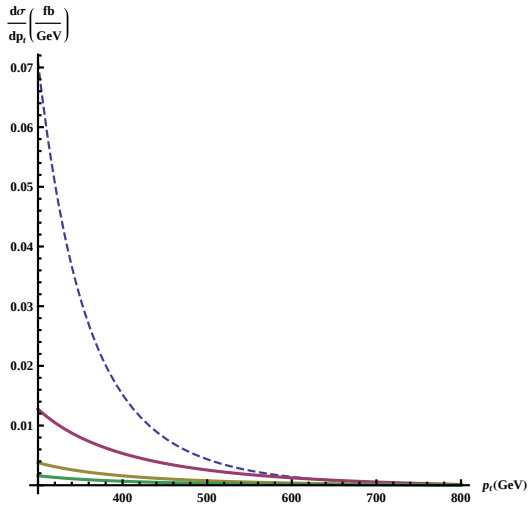

Figure 3. The KK graviton contribution to the dielectron production for $M_5 = 2$, 4, 6 TeV (solid curves, from above) vs. SM (Born) contribution (dashed curve) at $\sqrt{s} = 8$ TeV.

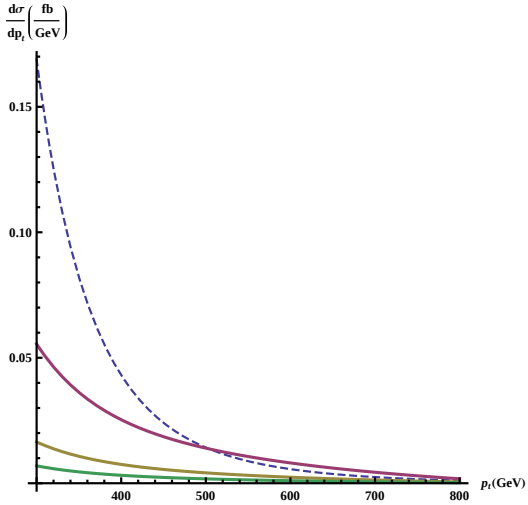

Figure 4. The same as in Fig. 4, but for $M_5 = 4$, 6, 8 TeV and $\sqrt{s} = 13$ TeV.

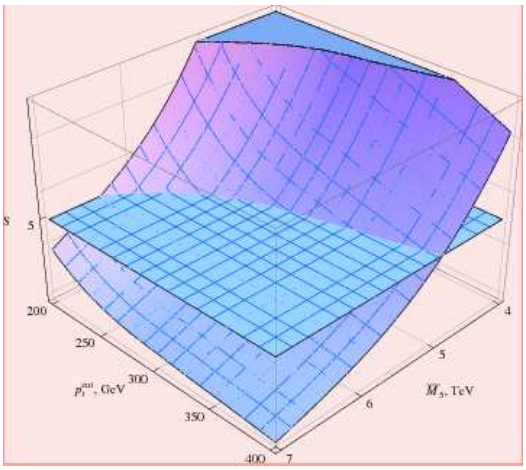

Figure 5. The statistical significance S for the dimuon production at the LHC for $\sqrt{s} = 7$ TeV and integrated luminosity 5 fb^{-1} as a function of the transverse momentum cut $p_\perp^{\rm cut}$ and reduced gravity scale $\bar{M}_5$. The plane $S = 5$ is also shown.

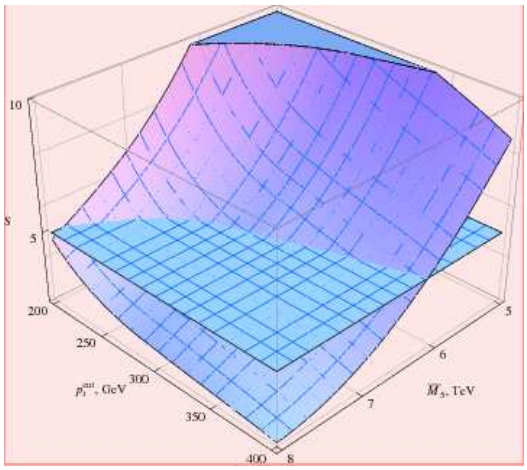

Figure 6. The same as in Fig. 5, but for $\sqrt{s} = 14$ TeV and integrated luminosity 30 fb^{-1}.

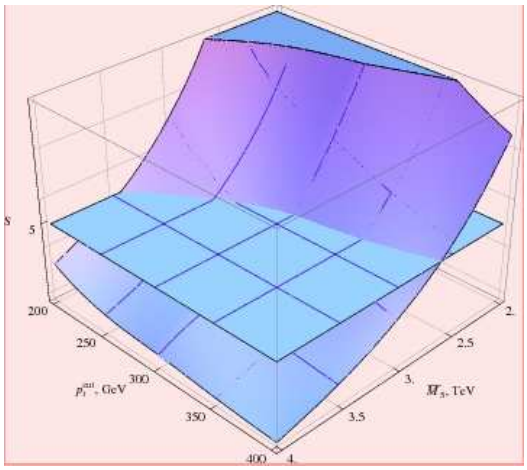

Figure 7. The statistical significance for the dielectron production at the LHC for $\sqrt{s} = (7 + 8)$ TeV and integrated luminosity (5+20) fb^{-1}.

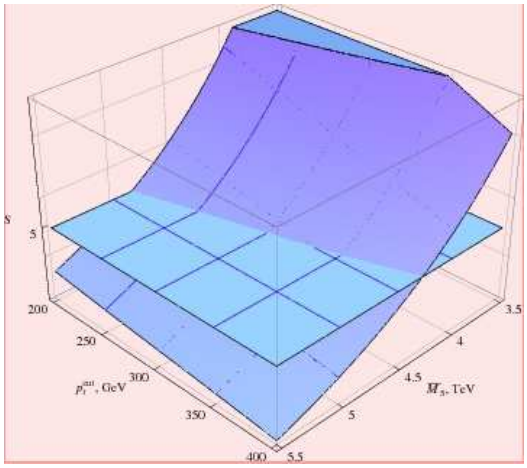

Figure 8. The same as in figure 7, but for $\sqrt{s} =$ 13 TeV and integrated luminosity 30 fb^{-1}.

significance for the dimuon events at $\sqrt{s} = 14$ TeV. The statistical significances for the dielectron events are shown in Fig. 7 and Fig. 8.

To take into account higher order contributions, the K-factor of 1.5 for the SM background was taken, while the factor $K = 1$ was used for the signal.

As a result, LHC discovery limits on the 5-dimensional Planck scale M_5 were obtained. In particular, for the (7+8) TeV LHC with the integrated luminosity (5+20) fb^{-1} the search limit in the dielectron production is equal to [2]

$$M_5 = 6.35 \text{ TeV} . \tag{25}$$

For the 13 TeV dielectron events with the integrated luminosity 30 fb^{-1} the search limit was found to be [2]

$$M_5 = 8.95 \text{ TeV} . \tag{26}$$

Let us underline that in the RSSC model these bounds do not depend on the curvature κ, contrary to the original RS model [6].

References

[1] A.V. Kisselev, JHEP **04**, 025 (2013) [arXiv:1210.3238].
[2] A.V. Kisselev, arXiv:1306.5402.
[3] G. F. Giudice, T. Plehn and A. Strumia, Nucl. Phys. **B 706**, 455 (2005) [hep-ph/0408320].
[4] A.V. Kisselev and V.A. Petrov, Phys. Rev. **D 71**, 124032 (2005) [hep-ph/0504203].
[5] A.V. Kisselev, Phys. Rev. **D 73**, 024007 (2006) [hep-th/0507145].
[6] L. Randall and R. Sundrum, Phys. Lett. **83**, 3370 (1999) [hep-ph/9905221].
[7] N. Arkani-Hamed, S. Dimopoulos and G. Dvali,Phys. Lett. **B 429**, 263 (1998) [hep-ph/9803315]; I. Antoniadis, N. Arkani-Hamed, S. Dimopoulos and G. Dvali, Phys. Lett. **B 436**, 257 (1998) [hep-ph/9804398]; N. Arkani-Hamed, S. Dimopoulos and G. Dvali, Phys. Rev. **D 59**, 086004 (1999) [hep-ph/9807344].
[8] A.D. Martin, W.J. Stirling, R.S. Thorne and G. Watt, Eur. Phys. J. C **63**, 189 (2009) [arXiv:0901.0002].
[9] CMS collaboration, Phys. Lett. **B 711**, 15 (2012) [arXiv:1202.3827].

Proceedings of the International School-seminar
"New Physics and Quantum Chromodynamics at External Conditions", pp. 25 – 32,
May 22-24, 2013, Dnipropetrovsk, Ukraine

ABOUT PHASE TRANSITIONS IN DENSE NEUTRON MATTER WITH GENERALIZED SKYRME FORCES TO SUPERFLUID STATES WITH ANISOTROPIC SPIN-TRIPLET PAIRING IN STRONG MAGNETIC FIELDS

A. N. Tarasov[a]

Akhiezer Institute for Theoretical Physics, NSC "Kharkov Institute of Physics and Technology", Kharkov, Ukraine

In the framework of generalized non-relativistic Fermi-liquid approach we study phase transitions in spatially uniform dense pure neutron matter from normal to superfluid states with spin-triplet p-wave pairing (similar to anisotropic superfluid phases $^3He-A_1$ and $^3He-A_2$) in steady and homogeneous strong magnetic field H (but $|\mu_n|H \ll E_c < \varepsilon_F(n)$, where μ_n is the magnetic dipole moment of a neutron, E_c is the cutoff energy and $\varepsilon_F(n)$ is the Fermi energy in neutron matter with density of particles n). The previously derived general formulas (valid for arbitrary parametrization of the effective Skyrme interaction in neutron matter) for phase transition (PT) temperatures $T_{c1,2}(n,H)$ (which are functions nonlinear of density n and linear of magnetic field H) are specified here for new generalized BSk20 and BSk21 parametrizations of the Skyrme forces (with additional terms dependent on density n) on the interval $0.1\cdot n_0 < n < 3.0\cdot n_0$, where $n_0 = 0.17$ fm^{-3} is nuclear density. Our main results are mathematical expressions and figures for PT temperatures in absence of magnetic field, $T_{c0,BSk20}(n) < 0.17$ MeV and $T_{c0,BSk21}(n) < 0.064$ MeV (at $E_c = 10$ MeV), and $T_{c1,2}(n,H)$ in strong magnetic fields (which may approach to 10^{17} G or even more as in liquid outer core of magnetars – strongly magnetized neutron stars). These are realistic non-monotone functions with bell-shaped density profile. We have obtained previously general formula (valid for arbitrary parametrization of the Skyrme forces) for magnetic susceptibility of superfluid pure neutron matter (SPNM) at zero temperature which is specified here for the new BSk18, BSk20 and BSk21 parametrizations of the Skyrme interaction. As a result from regular (nonsingular) behavior of magnetic susceptibility dependent on density we have concluded that for the model of SPNM with these generalized parametrizations of the Skyrme forces phase transition to ferromagnetic state does not occur neither at subnuclear nor at supranuclear densities.

1 Introduction

In August 1999 the NASA's *Chandra* X-ray Observatory detected the supernova remnant in Cassiopeia A (Cas A), which is the youngest known neutron star (NS) in the Milky Way Galaxy. Recently it was discovered unusually fast cooling of this NS [1, 2] and this fact has attracted considerable interest (see, e.g., [3, 4] and references therein). Several authors [3, 4] explain such rapid cooling of NS in Cas A during last years due to existence of spin-triplet superfluidity of neutrons inside high-density liquid outer core of this NS.

Neutrons are presumably the main constituent of neutron stars (NSs). In view of the fact that there is no decisive evidence that only $^3P_2$ pairing of neutrons [5, 6] occurs in outer core of NSs (it is not yet clear how n-n interaction in vacuum is modified in medium of NS at supra-saturation densities) and for lack of consensus in the calculated magnitude of neutron $^3P_2$ pairing gap at high densities [7, 8], we consider here another but somewhat simplified problem. Namely, in this work we shall focus our study on spin-triplet superfluid pure neutron matter (SPNM) which is spatially homogeneous (and, as a consequence, without spin-orbit coupling) at sub- and supra-nuclear densities from the interval $0.1 < n/n_0 < 3.0$ with p-wave pairing (similar to anisotropic superfluid phases ^{3}He – A$_1$ and ^{3}He – A$_2$, see [5]) in strong spatially uniform magnetic field **H**. Upper limit for magnetic fields studied here may be of the order 10^{17} G or even more (as inside cores of magnetars, i.e., strongly magnetized NSs [9, 10]).

General consensus is that relativistic effects are small up to densities $\sim 3\cdot n_0$ and Skyrme interaction is well justified for the description of nuclear matter consisting of nucleons (no strange baryons or mesons) (see, e.g., [11, 12] and references therein). That is why we shall use the generalized non-relativistic Fermi-liquid approach [13] which is the extension of the Landau's theory of normal Fermi-liquid to superfluid Fermi-liquids. The so-called generalized BSk20 and BSk21 parametrizations of Skyrme forces with additional unconventional terms depending on density (details in [15]) are used here as interactions in SPNM. Obtained previously [16–18] general formulas (valid for arbitrary parametrization of the effective Skyrme interaction in neutron matter (NM)) for phase transition (PT) temperatures (which are splitted in strong magnetic fields) are specified here for BSk20 and BSk21 parametrizations of the Skyrme forces (see also our recent work [19] with BSk18 Skyrme [14]).

e-mail: [a]antarasov@kipt.kharkov.ua

Furthermore, for comparison we represent our figures for PT temperatures dependent on density for NM with generalized parameterizations BSk18, BSk19, BSk20 and BSk21 of the Skyrme forces (for PT from normal to superfluid states with anisotropic triplet p-wave pairing) in zero magnetic field, $H = 0$.

Next we also study the equilibrium magnetic properties of the SPNM (with the same type of anisotropic spin-triplet p-wave pairing) with generalized Skyrme effective forces BSk18 [14] and BSk20, BSk21 [15] and we have come to the conclusion [20] about absence of ferromagnetic instability in SPNM with generalized forces. It is in contrast to the results about ferromagnetic instabilities in dense superfluid [21] and in normal NM (see, e.g., [22,23]) with conventional Skyrme forces [24]. In Conclusion the obtained results for the SPNM with triplet pairing in high magnetic field are briefly discussed and compared with some other works.

2 General equations for the EMF and OP for SPNM with conventional and generalized Skyrme forces between neutrons and anisotropic spin-triplet pairing

For theoretical description of dense SPNM with generalized effective Skyrme forces [14,15] and with anisotropic spin-triplet p-wave pairing of neutrons (spin and orbital momentum of the Cooper pair are equal to 1) in the presence of strong spatially homogeneous magnetic field $\mathbf{H}$ we have to write down here the order parameter (OP) for SPNM which is similar to the OP for superfluid $^3\mathrm{He}-\mathrm{A}_{1,2}$ (see [5] and [18,20]):

$$\Delta_\alpha{}^A(\mathbf{p}) \equiv (\mathbf{\Delta}_+\hat{\mathbf{d}}_\alpha + \imath\mathbf{\Delta}_-\hat{\mathbf{e}}_\alpha)\psi(\hat{\mathbf{p}}), \quad \psi(\hat{\mathbf{p}}) \equiv (\hat{\mathbf{m}}_\mathbf{j} + \imath\hat{\mathbf{n}}_\mathbf{j})\hat{\mathbf{p}}_\mathbf{j}, \quad \hat{\mathbf{p}} \equiv \frac{\mathbf{p}}{\mathbf{p}}. \tag{1}$$

Here $\Delta_\pm(T) \equiv (\Delta_\uparrow(T) \pm \Delta_\downarrow(T))/2$; $\hat{\mathbf{d}}$ and $\hat{\mathbf{e}}$ are mutually orthogonal real unit vectors in spin space, $\hat{\mathbf{d}}\cdot\hat{\mathbf{e}} = 0$, $\hat{\mathbf{d}}^2 = \hat{\mathbf{e}}^2 = 1$; $\hat{\mathbf{m}}$ and $\hat{\mathbf{n}}$ are mutually orthogonal real unit vectors in orbital space, $\hat{\mathbf{m}}\cdot\hat{\mathbf{n}} = 0$, $\hat{\mathbf{m}}^2 = \hat{\mathbf{n}}^2 = 1$. Note also that the superfluid phase of $^3\mathrm{He}-\mathrm{A}_1$ type may be realized at the condition, when $\Delta_\downarrow = 0$, $\Delta_\uparrow \neq 0$.

As a result, using general formulas (obtained by us previously [25,26]) for anomalous and normal distribution functions of quasiparticles (neutrons) for SPNM in magnetic field we have derived (see in [18,21] more details) in the framework of generalized Fermi-liquid approach [13] a set of integral equations for $\xi(p)$ and $\Delta_\uparrow^A$, $\Delta_\downarrow^A$. In this case for SPNM $\vec{\xi}(\mathbf{p}) = \xi(p)\mathbf{H}/H \equiv -\mu_n\mathbf{H}_{eff}(p)$ ($\mu_n \approx -0.60308\cdot10^{-17}$ (MeV/G) is the magnetic dipole moment of a neutron [27] and $\mathbf{H}_{eff}(p)$ is the effective magnetic field (EMF) renormalized inside SPNM) and for $\xi(p)$ we have the equation:

$$\xi(p) = -\mu_n H + (r + sp^2)K_2(\xi) + sK_4(\xi). \tag{2}$$

Here $r = t_0' + (t_3'/6)n^\alpha$ and $s = (t_1' - t_2')/(4\hbar^2)$, $n \equiv yn_0$ is density of neutron matter;

$$t_0' = t_0\cdot(1 - x_0), \quad t_3' = t_3\cdot(1 - x_3) \tag{3}$$

$$t_1'(n) = t_1\cdot(1 - x_1) + t_4\cdot(1 - x_4)\cdot n^\beta, \tag{4}$$

$$t_2'(n) = t_2\cdot(1 + x_2) + t_5\cdot(1 + x_5)\cdot n^\gamma, \tag{5}$$

and $1/12 \leq \alpha \leq 1/3$ are parameters of the generalized (improved) Skyrme interaction. It is important to note here that for the generalized Skyrme forces [14,15] new additional parameters t_4, t_5, x_4, x_5 and also additional power exponents of density dependence β and γ have originated in comparison with conventional Skyrme forces.

The functionals $K_\sigma(\xi)$ $(\sigma = 2, 4)$ in equation (2) have the same form as in [18,21]:

$$K_\sigma(\xi) = \frac{1}{8\pi^2\hbar^3}\int_{p_{min}}^{p_{max}} dqq^\sigma \int_0^1 dx\kappa(q,x), \tag{6}$$

where

$$\kappa(q,x) = \frac{z(q)+\xi(q)}{E_+(q,x^2)}\tanh\left(\frac{E_+(q,x^2)}{2T}\right) - \frac{z(q)-\xi(q)}{E_-(q,x^2)}\tanh\left(\frac{E_-(q,x^2)}{2T}\right), \tag{7}$$

$$E_\pm^2 = q^2\Delta_{\uparrow(\downarrow)}^2\cdot(1-x^2) + (z(q)\pm\xi(q))^2, \tag{8}$$

$z(q) = q^2/2m_n^* - \mu$ (m_n^* is the effective mass of neutron, μ is the chemical potential). We have taken into account that for SPNM with pairing of the $^3\mathrm{He}-\mathrm{A}_{1,2}$ type the OP can be written as $\Delta_{\uparrow(\downarrow)}^A(T,\xi,q) = q\Delta_{\uparrow(\downarrow)}(T,\xi)$, where functions $\Delta_{\uparrow(\downarrow)}(T,\xi)$ obey the following equations (which structure are similar to those from [18,21]):

$$\Delta_{\uparrow(\downarrow)}(T,\xi) = -\Delta_{\uparrow(\downarrow)}(T,\xi)\frac{c_3}{8\pi^2\hbar^3}\int_{p_{min}}^{p_{max}} dqq^4\int_0^1 dx(1-x^2)\frac{\tanh(E_\pm(q,x^2)/2T)}{E_\pm(q,x^2)}, \tag{9}$$

($p_{max} \gtrsim p_F$ and $(p_{max} - p_{min})/p_F < 1$, where p_F is the Fermi momentum). It is significant that here $c_3 \equiv t_2'(n)/\hbar^2 < 0$ is coupling constant leading to spin-triplet p-wave pairing of neutrons, which is expressed

through the generalized parameters $t'_2(n)$ (see (5)) of the Skyrme interaction. Note that in contrast with (9) for conventional Skyrme forces $c_3 \equiv t_2 \cdot (1 + x_2)/\hbar^2 < 0$ (see [18, 21]) does not depend on density n of SPNM. We consider here a model of neutron Cooper pairing in a shell symmetric with respect to the Fermi sphere, i.e. $p_{max} - p_F = p_F - p_{min}$.

This set of nonlinear integral equations (2) and (9) for the EMF and OP give us the possibility to describe thermodynamics of superfluid non-unitary phases of $^3\mathrm{He} - \mathrm{A}_{1,2}$ type in dense SPNM with generalized Skyrme forces [14,15] and with spin-triplet p-wave pairing in static uniform high magnetic field at arbitrary temperatures from the interval $0 \leq T \leq T_c(H)$. In general case these equations can't be solved analytically and it is necessary to use numerical methods for their solving. But we can solve equations (2), (9) using analytical methods in the limiting cases: 1) when the temperature ($T < T_{c0}$) is near the PT temperature T_{c0} of dense NM to superfluid state (and it is the theme of the next section 3), and 2) at zero temperature (see section 4 below).

3 Solutions of equations for the OP and EMF for dense neutron matter with generalized Skyrme forces near T_{c0}

Formulas (7)-(9) contain the effective mass of neutron m_n^*, which depends on the density $n \equiv y \cdot n_0$ of NM according to the general formula [20]:

$$\frac{m}{m_n^*} = 1 + \frac{myn_0}{4\hbar^2}[t'_1(n) + 3t'_2(n)], \tag{10}$$

where $m \approx (m_p + m_n)/2 \approx 938.91897\ (\mathrm{MeV})/c^2$ is mean value of free nucleon mass; density dependent parameters $t'_1(n)$ and $t'_2(n)$ (see (4) and (5)) have specific numerical values for each Skyrme parametrization. For NM with BSk20 and BSk21 parametrizations [15] of the Skyrme forces we have from (10) that

$$m^*_{n,BSk20}(y) = \frac{m}{1 + y \cdot (3.18344y^{1/12} - 0.305158y^{1/6} - 2.90372)}, \tag{11}$$

$$m^*_{n,BSk21}(y) = \frac{m}{1 + y \cdot (3.97930y^{1/12} + 0.0422618\sqrt{y} - 3.89571)}, \tag{12}$$

and the Fermi energies of NM for the BSk20 and BSk21 Skyrme forces have the following form

$$\varepsilon_{F,BSk20}(y) \approx y^{2/3} \cdot [1 + y \cdot (3.18344y^{1/12} - 0.305158y^{1/6} - 2.90372)] \cdot 60.902\ (\mathrm{MeV}), \tag{13}$$

$$\varepsilon_{F,BSk21}(y) \approx y^{2/3} \cdot [1 + y \cdot (3.97930y^{1/12} + 0.0422618\sqrt{y} - 3.89571)] \cdot 60.902\ (\mathrm{MeV}). \tag{14}$$

In zero magnetic field $H = 0$ equations (9) for the OP are reduced to single equation for the energy gap in SPNM from which we have obtained as a result the following expressions for PT temperatures of dense NM (with BSk20 and BSk21 Skyrme forces) to SPNM with anisotropic spin-triplet pairing of $^3\mathrm{He} - \mathrm{A}$ type:

$$\begin{aligned} T_{c0,BSk20}(E_c; y) &\approx 1.14055 \cdot E_c \cdot \exp\left[\frac{3}{16} \cdot \left(\frac{E_c}{\varepsilon_{F,BSk20}(y)}\right)^2 + \frac{3}{512} \cdot \left(\frac{E_c}{\varepsilon_{F,BSk20}(y)}\right)^4\right] \\ &\times \exp\left[\frac{1 + y \cdot (3.18344y^{1/12} - 0.305158y^{1/6} - 2.90372)}{y \cdot (2.12230y^{1/12} - 2.35266)}\right]\ (\mathrm{MeV}), \end{aligned} \tag{15}$$

$$\begin{aligned} T_{c0,BSk21}(E_c; y) &\approx 1.14055 \cdot E_c \cdot \exp\left[\frac{3}{16} \cdot \left(\frac{E_c}{\varepsilon_{F,BSk21}(y)}\right)^2 + \frac{3}{512} \cdot \left(\frac{E_c}{\varepsilon_{F,BSk21}(y)}\right)^4\right] \\ &\times \exp\left[\frac{1 + y \cdot (3.97930y^{1/12} + 0.0422618\sqrt{y} - 3.89571)}{y \cdot (2.65286y^{1/12} - 2.85028)}\right]\ (\mathrm{MeV}) \end{aligned} \tag{16}$$

(here E_c is the cutoff energy which is less than Fermi energies, $E_c < \varepsilon_{F,BSk20}(y)$ and $E_c < \varepsilon_{F,BSk21}(y)$).

Now we write down the final formulae (obtained from the equations (2) and (9)) for the PT temperatures $T_{c1;BSk20}(E_c; H, y)$ and $T_{c2;BSk20}(E_c; H, y)$ of dense NM in strong magnetic field H to superfluid states of $^3\mathrm{He} - \mathrm{A}_1$ and then to $^3\mathrm{He} - \mathrm{A}_2$ type respectively:

$$\begin{aligned} T_{c1,2;BSk20}(E_c; H, y) &\approx T_{c0,BSk20}(E_c; y) \cdot \left\{1 \mp \frac{Z \cdot 0.60308}{\varepsilon_{F,BSk20}(y) \cdot I_{0,BSk20}(E_c; y)}\left[A_{c0,BSk20}(E_c; y) \cdot I_{A,BSk20}(E_c; y)\right.\right. \\ &+ \left.\left. B_{c0,BSk20}(E_c; y) \cdot I_{B,BSk20}(E_c; y)\right]\right\}\ (\mathrm{MeV}), \end{aligned} \tag{17}$$

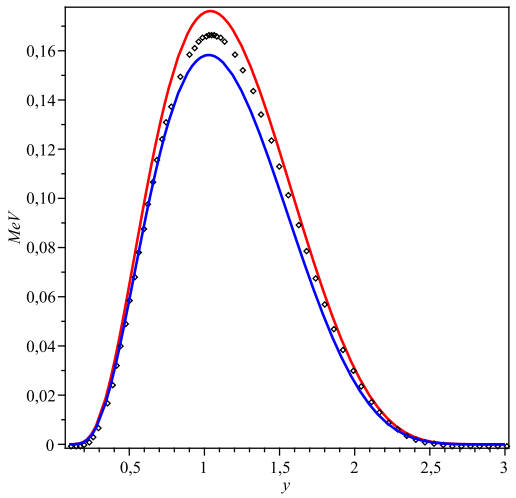

Figure 1. PT temperatures (15) and (17) for BSk20 at $E_c = 10$(MeV) and $H = 2 \cdot 10^{17}$(G) ($Z = 2$): $T_{c1;BSk20}(10; Z = 2, y)$ - upper curve; $T_{c0;BSk20}(10; y)$ - points; $T_{c2;BSk20}(10; Z = 2, y)$ - lower curve.

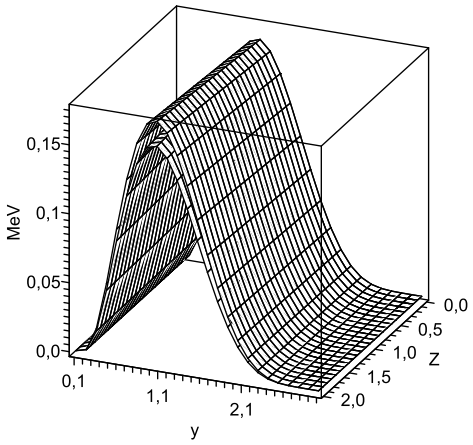

Figure 2. PT temperatures (17) for BSk20 at $E_c = 10$(MeV) and $0 < H < 2 \cdot 10^{17}$(G) : $T_{c1;BSk20}(10; Z, y) > T_{c2;BSk20}(10; Z, y)$.

where upper sign "-" corresponds to $T_{c1;BSk20}(E_c; H, y)$ and lower sign "+" - to $T_{c2;BSk20}(E_c; H, y)$. We have introduced here variable Z defined as $H \equiv Z \cdot 10^{17}$ (G), so that $\mid \mu_n H \mid \approx Z \cdot 0.60308$(MeV) $\ll E_c$. Note also that the functions $A_{c0,BSk20}(E_c; y)$, $B_{c0,BSk20}(E_c; y)$ and integrals $I_{0,BSk20}(E_c; y)$, $I_{A,BSk20}(E_c; y)$, $I_{B,BSk20}(E_c; y)$ in (17) are of the same form as general functions $A(a; y, t_{c0})$, $B(a; y, t_{c0})$ and integrals I_0, I_A, I_B in [18] (see also [17] and Appendix below) (which are valid for all Skyrme parametrizations) but with cutoff parameter $a \equiv E_c/\varepsilon_{F,BSk20}(y) < 1$ and with generalized BSk20 Skyrme parameters from [15].

It is obvious that the final formulae for the PT temperatures $T_{c1,2;BSk21}(E_c; H, y)$ for dense NM with BSk21 (or with any other properly selected parametrization of the Skyrme forces) in strong magnetic field H to superfluid states of $^3\mathrm{He} - \mathrm{A}_{1,2}$ type can be obtained analogously to (17) from the equations (2) and (9) and have the same general structure as (17) but with BSk21 (or with any other proper designations of Skyrme parametrizations) subscripts.

Now, for the definiteness, we select cutoff energy $E_c = 10$(MeV) so that $E_c < \varepsilon_{F,BSk20}(y)$ (and also $E_c < \varepsilon_{F,BSk21}(y)$) and plot figures for the PT temperatures (15) and (17) (at $H = 2 \cdot 10^{17}$(G), i.e. at $Z = 2$,- see Fig.1; and on the interval $0 < H < 2 \cdot 10^{17}$(G) - see Fig.2) of NM at sub- and supra-saturation densities on the interval $0.1 \cdot n_0 < n < 3.0 \cdot n_0 < n_C(BSk20) \approx 3.444 \cdot n_0$ (at critical density $n_C(BSk20)$ triplet superfluidity disappears, $T_{c0,BSk20}(E_c; y_C) = 0$). Figures for BSk21 are qualitatively similar to Fig.1 and Fig.2 for BSk20 but differ quantitatively (see also Fig.3 for comparison between $T_{c0,BSk}(E_c; y)$ for different BSk18-21 parametrizations of the generalized Skyrme forces).

Note also that similarly to our previous paper [18] we can use other cutoff procedure. Namely, we can select cutoff parameter $a \equiv \varepsilon_{max}/\varepsilon_F - 1 = const < 1$ which doesn't depend on density in contrast with our previous definition for $a(y) \equiv E_c/\varepsilon_F(y) < 1$. There is one to one correspondence between these cutoff parameters E_c and $a = const < 1$ if we demand that condition $max(T_{c0,Skyrme}(E_c; y)) = max(T_{c0,Skyrme}(a; y))$ should be fulfilled. Then we get similar results for the PT temperatures for NM but with maxima shifted on density (e.g., for BSk21 parametrization of the Skyrme forces in dense NM see Figs.4-5 with comparison between PT temperatures at $H = 0$ for two different selected cutoffs).

4 Solutions of equations for the OP and EMF in dense SPNM with conventional and generalized Skyrme forces at $T = 0$

Let us consider the SPNM at $T = 0$. In this case we have obtained from the integral equation (2) for the EMF on the Fermi surface the following solution to the first order in the small parameter $h_{ext} \equiv |\mu_n| \cdot H/\varepsilon_F \ll a < 1$:

$$\frac{|\mu_n| H_{eff}(p_F, H)}{\varepsilon_F(y)} = \frac{h_{ext}(H, y)}{1 - (r + 2sp_F{}^2)\nu_F/2}. \tag{18}$$

Here r and s (see after (2)) are density dependent combinations of the Skyrme parameters (3)-(5) and the density of states $\nu_F = (m_n^* p_F)/(\pi^2\hbar^3)$ at the Fermi surface is

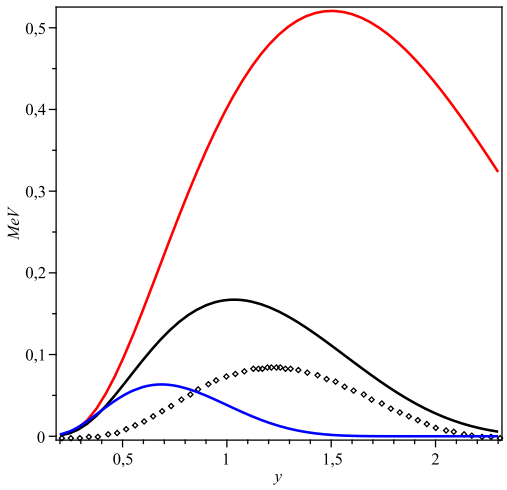

Figure 3. Comparison of PT temperatures of dense NM (with generalized parametrizations BSk18, BSk19, BSk20 and BSk21 of the Skyrme forces) from normal to superfluid states with anisotropic triplet p-wave pairing (in zero magnetic field $H = 0$): $T_{c0,BSk18}(10; y)$ - points, $T_{c0,BSk19}(10; y)$ - upper line, $T_{c0,BSk20}(10; y)$ - middle line (see (15)) and $T_{c0,BSk21}(10; y)$ - bottom line (see (16)) (here all PT temperatures were calculated with cutoff energy $E_c = 10$(MeV).

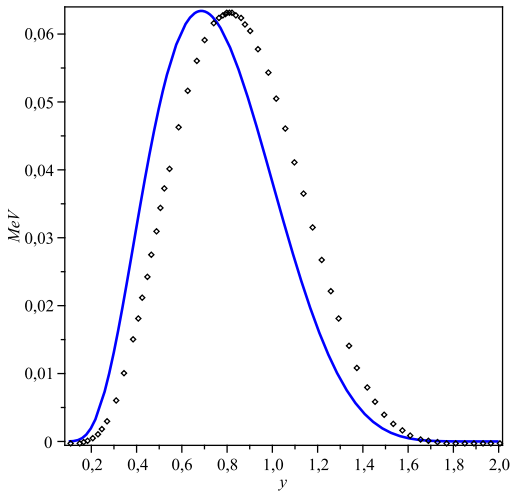

Figure 4. PT temperature for BSk21 at $E_c = 10$(MeV) and $H = 0$ (see (16)): $T_{c0,BSk21}(10; y)$ - left curve; and $T_{c0,BSk21}(0.197; y)$ - points (for other cutoff parameter $a = \varepsilon_{max}/\varepsilon_{F,BSk21} - 1 \approx 0.197$).

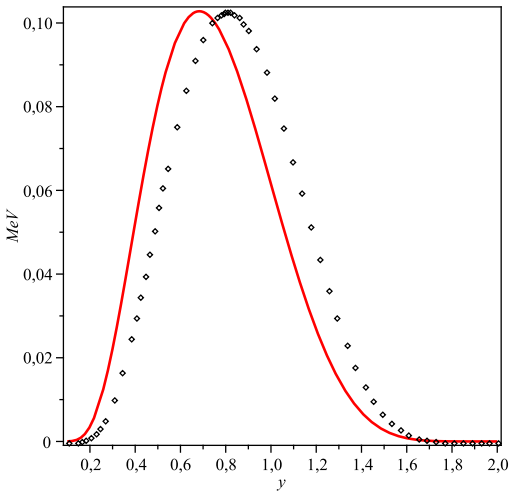

Figure 5. PT temperature for BSk21 at $E_c = 16$(MeV) and $H = 0$ (see (16)): $T_{c0,BSk21}(16; y)$ - left curve; and $T_{c0,BSk21}(0.316; y)$ - points (for other cutoff parameter $a = \varepsilon_{max}/\varepsilon_{F,BSk21} - 1 \approx 0.316$).

$$\nu_F(y) \approx 0.00419 \frac{m_n^*(y)}{m_n} y^{1/3} \ (\mathrm{MeV}^{-1}\mathrm{fm}^{-3}). \tag{19}$$

It should be emphasized that the general approximate formula (18) for $H_{eff}(p_F, H)$ is valid for all parametrizations (conventional and generalized) of the Skyrme forces admissible for NM [12, 24], and H_{eff} is independent of the cutoff parameter $a < 1$ ($a \equiv \varepsilon_{max}/\varepsilon_F - 1$) and of the energy gap in the energy spectrum of neutrons in the SPNM (to the first order).

Now let us consider generalized BSk18 [14], BSk20 and BSk21 [15] parametrizations of the Skyrme forces. This concretization give us the possibility to plot the figures for the ratio of paramagnetic susceptibility of SPNM with Skyrme interaction and susceptibility Pauli of free neutron gas (see (18))

$$\frac{\chi_{Skyrme}(y)}{\chi_{free}} = \frac{1}{1 - (r + 2sp_F^2)\nu_F/2}, \tag{20}$$

which describes a renormalization of magnetic field inside SPNM with triplet p-wave pairing of the $^3\mathrm{He} - \mathrm{A}_{1,2}$ type.

For SPNM with the generalized Skyrme forces BSk18, BSk20 and BSk21 the phase transition to ferromagnetic state is removed (in contrast to SPNM with the conventional Skyrme forces; more details see in [18, 20, 21]). Really, for the generalized BSk18 parametrization [14] of the Skyrme forces (with additional dependences on the density, see (3)-(5)) we have obtained from (20) the expression:

$$\frac{\chi_{BSk18}(y)}{\chi_{free}(y)} \approx \Big[1 - \frac{2y^{1/3} \cdot (0.373605 \cdot y^{3/10} - 1.11339)}{1 + 0.253920 \cdot y} - \frac{4 \cdot y \cdot (0.774775 - 0.209061 \cdot y)}{1 + 0.253920 \cdot y}\Big]^{-1}. \tag{21}$$

In a similar manner for the generalized BSk20 and BSk21 parametrizations [15] of the Skyrme forces relation (20) yields:

$$\frac{\chi_{BSk20}(y)}{\chi_{free}(y)} \approx \Big[1 - \frac{2y^{1/3} \cdot (1.35019 \cdot y^{1/12} - 1.82731)}{1 + y \cdot (3.18344 \cdot y^{1/12} - 0.305158 \cdot y^{1/6} - 2.90372)} - \\ - \frac{4 \cdot y \cdot (1.35095 - 0.228827 \cdot y^{1/6} - 0.795714 \cdot y^{1/12})}{1 + y \cdot (3.18344 \cdot y^{1/12} - 0.305158 \cdot y^{1/6} - 2.90372)}\Big]^{-1} \tag{22}$$

and

$$\frac{\chi_{BSk21}(y)}{\chi_{free}(y)} \approx \Big[1 - \frac{2y^{1/3} \cdot (-0.133544 \cdot y^{1/12} - 0.475909)}{1 + y \cdot (3.97930 \cdot y^{1/12} + 0.0422618 \cdot \sqrt{y} - 3.89571)} - \\ - \frac{4 \cdot y \cdot (1.35338 + 0.0316905 \cdot \sqrt{y} - 0.994643 \cdot y^{1/12})}{1 + y \cdot (3.97930 \cdot y^{1/12} + 0.0422618 \cdot \sqrt{y} - 3.89571)}\Big]^{-1}. \tag{23}$$

For comparison between the ratios of paramagnetic susceptibilities of SPNM with these generalized Skyrme interactions and susceptibility Pauli of free neutron gas we have plotted Fig.6 for the functions (21)-(23).

5 Conclusion

We have obtained that PT temperatures $T_{c0,BSk20}(10; y)$ and $T_{c0,BSk21}(10; y)$ (see (15) and (16)) of dense NM (in zero magnetic field) to superfluid state with anisotropic p-wave pairing of $^3He - A$ type and with generalized BSk20 and BSk21 Skyrme interactions [15] depend on density in non-monotone way (exhibit a bell-shaped density profile, see Fig.3). Such behavior of these PT temperatures are in qualitative agreement with results of recent articles [3, 4, 28] and is of the same order in magnitude at $E_c = 10$MeV (namely, $T_{c0,BSk20}(10; y) < 0.17$(MeV) for BSk20 - see Fig.1 and Fig.3 and $T_{c0,BSk21}(10; y) < 0.064$(MeV) for BSk21 - see Fig.4). It follows from (15) and (16) that $^3He - A$ type of triplet superfluidity disappears in NM when supra-saturation density $n > n_0$ tends to critical magnitude: $n_C(BSk20) \approx 3.444 \cdot n_0$ and $n_C(BSk21) \approx 2.38 \cdot n_0$. And our main results are expressions (17) (and Figs.1-2) for PT temperatures $T_{c1,2;BSk20}(E_c; H, y)$ (and similarly for BSk21) linear in strong magnetic fields (which may approach to 10^{17}(G) or even more as in liquid outer cores of magnetars [9, 10]) which have also a bell-shaped density profile (contrary to their monotone increase with density [18] for all previous conventional Skyrme parametrizations).

Here we have applied new generalized BSk20 and BSk21 Skyrme forces [15] which lead to equations of state (EOSs) of dense pure neutron matter (NM) which are consistent (see [29] for details) with the recently measured value of for the mass of pulsar PSR J1614-2230 ([30]). Note that EOS in NM with generalized Skyrme force BSk19 [15] is too soft at high (supra-saturation) densities and therefore detailed study of SPNM with BSk19

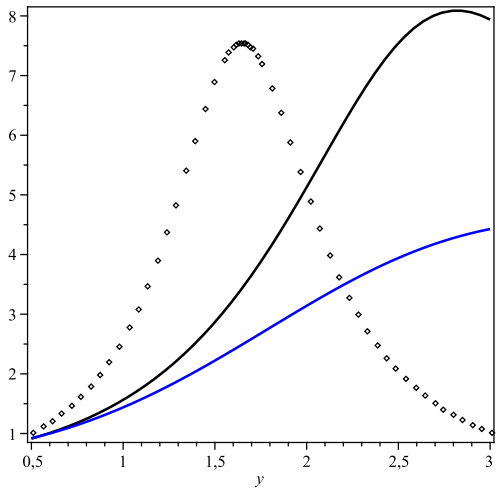

Figure 6. Ratio $\chi_{Skyrme}(y)/\chi_{free}$ (see (21), (22) and (23)) for SPNM with generalized parametrizations (BSk18 - points, BSk20 - upper line and BSk21 - lower line) of the Skyrme forces [14,15] and spin-triplet p-wave pairing of the ^{3}He − A type at $T = 0$ as a function of reduced density $y = n/n_0$.

parametrization (see upper curve in Fig.3) is eliminated here from our consideration (see [29] and also review [12] with analysis of different numerous parametrizations of the Skyrme forces).

Another our main result here is that for generalized Skyrme forces BSk18-BSk21 [14,15] introduction of new additional Skyrme parameters dependent on density (see (4), (5)) lead to removal of ferromagnetic instability not only in normal NM but also in SPNM with BSk18-BSk21 forces and anisotropic spin-triplet pairing of $^3He - A$ type in strong magnetic field. The density dependent ratio of magnetic susceptibilities $\frac{\chi_{BSk18-21}(y)}{\chi_{free}}$ have regular (nonsingular) behavior on the interval $0.5 < n/n_0 < 3.0$ (see Fig.6 and also (21)-(23)). Note, that superfluid corrections to $\frac{\chi_{BSk18-21}(y)}{\chi_{free}}$ have negligibly small values (which are of the order $(\Delta/\varepsilon_F)^2 \approx 10^{-6}$, where Δ is maximal magnitude of anisotropic energy gap in the spectrum (8) of quasiparticles (neutrons) in the SPNM considered here).

Note finally that the phenomenon of superfluidity in NM at very high densities $n/n_0 > 3.0$ (which may be realized inside the inner fluid cores of a sufficiently massive neutron stars and magnetars) should be investigated in the framework of a relativistic approach and with different interpretation of the hadron matter structure (including π mesons, K mesons, hyperons, quarks, and other possible constituents, see e.g., [31–34]).

Acknowledgements. I am grateful to Organizers of the International School-Seminar NPQCD-2013 and particularly to Professors V.V. Skalozub and A.I. Sokolovsky for invitation and warm hospitality in Dnipropetrovsk.

6 Appendix

The functions $A_{c0,Skyrme}(a;y) \equiv A_{Skyrme}(a;y,t_{c0}(a;y))$ and $B_{c0,Skyrme}(a;y) \equiv B_{Skyrme}(a;y,t_{c0}(a;y))$ with $t_{c0}(a;y) \equiv T_{c0}(a;y)/\varepsilon_{F,Skyrme}(y) \ll 1$ (see (17) with cutoff parameter $a = E_c/\varepsilon_{F,BSk20}(y) < 1$, where $y \equiv n/n_0$) have the following general form [18] for arbitrary Skyrme parametrization:

$$A(a;y,t_{c0}(a;y)) \equiv \frac{1}{D(a;y,t_{c0})}\left[1 + d_{12}y \cdot \frac{m_n^*(y)}{m_n} \cdot (i_1(a;t_{c0}) - i_3(a;t_{c0}))\right], \tag{24}$$

$$B(a;y,t_{c0}(a;y)) \equiv \frac{i_1(a;t_{c0})}{D(a;y,t_{c0})} d_{12}y \cdot \frac{m_n^*(y)}{m_n}, \tag{25}$$

$$D(a;y,t_{c0}(a;y)) \approx 1 - y^{1/3}(d_3 y^{\alpha} + d_0) \cdot \frac{m_n^*(y)}{m_n} i_1(a;t_{c0}) - 2d_{12}y \cdot \frac{m_n^*(y)}{m_n} i_3(a;t_{c0}) -$$

$$-d_{12}^2 y^2 \cdot \left(\frac{m_n^*(y)}{m_n}\right)^2 \left(i_1(a;t_{c0}) i_5(a;t_{c0}) - i_3^2(a;t_{c0})\right). \tag{26}$$

The dimensionless coefficients d_{12}, d_3, d_0 take the following general form for all Skyrme parameterizations:

$$d_{12} \equiv \frac{m_n c^2}{(\hbar c)^2}\frac{3n_0}{16} \cdot (t_1' - t_2') \approx (t_1' - t_2') \cdot 0.00076913765 \left(\text{MeV fm}^5\right)^{-1}, \tag{27}$$

$$d_3 \equiv \frac{m_n c^2}{2(\hbar c)^2}\left(\frac{3n_0}{8\pi^4}\right)^{1/3} n_0^{\alpha}\cdot\frac{t'_3}{6} \approx t'_3\cdot 0.0010474922\cdot(0.17^{\alpha}/6)\,\left(\text{MeV fm}^{3+3\alpha}\right)^{-1}, \tag{28}$$

$$d_0 \equiv \frac{m_n c^2}{2(\hbar c)^2}\left(\frac{3n_0}{8\pi^4}\right)^{1/3}\cdot t'_0 \approx t'_0\cdot 0.0010474922\,\left(\text{MeV fm}^{3}\right)^{-1}, \tag{29}$$

where Skyrme power index is $1/12 \le \alpha \le 1/3$, and dimensional Skyrme parameters t'_0, t'_3 and $t'_1(y)$, $t'_2(y)$ of the generalized Skyrme interaction are defined by formulas (3) and (4), (5) respectively (see also note after (5)).

Integrals $i_j(a;t)$ (j=1, 3, 5) in (24)-(26) are defined as follows ($0 < a < 1$):

$$i_j(a;t) \equiv \int_{-a}^{a} \mathrm{d}x\sqrt{(1+x)^j}\,\frac{\mathrm{d}}{\mathrm{d}x}\tanh\left(\frac{x}{2t}\right). \tag{30}$$

Integrals I_0, I_A and I_B, which appear in (17) for the PT temperatures $T_{c1,2;BSk20}(E_c;H,y)$ (and similarly for $T_{c1,2;BSk21}(E_c;H,y)$), are defined in the following way (with cutoff parameters $a = E_c/\varepsilon_{F,BSk20}(y) < 1$ and $a = E_c/\varepsilon_{F,BSk21}(y) < 1$, respectively):

$$I_0(a;y) \equiv \int_{-a}^{a} dx\frac{\sqrt{(1+x)^3}}{x}\tanh\left(\frac{x}{2t_{c0}}\right), \tag{31}$$

$$I_A(a;t_{c0}) \equiv \int_{-a}^{a} \mathrm{d}x\sqrt{(1+x)^3}\,\frac{\mathrm{d}}{\mathrm{d}x}\frac{\tanh(x/2t_{c0})}{x}, \tag{32}$$

$$I_B(a;t_{c0}) \equiv \int_{-a}^{a} \mathrm{d}x\sqrt{(1+x)^3}x\,\frac{\mathrm{d}}{\mathrm{d}x}\frac{\tanh(x/2t_{c0})}{x}. \tag{33}$$

References

[1] W.C.G. Ho and C.O. Heinke, Nature **462**, 71 (2009).
[2] C.O. Heinke and W.C.G. Ho, Astrophys. J. **719**, L167 (2010).
[3] D. Page, M. Prakash, J.M. Lattimer, and A.W. Steiner, Phys. Rev. Lett. **106**, 081101 (2011).
[4] P.S. Shternin, D.G. Yakovlev, C.O. Heinke *et al.*, MNRAS **412**, L108 (2011).
[5] D. Vollhardt and P. Wölfle, *The Superfluid Phases of Helium 3* (London, Taylor and Francis, 1990).
[6] T. Takatsuka and R. Tamagaki, Prog. Theor. Phys. Suppl. **112**, 27 (1993).
[7] M. Baldo, Ø. Elgaroy, L. Engvik *et al.*, Phys. Rev. C **58**, 1921 (1998).
[8] D.J. Dean and M. Hjorth-Jensen, Rev. Mod. Phys. **75**, 607 (2003).
[9] R.C. Duncan and C. Thompson, Astrophys. J. **392**, L9 (1992).
[10] S. Mereghetti, AIP Conf. Proc. **924**, 151 (2007).
[11] J.R. Stone and P.-G. Reinhard, Prog. Part. Nucl. Phys. **58**, 587 (2007).
[12] M. Dutra, O. Lourenco, J.S. Sa Martins, *et al.*, Phys. Rev. C **85**, 035201 (2012).
[13] A.I. Akhiezer, V.V. Krasil'nikov, S.V. Peletminskii, A.A. Yatsenko, Phys. Rep. **245**, 1 (1994).
[14] N. Chamel, S. Goriely, and J.M. Pearson, Phys. Rev. C **80**, 065804 (2009).
[15] S. Goriely, N. Chamel, and J.M. Pearson, Phys. Rev. C **82**, 035804 (2010).
[16] A.N. Tarasov, Physica B **329-333**, Part 1, 100 (2003).
[17] A.N. Tarasov, AIP Conf. Proc. **850**, 109 (2006).
[18] A.N. Tarasov, Cent. Eur. J. Phys. **9**, 1057 (2011).
[19] A.N. Tarasov, J. Phys.: Conf. Series **400**, 032101 (2012) [nucl-th/1301.5528].
[20] A.N. Tarasov, Ukr. J. Phys. **58**, 611 (2013).
[21] A.N. Tarasov, Ukr. J. Phys. **55**, 644 (2010).
[22] A. Vidaurre, J. Navarro, and J. Bernabeu, Astron. Astrophys. **135**, 361 (1984).
[23] A. Rios, A. Polls, and I. Vidana, Phys. Rev. C **71**, 055802 (2005).
[24] J.R. Stone, J.C. Miller, R. Koncewicz, P.D. Stevenson, and M.R. Strayer, Phys. Rev. C **68**, 034324 (2003).
[25] A.N. Tarasov, Low Temp. Phys. **26**, 785 (2000).
[26] A.N. Tarasov, Probl. At. Sci. Tech. **6**, 356 (2001).
[27] K. Nakamura *et al.* (Particle Data Group), J. Phys. G **37**, 075021 (2010).
[28] W. Zuo and U. Lombardo, Phys. Atom. Nucl. **72**, 1359 (2009).
[29] N. Chamel, A.F. Fantina, J.M. Pearson, and S. Goriely, Phys. Rev. C **84**, 062802(R) (2011).
[30] P.B. Demorest *et al.*, Nature **467**, 1081 (2010).
[31] T. Tatsumi and K. Sato, Phys. Lett. B **663**, 322 (2008).
[32] G.E. Brown, C.-H. Lee, and M. Rho, Phys. Rep. **462**, 1 (2008).
[33] M.G. Alford, A. Schmitt, K. Rajagopal, and T. Schafer, Rev. Mod. Phys. **80**, 1455 (2008).
[34] K. Sato and T. Tatsumi, Nucl. Phys. A **826**, 74 (2009).

Proceedings of the International School-seminar
"New Physics and Quantum Chromodynamics at External Conditions", pp. 33 – 40,
May 22-24, 2013, Dnipropetrovsk, Ukraine

QUANTUM THERMALIZATION IN RELATIVISTIC NUCLEAR COLLISIONS

S. V. Akkelin[a], Yu. M. Sinyukov[b]

Bogolyubov Institute for Theoretical Physics, Kiev, Ukraine

Based on common consideration of hydrodynamics as effective theory in domain of slow and long-length modes, we discuss the physical mechanisms responsible for the decoherence and emergence of the hydrodynamic behavior in relativistic heavy ion collisions, and demonstrate how such physical mechanisms work in the case of the scalar field model. We obtain the evolution equation for the Wigner function of long wavelength subsystem that describes its decoherence, isotropization and approach to thermal equilibrium induced by interaction with short wavelength modes. Our analysis supports an idea that decoherence, quantum-to-classical transition and thermalization in isolated quantum system are related to a particular procedure of decomposition of the whole quantum system into "relevant" and "unrelevant" from an observational viewpoint subsystems.

1 Introduction

One of the most important discoveries made at Relativistic Heavy Ion Collider (RHIC) and Large Hadron Collider (LHC) is applicability of nearly perfect fluid hydrodynamic models for description of hadron momentum spectra in central and non-central collisions. It is noteworthy that the agreement with data is achieved only if very early thermalization times (≤ 1 fm) of the produced quark-gluon matter are assumed [1]. In spite of intense efforts, an understanding of thermalization in relativistic nuclear collisions is still lacking. It seems that, at least partially, it is so because system created in a relativistic nucleus-nucleus collision can be considered as an isolated quantum system that does not interact with external environment, and unitary quantum evolution of an isolated system cannot increase its total entropy, no matter what happens during this evolution (e.g., deconfinement, etc.). Then such an isolated system can not be thermalized as whole, no matter how large and complex the system is. It distinguishes quantum system from a classical system where chaotic behavior can appear due to extreme sensitivity of a complex system on its initial conditions in the sense that the distance between the trajectories arising from different initial conditions increases exponentially in time. Unlike of it, in a quantum system the unitarity of the Schrödinger evolution preserves all scalar products and, so, all "distances" between quantum state vectors during the time, and no chaotic behavior is possible.

To avoid the problems with thermalization of an isolated quantum system, some approaches (see, e.g., [2–4]) utilize classical approximation for early time dynamics in heavy ion collisions. Whether or not such approaches can result in proper early thermalization in $A + A$ collisions is still unclear. Moreover, even if based on classical picture approach results in the early time estimate of the thermalization, it does not help to understand mechanism of thermalization in $A + A$ collisions. It is so because for any fixed $\hbar$ there is no violation of unitary evolution in closed system, and, so, there is no quantum-to-classical transition (see, e.g., [5]) in a completely quantum system, even for high population modes [6]. Any derivation of quantum-to-classical transition that is based on mathematical limit $\hbar \to 0$ (see, e.g., [7]) requires, in fact, that uncertainty in both position and momentum vanishes as $\hbar$ tends to zero, that is obviously impossible for any fixed $\hbar$ because of uncertainty relation.

Perhaps, a hope that the anti-de-Sitter/conformal-field-theory (AdS/CFT) correspondence [8] (for reviews see [9, 10]) can help to understand quantum-to-classical transition in a closed quantum system is one of the reasons why this approach, that pretends to explain the origin of decoherence and thermalization in $A + A$ collisions, has recently attracted much attention in heavy ion community. While AdS/CFT correspondence does not hold for QCD, it is generally believed that it provides correct qualitative picture of QCD dynamics in strongly coupled regime. The AdS/CFT correspondence is based on the holographic gauge/string duality between a 4-dimensional quantum field gauge theory such as $N = 4$ Super Yang-Mills gauge theory (which is a conformal field theory), and a 5-dimensional quantum string theory. The duality means an exact equivalence between two theories, i.e., it means that any calculated quantity can be expressed in terms of a dual partner theory. In practice, however, calculations in dual 5D quantum string theory are possible only under some limitations, that from the QCD viewpoint means that $N_c \to \infty$ and $\lambda \to \infty$, where N_c is number of colors and λ is QCD coupling constant. In dual 5D string theory these limits switch off interactions between strings and reduce (open and closed) strings to point particles. As a result of it, the 5D classical gravity theory in

e-mail: [a]akkelin@bitp.kiev.ua, [b]sinyukov@bitp.kiev.ua

Anti-de-Sitter space (with negative Λ term) substitutes for 5D quantum theory of closed strings. Under such conditions gauge/string duality is reduced to gauge/gravity duality between 4D quantum gauge theory and 5D classical gravity theory (so called AdS/CFT correspondence). In this correspondence, the radial coordinate r of additional spatial direction can be associated with the renormalization group energy scale (energy cutoff scale) in the gauge field theory [11], and asymptotically high values of radius parameter correspond to gauge field theory with asymptotically high energy cutoff. Therefore, the AdS/CFT correspondence can be treated as geometrization of a renormalization group. Phenomenon of thermalization of 4D quantum field theory in this approach is then associated with irreversible process of formation of black holes and corresponding event horizons (with non-zero entropies), see Refs. [12–14] and references therein. Specifically, it was found that the long wavelength (smoothed over short-scales) approximation of metrics induced by a large stationary black hole results in a thermal state of the gauge quantum field theory, and long wavelength approximation of metrics induced by a large nearly stationary black hole results in a nearly perfect hydrodynamical description of expectation value of energy momentum tensor of gauge quantum fields. The latter duality is sometimes named as the fluid/gravity correspondence [15]. Such a fluid/gravity correspondence can be useful tool to calculate viscosity for strongly interacting locally equilibrated systems [10]. Then, an increase of entropy, associated with black hole formations, takes place here only after substitution of *quantum* theory of closed strings by the *classical* general relativity. Such a substitution is justified by means of the limit where 5D "gravity constant" tends to zero and, then, classical configurations give the only contribution in the sense of saddle-point method. However, similar to ordinary quantum mechanics, for any fixed value of 5D "gravity constant" there is no quantum-to-classical transition that preserves unitarity. Indeed, in Ref. [16] it was demonstrated that taking the radial coordinate r of additional spatial direction to be close to the black hole horizon, the hydrodynamical behavior of 4D quantum field theory becomes exact, while for the theory defined at the holographic screen far from the black hole increasing deviations from hydrodynamical behavior are observed, and such a behavior takes place only in long wavelength approximation when short length modes are smeared and traced out. It means, according to the AdS/CFT correspondence and renormalization group ideas [11], that hydrodynamical behavior appears in coarse grained (with some energy cutoff) 4D quantum theory. Then, one can guess that 5D classical gravity is dual to long-wavelength dynamics of 4D gauge quantum field theory, and calculations based on AdS/CFT correspondence indicate that such quasiclassical properties as irreversible evolution, entropy creation and hydrodynamics are attributes of long wavelength modes of 4D quantum field theory.

In what follows, we suggest that decoherence and thermalization in heavy ion collisions happen for long wavelength modes that approach equilibrium due to interaction induced entanglement with short wavelength environment. Such an approach to (large-scale) thermalization in $A + A$ collisions is agreed with common consideration of hydrodynamics as effective theory in domain of slow and long-length modes [17]. We will focus mainly on the general quantitative features of the evolution of coarse graining quantities in a simple scalar field theory model to investigate the physical mechanisms responsible for the decoherence and emergence of the hydrodynamic behavior in $A + A$ collisions, and do not try to give a full treatment of the emergence of hydrodynamic behavior in quantum field theory (for recent developments in this direction see Refs. [18–22]).

2 Approach to equilibrium of the coarse-grained observables in quantum systems

Let us start with pointing out that necessary condition for emergence of hydrodynamic behavior is the decoherence, i.e., suppression of interference of some set of variables (local densities). It is well known that open system can be decohered (i.e., its state can be approximately diagonalized in some basis) and can acquire classical properties due to interactions with its environment containing the many degrees of freedom that is ignored from an observational point of view (for review see [23] and references therein). In contrast with the environment-induced decoherence, in a relativistic nucleus-nucleus collision the system remains isolated after preparation and until an observation at a large time t_{out} is performed. However, while decoherence of isolated system is impossible, the decoherence of its subsystems is still possible: interacting subsystems are not in the pure states (except initially, if it is the case), while the closed compound state keeps evolving unitarily.

To be more specific, let us assume that at $t = t_0$ the isolated composite state of two interacting systems is $|\Psi_{AB}\rangle = |\Psi_A\rangle \otimes |\Psi_B\rangle$. Then, for $t > t_0$ it is not a product state anymore, and can be represented as entangled state $|\Psi_{AB}\rangle = \sum_{m,n} c_{m,n}|\Psi_{A,m}\rangle \otimes |\Psi_{B,n}\rangle$. The pure entangled state of any two quantum systems can always be written as a single sum in the Schmidt diagonal canonical form $|\Psi_{AB}\rangle = \sum_i \sqrt{p_i}|\widetilde{\Psi}_{A,i}\rangle \otimes |\widetilde{\Psi}_{B,i}\rangle$ with some coefficients p_i, where the orthogonal states $|\widetilde{\Psi}_{A,i}\rangle$ and $|\widetilde{\Psi}_{B,i}\rangle$ forming the two bases are determined by the total state $|\Psi_{AB}\rangle$ and, so, are time-dependent and interaction-dependent. This instantaneous Schmidt representation determines the reduced density matrices $\hat{\rho}_A$ and $\hat{\rho}_B$ in their diagonal form, $\hat{\rho}_A = \sum_i |\widetilde{\Psi}_{A,i}\rangle p_i \langle\widetilde{\Psi}_{A,i}|$, $\hat{\rho}_B = \sum_j |\widetilde{\Psi}_{B,j}\rangle p_j \langle\widetilde{\Psi}_{B,j}|$. These density matrices are defined as $\hat{\rho}_A \otimes I_B = Tr^{(B)}|\Psi_{AB}\rangle\langle\Psi_{AB}|$ and $I_A \otimes \hat{\rho}_B = Tr^{(A)}|\Psi_{AB}\rangle\langle\Psi_{AB}|$, where symbols $Tr^{(A)}$, $Tr^{(B)}$ mean the operation of taking the partial trace that is carried over in space of states of A, B, respectively, and I_A, I_B are identity operators in the corresponding space of states.

The state of a subsystem of a composite system can be described as reduced statistical operator represented by the partial trace of composite system pure state statistical operator. The key point here is quantum entanglement: interacting quantum subsystems become entangled in course of unitary evolution of the system as whole and, as a result, the quantum states of subsystems become mixed states. The total entropy, however, remains zero: due to the quantum entanglement, the entropy of a whole quantum system is not equal to the sum of the entropies of its parts that are defined as the von Neumann entropies of the corresponding reduced density matrices. Entropy then is a measure for the entanglement, and the equilibrium state of the relevant subsystem is just state when its entanglement entropy reaches a maximum due to the build-up of entanglement of the considered system with its environment induced by the interaction [24]. Noteworthy, such mixed states generation has nothing to do with formation of statistical ensembles when the weights of the states has no relation to the exact dynamical equations.

Then, to explain success of hydrodynamics in $A+A$ collisions [1], one can utilize idea that unitary quantum evolution of the closed system allows thermalization of a relevant subsystem. Of course, a closed system can be resolved into parts ("subsystems") in various ways. Because of quantum non-separability [25], the evolution of such a decomposition is not equivalent to the evolution of the whole system, and evolutions of different sets of subsystems are not equivalent to each other. An ambiguity of a splitting procedure is removed by requirement that such a splitting must be done in an observer dependent way. In fact, specific way of division of a closed system into subsystems depends on a certain experimental context and is just a way to select the relevant observables and disregard inaccessible for the observer or ignored degrees of freedom of the closed system. The appropriate separation is determined by initial and observational conditions, the latter usually reflect the degree of precision in a measurement of relevant observables, and not complete analysis of all available information such as all n-particle correlations, quantum interference effects, etc. Then, decoherence and thermalization in $A+A$ collisions can be understood via the approximations introduced by the coarse-graining procedure when a system is decomposed into the fast short-length modes that represent irrelevant (i.e., observationally inaccessible or ignored) degrees of freedom, and slow long-length modes that represent relevant (i.e., observationally accessible) degrees of freedom. The former act as environment and ensure decoherence and approach to (local) equilibrium for the latter (see e.g. [19, 26]).

The evolution of the relevant subsystem of closed system can be studied by means of utilizing powerful mathematical methods, e.g., by means of the projection operator technique (for review see, e.g., Ref. [21]) and renormalization group technique (for recent review see, e.g., [27]). Note, however, that application of these methods to non-equilibrium quantum field theory is usually rather complicated and sometimes ambiguous, and physics is often hidden by mathematical formalisms. Therefore, for illustrative purposes, we will utilize here more heuristic coarse graining approach aiming to make clear origin of decoherence of relevant observables in $A+A$ collisions and their subsequent evolution towards to equilibrium. Due to the complexity of the problem, we restrict ourselves to a φ^4 quantum field model, whose dynamics is determined by the Lagrangian density

$$L = \frac{1}{2}\partial_\mu\varphi\partial^\mu\varphi - \frac{\lambda}{4!}\varphi^4, \tag{1}$$

where λ is coupling constant. In the following, we utilize the Heisenberg representation. Expectation values are defined as $\langle O\rangle = Sp(\hat{\rho}O)$, where $\hat{\rho}$ denotes the statistical operator associated with an initial (pure) state of the system.

Expectation value of energy momentum tensor, $\langle T_{\mu\nu}\rangle$, satisfies to energy-momentum conservation equations

$$\partial^\mu\langle T_{\mu\nu}\rangle = 0, \tag{2}$$

that follows from the field evolution equation. Many studies of the $\langle T_{\mu\nu}\rangle$ evolution were based on classical field approximation of the energy momentum tensor,

$$\langle T^{\mu\nu}(x)\rangle \approx T^{\mu\nu}[\langle\varphi\rangle] = \partial^\mu\langle\varphi\rangle\partial^\nu\langle\varphi\rangle - g^{\mu\nu}\left[\frac{1}{2}(\partial_\alpha\langle\varphi\rangle)^2 - \frac{\lambda}{4!}\langle\varphi\rangle^4\right]. \tag{3}$$

It is worth to note here that such an approximation does not mean that the evolution of $\langle T_{\mu\nu}\rangle$ proceeds as in classical field theory. It is so because the expectation value of the field, $\langle\varphi\rangle$, is governed by the equation

$$\partial^\mu\partial_\mu\langle\varphi\rangle = -\frac{\lambda}{3!}\langle\varphi^3\rangle, \tag{4}$$

where $\langle\varphi^3\rangle$ in the right hand side contains correlations of quantum fluctuations. It is known that for initial conditions associated with $A+A$ collisions the classical field evolution does not lead to hydrodynamics in $A+A$ collisions, at least in due times [4]. To get phenomenologically reasonable start of hydrodynamical behavior in $A+A$ collisions, it was proposed [4] to account for quantum fluctuations around classical approximation in evolution equation. However, such an approach does not look fully self-consistent, because classical equations can

approximate the underlying microscopic quantum dynamics only as result of environment-induced decoherence, and without decoherence any classical approximation in a completely quantum system is impossible, even for high population modes. If, instead, we assume that thermalization in $A + A$ collisions does not occur for the whole system but for relevant subsystem only, and associate the latter with long wavelength modes subsystem (i.e., with momentum scales k smaller than the some characteristic scale $k^\star$), then utilization of classical approximation for expectation values of long wavelength observables can be justified, and quantum fluctuations can be accounted for short-length modes only.

Let us split the quantum field φ at $t = t_0$ into long wavelength modes $\varphi_L^{t_0}$, and short wavelength modes $\varphi_S^{t_0}$: $\varphi = \varphi_L^{t_0} + \varphi_S^{t_0}$. We assume that the initial long wavelength field, $\varphi_L^{t_0}$, corresponds to a convolution of field operator φ with a "window" function W_V, $\int W_V = 1$, that makes smoothing/averaging of the field over domain of size $V = 1/k^{*3}$,

$$\varphi_L^{t_0}(x, t_0) = \int d^3x' W_V(x - x')\varphi(x', t_0). \tag{5}$$

Also, we split a state of the system into L and S subsystems: $\hat{\rho}_L \otimes \hat{\rho}_S$, assuming that observables correspond to operators acting on L states only. Such a splitting is conditioned by the experimental context because of limited region and accuracy in particle momentum spectra measurements and, also, because whole correlations between all emitted particles are unobservabled.

The evolution equation for expectation value of long-length modes with initial condition defined according to (5) reads

$$\partial^\mu\partial_\mu\langle\varphi_L^{t_0}\rangle = -\partial^\mu\partial_\mu\langle\varphi_S^{t_0}\rangle - \frac{\lambda}{3!}\langle(\varphi_L^{t_0} + \varphi_S^{t_0})^3\rangle. \tag{6}$$

One can see that in course of evolution initially smeared field becomes dependent on short wavelength modes. Then, to calculate observables associated with long wavelength modes, one needs to supplement this exact motion with an operation that prevents the state to deviate too much from L. It can be done by dividing evolution into time interval, and choosing initial conditions for each time step with $\varphi_L^{t_i}$ being replaced at the time $t_{i+1} = t_i + \delta t$ by the associated $\varphi_L^{t_{i+1}}(x, t_{i+1}) = \int d^3x' W_V(x - x')(\varphi_L^{t_i}(x', t_{i+1}) + \varphi_S^{t_i}(x', t_{i+1}))$. Then for $t_{i+1} < t < t_{i+2} = t_{i+1} + \delta t$,

$$\partial^\mu\partial_\mu\langle\varphi_L^{t_{i+1}}\rangle = -\partial^\mu\partial_\mu\langle\varphi_S^{t_{i+1}}\rangle - \frac{\lambda}{3!}\langle(\varphi_L^{t_{i+1}} + \varphi_S^{t_{i+1}})^3\rangle, \tag{7}$$

and we have piecewise continuous description of L-modes evolution. Now, let us neglect in each δt-interval contribution of long-scale quantum fluctuations and contribution of the short wavelength modes into right hand side of the evolution equations. Then we get chain of equations

$$\partial^\mu\partial_\mu\langle\varphi_L^{t_0}\rangle = -\frac{\lambda}{3!}\langle\varphi_L^{t_0}\rangle^3, t_0 < t < t_1, \tag{8}$$

$$\ldots$$

$$\partial^\mu\partial_\mu\langle\varphi_L^{t_n}\rangle = -\frac{\lambda}{3!}\langle\varphi_L^{t_n}\rangle^3, t_{n-1} < t < t_n, \tag{9}$$

that approximates piecewise continuous description of L-modes till some time t_n. Such a set of piecewise continuous evolutions can be approximated by the continuous one,

$$\partial^\mu\partial_\mu\langle\varphi_L\rangle_\xi = -\frac{\lambda}{3!}(\langle\varphi_L\rangle_\xi^3 + \xi), \tag{10}$$

where ξ accounts for random discontinuity $\langle\varphi_L^{t_i}\rangle(t_{i+1}) \neq \langle\varphi_L^{t_{i+1}}\rangle(t_{i+1})$ and, so, is associated with fluctuations of the expectation value of long wavelength modes. As we discussed above, such a discontinuity is caused by the interaction of long wavelength modes with the short wavelength ones, in particular, by the interaction with the short-scale quantum fluctuations that typically are more enhanced than the long-scale ones. Because the information transferred towards the irrelevant variables is discarded at the beginning of each time interval, ξ becomes a stochastic "noise" variable, and induces a continuous time random walk stochastic dynamics for $\langle\varphi_L\rangle_\xi$. Then, to get true long wavelength observables without "trembles" that are associated with different projection histories, one needs to average such observables over ξ. Such an averaging means, in fact, smearing over time interval δt for set of projection histories, and is not associated with statistical ensemble of initial events. The necessary condition for hydrodynamical approximation to be valid is the allowance to neglect, after such an averaging, non-conservation of energy momentum due to interactions with short wavelength modes, i.e., assumption that such a interaction results in information loss only.

Direct calculation of $T_{\mu\nu}[\langle\varphi_L\rangle_\xi]$ based on evolution equations for $\langle\varphi_L\rangle_\xi$ is rather uneasy task, that can hardly be done analytically. Therefore, here we proceed in more heuristic way and express $T_{\mu\nu}[\langle\varphi_L\rangle_\xi]$ through

expectation value of corresponding Wigner operator (see, e.g., [28]), and obtain for the latter kinetic transport equation.

Let us define (reduced) Wigner function describing the state of the long-wavelength modes, $N_L(x,p)$, as

$$N_L(x,p) = \sum_\xi N_L^\xi(x,p), \tag{11}$$

where

$$N_L^\xi(x,p) = (2\pi)^{-4} \int d^4v e^{-ipv} \langle\varphi_L\rangle_\xi(x+\frac{1}{2}v)\langle\varphi_L\rangle_\xi(x-\frac{1}{2}v), \tag{12}$$

and symbol $\sum_\xi$ means that we perform in (11) the average with respect to random ξ fluctuations, as was discussed above.

Using (10), we obtain the following time evolution of the Wigner function:

$$p_\mu\partial^\mu N_L(x,p) = \\ \frac{i}{2(2\pi)^4}\sum_\xi \int d^4v e^{-ipv}\left(\rho_\xi(x-\frac{v}{2})\langle\varphi_L\rangle_\xi(x+\frac{v}{2}) - \langle\varphi_L\rangle_\xi(x-\frac{v}{2})\rho_\xi(x+\frac{v}{2})\right). \tag{13}$$

Here $\rho_\xi = -\frac{\lambda}{3!}(\langle\varphi_L\rangle_\xi^3 + \xi)$. Then, performing the Tailor expansion of $(\varrho_\xi(x-\frac{v}{2}) - \varrho_\xi(x+\frac{v}{2}))$, $\varrho_\xi = \frac{\rho_\xi}{\langle\varphi_L\rangle_\xi}$, in powers of v and integrating over v, we get

$$p_\mu\partial^\mu N_L(x,p) = \frac{1}{4}\sum_\xi \partial^\mu\varrho_\xi(x)\frac{\partial}{\partial p^\mu}N_L^\xi(x,p), \tag{14}$$

where we used (12) and assumed that averaging over ξ reduces high derivatives terms. Then in such an approximation

$$p_\mu\partial^\mu N_L(x,p) = \frac{1}{4}\sum_\xi \partial^\mu\varrho_\xi(x)\frac{\partial}{\partial p^\mu}N_L^\xi(x,p), \tag{15}$$

and $N_L^\xi(x,p)$, as follows from (11), is governed by the equation

$$p_\mu\partial^\mu N_L^\xi(x,p) = \frac{1}{4}\partial^\mu\varrho_\xi(x)\frac{\partial}{\partial p^\mu}N_L^\xi(x,p). \tag{16}$$

Let us define

$$\delta N_L^\xi = N_L^\xi - N_L, \qquad \delta\varrho_\xi = \varrho_\xi - \varrho, \tag{17}$$

here $\varrho = \sum_\xi \varrho_\xi$. Then, using (17), Eq. (14) reads

$$p_\mu\partial^\mu N_L(x,p) = \frac{1}{4}\partial^\mu\varrho(x)\frac{\partial}{\partial p^\mu}N_L(x,p) + \frac{1}{4}\sum_\xi[\partial^\mu\delta\varrho_\xi(x)\frac{\partial}{\partial p^\mu}\delta N_L^\xi(x,p)]. \tag{18}$$

Now one needs to calculate second term in the right hand side of the above equation. Assuming that initially $\delta N_L^\xi = 0$ and keeping only lowest terms in δ, one can get after some mathematics

$$p_\mu\partial^\mu N_L(x,p) = \\ \frac{1}{4}\partial^\mu\varrho(x)\frac{\partial}{\partial p^\mu}N_L(x,p) + \frac{1}{16}\frac{\partial}{\partial p^\mu}\int d^4y G_p(x-y)\sum_\xi[\delta\varrho_\xi^\mu(x)\delta\varrho_\xi^\nu(y)]\frac{\partial}{\partial p^\nu}N_L(y,p). \tag{19}$$

Here $\varrho^\mu \equiv \partial^\mu\varrho$, $\delta\varrho_\xi^\mu \equiv \partial^\mu\delta\varrho_\xi$, and

$$p^\mu\partial_\mu G_p(x) = \delta^{(4)}(x), \tag{20}$$

$$G_p(x) = p_0^{-1}\Theta(t)\delta^{(3)}(\mathbf{r} - (\mathbf{p}/p_0)t). \tag{21}$$

In general, we cannot compute exactly the contributions of the fluctuations (otherwise we could solve exactly the model): approximations are necessary. Then, to proceed further we have to specify the stochastic properties of the random quantities $\delta\varrho_\xi^\mu(x)$. We take the simplest ansatz assuming that the backreaction is negligible

$$\sum_\xi[\delta\varrho_\xi^\mu(x)\delta\varrho_\xi^\nu(y)] = \tau^{\mu\nu}(x,y)\delta(t_x - t_y). \tag{22}$$

The assumption of a $\delta-$function in time difference means that the auto-correlation time of the fluctuations is small compared to the time scale of the motion of the averaged fields. The fluctuations thus appear as uncorrelated on the time scale of the motion of the averaged fields. This assumes a clear separation of scales between short time scale of irrelevant degrees of freedom, and the "relaxation time", which characterizes the dynamics of the relevant degrees of freedom. Then

$$p_\mu \partial^\mu N_L(x,p) = \frac{1}{4}\partial^\mu \varrho(x)\frac{\partial}{\partial p^\mu}N_L(x,p) + \frac{1}{16}\tau^{\mu\nu}\frac{\partial}{\partial p^\mu}\frac{1}{p_0}\frac{\partial}{\partial p^\nu}N_L(x,p), \tag{23}$$

here $\tau^{\mu\nu} \equiv \tau^{\mu\nu}(x,x)$. As usual, irreversible transport equation for "relevant" subsystem is valid only for finite time scales where the short-memory approximation (i.e., "white noise" approximation) is justified. It is worth to note similarity of Eq. (23) with the Fokker-Plank equation, the latter is often utilized for description of approach to (local) equilibrium. In the utilized approximation, see Eqs. (9) and (10), we do not account for explicit contribution of short wavelength modes, so $\sum_\xi \xi = 0$ and $\varrho = \sum_\xi \varrho_\xi = -\frac{\lambda}{3!}\langle\varphi_L\rangle^2$. Then the first term in r.h.s. of Eq. (23) is reduced to a familiar Vlasov term, and the second term in r.h.s. of Eq. (23) is associated with correlators of fluctuations induced by interactions with short-length modes. In such an approximation, the above equation cannot describe thermalization, but it still can describe process of momentum isotropization and spatial decoherence of the long-length modes, that precede thermal equilibration acting on a shorter time scale and are necessary condition for thermalization and hydrodynamics.

Isotropization of the relevant subsystem can happen, evidently, only because of interactions with irrelevant modes. In more mathematical terms, it can happen if diffusion term, that is associated with correlators of fluctuations, has appropriate properties. Namely, let us assume that $\tau^{\mu\nu} \sim \delta^{\mu\nu}$, i.e., the corresponding fluctuations are isotropic. Then, to find steady (quasistationary) state, we suppose that r.h.s. of Eq. (23) is equal to zero:

$$\begin{aligned} &\frac{1}{2}\partial^0\varrho(x)\frac{\partial}{\partial p_0^2}N_L(x,p) + \frac{1}{4}\frac{\partial}{\partial p_0^2}\frac{\partial}{\partial p_0^2}\tau^{00}N_L(x,p) + \\ &\frac{1}{4p_0}\partial^i\varrho(x)\frac{\partial}{\partial p^i}N_L(x,p) + \frac{1}{16p_0^2}\frac{\partial}{\partial p^i}\frac{\partial}{\partial p^i}\tau^{ii}N_L(x,p) = 0. \end{aligned} \tag{24}$$

Here for convenience we divided r.h.s. of Eq. (23) on p_0. Just to demonstrate that solution of the above equation can be associated with isotropic steady state, let us find approximate analytic solution of Eq. (23) for $|\mathbf{p}|/|p_0| \ll 1$. One can easy see that it is

$$N_L(x,p) \sim \exp\left[-2p_0\left(\frac{p_0\partial^0\varrho(x)}{\tau^{00}} + \frac{2p_i\partial^i\varrho(x)}{\tau^{ii}}\right)\right]. \tag{25}$$

Notice, that such a steady state is obtained without account of energy-momentum dispersion relation. So, it is valid, in fact, only if mass shell constraint on p_μ is not strongly peaked like the delta-function but, instead, is wide enough, having, however, some limited virtuality. For an expanding system one can expect that $\partial^\mu\varrho > 0$ because $\varrho < 0$. Then this steady state has quasi-local equilibrium form with "effective temperature" that is $\sim 1/p_0$, and "effective collective four-velocity" that is $\sim \partial^\mu\varrho$, and can be related to the so-called prethermalization stage [29]. Also, one can see that (25) demonstrates spatiotemporal decoherence of the long wavelength subsystem. Indeed, the lengths of coherence are associated with values of the off-diagonal elements of the corresponding density matrix, $\rho_L(x+\frac{1}{2}\Delta x, x-\frac{1}{2}\Delta x) = \int d^4p \exp(ip\Delta x)N_L(x,p)$. The structure like (25) for $N_L(x,p)$ leads typically to finite coherence length. Because we do not fix dispersion relation, we just illustrate our conclusion analytically supposing particles on zero-mass shell. Then, calculating the density matrix in the "rest frame", it is easy to see that in the time direction nondiagonal elements of the density matrix will be proportional to $e^{-\Delta t^2/\lambda_t^2}$ with temporal correlation length in this rest system to be $\lambda_t^2 \propto \partial^0\rho/\tau^{00}$. During this time the long-length state looses coherence. In space directions there are also exponential cuts in nondiagonal elements of the density matrix. So one can conclude that coherence lengths in this steady state are finite and are caused by the "hydrodynamical" parameters and energy momentum dispersion relation. In a similar way, thermal wave length $\lambda_{th}^2 \propto 1/mT$ defines the off-diagonal elements of the corresponding density matrix and, so, spatial coherence lengths of the non relativistic Boltzmann distribution. Because sufficient degree of isotropy in the locally co-moving frame and decoherence of densities are the basic premises for applicability of hydrodynamics, one can conjuncture that energy momentum tensor of the long wavelength modes can, eventually, approach to energy momentum tensor of an effective viscous fluid.

3 Conclusions

In this paper, we discuss a physical mechanism which can explain the source of decoherence at early stage of matter evolution in ultrarelativistic nucleus-nucleus collisions, and subsequent approach to hydrodynamical behavior. Motivated by the phenomenological success of application of hydrodynamics in $A+A$ collisions, and

taking into account that any measurement is projection into macrostate with experimental errors that much exceed the quantum limit, we proposed to split the system into long-length modes subsystem and short-length modes subsystem, and consider the former as a relevant subsystem. Because long-length modes in initial stage of $A + A$ collision are highly populated [30], it allows to consider evolution of the corresponding expectation value of the quantum field in the quasiclassical approximation with noise term. The latter is associated with quantum fluctuations that are mostly contributed by the irrelevant from an observational viewpoint short-length modes.

We demonstrate how such a physical mechanism works by means of scalar field model. We derived evolution equation of the Fokker-Planck type for the Wigner function of a relevant part of a system and demonstrated, after some simplifying assumptions, that this equation can describe decoherence and isotropization at prethermalization stage that are necessary conditions for eventual thermalization and hydrodynamics. Notice that it happens as result of interactions with the irrelevant (i.e., observationally inaccessible) degrees of freedom, and no averaging over ensemble of initial conditions is needed for such a quantum thermalization. The generated non-zero entropy can be understood as the entanglement entropy of long-length subsystem of system created by nucleus-nucleus collision, while the entropy of the whole closed system does not change with time due to the unitarity of the time evolution.

Our analysis supports an idea that thermalization and transition to hydrodynamics are contextual, and are related to a particular procedure of decomposition of the whole quantum system into subsystems that contain a large enough number degrees of freedom (evidently, one should not expect a similar behavior in systems with few degrees of freedom). A fluid dynamics then appears as effective long wavelength theory. Hydrodynamical description is, in fact, inappropriate for an artificial "observer" who wholly measures of an isolated quantum system, such an "observer" then will have to calculate whole quantum evolution of a system in interest to predict results of such a "complete" experiment. On the other hand, utilization of a full unitary quantum evolution of a closed system with subsequent projection into relevant coarse-grained subspace at the measurement will result in the same predictions for statistical ensemble of experimental data as utilization of a relevant coarse-grained effective theory that follows to instantaneous decomposition of the composite state into relevant and irrelevant subsystems/observables. Finally, note that great efforts are currently focused on computing viscous transport coefficients from microscopic models, see, e.g., Ref. [31] where contribution of correlation of fluctuations to viscous coefficients was studied. In our opinion, understanding of the dynamical mechanisms of decoherence and thermalization should create the necessary prerequisites for unambiguous calculation of viscous coefficients in $A + A$ collisions, and we hope that our analysis can be useful for this aim.

Acknowledgements. The research was carried out within the scope of the EUREA: European Ultra Relativistic Energies Agreement (European Research Group: "Heavy Ions at Ultrarelativistic Energies") and is supported by the National Academy of Sciences of Ukraine (Agreement F4 – 2013).

References

[1] U. Heinz, in "Relativistic Heavy Ion Physics", Landolt-Boernstein New Series, Vol. I/23, edited by R. Stock (Springer Verlag, New York, 2010), Chap. 5 [arXiv:0901.4355]; D.A. Teaney, arXiv:0905.2433; H. Song, arXiv:1207.2396; U. Heinz, R. Snellings, Annu. Rev. Nucl. Part. Sci. **63**, 123 (2013) [arXiv:1301.2826]; C. Gale, S. Jeon, B. Schenke, Int. J. Mod. Phys. A **28**, 1340011 (2013) [arXiv:1301.5893].

[2] A. El, Z. Xu, C. Greiner, Nucl. Phys. A **806**, 287 (2008) [arXiv:0712.3734]; Z. Xu, L. Cheng, A. El, K Gallmeister, C. Greiner, J. Phys. G **36**, 064035 (2009) [arXiv:0812.3839].

[3] St. Mrówczyński, Acta Phys. Polon. B **37**, 427 (2006) [arXiv:hep-ph/0511052]; S.V. Akkelin, Phys. Rev. C **78**, 014906 (2008) [arXiv:0801.1628]; St. Mrówczyński, B. Müller, Phys. Rev. D **81**, 065021 (2010) [arXiv:0912.5108]; J. Peralta-Ramos, E. Calzetta, Phys. Rev. D **86**, 125024 (2012) [arXiv:1208.2715] M. Attems, A. Rebhan, M. Strickland, Acta Phys. Polon. Supp. **6**, 393 (2013) [arXiv:1302.5098].

[4] K. Dusling, T. Epelbaum, F. Gelis, R. Venugopalan, Nucl. Phys. A **850**, 69 (2011) [arXiv:1009.4363]; T. Epelbaum, F. Gelis, Nucl. Phys. A **872**, 210 (2011) [arXiv:1107.0668]; J.-P. Blaizot, F. Gelis, J. Liao, L. McLerran, R. Venugopalan, Nucl. Phys. A **873**, 68 (2012) [arXiv:1107.5296]; K. Dusling, T. Epelbaum, F. Gelis, R. Venugopalan, arXiv:1207.5401; arXiv:1210.6053.

[5] S. Habib, K. Jacobs, H. Mabuchi, R. Ryne, K. Shizume, B. Sundaram, Phys. Rev. Lett. **88**, 040402 (2002) [arXiv:quant-ph/0010093]; U. Klein, Am. J. Phys. **80**, 1009 (2012) [arXiv:1201.0150].

[6] G.G. Cabrera, M. Kiwi, Phys. Rev. A **36**, 2995 (1987).

[7] L.G. Yaffe, Rev. Mod. Phys. **54**, 407 (1982) ; J.R. Klauder, arXiv:1008.4307.

[8] J.M. Maldacena, Adv. Theor. Math. Phys. **2**, 231 (1998) [arxiv:hep-th/9711200]; E. Witten, Adv. Theor. Math. Phys. **2**, 253 (1998) [arXiv:hep-th/9802150].

[9] O. Aharony, S.S. Gubser, J. Maldacena, H. Ooguri, Y. Oz, Phys. Rep. **323**, 183 (2000) [arXiv:hep-th/9905111]; J.M. Maldacena, arXiv:hep-th/0309246; arXiv:1106.6073.

[10] J. Casalderrey-Solana, H. Liu, D. Mateos, K. Rajagopal and U. A. Wiedemann, arXiv:1101.0618; D. Mateos, J. Phys. G: Nucl. Part. Phys. **38**, 124030 (2011) [arXiv:1106.3295]; J.-P. Blaizot, Acta Phys. Pol. B Proc. Suppl. **4**, 641 (2011) [arXiv:1108.3049].

[11] V. Balasubramanian, P. Kraus, Phys. Rev. Lett. **83**, 3605 (1999) [arXiv:hep-th/9903190]; T. Faulkner, H. Liu, M. Rangamani JHEP **1108**, 051 (2011) [arXiv:1010.4036]; I. Heemskerk, J. Polchinski, JHEP **1106**, 031 (2011) [arXiv:1010.1264]; L. Susskind, E. Witten, arXiv:hep-th/9805114; I. Papadimitriou, K. Skenderis, arXiv:hep-th/0404176.

[12] Ho-Ung Yee, arXiv:1212.2584.

[13] A. Bernamonti, R. Peschanski, Nucl. Phys. Proc. Suppl. **216**, 94 (2011) [arXiv:1102.0725].

[14] V. Balasubramanian, A. Bernamonti, J. de Boer, N. Copland, B. Craps, E. Keski-Vakkuri, B. Müller, A. Schäfer, M. Shigemori, and W. Staessens, Phys. Rev. D **84**, 026010 (2011) [arXiv:1103.2683].

[15] S. Bhattacharyya, V.E. Hubeny, S. Minwalla, M. Rangamani, JHEP **0802**, 045 (2008) [arXiv:0712.2456]; M. Rangamani, Class. Quant. Grav. **26**, 224003 (2009) [arXiv:0905.4352]; V.E. Hubeny, M. Rangamani, Adv. High Energy Phys. **2010**, 297916 (2010) [arXiv:1006.3675]; V.E. Hubeny, S. Minwalla, M. Rangamani, arXiv:1107.5780; V.E. Hubeny, Class. Quant. Grav. **28**, 114007 (2011) [arXiv:1011.4948].

[16] I. Bredberg, C. Keeler, V. Lysov, A. Strominger, JHEP **1103**, 141 (2011) [arXiv:1006.1902].

[17] S. Bhattacharyya, R. Loganayagam, I. Mandal, S. Minwalla, A. Sharma, JHEP **0812**, 116 (2008) [arXiv:0809.4272]; R. Baier, P. Romatschke, D. T. Son, A. O. Starinets, M. A. Stephanov, JHEP **0804**, 100 (2008) [arXiv:0712.2451]; P. Kovtun, J. Phys. A: Math. Theor. **45**, 473001 (2012) [arXiv:1205.5040].

[18] P. Danielewicz, Annals of Physics **152**, 239 (1984); J.-P. Blaizot, E. Iancu, Phys. Rep. **359**, 355 (2002) [arXiv:hep-ph/0101103]; J. Berges, AIP Conf.Proc. **739**, 3 (2005) [arXiv:hep-ph/0409233]; J. Rammer, *Quantum Field Theory of Non-Equilibrium States*, (Cambridge University Press, 2007); W. Cassing, Eur. Phys. J. ST **168**, 3 (2009) [arXiv:0808.0715].

[19] E.A. Calzetta, B.L. Hu, F.D. Mazzitelli, Phys. Rep. **352**, 459 (2001) [arXiv:hep-th/0102199]; E. Calzetta and B.-L. Hu, *Nonequilibrium Quantum Field Theory*, (Cambridge University Press, 2008).

[20] Yu. B. Ivanov, J. Knoll, D. N. Voskresensky, Nucl. Phys. A **672**, 313 (2000) [arXiv:nucl-th/9905028]; G. Aarts, G.F. Bonini, C. Wetterich, Nucl. Phys. B **587**, 403 (2000) [arXiv:hep-ph/0003262]; A.H. Mueller, D.T. Son, Phys. Lett. B **582**, 279 (2004) [arXiv:hep-ph/0212198]; S. Jeon, Phys. Rev. C **72**, 014907 (2005) [arXiv:hep-ph/0412121]; A. Arrizabalaga, J. Smit, A. Tranberg, Phys. Rev. D **72**, 025014 (2005) [arXiv:hep-ph/0503287]; M. Lindner, M.M. Muller, Phys. Rev. D **73**, 125002 (2006) [arXiv:hep-ph/0512147]; A. Nishiyama, Nucl. Phys. A **832**, 289 (2010) [arXiv:0810.5003].

[21] J. Rau, B. Müller, Phys. Rep. **272**, 1 (1996) [arXiv:nucl-th/9505009]; H. Grabert, *Projection Operator Techniques in Nonequilibrium Statistical Mechanics*, (Springer, Berlin, Heidelberg, 1982).

[22] T.Koide, M.Maruyama, F.Takagi, Prog. Theor. Phys. **107**, 1001 (2002) [arXiv:hep-ph/0102272]; T. Koide, Prog. Theor. Phys. **107**, 1001 (2002) [arXiv:hep-ph/0102272]; X.-G. Huang, T. Kodama, T. Koide, D.H. Rischke, Phys. Rev. C **83**, 024906 (2011) [arXiv:1010.4359]; X.-G. Huang, T. Koide, Nucl. Phys. A **889**, 73 (2012) [arXiv:1105.2483].

[23] E. Joos, H.D. Zeh, Z. Phys. B **59**, 223 (1985); W.H. Zurek, Rev. Mod. Phys. **75**, 715 (2003) [arXiv:quant-ph/0105127]; D. Guilini, E. Joos, C. Kiefer, J. Kupsch, I.-O. Stamatescu, H.D. Zeh, *Decoherence and the Appearance of a Classical World in Quantum Theory*, (Springer-Verlag Berlin Heidelberg 1996); M. Schlosshauer, Rev. Mod. Phys. **76**, 1267 (2004) [arXiv:quant-ph/0312059]; H.D. Zeh, *The Physical Basis of the Direction of Time*, (Springer-Verlag Berlin Heidelberg 2007).

[24] J. Gemmer, M. Michel, G. Mahler, *Quantum Thermodynamics. Emergence of Thermodynamic Behavior Within Composite Quantum Systems*. Lect. Notes Phys. **657** (Springer, Berlin Heidelberg 2004).

[25] B. d'Espagnat, Phys. Rep. **110**, 201 (1984); *Conceptual Foudations of Quantum Mechanics*, (Perseus Books 1999).

[26] F. Lombardo, F. Mazzitelli, Phys. Rev. D **53**, 2001 (1996) [arXiv:hep-th/9508052].

[27] M. E. Fisher, Rev. Mod. Phys. **70**, 653 (1998); C. Bagnuls and C. Bervillier, Phys. Rep. **348**, 91 (2001) [arXiv:hep-th/0002034]; J. Berges, N. Tetradis, and C. Wetterich, Phys. Rep. **363**, 223 (2002) [arXiv:hep-ph/0005122]; B. Delamotte, arXiv:cond-mat/0702365; O.J. Rosten, Phys. Rep. **511**, 177 (2012) [arXiv:1003.1366]; J. Berges, D. Mesterházy, arXiv:1204.1489.

[28] S.R. de Groot, W.A. van Leeuwen, Ch. G. van Weert, *Relativistic Kinetic Theory*, (North-Holland Publ. Comp., Amsterdam, 1980); H.-Th. Elze, AIP Conf. Proc. **631**, 229 (2002) [arXiv:hep-ph/0204309].

[29] J. Berges, S. Borsanyi, C. Wetterich, Phys. Rev. Lett. **93**, 142002 (2004) [hep-ph/0403234].

[30] F. Gelis, E. Iancu, J. Jalilian-Marian, R. Venugopalan, Ann. Rev. Nucl. Part. Sci. **60**, 463 (2010) [arXiv:1002.0333]; T. Lappi, Int. J. Mod. Phys. E **20**, 1 (2011) [arXiv:1003.1852] ; L. McLerran, Prog. Theor. Phys. Suppl. **187**, 17 (2011) [arXiv:1011.3204]; F. Gelis, arXiv:1211.3327.

[31] P. Kovtun, G.D. Moore, P. Romatschke, Phys. Rev. D **84**, 025006 (2011) [arXiv:1104.1586]; J.I. Kapusta, B.Müller, M. Stephanov, Phys. Rev. C **85**, 054906 (2012) [arXiv:1112.6405].

Proceedings of the International School-seminar
"New Physics and Quantum Chromodynamics at External Conditions", pp. 41 – 48,
May 22-24, 2013, Dnipropetrovsk, Ukraine

SPONTANEOUS SYMMETRY BREAKING IN THE $O(4)$ MODEL ON A LATTICE

V. I. Demchik[a], A. V. Gulov[b], V. V. Skalozub[c]

Dnipropetrovsk National University, Dnipropetrovsk, Ukraine

The dependence of the symmetry breaking phenomenon on the coupling constant λ values in the $O(N)$ scalar field models is investigated on a lattice. As particular case, the $O(4)$ model is considered. The general case of $O(N)$ model is reduced to the one component theory in spherical coordinates by integrating over Goldstone's modes in the functional integral. The partition function Z of the $O(N)$ models is calculated analytically. Monte Carlo simulations are performed with QCDGPU software package on HGPU cluster. It is shown for $O(4)$ model that symmetry breaking does not happen for $\lambda < 10^{-3}$, the phase transition holds for $10^{-3} < \lambda < 10^{-1}$ and temperature restoration of the symmetry is observed.

1 Introduction

The problems on the phase transitions and symmetry breaking in the $O(N)$ models are of a great importance for QFT. They have been investigated in numerous publications (see Refs. [3]- [5] and references therein) by using different methods of calculations, in particular, in Monte Carlo (MC) simulations on a lattice.

Recently in [6] it has been determined in MC simulations for the $O(1)$ model that the type of the phase transition at finite temperature depends on the value of coupling constant λ. So, this problem is of interest for other $O(N)$ models. For $N \geq 2$ this problem is much complicated because of an number of reasons: "triviality", dependence on the space dimensions, Goldstone theorem, etc. In fact, one needs in a reliable order parameter which distinguishes the phases of the system and the dependence of them on the λ value. Traditionally, in investigating this problem an effective potential approach is used. In the present file, having as a goal to introduced an order parameter useful in lattice MC calculations, we investigate the property of the partition function Z as a function of λ. In fact, in analytic calculations it serves as a normalization factor which disappears in calculation of an effective potential or other functions, when a functional integral is calculated. However, it may be of interest for lattice investigations announced.

Here, we develop a general approach for solving this problem by using the representation of the partition function (PF) in the spherical coordinates. The main problem here is to integrate out Goldstone's modes before doing a lattice investigations.

2 The model

The Lagrangian of O(N) ϕ^4-model is

$$L = \frac{1}{2}\sum_{i=1}^{N} \partial_\mu \varphi_i(x)\partial_\mu \varphi_i(x) - V(\varphi),$$
$$V(\varphi) = \frac{m^2}{2}\varphi^2(x) + \frac{\lambda}{4}(\varphi^2(x))^2, \qquad (1)$$

where $\varphi^2(x) = \sum_{i=1}^{N} \varphi_i(x)\varphi_i(x)$, φ is real N-component scalar field. For $m^2 < 0$ a spontaneous symmetry breaking (SSB) takes place.

Let us turn to the spherical coordinates and parameterize the field as follows. First we separate the absolute value from direction of the vector:

$$\varphi_i(x) = R(x)n_i(x),$$

where $R(x) \in [0, \infty)$ and $n^2(x) = \sum_i n_i(x)n_i(x) = 1$ holds.

The angular variables in the spherical coordinates

$$n_1 = \sin\theta_1 ... \sin\theta_{N-1},$$

e-mail: [a]vadimdi@yahoo.com, [b]alexey.gulov@gmail.com, [c]skalozubv@daad-alumni.de

$$\begin{aligned} n_i &= \sin\theta_1 ... \sin\theta_{N-1}\cos\theta_{N-i+1}, \quad i = 2, ..., N-1 \\ n_N &= \cos\theta_1, \end{aligned} \tag{2}$$

with angles $\theta_{1,...,N-2}(x) \in [0, \pi]$ and $\theta_{N-1}(x) \in [0, 2\pi]$.

In these variables the Lagrangian has the form,

$$L = \frac{1}{2}\frac{\partial R}{\partial x_\mu}\frac{\partial R}{\partial x_\mu} - \frac{1}{2}R^2 n^i \frac{\partial^2 n^i}{\partial x_\mu \partial x_\mu} - V(R), \tag{3}$$

where we have taken into consideration the total derivative $\partial(R^2 n_i \partial n_i/\partial x_\mu)/\partial x_\mu$ and the condition $\partial(n_i n_i)/\partial x_\mu = 0$.

From the Lagrangian (3) the equations follow:

$$R^2(x)\frac{\partial^2 n^i}{\partial x_\mu \partial x_\mu} + 2R(x)\sum_i n^i \frac{\partial n^i}{\partial x_\mu}\frac{\partial R}{\partial x_\mu} = 0, \tag{4}$$

and

$$\frac{\partial^2 R(x)}{\partial x_\mu \partial x_\mu} + \frac{\partial V(R)}{\partial R} + 2R\sum_i \frac{\partial n^i}{\partial x_\mu}\frac{\partial n^i}{\partial x_\mu} = 0. \tag{5}$$

In Eq.(4), the last term has to be transformed to account for the dependence of the fields n_i. These relations are dependent on the number N and therefore could not be written in an explicit form in general. As we see, the first equation describes the massless models corresponding to the motions along the coordinate lines. At $R = const$ these are the equations for the Goldstone modes appeared after symmetry breaking.

Our main problem in what follows is to calculate the partition function Z in spherical coordinates in some a way. We shell do that in two steps. In the next section, we calculate a usual Gaussian integral in this coordinates. And then a functional integral of interest is computed.

3 Integration in spherical coordinates

It is well known that the continual integrals of interest in the QFT are of the Gaussian types. In spherical coordinates an additional Jacobian factor as in Eq.(14) presents in the integrand. That needs to work out a procedure for the calculation of the such type integrals. As a first step, we calculate the usual Gaussian integrals in spaces with different dimensions.

First, we consider the 2-dimensional integral

$$I_2 = \int_{-\infty}^{\infty} dxdy e^{-ax^2} e^{-ay^2} = \frac{\pi}{a}. \tag{6}$$

Now, we calculate it in the way interested for the generalization to the functional integrals. We write

$$I_2 = \int_0^{\infty} RdR \int_0^{2\pi} d\theta e^{-aR^2}. \tag{7}$$

This integral we calculate by the saddle-point method. Namely, we integrate over the angular variable and transform the integrand to the form

$$I_2 = 2\pi \int_0^{\infty} dR e^{-aR^2 + \log R}. \tag{8}$$

The stationary points are determined from the equation for the function $F(R) = -aR^2 + \log R$ standing in the exponential,

$$\frac{\partial F(R)}{\partial R} = -2aR + \frac{1}{R}. \tag{9}$$

Hence we find $R_0 = \frac{1}{\sqrt{2a}}$ and the function can be written in the standard form: $F(R) = -1/2 - 2a(R - R_0)^2 + ...$ The Eq.(8) takes the form

$$I_2 = 2\pi \frac{e^{-1/2}}{\sqrt{2a}} \int_0^{\infty} dR e^{-2a(R-R_0)^2}. \tag{10}$$

Then, as in a standard saddle-point procedure, we extend the integration interval near the point R_0 to the infinity and obtain,

$$I_2 = 2\pi \frac{e^{-1/2}}{\sqrt{2a}} \sqrt{\frac{\pi}{2a}} = \frac{\pi}{a}\sqrt{\frac{\pi}{e}}. \tag{11}$$

This expression is very close to the exact value π/a. The difference is decreased if the next-to-leading terms of the asymptotic expansion are taken into consideration. This simple example demonstrate how to proceed in the case of Gaussian's integrals in the spherical coordinates. The procedure is reduced to the standard saddle-point calculations with the functions $F(R)$ coming from the exponentiation of the Jacobian and calculation the corresponding saddle-points. The angular integration is carried out explicitly as in the previous section for the functional integral. Actually, the role of the Jacobian is reduced to the detecting of the saddle-point position in the radial direction.

Adduce the values of the integrals obtained in the leading approximation for the 3-dimensional and 4-dimensional cases:

$$I_3 = \left(\frac{\pi}{a}\right)^{3/2} \cdot \left(\frac{4}{e\sqrt{2}}\right), \tag{12}$$

$$I_4 = \left(\frac{\pi}{a}\right)^{2} \cdot \left(\frac{3^{3/2}\sqrt{\pi}}{e^{3/2}}\right). \tag{13}$$

These are close to the exact values.

From these examples it becomes clear how to proceed in the case of the functional integrals in the spherical coordinates and calculate the Z factor.

4 Partition function

In this section we present the partition function of the $O(N)$ model in terms of new variables. It reads

$$\begin{aligned} Z &= \int D\phi \exp(\int d^4x L) \\ &= \int_0^\infty R^{N-1} DR(x) \int d^{N-1}\Omega(x) \exp(\int d^4x L). \end{aligned} \tag{14}$$

(the integration over angular variables is assumed). We shall look for constant solutions $R_c = const$, $\theta_i = const$ and calculate Z.

A usual procedure in this case is to calculate an effective potential $V(\phi_c)$ and apply a steepest descent method. For constant fields, the equations for determining the saddle point is simplified and the integration in the functional integral can be easily fulfilled.

5 Calculation of an overall factor

We proceed with the $O(4)$ model and consider the Z factor given in Eq.(14). Information on the free field case as well as a general theory on continual integration is given in numerous books (see, for example, [7]). In this section we work out a procedure for calculation in the form convenient for lattice investigations and related to the one in previous files. That is, we assume that a lattice is introduced having a spacing a in the Euclidian 4-space. The field $R(x)$ is determined by its values in each site x of the lattice. At this moment we consider a zero temperature case. So, the partition function can be written in the form,

$$Z = \sum_x \int_0^\infty DR(x) \int d^{4-1}\Omega(x) e^{3\log R(x)} e^{a^4 L(\tilde{x})}. \tag{15}$$

The "effective potential" for this case is

$$\tilde{V}(R) = \sum_x a^4 \left(\frac{1}{2}m^2R^2 - \frac{\lambda}{4}R^4\right) + \sum_x (3\log R). \tag{16}$$

In fact, this is not a usual effective potential, considered as a Legendre transform but a useful tool to calculate the partition function by using the steepest descent method.

We introduce the notation $\Omega = 1/a^4$. The stationary equation, $\partial\tilde{V}/\partial R = 0$, reads

$$y^2 - \frac{m^2}{\lambda}y - \frac{3\Omega}{\lambda} = 0, \tag{17}$$

where $y = R^2$. It has one positive solution

$$y_0 = R_0^2 = \frac{m^2}{2\lambda} + \sqrt{\left(\frac{m^2}{2\lambda}\right)^2 + \frac{3\Omega}{\lambda}}. \tag{18}$$

For small λ it can be written as $y_0 = \frac{m^2}{\lambda} + \frac{3\Omega}{m^2}$. The second derivative in the vicinity R_0^2 equals to $\tilde{V}''(R_0) = -\kappa^2 = -\left(\frac{12\lambda}{m^2} + \frac{3\Omega}{m^2}\right)$. Hence, the effective potential can be presented as follows,

$$\tilde{V}(R) = \tilde{V}(R_0) - \frac{1}{2}\kappa^2\rho^2, \tag{19}$$

where

$$\tilde{V}(R_0) = \log\left(\frac{m^2}{\lambda} + \frac{3\Omega}{m^2}\right)^{3/2} + \frac{m^4}{4\lambda\Omega} - \frac{9}{4}\frac{\lambda\Omega}{m^4} \tag{20}$$

and $\rho = R(x) - R0$. After that the integration over the field ρ is simply carried out even with accounting for the kinetic term in the action. But it does not matter at this moment because we observe the important distinguishable behavior of the functional integral over ρ - it is proportional to

$$z_0 = \sum_x \left(\frac{m^2}{\lambda} + \frac{3\Omega}{m^2}\right)^{3/2} \exp\left(\frac{m^4}{4\lambda\Omega}\right) \exp\left(-\frac{9}{4}\frac{\lambda\Omega}{4m^4}\right), \tag{21}$$

and two first factors are diverging for λ goes to zero. This is the distinguishable feature of the spontaneous symmetry breaking. Note that for the positive values of m^2, that is the symmetric phase, the integral is proportional to $(\frac{3\Omega}{m^2})^{3/2}$ and not dependent on λ in the limit of $\lambda \to 0$.

The factor z_0 stands independently of the operator structure of the kinetic part. So, this property of Z can be used to determine the phase transition (or symmetry breaking) as a function of λ. Due to such type behavior, the partition function can serve as an order parameter for symmetry breaking in the $O(N)$ models. Of course, this behavior may be changed when the part due to other terms standing in the functional integral. But one may expect that the spontaneous symmetry breaking is expressed in divergent behavior of the partition function in the limit $\lambda \to 0$. Other details on the behavior of Z will be discussed in what follows. Note that at this level of approximation it is possible to replace the value R_0 in the effective action by the "classical field" R_c derived via a Legendre transform [8]. Then via a steepest descent method the loop expansion of the partition function can be done.

6 One-loop contributions

In this section, we calculated the first loop correction contributions to the Z assuming "classical field" R_c is a constant. This approximation corresponds for any effective potential $V(R_c)$ the terms of the order h in a loop expansion.

For simplicity, we now tern to the $O(2)$ model. So, the integration measure in Eq.(14) is: $RDRD\theta$. We introduce the fields of small deviations from the stationary point solution $R_c = R_0 + \theta$ and $\theta_c = \Theta_0 + \alpha$ and calculate new integral over these fields. Here, we are interested in the effective potential. And the term $\sim \partial_\mu\theta\partial_\mu\theta$ in the Lagrangian corresponds to the varying in space field configurations and therefore contributes to the next term in derivative expansion of the effective action. So, they do not relevant and can be neglected in what follows.

We substitute new variables in the effective action to get,

$$L' = \frac{1}{2}\frac{\partial\rho}{\partial x_\mu}\frac{\partial\rho}{\partial x_\mu} - \frac{m_c^2}{2}\rho^2 + \frac{1}{2\Omega}\left[m^2R_0^2 - \frac{\lambda}{2}R_0^4\right] + \log R_0 + O(\rho)^3 + \frac{1}{2\Omega}R_0^2[\frac{\partial\alpha}{\partial x_\mu}\frac{\partial\alpha}{\partial x_\mu}], \tag{22}$$

where the linear in ρ terms are canceled via the stationary condition (18) and the "mass term" is $m_c^2 = \frac{1}{\Omega}(\lambda R_c^2 - m^2) + \frac{2}{R_c^2}$. The last term here is coming from a series expansion of the logarithm $\log(R_0 + \rho)$. Note that the term λR^2 appears because of the term $\log R$ instead $\log R^3$ in Eq.(16).

The calculation procedure is straightforward and well known ([8]). One has to construct the symmetric kernel for the operator standing in Eq.(22)

$$K_{xy}(m_c) = (\partial_x\partial_y + m_c^2)\delta^4(x-y) = \int \frac{d^4k}{(2\pi)^4}(k^2 + m_c^2)\exp[ik(x-y)]. \tag{23}$$

Hence we obtain for the trace:

$$\tilde{V}^1 = \frac{1}{2}\log K(m_c) = \frac{1}{2}\int \frac{d^4k}{(2\pi)^4}\log[(k^2 + m_c^2)] + AR_c^2 + BR_c^4, \tag{24}$$

where A and B are renormalization constants. To determine a finite expression and fix the constants some renormalization conditions have to be applied. Here, we apply the conditions of the renormalization in the vicinity of the tree-level effective potential Eq.(16):

$$\left(\frac{\partial\tilde{V}}{\partial R_c^2}\right)|_{R_c=R_0}=0,\quad \left(\frac{\partial^2\tilde{V}}{\partial(R_c^2)^2}\right)|_{R_c=R_0}=-\kappa^2. \tag{25}$$

For the one-loop terms, this means that both of the derivatives equal to zero. In fact, this is a well known ubiquitous procedure giving a finite potential.

It is not difficult to carry out all these calculations by using, for example, the k-space cut off regularization. For the integral we get,

$$I^1=\frac{1}{64\pi^2}[4Lm_c^2+2m_c^4\log m_c^2-2m_c^4\log L-m_c^4]+am_c^2+bm_c^4, \tag{26}$$

where L is a cutoff parameter. Then, it has to be renormalized according to Eq.(25). Hence one can obtain the A and B coefficients. In fact, to simplify the representation we express the conditions (25) in a little bit modified form and write

$$\left(\frac{\partial\tilde{V}(R_c^2)}{\partial R_c^2}\right)=\left(\frac{\partial\tilde{V}(R_c^2)}{\partial m_c^2}\right)\left(\frac{\partial m_c^2}{\partial R_c^2}\right). \tag{27}$$

After that the expressions for renormalization of I^1 (26) read

$$\left(\frac{\partial\tilde{V}^1}{\partial m_c^2}\right)|_{m_c=m_0}=0,\quad \left(\frac{\partial^2\tilde{V}^1}{\partial(m_c^2)^2}\right)|_{m_c=m_0}=0, \tag{28}$$

where $m_0^2=m_c^2(R_0)=\frac{1}{\Omega}(\lambda y_0-m^2)+2/y_0$ and y_0 is given in Eq.(18). For the coefficients a and b we find

$$a = \frac{1}{16\pi^2}(m_0^2-L), \tag{29}$$

$$b = -\frac{1}{16\pi^2}\frac{1}{2}[1-\log(L/m_0^2)]. \tag{30}$$

Hence the renormalized one-loop contribution follows:

$$\tilde{V}^1_{ren.}=\frac{1}{64\pi^2}[2m_c^4\log\left(\frac{m_c^2}{m_0^2}\right)-3m_c^4+4m_c^2m_0^2]. \tag{31}$$

Adding this term to Eq.(22), we derive the first two terms of the expansion of the partition function Z. It is also convenient to pass to dimensionless variables

It is also convenient to pass to dimensionless variables:

$$r_c=\frac{R_c}{m},\quad \mu^4=\frac{m^4}{\Omega}=(am)^4, \tag{32}$$

where now a is the lattice spacing. Let us present the result (31) in these variables and substitute as m_0^2 its value in the small λ limit, $m_0^2=3\lambda/m^2$. In this case we obtain:

$$\tilde{V}^1_{ren.}=\frac{1}{64\pi^2}\frac{1}{m^4}\left(\mu^4(\lambda r_c^2-1)+\frac{2}{r_c^2}\right)^2\left[2\log\left(\frac{\mu^4}{3}(r^2-1/\lambda)+\frac{2}{3\lambda r_c^2}\right)-3+\frac{4}{3}\left(\mu^4(r^2-1/\lambda)+\frac{2}{\lambda r_c^2}\right)\right]. \tag{33}$$

The same can be done for the tree level terms in Eq.(22):

$$\tilde{V}^0=\frac{\mu^4}{2}\left(r_c^2-\frac{\lambda}{2}r_c^4\right)+\log(mr_c). \tag{34}$$

Thus, in this limit, the explicit dependence on the coupling λ is present. Remind here that the point R_0 is not a stationary point for the effective potential $V(R)$ standing in the Lagrangian but the one to calculate the partition function Z in one-loop approximation.

As concerns the integration over the field α, it can also be done by the standard steepest descent method near the stationary point Θ_0. The calculation procedure is quite similar to the previous one. More precise, we have to transform the last term in Eq.(22) to the form $-\frac{1}{2}\frac{R_0^2}{\Omega}\alpha\partial_\mu^2\alpha$ and integrate over α in the functional

integral. Since the integral in Gaussian we can extend the limits of integration to infinity, as usually is doing in the steepest descent method. Thus, the integral is reduced to

$$\int_{-\infty}^{+\infty} d\alpha e^{-\frac{1}{2}\frac{R_0^2}{\Omega}\alpha\partial_\mu^2\alpha} = \int_{-\infty}^{+\infty} d\xi \frac{\Omega^{1/2}}{R_0} e^{-\frac{1}{2}\xi\partial_\mu^2\xi}, \tag{35}$$

where new integration variable $\xi = \alpha\frac{R_0}{\Omega^{1/2}}$ is introduced. The integration over ξ is fulfilled as before and resulted in the field independent factor which is not important for what follows. Hence, the main result of this integration is the appearance of the factor $1/R_0$. This factor being transformed into exponential cancels the term $\log R_0$ in Eq.(22) or the last one in Eq.(34). As a result, the divergent factor in Eq.(21) becomes

$$z_0' = \sum_x \exp\left(\frac{m^4}{4\lambda\Omega}\right)\exp\left(-\frac{9\lambda\Omega}{4m^4}\right). \tag{36}$$

Thus, the singular behavior of Z in the limit of $\lambda \to 0$ remains and the partition function is a good order parameter.

Of course, this calculation may serves as a rough estimate to Z and actual calculations must be carried out on a lattice. However, it demonstrates some general features of the problem of interest. In fact, integration over x must be done in a standard way used for lattice calculations.

7 Monte Carlo lattice simulations

For MC simulations we use symmetric hypercubic lattice with hypertorous geometry L^4. The temperature is introduced into a lattice through anisotropic lattice spacings: the spatial and a temporal lattice spacing a_s and $a_t = a_s/\zeta$ with $\zeta \geq 1$, respectively. The scalar field $\varphi_i(x)$ is defined in the lattice sites.

General procedure for investigations of the phase transitions in the $O(N)$ models.

- We can start from the effective one-component Lagrangian consisting of the initial one written in the spherical coordinates where we can omit the angular terms and add the term $\log(R/R_0)^{(N-1)}$.
- The value of the R_0 has to be calculated from the "EP" $\tilde{V}(R)$ for fixed angular variables.
- The integration over continuum compact variables is carried out explicitly.

The most important feature of this approach is the order parameter which is related with mean value of $R^2(x)$. The procedure of dealing with the one component field $R(x)$ can be simply realized on the lattices similarly to the $O(1)$ model investigated already [6].

To perform a computer simulations we must have a procedure to generate uniformly distributed $R(x)$ in interval $[0,\infty)$. But there is no uniform random number generator to realize uniformly distributed numbers in infinite interval directly on a computer.

So, we introduce one-to-one transformation

$$R(x) \to U(x), \qquad U(x) \in (0, U_{max}), U_{max} < 1. \tag{37}$$

The final lattice action is the follow

$$\begin{aligned} S &= \frac{1}{z}\sum_x \Phi_x\left(\Phi_x - 1 + \frac{1}{4}\sqrt{\frac{z}{\lambda\zeta}}\sum_\mu\left(\zeta_\mu^2\log^2\frac{\Phi_{x+a_\mu\hat{\mu}}}{\Phi_x}\right)\right) \\ &- \sum_x \frac{N-1}{2}\log\left(1-\sqrt{2\Phi_x}\right) \\ &- \sum_x \log\frac{1-\eta\log(1-U_x)}{1-U_x}. \end{aligned} \tag{38}$$

$$\Phi_x = \frac{b}{2}\left[\left(-1+\frac{\eta}{2}\log(1-U_x)\right)\log(1-U_x)\right]^2 \tag{39}$$

In Monte-Carlo procedure we try successively change the field Φ_x by new one according to the standard Metropolis technique with action (38).

Physical fields (the classical condensate $\varphi_0 = m/\sqrt{\lambda}$ can be set as a unit) are read as

$$\frac{\varphi(x)}{\varphi_0} = \sqrt{2\Phi_x}. \tag{40}$$

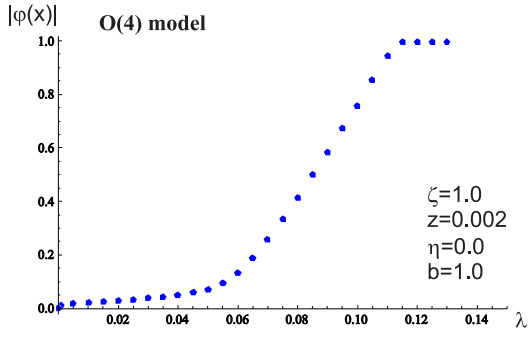

Figure 1. Dependence of symmetry behavior on the coupling constant λ at zero temperature ($\zeta = 1$) on a lattice 16^4.

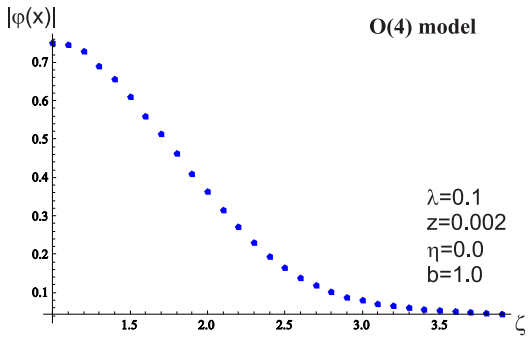

Figure 2. Temperature dependence of symmetry behavior at finite temperature on a lattice 16^4.

The dependence of symmetry behavior on the coupling constant λ at zero temperature (isotropic lattice, $\zeta = 1$) on a lattice 16^4 is present in Fig.1. The phase transition is observed with the increasing of the value of coupling constant λ. The temperature dependence of symmetry behavior at finite temperature on a lattice 16^4 is shown in Fig.2. It can be seen that the symmetry is restored at high temperatures ($\zeta \sim 3.5$). The temperature dependence of field condensate is not sensitive to the initial configuration. Both cold and hot starts lead to the same behavior of field condensate for various ζ.

8 Monte Carlo simulations on GPU

Study of phase transition phenomena on a computer is always connected with the need to get huge statistics. The use of traditional computing resources are insufficient. The new computing platform – GPGPU provides a performance increase tenfold over conventional computing resources. For example, the peak performance of modern high-end computing accelerators (nVidia Tesla K20 and AMD Radeon HD7970 GPUs as well as Intel Xeon Phi accelerator) is about 20-50 times faster than that of comparable CPUs. Along last five years the GPU performance has been increasing twice per each year. Thanks to a substantially lower cost (per Flops[1]), as well as high rates of productivity growth compared to CPUs the graphics accelerators have become a very attractive platform for high performance computing.

Current overall maximal performance of all computer systems ranked in the last TOP-500 (list of the most powerful (non-distributed) computer systems in the world [1]) list is about 224 PFlops.

The number of computer systems for different countries is: USA - 253 computers (50.6%), China - 65 (13.0%), Japan - 30 (6.0%), UK - 29 (5.8%), France - 23 (4.6%), Germany - 19 (3.8%), Russia - 8 (1.6%). Fifty three of these supercomputer systems, equipped with computing accelerators are shown in Table 1 (peak performance of corresponding system measured in GFlops is show in the last column).

Rank	Computer	Country	Year	Cores	R_{max}	R_{peak}
1	Tianhe-2, Intel Xeon Phi	China	2013	3120000	33862700	54902400
2	Titan, Cray XK7, Nvidia GPU	USA	2012	560640	17590000	27112550
3	Sequoia, BlueGene/Q	USA	2011	1572864	17173224	20132659
4	K computer	Japan	2011	705024	10510000	11280384
5	Mira, BlueGene/Q	USA	2012	786432	8586612	10066330
6	Stampede, PowerEdge C8220, Intel Xeon Phi	USA	2012	462462	5168110	8520112
10	Tianhe-1A, NUDT YH MPP, Nvidia GPU	China	2010	186368	2566000	4701000
16	Nebulae, Dawning TC3600 Blade System, Nvidia GPU	China	2010	120640	1271000	2984300
21	TSUBAME 2.0, HP ProLiant SL390s, Nvidia GPU	Japan	2010	73278	1192000	2287630
28	Conte, Cluster Platform SL250s, Intel Xeon Phi	USA	2013	77520	943380	1341096
31	Lomonosov, T-Platforms T-Blade2/1.1, Nvidia GPU	Russia	2011	78660	901900	1700210
500	Cluster Platform 3000SL SL170s/160z	USA	2012	17904	96619	190499

Table 1: Some computer systems in TOP-500 list of Worlds Supercomputers [1]

Obviously, the software for Monte Carlo simulations require a totally new approach. Therefore, we developed a common software environment **QCDGPU** that allows Monte Carlo simulations for a number of the most frequently studied models – $SU(N)$ gluodynamics and $O(N)$ scalar field model. The software environment is a stand-alone set of software that has important properties for performing long-intensive simulations:

1. OpenCL package for MC simulations of $SU(N)$ and $O(N)$ models is developed
2. huge lattices stay available to study – lattices 128^4 could be researched
3. MC simulations can be performed on single- or multi-GPU systems simultaneously
4. during long simulations package can write lattice configuration states to HDD for further simulations

[1]Flops (*floating point operations per second*) – is a measure of computer's performance

5. simulations can be performed with single, double and mixed precision

All simulations are performed on heterogeneous distributed **HGPU** cluster [2].

9 Conclusions

In this paper we have study the spontaneous symmetry breaking behavior in $O(N)$ scalar field model. It is shown in MC simulations on a lattice that the symmetry breaking phenomenon is dependent on the coupling constant λ values. The effective theory which reduces $O(N)$ theory to $O(1)$ model is developed. It is proposed MC procedure for study the dependence of the symmetry breaking phenomenon on the coupling constant λ values in the $O(N)$ scalar field models on a lattice.

We have obtained that in O(4) scalar field theory the symmetry breaking does not happen for small coupling constant values, $\lambda < 10^{-3}$, whereas the phase transition holds for $10^{-3} < \lambda < 10^{-1}$. Also, the temperature restoration of the symmetry is observed.

We developed the software package QCDGPU for MC simulations of $SU(N)$ and $O(N)$ models on GPU.

References

[1] The Top-500 list, http://www.top500.org/ (Last access: jun.2013)
[2] High performance computing on graphics processing units, http://hgpu.org/ (Last access: jun.2013)
[3] J. Zinn-Justin, Int. Ser. Monogr. Phys. **92**, 1 - 1008 (1996).
[4] J. Berges, N. Tetradis and C. Wetterich, Phys. Rept. **363**, 223 (2002).
[5] P. Cea, M. Consoli, L. Cosmai [hep-lat/0407024]; [hep-ph/0311256]; Nucl. Phys. Proc. Suppl. **106**, 953 (2002).
[6] M. Bordag, V. Demchik, A. Gulov and V. Skalozub, Int. J. Mod. Phys. A **27**, 1250116 (2012) [arXiv:1204.0651 [hep-lat]].
[7] A. Shvartz, Springer, Lecture Notes in Mathematics, Volume 307, pp.274 (1993).
[8] J. Iliopoulos, C. Itzykson and A. Martin, Rev. Mod. Phys. **47**, 165 (1975).

Proceedings of the International School-seminar
"New Physics and Quantum Chromodynamics at External Conditions", pp. 49 – 56,
May 22-24, 2013, Dnipropetrovsk, Ukraine

NEUTRINO MAGNETIC MOMENT AS A SIGNAL OF NEW PHYSICS

O.M.Boyarkin [a], G.G.Boyarkina [b]

Belarus State Pedagogical University, Minsk, Belarus

Within the left-right model with Majorana neutrinos the corrections to neutrino dipole magnetic moments (DMM) coming from the $\tilde{\delta}^{(\pm)}$-Higgs bosons are considered. It is shown that when $\tilde{\delta}^{(\pm)}$-bosons are on the electroweak scale then their contributions to the DMM are comparable with, and even could exceed, the contributions of the charged gauge bosons. The behavior of a neutrino flux in matter and a magnetic field is investigated. It was proven that even at $E_\nu > m_N$ the resonance transitions between the light and heavy neutrinos are forbidden. Investigation of the collider experiments with the light neutrino beam revealed that we can detect both the μ^{NN} and $\mu^{\nu N}$ moments. The most perspective reactions are

$$\nu_{\mu L} + p \to N_{\mu R} + X, \qquad p + p \to \gamma^* \to N_{eR} + \overline{\nu}_{eL} + X, \qquad p + p \to W_R^* \to e + N_e \to e + \nu_e + \gamma + X.$$

1 Introduction

At the end of 2002 as consequence of series of experiments with solar, atmospheric and reactor neutrinos the existence of the neutrino oscillations has been established. This, in turn, meant that the neutrino has a mass and the partial lepton flavor violation takes place. At the same time monitoring of the Galaxy by the net of neutrino telescopes aimed to detect a neutrino signal from the expected galactic supernova explosion has been starting. Neutrinos also find a use for solution of applied problems as evidenced by the application of antineutrino detectors for nuclear reactor monitoring in the "on-line" regime and the appearance of a neutrino geotomography (see, for review, [1]). All this puts forward the neutrino physics in the forefront of natural sciences. However, in spite of achieved progress there are series unsolved problems in the neutrino physics. Among these first of all are: (i) the smallness of the neutrino mass $m_\nu \approx 10^{-6} m_e$; (ii) the value of the neutrino dipole magnetic moment (DMM); (iii) the neutrino nature (Dirac or Majorana).

Models with the see-saw mechanism give successful explanation of the first problem. In these models heavy right-handed neutrinos being see-saw partners of light left-handed neutrinos appear. Introducing of heavy neutrinos N_i $(i = 1, 2, 3)$ helps to solve some cosmological problems as well. For example, these neutrinos are used for explanation of the observed baryon asymmetry in the Universe thanks to the leptogenesis.

Interest in electromagnetic neutrino properties is primarily caused by the fact that there exist plenty of astrophysical systems with intensive magnetic fields where neutrino physics plays an important part. Large magnetic fields are present in supernovas, neutron stars and white dwarfs, and fields as large as $B_e = m_e^2/e \simeq 4.41 \times 10^{13}$ G can arise in supernova explosions or coalescing neutron stars.

In the standard model (SM) neutrinos are massless particles and the mixing of neutrino states do not take place. Reconstruction of the neutrino sector of the SM is usually achieved by introducing a right-handed neutrino singlet (minimally extended SM). However, the explanation of the neutrino mass smallness is absent. DMM's predicted by the SM are so small that they are not of any physical interest. It should be also noted that in the SM the satisfactory mechanism to produce a baryonic asymmetry in the universe is absent. All this taken together provides strong evidence of Physics beyond the SM.

The purpose of our work is investigation of the neutrino electromagnetic properties in the context of the left-right-symmetric model (LRM).

2 The left-right-symmetric model

For the first time the model based on the $SU(2)_L \times SU(2)_R \times U(1)_{B-L}$ gauge group (LRM) was proposed at the beginning of the 1970s [2]. In the LRM quarks and leptons enter into the left- and right-handed doublets

$$Q_L^a(\frac{1}{2}, 0, \frac{1}{3}) = \begin{pmatrix} u_L^a \\ d_L^a \end{pmatrix}, \qquad Q_R^a(0, \frac{1}{2}, \frac{1}{3}) = \begin{pmatrix} u_R^a \\ d_R^a \end{pmatrix},$$

e-mail: [a]oboyarkin@tut.by, [b]boyarkin@front.ru

$$\Psi^a_L(\frac{1}{2},0,-1)=\begin{pmatrix}\nu_{aL}\\ l_{\alpha L}\end{pmatrix},\qquad \Psi^a_R(0,\frac{1}{2},-1)=\begin{pmatrix}N_{aR}\\ l_{aR}\end{pmatrix}. \tag{1}$$

where $a=1,2,3$, in brackets the values of S^W_L, S^W_R and $B-L$ are given, S^W_L (S^W_R) is the weak left (right) isospin while B and L are the baryon and lepton numbers. The gauge boson sector include four charged bosons ($W^{\pm}_L$, $W^{\pm}_R$) and two neutral bosons (Z_L and Z_R). There are two possibilities of defining the LR symmetry as a generalized parity P and as a generalized charge conjugation C. It was found that $m_{W_2}>2.5$ TeV if LR=C and $m_{W_2}>4$ TeV if LR=P. We remind that there is the theoretical relation $m_{Z_R}\approx 1.7 m_{W_R}$ too.

The Higgs sector structure determines the neutrino nature. The mandatory element of the Higgs sector is the bi-doublet $\Phi(1/2,1/2,0)$. For the neutrino to be a Majorana particle, the Higgs sector must include two triplets $\Delta_L(1,0,2)$, $\Delta_R(0,1,2)$.

The SSB according to the chain

$$SU(2)_L\times SU(2)_R\times U(1)_{B-L}\to SU(2)_L\times U(1)_Y\to U(1)_Q$$

is realized for the following choice of the VEVs:

$$<\delta^0_{L,R}>=\frac{v_{L,R}}{\sqrt{2}},\qquad <\Phi^0_1>=k_1,\qquad <\Phi^0_2>=k_2, \tag{2}$$

$$v_L<<\max(k_1,k_2)<<v_R. \tag{3}$$

After the SSB we are left with 14 physical Higgs bosons: four doubly-charged scalars $\Delta^{(\pm)}_{1,2}$, four singly-charged scalars $\tilde{\delta^{(\pm)}}$ and $h^{(\pm)}$, four neutral scalars $S_{1,2,3,4}$, and two neutral pseudoscalars $P_{1,2}$. The detailed discussion of the Higgs sector structure has been done in [3].

It could be shown that the $\tilde{\delta^{(\pm)}}$-boson whose mass is defined as

$$m^2_{\tilde{\delta}}=(\rho_3/2-\rho_1)v^2_R-\frac{\beta^2k^2_0}{\alpha+\rho_1-\rho_3/2}, \tag{4}$$

where

$$k_{\pm}=\sqrt{k^2_1\pm k^2_2},\qquad k_0=\frac{k^2_-}{\sqrt{2}k_+},\qquad \alpha=\frac{\alpha_3k^2_+}{2k^2_-},\qquad \beta=\frac{k^2_+(\beta_1k_1+2\beta_3k_2)}{2k^2_-k_0}, \tag{5}$$

$k_+=174$ GeV, and $\beta_1,\beta_3,\alpha_3,\rho_1,\ \rho_3$ are the constants entering into the Higgs potential, may lie on the electroweak scale (EWS). It is possible under conditions

$$\alpha\approx 1,\qquad (\rho_3/2-\rho_1)\approx\frac{k^2_+ +3\beta^2k^2_0}{3v^2_R}. \tag{6}$$

Note, when this scenario is realized two physical Higgs bosons S_4 and P_2 whose masses are

$$m^2_{S_4}=(\rho_3/2-\rho_1)v^2_R,\qquad m^2_{P_2}=(\rho_3/2-\rho_1)v^2_R \tag{7}$$

lie on the EWS too.

For a massive Dirac neutrino the most general form of the matrix element for the conserved neutrino electromagnetic current J^{em}_μ is given by the expression

$$<\nu^D_i(p')|J^{em}_\mu|\nu^D_j(p)>=<\nu^D_i(p')|i\sigma_{\mu\lambda}q^\lambda[F_M(q^2)+F_E(q^2)\gamma_5]+(q^2\gamma_\mu-q_\mu\hat{q})[F_V(q^2)+F_A(q^2)\gamma_5]|\nu^D_j(p)>, \tag{8}$$

where $q=p'-p$, $F_M(q^2)$, $F_E(q^2)$, $F_A(q^2)$ and $F_V(q^2)$ are the magnetic, electric, anapole and reduced Dirac formfactors, respectively. In the static limit ($q^2=0$) $F_M(q^2)$ and $F_E(q^2)$ define (anomalous) dipole magnetic moment μ_{ij} and dipole electric moment d_{ij}, respectively. At $i=j$ and $q^2=0$, $F_A(q^2)$ represents the anapole neutrino moment.

For a Majorana neutrino all the formfactors, except the axial one F_A, are identically equal to zero. As regards non-diagonal elements, the situation depends on the fact whether CP-parity is conserved or not. For the CP non-variant case all the four formfactors are nonzero. When CP invariance takes place and the $|\nu^M_i>$- and $|\nu^M_j>$-states have identical (opposite) CP-parities, then $(F_E)_{ij}$ and $(F_A)_{ij}$ ($(F_M)_{ij}$ and $(F_V)_{ij}$) are different from zero.

By now we have information concerning the DMMs of ordinary left-handed neutrinos ν_{aL} while any experimental data associated with the DMMs of heavy right-handed neutrinos N_{aR} is absent. The most sensitive and established method for the experimental investigation of the neutrino DMMs is provided by direct laboratory measurements of electron (anti)neutrino-electron scattering at low energies in solar, accelerator and reactor experiments. The best limit was obtained in the work [4]

$$\mu_\nu\le 3.2\times 10^{-11}\mu_B.$$

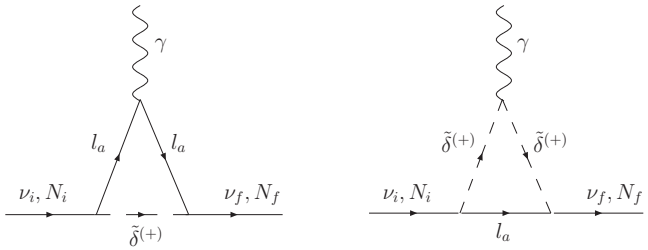

Figure 1. The Feynman diagrams caused by the virtual singly charged boson only.

Contributions to the neutrino DMMs coming from the diagrams with the virtual charged gauge bosons W_1 and W_2 have the following form [5]:

$$\mu_{ii'}^{\nu\nu} = -\frac{3g_L^2 m_e(m_{\nu_i} + m_{\nu_{i'}})\mu_B}{32\pi^2} \sum_a \left[\frac{\cos^2\xi}{m_{W_1}^2}\epsilon_a^{(1)} + \frac{\sin^2\xi}{m_{W_2}^2}\epsilon_a^{(2)} \right] \times \mathrm{Im}[U_{i'a}^\dagger U_{ai}], \tag{9}$$

$$\mu_{jj'}^{NN} = \mu_{ii'}^{\nu\nu}(g_L \to g_R, U_{ai} \to V_{aj}, m_{\nu_i} \to m_{N_j}, \xi \to \xi + \pi/2), \tag{10}$$

$$\mu_{ij}^{\nu N} = \frac{g_L g_R m_e \mu_B}{2\pi^2} \sin\xi\cos\xi \sum_a m_a \mathrm{Im}\left[e^{-i\phi}U_{ja}^\dagger V_{ai}\right] \left\{ \sum_{k=1}^{2} \frac{(-1)^k}{m_{W_k}^2} \left[1 + \epsilon_a^{(k)} \left(\ln\epsilon_a^{(k)} + \frac{9}{8} \right) \right] \right\}, \tag{11}$$

where

$$\nu_{iL} = U_{ia}^\dagger \nu_{aL}, \qquad N_{iR} = V_{ia}^\dagger N_{aR}, \qquad \epsilon_a^{(k)} = \frac{m_a^2}{m_{W_k}^2}, \qquad k = 1, 2,$$

and U_{ia} (V_{ia}) is the mixing matrix in the light (heavy) neutrino sector while ξ is the mixing angle in the charged gauge boson sector. Assuming that

$$g_L = g_R, \qquad m_{W_2} = 4 \text{ TeV}, \qquad \xi = 2 \times 10^{-4}, \tag{12}$$

and N_j, $N_{j'}$ are on the EWS, we obtain the small value for $\mu_{ii'}^{\nu\nu}$ as before, while

$$|\mu_{jj'}^{NN}| \approx 10^{-11}\mu_B \qquad \text{and} \qquad |\mu_{ij}^{\nu N}| \approx 2 \times 10^{-13}\mu_B. \tag{13}$$

Contributions to the neutrino DMM coming from the $\tilde{\delta}^{\pm}$-bosons were found in [6]. They are caused by the diagrams pictured on Fig. 1. The results are as follows ($i \neq f$)

$$(\mu^{\nu\nu})_{if} = \frac{m_e\mu_B}{2\pi^2} \sum_{l_a} \frac{\alpha_{\nu_a\tilde{\delta}l_a}\alpha_{\nu_a\tilde{\delta}l_a}}{(m_{\nu_i} - m_{\nu_f})} \int_0^1 xdx \left[\ln\left|\frac{M_{\nu_i\tilde{\delta}}}{M_{\nu_f\tilde{\delta}}}\right| + \ln\left|\frac{M_{\nu_i l_a}}{M_{\nu_f l_a}}\right| \right] \times \mathrm{Im}[(\mathcal{D}_{fl_a}^{\nu\nu})^\dagger \mathcal{D}_{l_a i}^{\nu\nu}], \tag{14}$$

$$(\mu^{NN})_{if} = (\mu^{\nu\nu})_{if}(\nu_i \longrightarrow N_i, \nu_f \longrightarrow N_f), \tag{15}$$

$$(\mu^{\nu N})_{if} = -\frac{m_e\mu_B}{2\pi^2} \sum_{l_a} \alpha_{N_a\tilde{\delta}l_a}\alpha_{\nu_a\tilde{\delta}l_a} m_{l_a} \int_0^1 dx \left[\frac{1}{m_{N_i}^2} \ln\left|\frac{M_{\nu_f\tilde{\delta}}}{M_{N_i\tilde{\delta}}}\right| - \right.$$
$$\left. - \frac{x}{m_{N_j}^2(1-x) + m_{\nu_i}^2 x} \ln\left|\frac{M_{\nu_i l_a}}{M_{N_j l_a}}\right| \right] \times \mathrm{Im}[\mathcal{U}_{jl_a}^\dagger \mathcal{U}_{l_a i}], \tag{16}$$

where

$$M_{N_i\tilde{\delta}} = (m_{\tilde{\delta}}^2 - m_{N_i}^2)x + m_{N_i}^2 x^2 + m_{l_a}^2(1-x), \qquad M_{N_i l_a} = (m_{l_a}^2 - m_{N_i}^2)x + m_{N_i}^2 x^2 + m_{\tilde{\delta}}^2(1-x).$$

$$M_{\nu_i l_a} = (m_{l_a}^2 - m_{\nu_i}^2)x + m_{\nu_i}^2 x^2 + m_{\tilde{\delta}}^2(1-x), \qquad M_{\nu_i\tilde{\delta}} = (m_{\tilde{\delta}}^2 - m_{\nu_i}^2)x + m_{\nu_i}^2 x^2 + m_{l_a}^2(1-x).$$

Besides the diagrams pictured on Fig.1 the contributions to the neutrino DMM come from diagrams shown on Fig.2.

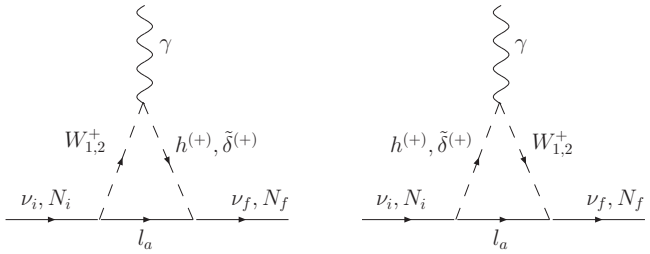

Figure 2. The Feynman diagrams caused by both the virtual singly charged boson and charged gauge boson.

These diagrams give the following contributions to the neutrino DMMs

$$(\mu'^{\nu\nu}_{\tilde{\delta}})_{ii'} = \frac{ig_L m_e \mu_B}{32\sqrt{2}\pi^2} \sum_{l_a} \alpha_{\nu_a \tilde{\delta} l_a} \alpha_{W\tilde{\delta}\gamma} \left\{ \frac{\sin 2\xi}{m^2_{W_1}} \int_0^1 dx \left[\frac{1}{M_{\nu_{i'}\tilde{\delta}} - M_{\nu_i W_1}} \ln \left| \frac{M_{\nu_{i'}\tilde{\delta}}}{M_{\nu_i W_1}} \right| \times \right.\right.$$
$$\times \left(x^2 m^2_{W_1} + 2(2x - 3x^2) M_{\nu_i W_1} + (x^3 - x^4)(m^2_{\nu_i} + m^2_{\nu_{i'}}) + x^2(m^2_{\nu_i} + \right.$$
$$\left. + m_{\nu_i} m_{\nu_{i'}}) \right) + 2(3x^2 - 2x) \left(\ln \left| \frac{l^\nu_h}{M_{\nu_{i'}\tilde{\delta}}} \right| + \frac{l^\nu_{W_1}}{l^\nu_{\tilde{\delta}} - l^\nu_{W_1}} \ln \left| \frac{l^\nu_{\tilde{\delta}}}{l^\nu_{W_1}} \right| \right) \Bigg] \times \mathrm{Im}[\mathcal{U}^\dagger_{i' l_a} \mathcal{U}_{l_a i}] -$$
$$\left. - (W_1 \longrightarrow W_2, \mathcal{U}^\dagger_{i' l_a} \longrightarrow \mathcal{U}^\dagger_{i' l_a} e^{i\phi}) \right\} + (m_{\nu_i} \leftrightarrow m_{\nu_{i'}}), \qquad (17)$$

$$(\mu'^{NN}_{\tilde{\delta}})_{jj'} = \frac{ig_L m_e \mu_B}{16\sqrt{2}\pi^2} \sum_{l_a} \alpha_{N_a \tilde{\delta} l_a} \alpha_{W\tilde{\delta}\gamma} \left\{ \frac{\cos^2 \xi}{m^2_{W_2}} \int_0^1 dx \left[\frac{1}{M_{N_{j'}\tilde{\delta}} - M_{N_j W_2}} \ln \left| \frac{M_{N_{j'}\tilde{\delta}}}{M_{N_j W_2}} \right| \times \right.\right.$$
$$\times \left(x^2 m^2_{W_2} + 2(2x - 3x^2) M_{N_j W_2} + (x^3 - x^4)(m^2_{N_j} + m^2_{N_{j'}}) + x^2(m^2_{N_j} + \right.$$
$$\left. + m_{N_j} m_{N_{j'}}) \right) + 2(3x^2 - 2x) \left(\ln \left| \frac{l^N_{\tilde{\delta}}}{M_{N_{j'}\tilde{\delta}}} \right| + \frac{l^N_{W_2}}{l^N_{\tilde{\delta}} - l^N_{W_2}} \ln \left| \frac{l^N_{\tilde{\delta}}}{l^N_{W_2}} \right| \right) \Bigg] \times \mathrm{Im}[\mathcal{U}^\dagger_{j' l_a} \mathcal{U}_{l_a j}] +$$
$$\left. + (W_2 \to W_1, \xi \to \xi + \pi/2, \mathcal{U}^\dagger_{j' l_a} \longrightarrow \mathcal{U}^\dagger_{j' l_a} e^{-i\phi}) \right\} + (m_{N_j} \leftrightarrow m_{N_{j'}}),$$
$$(\mu'^{\nu N}_{\tilde{\delta}})_{ij} = -\frac{ig_L m_e \mu_B}{64\sqrt{2}\pi^2} \sum_{l_a} \alpha_{W\tilde{\delta}\gamma} \alpha_{N_a \tilde{\delta} l_a} m_{l_a} \left\{ \frac{\sin 2\xi}{m^2_{W_1}} \int_0^1 \frac{dx}{M_{N_j\tilde{\delta}} - M_{\nu_i W_1}} \ln \left| \frac{M_{N_j\tilde{\delta}}}{M_{\nu_i W_1}} \right| \times \left[x^3(m_{N_j} + m_{\nu_i}) - \right.\right.$$
$$\left. - x^2(3m_{\nu_i} + m_{N_j}) + 2x m_{\nu_i} \right] \times \mathrm{Im}[e^{-i\phi} \mathcal{U}^\dagger_{j l_a} \mathcal{U}_{l_a i}] + (W_1 \longrightarrow W_2, \phi \longrightarrow 0) \Bigg\} + (m_{N_j} \leftrightarrow m_{\nu_i}), \qquad (18)$$

where

$$l^\nu_{W_k} = (m^2_{W_k} - m^2_{\nu_i})x + m^2_{l_a}(1 - x), \qquad l^N_{W_k} = l^\nu_{W_k}(\nu_i \to N_j),$$
$$l^\nu_{\tilde{\delta}} = (m^2_{\tilde{\delta}} - m^2_{\nu_i})x + m^2_{l_a}(1 - x), \qquad l^N_{\tilde{\delta}} = l^\nu_{\tilde{\delta}}(\nu_i \to N_j), \qquad l^\nu_{W_k} + m^2_{\nu_i} x^2 = M_{\nu_i W_k},$$
$$M_{\nu_i \tilde{\delta}} = l^\nu_{\tilde{\delta}} + m^2_{\nu_i} x^2, \qquad M_{N_j W_k} = M_{\nu_i W_k}(\nu_i \to N_j), \qquad l^N_{\tilde{\delta}} + m^2_{N_j} x^2 = M_{N_j \tilde{\delta}}.$$

Let us estimate the expressions for the DMMs obtained in this work using the values of the LRM parameters (12) and assuming that $m_{\tilde{\delta}} = 100$ GeV. As will be shown later, in the heavy neutrino sector only two scenarios are possible: (i) the heavy neutrino masses are (quasi) degenerated and the mixing angles between heavy and light neutrinos are equal (quasi mass degeneracy — QMD); (ii) the heavy neutrino masses are arbitrary and the mixing inside the same generation is absent (no mass degeneracy — NMD). Then, we get

$$(\mu^{\nu\nu})_{if} \approx -10^{-12} \mu_B, \qquad (\mu^{NN})_{if} \approx -5 \times 10^{-13} \mu_B, \qquad (\mu^{\nu N})_{if} \approx 10^{-10} \mu_B$$

for the QMD case and

$$(\mu^{\nu\nu})_{if} \approx -5 \times 10^{-11} \mu_B, \qquad (\mu^{NN})_{if} \approx 10^{-8} \mu_B, \qquad (\mu^{\nu N})_{if} \approx 10^{-8} \mu_B$$

for the NMD case.

3 Phenomenology of heavy neutrinos

Let us consider the motion of the high-energy beam of the left-handed electron neutrinos in matter and a twisting magnetic field. We shall be constrained by the two flavor approximation. The object of our investigation represents the system with the wave function $\Psi^T = (\nu_{eL}, \nu_{\mu L}, N_{eR}, N_{\mu R})$ and with the mixing matrix of the form

$$\mathcal{U} = \begin{pmatrix} \cos\theta_{12}^{\nu} & \sin\theta_{12}^{\nu} & 0 & 0 \\ -\sin\theta_{12}^{\nu} & \cos\theta_{12}^{\nu} & 0 & 0 \\ 0 & 0 & \cos\theta_{12}^{N} & \sin\theta_{12}^{N} \\ 0 & 0 & -\sin\theta_{12}^{N} & \cos\theta_{12}^{N} \end{pmatrix} \begin{pmatrix} \cos\theta_{11} & 0 & \sin\theta_{11} & 0 \\ 0 & \cos\theta_{22} & 0 & \sin\theta_{22} \\ -\sin\theta_{11} & 0 & \cos\theta_{11} & 0 \\ 0 & -\sin\theta_{22} & 0 & \cos\theta_{22} \end{pmatrix}. \tag{19}$$

The corresponding Hamiltonian is determined by the expression

$$\mathcal{H} = \begin{pmatrix} \mathcal{H}_{\nu\nu} & \mathcal{H}_{\nu N} \\ \mathcal{H}_{\nu N}^{\dagger} & \mathcal{H}_{NN} \end{pmatrix}, \tag{20}$$

where

$$\mathcal{H}_{\nu\nu} = \begin{pmatrix} c_{\theta_{11}}^2\Delta_c^{\nu} + s_{\theta_{11}}^2\Delta_c^{N} + c_{2\theta_{11}}\Sigma + V_{eL} - \dot{\Phi}/2 & c_{\theta_{11}}c_{\theta_{22}}\Delta_s^{\nu} + s_{\theta_{11}}s_{\theta_{22}}\Delta_s^{N} + \mu_{\nu_e\nu_\mu}B_{\perp} \\ c_{\theta_{11}}c_{\theta_{22}}\Delta_s^{\nu} + s_{\theta_{11}}s_{\theta_{22}}\Delta_s^{N} + \mu_{\nu_e\nu_\mu}B_{\perp} & -c_{\theta_{22}}^2\Delta_c^{\nu} - s_{\theta_{22}}^2\Delta_c^{N} + c_{2\theta_{22}}\Sigma + V_{\mu L} - \dot{\Phi}/2 \end{pmatrix},$$

$$\mathcal{H}_{\nu N} = \begin{pmatrix} \frac{s_{2\theta_{11}}}{2}(\Delta_c^{N} - \Delta_c^{\nu} - 2\Sigma) + \mu_{\nu_e N_e}B_{\perp} & s_{\theta_{11}}c_{\theta_{22}}\Delta_s^{N} - c_{\theta_{11}}s_{\theta_{22}}\Delta_s^{\nu} + \mu_{\nu_e N_\mu}B_{\perp} \\ c_{\theta_{11}}s_{\theta_{22}}\Delta_s^{N} - s_{\theta_{11}}c_{\theta_{22}}\Delta_s^{\nu} + \mu_{\nu_e N_\mu}B_{\perp} & \frac{s_{2\theta_{22}}}{2}(\Delta_c^{\nu} - \Delta_c^{N} - 2\Sigma) + \mu_{\nu_\mu N_\mu}B_{\perp} \end{pmatrix},$$

$$\mathcal{H}_{NN} = \mathcal{H}_{\nu\nu}\big(\theta_{11} \to \theta_{11} + \frac{\pi}{2}, \theta_{22} \to \theta_{22} + \frac{\pi}{2}, V_{eL} \to V_{eR}, V_{\mu L} \to V_{\mu R}, \dot{\Phi} \to -\dot{\Phi}\big),$$

$$\Delta_{c(s)}^{\nu} = \frac{m_{\nu_2}^2 - m_{\nu_1}^2}{4E}\cos 2\theta_{12}^{\nu}(\sin 2\theta_{12}^{\nu}), \qquad \Delta_{c(s)}^{N} = \frac{m_{N_2}^2 - m_{N_1}^2}{4E}\cos 2\theta_{12}^{N}(\sin 2\theta_{12}^{N}),$$

$$\Sigma = \frac{m_{\nu_1}^2 + m_{\nu_2}^2 - m_{N_1}^2 - m_{N_2}^2}{8E}, \qquad c_{2\theta_{kk}} = \cos 2\theta_{kk}, \qquad k = 1, 2,$$

V_{eL} (V_{eR}) and $V_{\mu L}$ ($V_{\mu R}$) are the matter potentials (MPs) describing the matter interaction with the left(right)-handed electron neutrino and muon neutrino:

$$V_{eL} = \sqrt{2}G_F(N_e - N_n/2) + V_{eL}^H, \qquad V_{\mu L} = -\sqrt{2}G_F N_n/2 + V_{\mu L}^H,$$
$$V_{eR} = \frac{g^2 N_e}{4m_{W_2}^2} - \frac{g^2 c_{\theta_W}^2 N_n}{8(c_{\theta_W}^2 - s_{\theta_W}^2)m_{Z_2}^2}, \quad V_{\mu R} = -\frac{g^2 c_{\theta_W}^2 N_n}{8(c_{\theta_W}^2 - s_{\theta_W}^2)m_{Z_2}^2}, \quad V_{aL}^H = \left(\frac{\alpha_{ea}^2}{2m_h^2} - \frac{f_{ea}^2}{m_{\tilde{\delta}}^2}\right)N_e, \tag{21}$$

where N_e (N_n) is the density of electrons (neutrons), $c_{\theta_W} = \cos\theta_W$, $s_{\theta_W} = \sin\theta_W$, θ_W is the Weinberg angle and we have neglected the mixing in the gauge boson sector.

Equalling the corresponding elements of the Hamiltonian (20), we can find all the totality of the resonance conversions in the case under consideration. Under fulfillment of the condition

$$V_{eL} - V_{\mu L} = -(c_{22}^2 + c_{11}^2)\Delta_c^{\nu} - (s_{22}^2 + s_{11}^2)\Delta_c^{N} + (c_{2\theta_{22}} - c_{2\theta_{11}})\Sigma \tag{22}$$

the $\nu_{eL} \to \nu_{\mu L}$-resonance (Mikheyev-Smirnov-Wolfenstein — MSW) occurs. Since the description of the MSW-resonance within the SM is sufficiently successful, then corrections to the SM predictions must be small in any SM extensions. Let us find out constraints on the LRM parameters that follow from this demand. The right-handed side of Eq. (22) will be close to the SM predictions in two cases: (i) the heavy neutrino masses m_{N_1} and m_{N_2} are arbitrary while the mixing inside generations is absent (NMD)

$$\theta_{11} = \theta_{22} = 0; \tag{23}$$

(ii) the angles θ_{11} and θ_{22} are equal to each other but not equal to zero whereas the heavy neutrino masses are (quasi)degenerated (QMD)

$$\theta_{11} = \theta_{22} \qquad \text{and} \qquad (m_{N_2}^2 - m_{N_1}^2)\cos 2\theta_{12}s_{22}^2 \approx (m_{\nu_2}^2 - m_{\nu_1}^2). \tag{24}$$

If the conditions

$$V_{eL} - V_{eR} - \dot{\Phi} = (\delta_c^{21} - \delta_c^{43})(s_e^2 - c_e^2) - 2c_{2\theta_e}\Delta, \tag{25}$$

and

$$V_{eL} - V_{eR} - \dot{\Phi} = -\delta_c^{21}(c_e^2 + s_\mu^2) - \delta_c^{43}(s_e^2 + c_\mu^2) - \Delta(c_{2\theta_e} + c_{2\theta_\mu}) \tag{26}$$

are fulfilled, we would have the $\nu_{eL} \to N_{eR}$- and $\nu_{eL} \to N_{\mu R}$ resonance transitions, respectively. It is clear that both the NMD- and QMD-schemes do not allow the existence of this resonances. So we may conclude, in spite of rather big values of $\mu_{ij}^{\nu N}$, in oscillation experiments with left-handed light neutrinos beam we have not the ghost of a chance to observe the heavy neutrinos production even at energies $E_\nu > m_N$.

Now we proceed to collider experiments. First we consider the process of the heavy neutrino production under collision of light neutrino beam with the proton target

$$\nu_{\mu L} + p \to \gamma^* \to N_{\mu R} + X, \tag{27}$$

where X is a nondetecting hadron state. The corresponding subprocesses are

$$\nu_{\mu L} + q_i \to \gamma^* \to N_{\mu R} + q_i, \tag{28}$$

$$\nu_{\mu L} + \overline{q}_i \to \gamma^* \to N_{\mu R} + \overline{q}_i. \tag{29}$$

Let us set the light neutrino mass equal to zero and do not take interest in the polarization of the initial and final particles. Calculations lead to the following value of the total cross section

$$\sigma(\nu_\mu p \to N_\mu X) = \frac{2\alpha^2|\mu^{\nu N}|^2\pi}{\mu_B^2 m_e^2 s^2} \sum_{q_i} n_{q_i}^2 \int_0^1 \frac{dx}{x^2} \left[f_{q_i}(x) + f_{\overline{q}_i}(x)\right] \left[2m_N^2 xs - 2x^2 s^2 - \right.$$
$$\left. -2m_{q_i}^4 - m_N^4\right] \ln\left|\frac{\beta_+(xs)}{\beta_-(xs)}\right| + \left[\beta_+(xs) - \beta_-(xs)\right]\left(2m_{q_i}^2 - 2xs + m_N^2 - \frac{2m_N^4 m_{q_i}^2}{\beta_+(xs)\beta_-(xs)}\right], \tag{30}$$

where s is the total energy squared of the colliding ν_μ-neutrino and proton in the center-of-mass frame, $f_{q_i}(x)$ and $f_{\overline{q}_i}(x)$ are the distribution functions of quarks and antiquarks inside the proton. When $\mu^{\nu N} = 10^{-8}\mu_B$ and $s = 10$ TeV, we have $\sigma(\nu_\mu p \to N_\mu p X) \approx 10$ fb. It is clear that at the existing experiment technique we could detect this process.

Further we consider possibilities of the observation of the transit DMM of the heavy neutrino at LHC. We start with the single heavy neutrino production in the process

$$p + p \to \gamma^* \to N_e + \overline{\nu}_e + X. \tag{31}$$

The differential cross section for the corresponding subprocess is given by the expression

$$\frac{d\hat{\sigma}}{d\hat{t}}(q_i\overline{q}_i \to N_e\overline{\nu}_e) = \frac{2n_{q_i}^2\alpha^2|\mu^{\nu N}|^2\pi}{m_e^2\mu_B^2\hat{s}^4}\left\{2\hat{s}\hat{u}\hat{t} + \hat{s}^2(m_N^2 + 2m_{q_i}^2) - \hat{s}(2m_{q_i}^4 + m_N^4) - 2m_N^4 m_{q_i}^2\right\}. \tag{32}$$

To integrate the expression (32) gives

$$\hat{\sigma}(q_i\overline{q}_i \to N_e\overline{\nu}_e) = \frac{2n_{q_i}^2\alpha^2|\mu^{\nu N}|^2\pi}{m_e^2\mu_B^2\hat{s}^4}\left\{\frac{\hat{s}^4}{3} + 2m_{q_i}^2\hat{s}^3 - \hat{s}^2\left[m_N^4 + 2m_N^2 m_{q_i}^2 + 2m_{q_i}^4\right] + \right.$$
$$\left. +2\hat{s}\left[\frac{m_N^6}{3} - m_N^4 m_{q_i}^2 + m_N^2 m_{q_i}^4\right] + 2m_N^6 m_{q_i}^2\right\}. \tag{33}$$

With the help of the obtained expression one can find $\sigma(pp \to \overline{\nu}_e N_e X)$. At the LHC energies and $\mu^{\nu N}$ being equal to $10^{-8}\mu_B$ the cross section of the reaction (31) is in the region of very small values 10^{-2} fb.

Let us approach to the problem of detecting the transit DMM $\mu^{\nu N}$ on the other hand. With zero value of $\mu^{\nu N}$, the dominant decay channel of the heavy neutrino is

$$N_a \to l_a + W_R^* \to l_a + 2j. \tag{34}$$

The corresponding decay width is defined by the expression

$$\Gamma(N \to lW_R^* \to ljj) \simeq N_c \frac{g_R^4 m_N^5}{1024\pi^3 m_{W_R}^4} \tag{35}$$

where the fermion masses have been neglected and the both lepton channels $\Gamma(N \to l^+ W_R^{-*}) = \Gamma(N \to l^- W_R^{+*})$ have been summed. However, if the $\mu_{ij}^{\nu N}$ moment has nonzero value, the heavy neutrino may also decay into the channel

$$N_l \to \gamma + \nu_l. \tag{36}$$

The decay width will look like

$$\Gamma(N_l \to \gamma\nu_l) = \frac{2\alpha|\mu^{\nu N}|^2 m_{N_l}^3}{\mu_B^2 m_e^2}. \tag{37}$$

We see that when $m_{N_l} = 100$ GeV and $\mu^{\nu N} = 10^{-8}\mu_B$ the decay width $\Gamma(N_{l_a} \to \gamma\nu_{l_a})$ could exceed $\Gamma(N_{l_a} \to \gamma l_a 2j)$ over several orders of magnitude. Note, that the DMM $\mu^{\nu N}$ rapidly decreases with the growth of m_N and in the region of $m_N \approx 300$ GeV the both decay widths have the same order of magnitude $\sim 10^{-6}$ GeV. Further one may choose the process of the heavy neutrino production having the most cross section and detect the heavy neutrino through the decay channel (36).

At LHC there are two possibilities for observing the heavy neutrino production. The former is the single heavy neutrino production that may take place due to the reaction

$$p + p \to W_R^* \to e^+ + N_e + X. \tag{38}$$

At $m_{W_R} = 4$ TeV, the cross section of this reaction is as high as 3×10^{-3} pb. This estimate of $\sigma(pp \to eN_eX)$ is valid for $m_N = 100$ GeV and are not practically changed to the extent $m_N \simeq 0.6 m_{W_R}$. Pair production of heavy neutrinos take place in the reaction

$$p + p \to Z_R^* \to N_e + \overline{N}_e + X. \tag{39}$$

Supposing the fulfillment of $m_{Z_R} = 1.7 m_{W_R} = 6.8$ TeV we have

$$\sigma(pp \to Z_R^* \to N_e N_e X) \simeq 3 \times 10^{-5} \text{ pb}. \tag{40}$$

The value (40) is also given for $m_N = 100$ GeV and it is weakly changed up to $m_N \simeq 0.4 m_{Z_R}$. So, we see, that for detecting heavy neutrinos the reaction (38) is the most perspective.

For m_{N_a} in the range of several hundreds GeV, the total N_a width is at most a few percents of m_a. Thus, we can take the narrow width approximation:

$$\sigma(pp \to W_R^* \to eN_e \to e\nu_e\gamma) \simeq \sigma(pp \to W_R^* \to eN_e) Br(N_e \to \nu_e\gamma). \tag{41}$$

Then, assuming that $m_{N_e} = 100$ GeV, $m_{W_R} = 4$ TeV and $\mu^{\nu N} = 10^{-8}\mu_B$, we obtain

$$\sigma(pp \to W_R^* \to eN_e \to e\nu_e\gamma) \simeq 3 \text{ fb}. \tag{42}$$

So, under the integrated luminosity $\int Ldt = 10$ fb^{-1} we shall observe 30 events. However, under increasing the heavy neutrino mass $Br(N_e \to \nu_e\gamma)$ is sharply decreased. For example, when $m_{N_e} = 300$ GeV there will be 15 events only.

Let us proceed to detection of μ^{NN}. We address to the pair production of the heavy neutrinos taking into account the DMM μ^{NN}. Then, we shall have

$$p + p \to Z_R^*, \gamma^* \to N_a + \overline{N}_b + X. \tag{43}$$

Note, that the weak and electromagnetic diagrams do not interfere. The corresponding subprocesses are as follows

$$q_i + \overline{q}_i \to Z_R^* \to N_a + N_b, \tag{44}$$

$$q_i + \overline{q}_i \to \gamma^* \to N_a + N_b \tag{45}$$

The cross section of (45) looks like

$$\sigma_{em} = \frac{2\alpha^2 |\mu^{N_a N_b}|^2 \pi}{3\mu_B^2 m_e^2} \sqrt{1 - \frac{4m_{N_a}^2}{s}}. \tag{46}$$

When $\mu^{NN} \approx 10^{-8}\mu_B$ and $m_{Z_R} = 6.8$ TeV, then the ratio

$$R = \sigma(pp \to \gamma^* \to N_a\overline{N}_a)/\sigma(pp \to Z_R^* \to N_a\overline{N}_a)$$

is close to one.

4 Conclusion

Within the left-right-symmetric model contributions to the neutrino dipole magnetic moments coming from the sectors of the gauge bosons and Higgs bosons have been considered. It has been shown that the contributions caused by the singly charged $\tilde{\delta}^{(\pm)}$-Higgs bosons could exceed that caused by the charged gauge bosons.

Investigation of the resonance conversion $\nu_{eL} \to \nu_{\mu L}$ (Mikheyev-Smirnov-Wolfenstein resonance) has revealed that in the heavy neutrino sector only two scenarios could be realized: (i) the heavy neutrino masses are quasi-degenerated and the mixing angles between heavy and light neutrinos are equal; (ii) the heavy neutrino masses are arbitrary and the mixing inside the same generation is absent.

It was proven that in oscillation experiments with left-handed light neutrinos beam we cannot observe the heavy neutrinos production even at energies $E_\nu > m_N$.

In collider experiments we can detect both the μ^{NN} and $\mu^{\nu N}$ moments. The most promising reactions are as follows

$$\nu_{\mu L} + p \to N_{\mu R} + X \qquad (\sigma \leq 10 \text{ fb}),$$
$$p + p \to \gamma^* \to N_{eR} + \overline{\nu}_{eL} + X \qquad (\sigma \leq 10^{-2} \text{ fb}).$$

The nonzero value of $\mu^{\nu N}$ could be also observed through the decay

$$N_{eR} \to \gamma^* \to \nu_{eL}.$$

A good example is the process

$$p + p \to W_R^* \to e + N_e \to e + \nu_e + \gamma + X.$$

Using the narrow width approximation we get

$$\sigma(pp \to W_R^* \to eN_e \to e\nu_e\gamma) \simeq \sigma(pp \to W_R^* \to eN_e)Br(N_e \to \nu_e\gamma) \leq 3 \text{ fb}.$$

References

[1] O.M.Boyarkin *Advanced Particles Physics, Volume II* (Taylor and Francis Group, New York, 2011).
[2] J.C.Pati and A.Salam, Phys. Rev. **D10**, 275 (1974).
[3] G.Boyarkina, O.Boyarkin, Eur. Phys. J. **C13**, 99, 2000.
[4] A.G.Beda *et al.*, Phys. Part. Nucl. Lett. **7**, 406 (2010).
[5] J.Kim, Phys. Rev. **D14**, 3000 (1976).
[6] O.M.Boyarkin, G.G.Boyarkina, Phys. Atom. Nucl. **76**, 504 (2013).

Proceedings of the International School-seminar
"New Physics and Quantum Chromodynamics at External Conditions", pp. 57 – 64,
May 22-24, 2013, Dnipropetrovsk, Ukraine

CHIRAL SYMMETRY BREAKING AND CENTER VORTICES

M. Faber[a], R. Höllwieser[b]

Institute of Atomic and Subatomic Physics, Vienna University of Technology, Operngasse 9, 1040 Vienna, Austria

We investigate the chiral properties of near-zero modes for thick classical center vortices in $SU(2)$ lattice gauge theory as examples of the phenomena which may arise in a vorex vacuum. In particular we analyze the creation of near-zero modes from would-be zero modes of various topological charge contributions from center vortices. We show that colorful spherical vortex and instanton ensembles have very similar Dirac eigenmodes and also vortex intersections are able to give rise to a finite density of near-zero modes, leading to chiral symmetry breaking via the Banks-Casher formula. We discuss the influence of the magnetic vortex fluxes on quarks and how center vortices may break chiral symmetry.

1 Introduction

The breaking of chiral symmetry is an effect which is strongly related to the structure of the non-perturbative vacuum of QCD. The only method at present available to tackle this non-perturbative problem is lattice QCD (LQCD). A well established theory of χSB relies on instantons [1–3], which are localized in space-time and carry a topological charge of modulus 1. According to the Atiyah-Singer index theorem [4], a zero mode of the Dirac operator arises, which is concentrated at the instanton core. In the instanton liquid model [5, 6] overlapping would-be zero modes split into low-lying nonzero modes which create the chiral condensate. Center vortices [7], closed magnetic flux tubes, are promising candidates for explaining confinement. The vortex model of confinement is theoretically appealing and was confirmed by a multitude of numerical calculations, both, in lattice Yang-Mills theory and within a corresponding infrared effective model, see *e.g.* [8, 9]. Lattice simulations indicate that vortices are responsible for topological charge and χSB as well [10–12], and thus unify all nonperturbative phenomena in a common framework. A similar picture to the instanton liquid model exists insofar as lumps of topological charge arise at the intersection and writhing points of vortices. The colorful, spherical SU(2) vortex was introduced in previous article of our group [13] and may act as a prototype for this picture, as it contributes to the topological charge by its color structure, attracting a zero mode like an instanton. We show how the interplay of various topological structures from center vortices (and instantons) leads to near-zero modes, which by the Banks-Casher relation [14] are responsible for a finite chiral condensate. We compute a varying number of the lowest-lying overlap Dirac eigenfunctions and visualize their chiral density.

2 Free Dirac eigenmodes

Fig. 1 shows the chiral density of free overlap eigenmodes obtained numerically using the MILC code. The modes are found with the Ritz functional algorithm [15, 16] with random start and for degenerate eigenvalues the eigenmodes span a randomly oriented basis in the degenerate subspace. Therefore the numerical modes presented in Fig. 1 are linear combinations of plane waves with momenta $\pm p_\mu$ and show plane wave oscillations of $2p_\mu$ in the chiral density. The first eight degenerate modes consist of plane waves with $p_4 = \pm\pi/24$, hence there is one sine (cosine) oscillation in time direction, the next eight have $p_4 = \pm 3\pi/24$, *i.e.*, three oscillations in the time direction. The oscillations of χ_R and χ_L are separated by half an oscillation length, *i.e.*, the maxima of ρ_+ correspond to minima of ρ_- and vice versa. Accordingly, the scalar density $\rho(x_\mu) = \frac{1}{2}(\chi_R^\dagger(x_\mu)\chi_R(x_\mu) + \chi_L^\dagger(x_\mu)\chi_L(x_\mu)) = 1/N_V$ is constant ($N_V \ldots$ lattice volume).

3 The Colorful Spherical Vortex

The spherical vortex was introduced in [13] and analyzed in more detail in [17] and [18]. It is constructed with t-links in a single time slice at fixed $t = t_i$, given by $U_t(x^\nu) = \exp\left(\mathrm{i}\alpha(|\vec{r} - \vec{r}_0|)\vec{r}/r \cdot \vec{\sigma}\right)$, where $\vec{r}$ is the spatial part of x_ν. The profile function $\alpha(r)$ changes from π to 0 in radial direction for the negative spherical vortex, or from π to 2π for the positive (anti-)vortex. This gives a hedgehog- like configuration, since the color vector points in (or against) the radial direction at the vortex radius R. The hedgehog-like structure is crucial for our

e-mail: [a]faber@kph.tuwien.ac.at, [b]hroman@kph.tuwien.ac.at

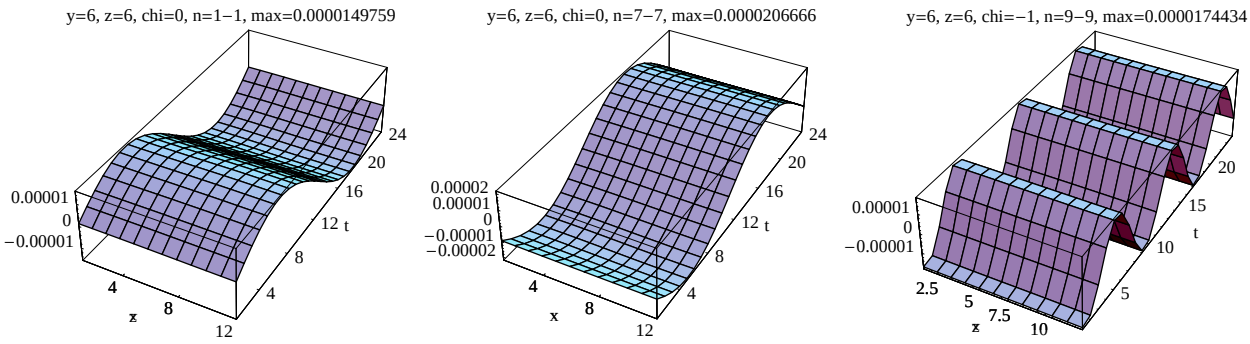

Figure 1. Chiral density of the low-lying eigenmodes of the free overlap Dirac operator: $\rho_5\#1$ (left), $\rho_5\#7$ (center) $\rho_5\#9$ (right). The modes clearly show the plane wave behavior with oscillations of $2p_\mu$ (see text).

analysis. The t-links of the spherical vortex define a map $S^3 \to SU(2)$, characterized by a winding number

$$N = -\frac{1}{24\pi^2}\int d^3x\, \epsilon_{ijk}\, \mathrm{Tr}[(U^\dagger\partial_i U)(U^\dagger\partial_j U)(U^\dagger\partial_k U)], \tag{1}$$

resulting in $N = -1$ for positive (anti-) and $N = +1$ for negative spherical vortices. Obviously such windings influence the Atiyah-Singer index theorem giving a topological charge $Q = -1$ for positive and $Q = +1$ for negative spherical vortices (anti-vortices). Hence, spherical vortices attract Dirac zero modes similar to instantons. In [18] we showed that the spherical vortex is in fact a vacuum-to-vacuum transition in the time direction which can even be regularized to give the correct topological charge also from gluonic definitions. In Fig. 2a we see that a single instanton has nearly exactly the same eigenvalues as a single spherical vortex. We interpreted the nonzero modes as eigenmodes of the free Dirac operator, which are shifted slightly because of their interaction with the nontrivial gauge field content. In Fig. 5 we show that even the chiral densities of the lowest eigenmodes distribute similarly, except for the fact that the response of the fermions to the spherical vortex is squeezed in the time direction, since the vortex is localized in a single time slice ($t = 5$). Another interesting issue is that the nonzero eigenmodes show plane wave oscillations, like the free eigenmodes in Fig. 1. We further plot the spectra of instanton–anti-instanton, spherical vortex-anti-vortex and instanton-anti-vortex pairs in Fig. 2a. We again see nearly exactly the same eigenvalues for instanton or spherical vortex pairs, but now we get instead of two would-be zero modes a near-zero mode for each pair. The chiral density plots in Fig. 6 for the instanton–anti-instanton pair and Fig. 7 for the spherical vortex-anti-vortex pair show, besides the similar densities, that the near-zero mode is a result of two chiral parts corresponding to the two constituents of the pairs. The nonzero modes can again be identified with the free overlap modes with the same side remark for mode #8. Finally in Fig. 2b we plot the eigenvalues of two (anti-)instantons and two spherical (anti-)vortices

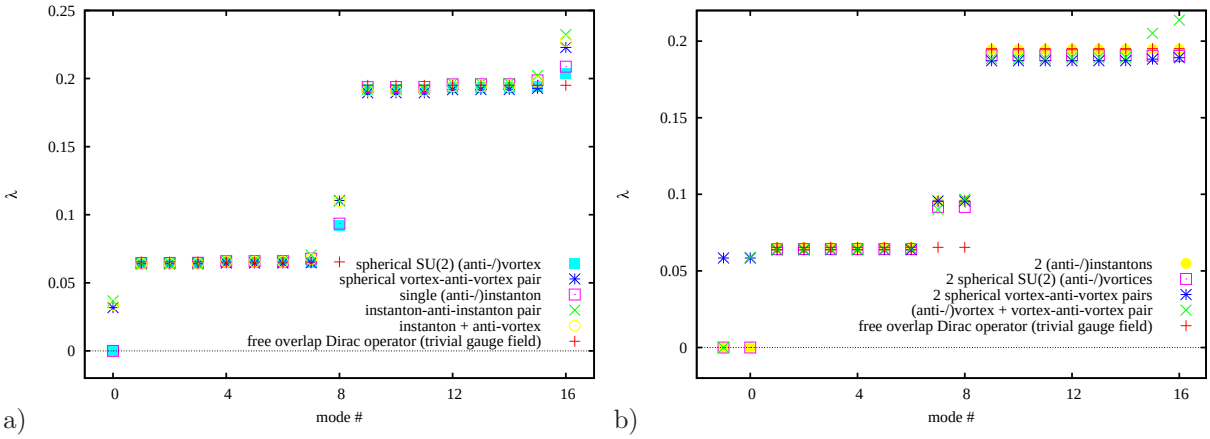

Figure 2. The lowest overlap eigenvalues for instanton and spherical vortex configurations compared to the eigenvalues of the free (overlap) Dirac operator.

giving topological charge $Q = 2$ ($Q = -2$) and therefore two zero modes, two vortex-anti-vortex pairs with two near-zero modes and a configuration with two vortices and an anti-vortex (*i.e.*, a single vortex plus one vortex-anti-vortex pair) giving one zero mode ($Q = 1$) and one near-zero mode. The results clearly show that

we may draw the same conclusions for spherical vortices as for instantons concerning the creation of near-zero modes.

4 Plane vortices

We define plane vortices parallel to two of the coordinate axes by links varying in a $U(1)$ subgroup of $SU(2)$. This $U(1)$ subgroup is generated by one of the Pauli matrices σ_i, *i.e.*, $U_\mu = \exp(\mathrm{i}\phi\sigma_i)$. Upon traversing a vortex sheet, the angle ϕ increases or decreases by π within a finite thickness of the vortex. Since we use periodic (untwisted) boundary conditions for the links, vortices occur in pairs of parallel sheets, each of which is closed by virtue of the lattice periodicity. We call vortex pairs with the same vortex orientation parallel vortices and vortex pairs of opposite flux direction anti-parallel. If thick, planar vortices intersect orthogonally, each intersection carries a topological charge $|Q| = 1/2$, whose sign depends on the relative orientation of the vortex fluxes [19], see Fig. 3. Fig. 3b indicates the position of the vortices after center projection, leading to (thin) P-vortices at half the thickness [8].

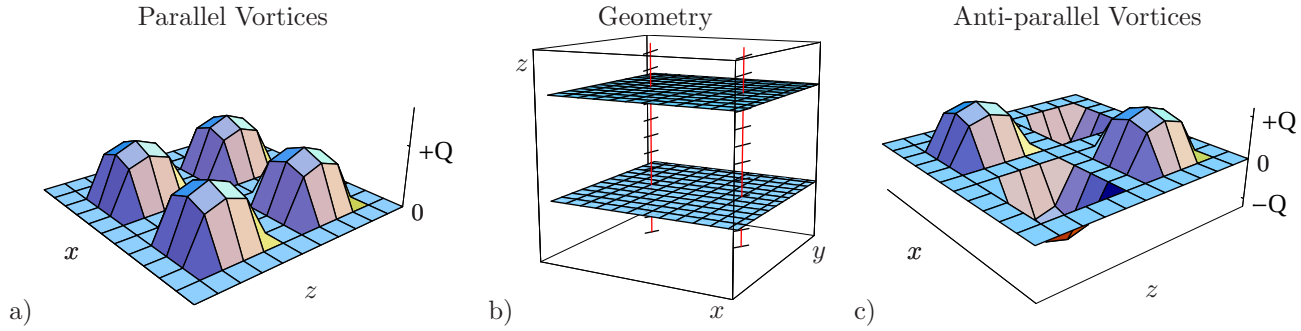

Figure 3. A single time-slice of a 12^4-lattice with intersecting vortices (center). The horizontal planes are the xy-vortices, which exist only at this time. The vertical lines are the zt-vortices, which continue over the whole time axis. The vortices intersect in four points, giving topological charge $Q = 2$ for parallel vortices (lhs) or $Q = 0$ for anti-parallel vortices (rhs).

For the configuration in Fig. 3a we get two real zero modes, according to the total topological charge $Q = 2$ of the four intersections. These modes we analyzed in [20], they peak at least at two of the four topological charge contributions of $Q = 1/2$. If we intersect anti-parallel vortex pairs orthogonally we get two intersection points with topological charge $Q = +1/2$ and two intersection points with topological charge $Q = -1/2$ (Fig. 3b), hence total $Q = 0$. For such a configuration we get four real near-zero modes, with local chirality peaks at the intersection points, according to their topological charge contribution, see Fig. 4b and compare to Fig. 3 c. Now, the mechanism of Sec. 3 or the analog instanton liquid model does not directly apply to the case of planar vortices, since there are no localized lumps of topological charge $Q = \pm 1$. Nevertheless the vortices attract chiral (near-)zero modes via their intersections with topological charge $Q = \pm 1/2$, which can be related to merons [21] and calorons [22]. We expect that vortex intersections, writhing points and even color structure contributions of vortices to topological charge are able to create a finite density of near-zero modes and break chiral symmetry via the Banks-Casher relation.

5 Conclusions

Fermions do not seem to make much of a difference between instantons and spherical vortices and the instanton liquid model can be extended to colorful spherical center vortices. Further also vortex intersections attract (would-be) zero modes which contribute via interactions to a finite density of near-zero modes with local chiral properties, *i.e.*, local chirality peaks at corresponding topological charge contributions. In Monte Carlo configurations we do not, of course, find perfectly flat or spherical vortices, as one does not find perfect instantons. The general picture of topological charge from vortex intersections, writhing points and even color structure contributions or instantons can provide a general picture of χSB: any source of topological charge can attract (would-be) zero modes and produce a finite density of near-zero modes leading to chiral symmetry breaking via the Banks-Casher relation. Here one also has to ask what could be the dynamical explanation of χSB. We can try the conjecture that only a combination of color electric and magnetic fields leads to χSB, electric fields accelerating color charges and magnetic fields trying permanently to reverse the momentum directions on spiral shaped paths. Such reversals of momentum keeping the spin of the particles should especially happen for very slowly moving color charges. Alternatively we could argue that magnetic color charges are able to flip the spin of slow quarks, *i.e.* when they interact long enough with the vortex structures. Finally, it seems that vortices not only confine quarks into bound states but also change their helicity in analogy to the instanton liquid model. In accordance with Casher's argument, a force strong enough to confine quarks is also generally expected to break

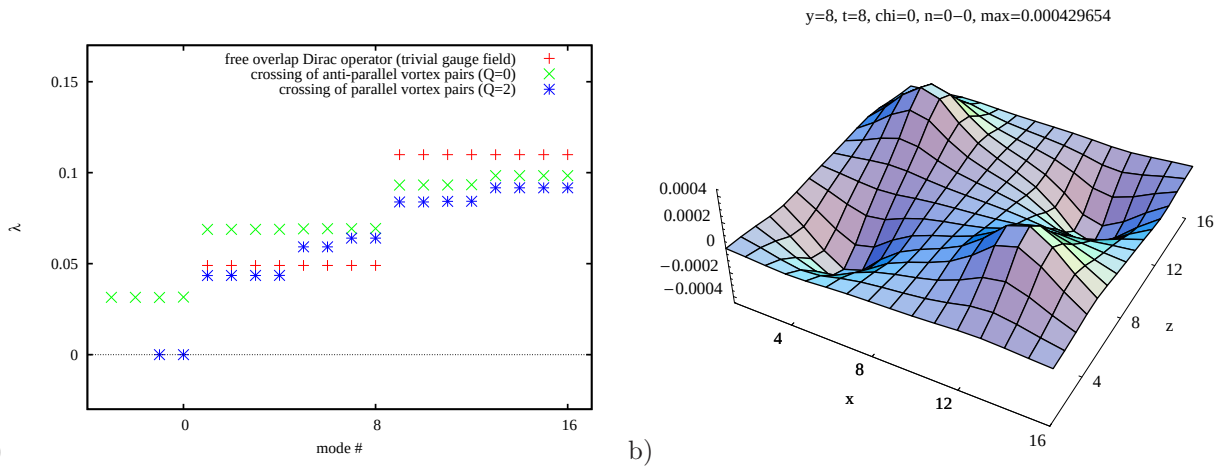

Figure 4. a) The lowest overlap eigenvalues for plane vortex configurations compared to the eigenvalues of the free (overlap) Dirac operator (red crosses) and spherical vortex configurations. b) Chiral density $\rho_5\#0$ in the intersection plane of all four near-zero modes of crossing flat vortex pairs with opposite flux direction ($Q = 0$).

chiral symmetry [23], we therefore conclude that the center vortex model of quark confinement may indeed be capable of describing chiral symmetry breaking. We should also mention that other mechanisms of chiral symmetry breaking in addition to the instanton liquid paradigm may be operative in the Yang-Mills vacuum. For instance, it also seems possible that, even in the absence of would-be zero modes, the random interactions of quarks with the vortex background may be strong enough to smear the free dispersion relation such that a finite Dirac operator spectral density at zero virtuality is generated. In fact, a confining interaction by itself generates chiral symmetry breaking, independent of any particular consideration of would-zero modes connected to topological charge. However, this effect on its own is not sufficiently strong for a quantitative explanation of the chiral condensate; other effects, among them possibly the ones considered in this article, must play a role. We cannot give a conclusive answer to the question of a dynamical explanation for the mechanism of χSB and only speculate on the importance of our results for Monte Carlo configurations, since there vortices are neither perfectly flat nor spherical, as there are no perfect instantons either. But the importance of the long-range nature of low-dimensional topological structures for the understanding of the mechanism of χSB in QCD was underlined by various results of different groups [24–30], and agrees well with a vortex picture of χSB. For more details see [31].

Acknowledgements. We thank Štefan Olejník and Michael Engelhardt for helpful discussions. This research was supported by the Austrian Science Fund FWF ("Fonds zur Förderung der wissenschaftlichen Forschung") under Contract No. P22270-N16 (R.H.).

References

[1] A. A. Belavin, A. M. Polyakov, A. S. Schwartz, and Y. S. Tyupkin, "Pseudoparticle solutions of the Yang-Mills equations," *Phys. Lett.* **B59**, 85–87 (1975).

[2] A. Actor, "Classical Solutions of SU(2) Yang-Mills Theories," *Rev. Mod. Phys.* **51**, 461 (1979).

[3] G. 't Hooft, "Computation of the quantum effects due to a four- dimensional pseudoparticle," *Phys. Rev.* **D14**, 3432–3450 (1976).

[4] M. F. Atiyah and I. M. Singer, "The Index of elliptic operators. 5", *Annals Math.* **93**, 139–149 (1971).

[5] E.-M. Ilgenfritz and M. Muller-Preussker, "Statistical Mechanics of the Interacting Yang-Mills Instanton Gas", *Nucl. Phys.* **B184**, 443 (1981).

[6] D. Diakonov and V. Y. Petrov, "Chiral Condensate in the Instanton Vacuum," *Phys. Lett.* **B147**, 351–356 (1984).

[7] G. 't Hooft, "On the phase transition towards permanent quark confinement," *Nucl. Phys.* **B138**, 1 (1978).

[8] L. Del Debbio, and M. Faber, and J. Greensite, and Š. Olejník, "Center dominance and Z(2) vortices in SU(2) lattice gauge theory," *Phys. Rev.* **D55**, 2298–2306 (1997).

[9] M. Engelhardt and H. Reinhardt, "Center vortex model for the infrared sector of Yang-Mills theory: Confinement and deconfinement," *Nucl. Phys.* **B585**, 591–613 (2000).

[10] P. de Forcrand and M. D'Elia, "On the relevance of center vortices to QCD," *Phys.Rev.Lett.* **82**, 4582–4585 (1999).

[11] M. Engelhardt, "Center vortex model for the infrared sector of Yang-Mills theory: Quenched Dirac spectrum and chiral condensate," *Nucl.Phys.* **B638**, 81–110 (2002).

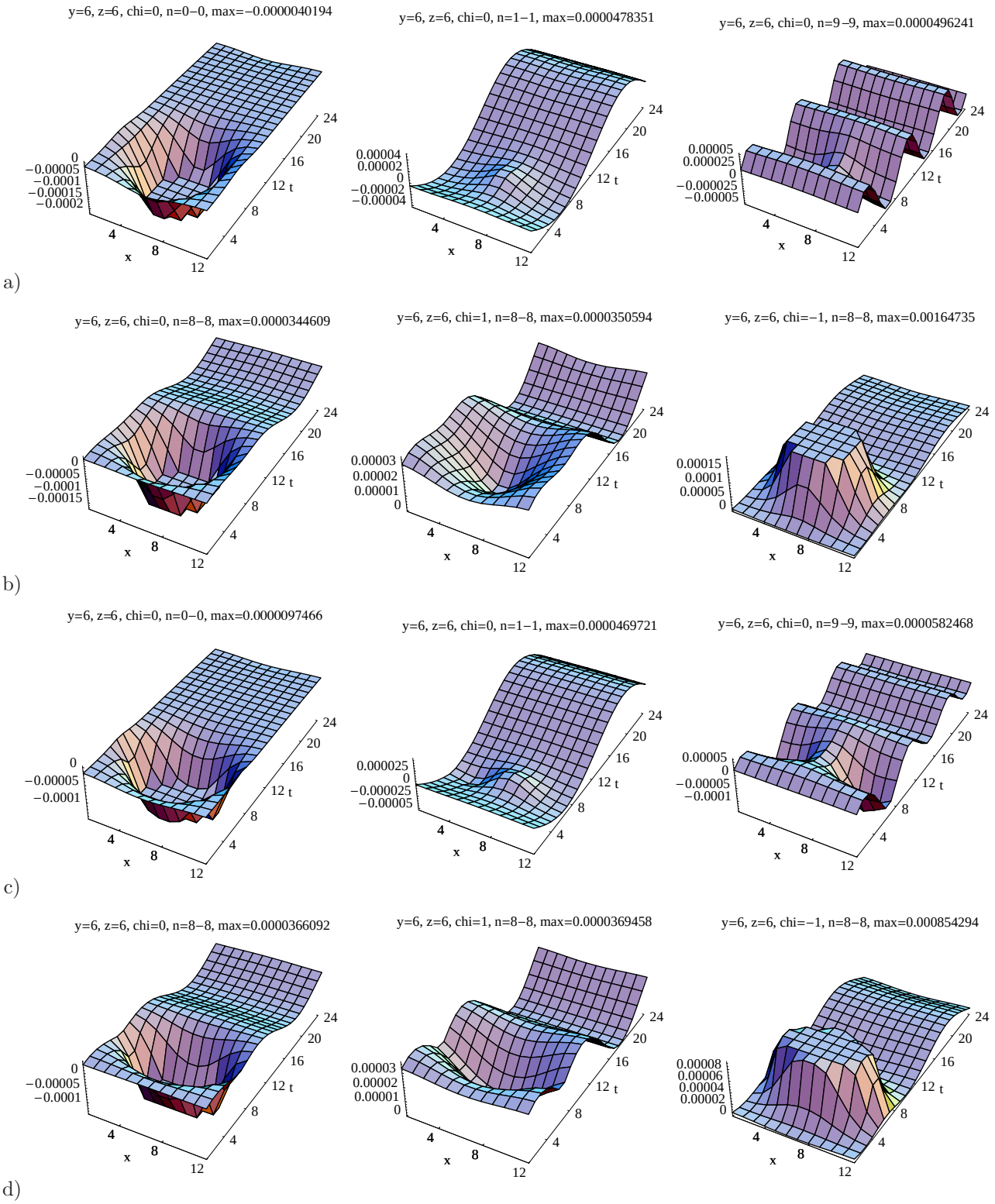

Figure 5. Chiral densities of overlap eigenmodes: a) zero mode (left), first (center), ninth (right) and b) eighth (ρ_5 left, ρ_+ center and ρ_- right) nonzero modes for an instanton; c) and d) the same as a) and b) but for a spherical vortex.

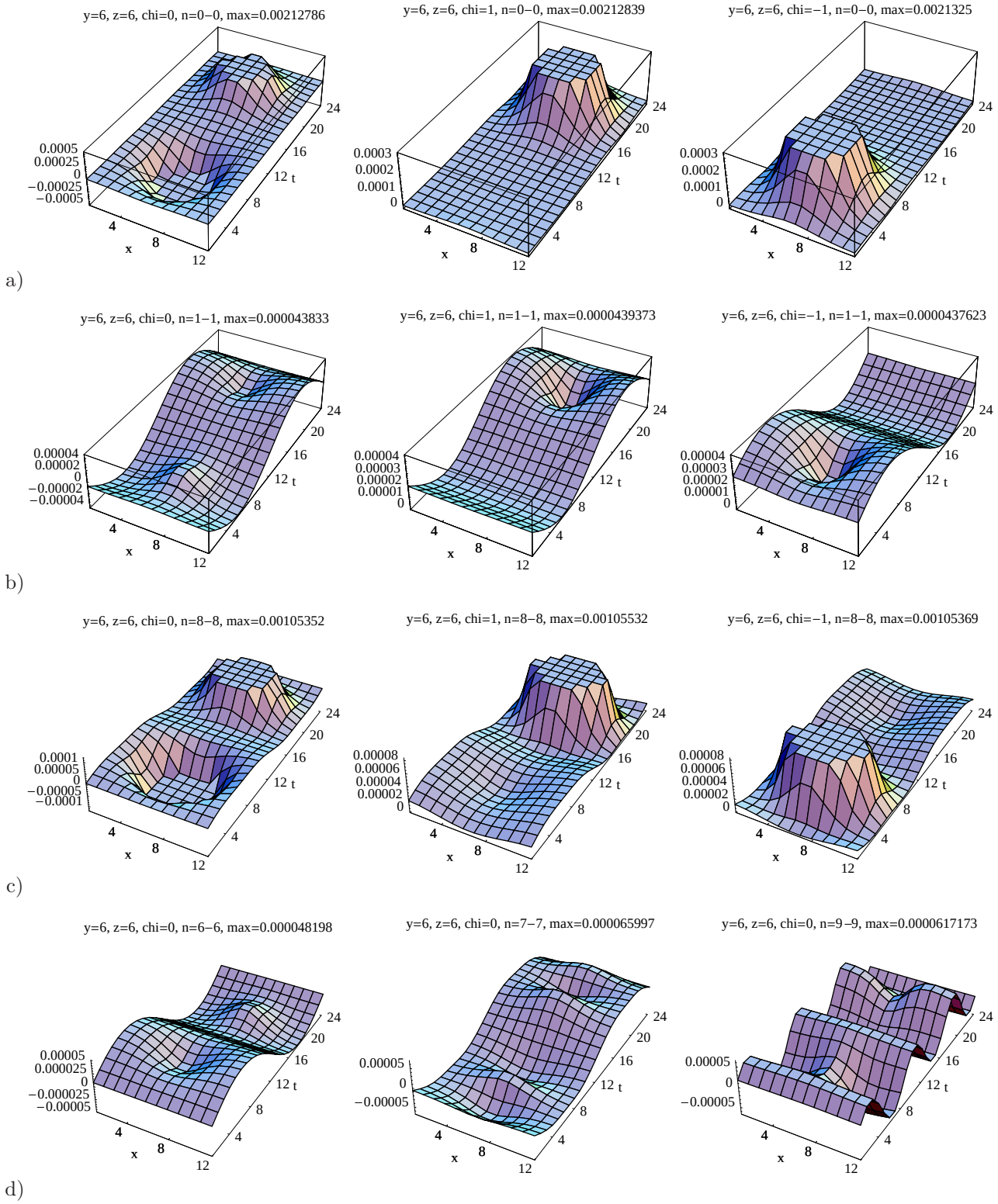

Figure 6. Chiral densities (ρ_5 left, ρ_+ center and ρ_- right column) of the a) lowest (near-zero), b) second-lowest (nonzero) and c) eighth (nonzero) eigenmode of the overlap Dirac operator for an instanton–anti-instanton pair. d) ρ_5 of the sixth (left), seventh (center) and ninth (right) eigenmode.

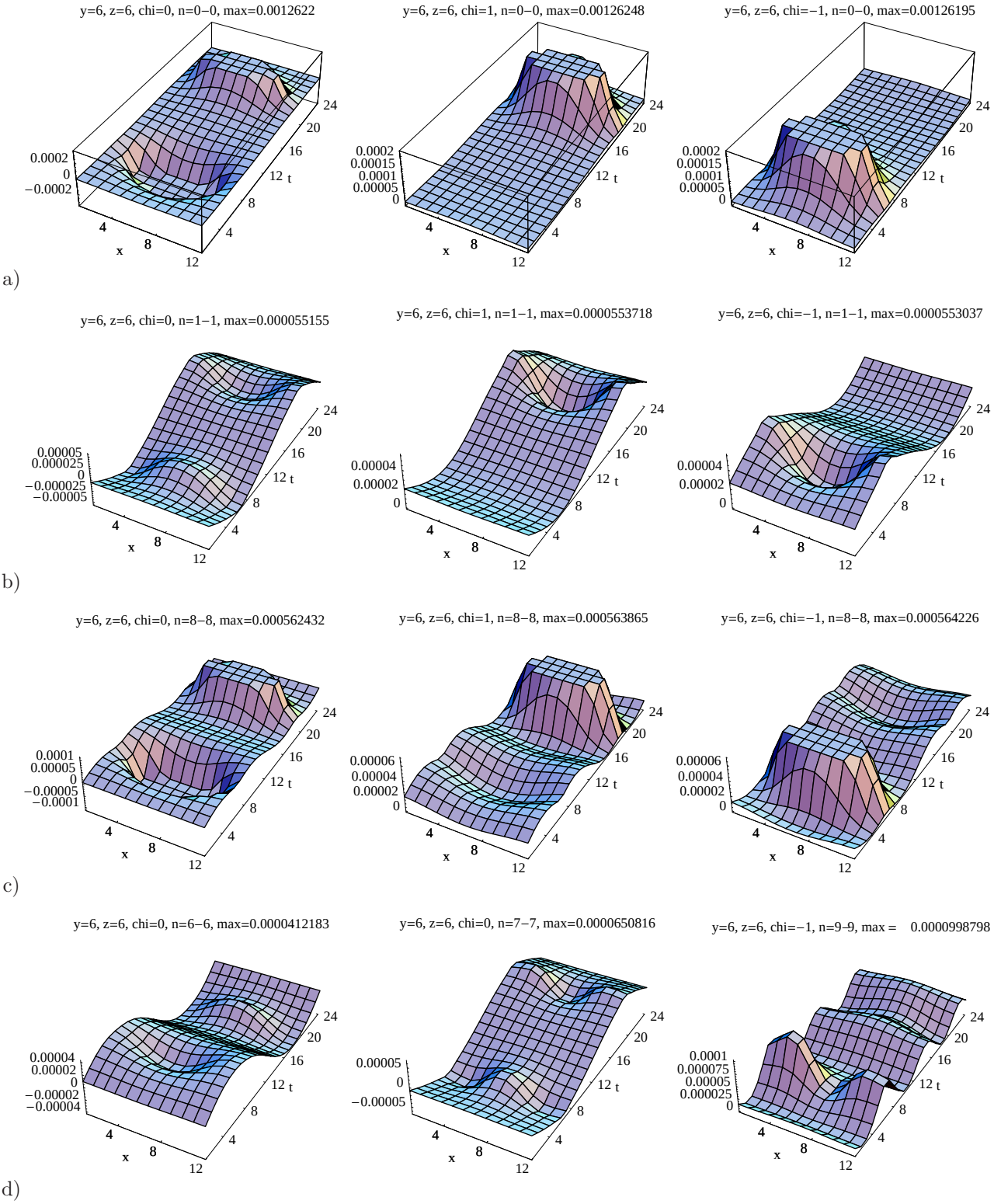

Figure 7. Same as Fig. 6 but for a spherical vortex-anti-vortex pair. Chiral densities (ρ_5 left, ρ_+ center and ρ_- right column) of the a) lowest (near-zero), b) second-lowest (nonzero) and c) eighth (nonzero) eigenmode. d) ρ_5 of the sixth (left), seventh (center) and ninth (right) eigenmode.

[12] R. Höllwieser, and M. Faber, and J. Greensite, and U.M. Heller, and Š. Olejník, "Center Vortices and the Dirac Spectrum," *Phys. Rev.* **D78**, 054508 (2008).

[13] G. Jordan, and R. Höllwieser, and M. Faber, and U.M. Heller, "Tests of the lattice index theorem," *Phys. Rev.* **D77**, 014515 (2008).

[14] T. Banks and A. Casher, "Chiral Symmetry Breaking in Confining Theories," *Nucl. Phys.* **B169**, 103 (1980).

[15] B. Bunk, K. Jansen, B. Jegerlehner, M. Lüscher, H. Simma, *et. al.*, "A New simulation algorithm for lattice QCD with dynamical quarks," *Nucl.Phys.Proc.Suppl.* **42**, 49–55 (1995).

[16] T. Kalkreuter and H. Simma, "An Accelerated conjugate gradient algorithm to compute low lying eigenvalues: A Study for the Dirac operator in SU(2) lattice QCD," *Comput.Phys.Commun.* **93**, 33–47 (1996).

[17] R. Höllwieser, and M. Faber, and U.M. Heller, "Lattice Index Theorem and Fractional Topological Charge, arxiv:1212.3737.

[18] T. Schweigler, R. Höllwieser, M. Faber, and U.M. Heller, "Colorful SU(2) center vortices in the continuum and on the lattice, arxiv:.

[19] M. Engelhardt and H. Reinhardt, "Center projection vortices in continuum Yang-Mills theory," *Nucl. Phys.* **B567**, 249 (2000).

[20] R. Höllwieser, and M. Faber, and U.M. Heller, "Intersections of thick Center Vortices, Dirac Eigenmodes and Fractional Topological Charge in SU(2) Lattice Gauge Theory," *JHEP* **1106**, 052 (2011).

[21] H. Reinhardt and T. Tok, "Merons and instantons in laplacian abelian and center gauges in continuum Yang-Mills theory", *Phys. Lett.* **B505**, 131–140 (2001).

[22] F. Bruckmann, E.-M. Ilgenfritz, B. Martemyanov, and B. Zhang, "The Vortex Structure of SU(2) Calorons," *Phys. Rev.* **D81**, 074501 (2010).

[23] A. Casher, "Chiral Symmetry Breaking in Quark Confining Theories," *Phys. Lett.* **B83**, 395 (1979).

[24] I. Horvath, S. Dong, T. Draper, K. Liu, N. Mathur, *et. al.*, "Uncovering low dimensional topological structure in the QCD vacuum, hep-lat/0212013.

[25] I. Horvath, S. Dong, T. Draper, F. Lee, K. Liu, *et. al.*, "Low dimensional long range topological structure in the QCD vacuum," *Nucl.Phys.Proc.Suppl.* **129**, 677–679 (2004).

[26] P. O. Bowman, K. Langfeld, D. B. Leinweber, A. Sternbeck, L. von Smekal, *et. al.*, "Role of center vortices in chiral symmetry breaking in SU(3) gauge theory," *Phys.Rev.* **D84**, 034501 (2011).

[27] V. Braguta, P. Buividovich, T. Kalaydzhyan, S. Kuznetsov, and M. Polikarpov, "The Chiral Magnetic Effect and chiral symmetry breaking in SU(3) quenched lattice gauge theory," *Phys.Atom.Nucl.* **75**, 488–492 (2012).

[28] E.-A. O'Malley, W. Kamleh, D. Leinweber, and P. Moran, "SU(3) centre vortices underpin confinement and dynamical chiral symmetry breaking," *Phys.Rev.* **D86**, 054503 (2012).

[29] P. Buividovich, T. Kalaydzhyan, and M. Polikarpov, "Fractal dimension of the topological charge density distribution in SU(2) lattice gluodynamics," *Phys.Rev.* **D86**, 074511 (2012).

[30] V. Braguta, P. Buividovich, T. Kalaydzhyan, and M. Polikarpov, "Topological and magnetic properties of the QCD vacuum probed by overlap fermions," *PoS* **ConfinementX**, 085 (2012).

[31] R. Höllwieser, T. Schweigler, M. Faber, and U. M. Heller, "Center Vortices and Chiral Symmetry Breaking in SU(2) Lattice Gauge Theory, arxiv:1304.1277.

Proceedings of the International School-seminar
"New Physics and Quantum Chromodynamics at External Conditions", pp. 65 – 72,
May 22-24, 2013, Dnipropetrovsk, Ukraine

HOLOGRAPHIC SUPERCONDUCTIVITY: THE PAST, THE PRESENT, AND THE FUTURE

A. J. Nurmagambetov[a]

A.I. Akhiezer Institute for Theoretical Physics NSC KIPT, 1 Akademicheskaya St., 61108 Kharkiv, Ukraine

I review one of the recently found magic relations of "artificial" (from the CMP audience point of view) String Theory to real problems in Condensed Matter Physics.

1 Prologue

The theory of High-T superconductivity (HTS) [1] is still a theorists' battle field. Two most common approaches in the mid of 80th, partially explaining the experimental data for both, were the emergency of HTS from antiferromagnetic spin fluctuations in a doped system [2], and the interlayer coupling model of a BCS-type [3].[1] Recent experiments with cuprates [8] gave more precise data in favour of the first approach, based on the Habbard-type Hamiltonian [9]. However, the second (third, forth etc., see [4]– [7] among them) approach can not be a priori rejected for other HT superconductors.

Prospects in establishing the complete HTS theory are widely discussed in literature (see, e.g., the discussion in [10]), though the community is rather sceptical on finding the solution within the present paradigm of superconductivity – electron-electron, electron-phonon interactions, spin fluctuations etc. New ideas are welcome and really wanted to resolve this puzzle. One of the new ideas that may refresh the old-school CMP theoretical ground came recently from Strings [11] (see also the recent Lecture Notes [12] on the subject, and Refs. therein). The approach of Holographic Superconductivity (HSC) to the description of the HTS was so unexpected and "alchemical" for the CMP audience, that at the first stage of its development it was almost ignored on the traditional CMP side. Later on, some lingering criticism was addressed to the HSC approach (I will postpone the discussion around to the main body of the paper), but now ideas of the AdS/CMT correspondence are germinating into the CMP ground, mostly by efforts of distinguished persons like Subir Sachdev and Jan Zaanen.

The aim of these notes is twofold: On one hand, to make formalism of the AdS/CFT correspondence slightly convenient in use for CMP practitioners; perhaps, some of them will be interested in applying the AdS/CMT correspondence for solving specific tasks. On the other hand, the notes are aimed at explaining in brief key ideas of HTS theory to QFT or String theory practitioners; perhaps, some of them will get new excitement of doing something in another branch of physics. Limited in volume, these notes are neither comprehensive, nor pedagogical; I make no claim of originality for the content. But the hope is somebody will find the discussed subject interesting enough to start the own researches in a highly non-trivial interplay between String Theory and Condensed Matter Physics.

2 Holographic Superconductivity: the Presence

Attempts to resolve the HTS problem on the CMP side led to the important conclusion: Whatever the final theory would be, it should be a theory with a strong coupling constant. This conclusion is easy to reach, because the standard theory of superconductivity – the BCS theory – does not describe the HTS et all. Recall, the BCS theory is one of the most profound and successful theories for physical systems in the weak coupling constant regime. But the analysis of common features of different HTS samples (see, e.g., [13]) showed the strong difference between corresponding mechanisms of forming the superconducting state in conventional[2] and non-conventional[3] superconductors. Moreover, magnetism, playing the destructive role for conventional superconductors, is in the ground of new mechanism of the HTS state forming. Roughly, the BCS theory with an electric-type coupling constant has to be dual to the HTS theory with a magnetic-type coupling constant, similar to the Dirac electric-magnetic duality in QED. These reasons lead the HTS to a theory at a strong

[1] I would like to refer to less common, if not marginal, approaches to the HTS [4]– [7], which, for my opinion, are also worth mentioning.

[2] like mercury or lead

[3] like cuprates, iron-based HT superconductors, organic compounds and heavy fermion (uranium-based) exotic compounds with superconducting properties

e-mail: [a]ajn@kipt.kharkov.ua

coupling constant. We know, mostly from the QCD experience, that if a model with the strong coupling constant possesses non-trivial properties, they are hard to analyze with perturbative tools. Non-perturbative tools are also restrictive, that is why a real progress in formulation of the HTS theory within conventional CMP wisdom is almost stopped. But a crucial observation in Stringy description of Black Hole physics, now recognized as the AdS/CFT correspondence [15], [16], [17], gives a possibility to equate, in the strong version of this duality, non-perturbative and perturbative physics, but in framework of two different dual theories. Following the AdS/CFT, one of the dual theories, in the weak coupling constant regime, is a gravitation theory with matter on AdS background. Hence the main question in the context of High-T superconductivity is: What is the dual classical theory of gravity with matter for the strongly coupled quantum states of the HTS theory?

Even at this point some "mystery" has been appeared. The way to describe HTS models through AdS gravity with matter looks really strange from a CMP practitioner point of view. To resolve this puzzle, one should have in mind, the AdS/CFT prescription is just a convenient way to reformulate the problem in more tractable manner: *There is not any gravity inside a superconductor et all! It's just a recipe to compute observables on the dual field theory side.*[4]

But it is not the end of the story. When the CMP practitioner realizes that the Black Hole presence on the gravity side becomes crucial for modelling the HTS properties, his/her reaction is easy to predict: "It's a mess!" That's why only a small amount of real critics was addressed, up to now, from the CMP community side to the Holographic Superconductivity approach: People can not understand how it works.

Something interesting and important for traditional CMP practitioners is missing in this way. To realize the missing points of the Holographic Superconductivity approach, let's try to understand details.

2.1 The "alchemy" of AdS/CFT

The HSC is a part of more wide AdS/CMT correspondence – the correspondence between gravitational theories in the AdS bulk and non-gravitational Condensed Matter theories on the boundary of the AdS space.[5] Models of AdS/CMT are united by common features. Strong coupling constant, non-zero temperature, finite density of states/charges are among them. These models are featured by rejection of some CMP concepts like particles, quasi-particles, crystal lattice and their interplay, which are in the ground of any solid state theory, including the BCS theory. The AdS/CMP correspondence deals with effective ensembles/condensates instead, which come after integration over the Condensed Matter field theory degrees of freedom in the special limit, when the number of d.o.f. comes to infinity. Last but not least, all of the AdS/CMT models are effectively described in terms of gravitational theories.

To realize the gravity/field theory duality, one should follow the prescriptions proposed in early papers on the AdS/CFT [15], [16], [17]. These prescriptions were confirmed in case by case studies later on. Though there is not any explicit proof of the AdS/CFT correspondence till now, a counterexample, which falls into the requirements for such a duality, has not been found yet.

As it has been noticed, the AdS/CFT correspondence is the duality between gauge theory on the boundary of $\mathrm{AdS}_{\mathrm{d}+1}$, at the strong coupling constant regime, to gravitational theory with matter on $\mathrm{AdS}_{\mathrm{d}+1}$, at the weak coupling constant regime. Fields and their characteristics on $\mathrm{AdS}_{\mathrm{d}+1}$ are in the following correspondence with d-dimensional gauge theory observables:

$$\begin{aligned}
&\bullet\ \text{Matter fields in AdS} \rightsquigarrow \text{local boundary CFT operators;}\\
&\bullet\ \text{Spin } s\text{/mass } m \text{ of fields} \quad \rightsquigarrow \quad \text{spin } s\text{/scaling dimension } \Delta \text{ of local operators;}\\
&\bullet\ \text{Gauge fields in AdS} \rightsquigarrow \text{boundary currents.}
\end{aligned} \tag{1}$$

This short list can be further extended if necessary (see, e.g., [14]).

The first point of the duality (1) is the correspondence between matter fields in AdS to local Conformal Field Theory (CFT) operators. If fields, even on a constant curvature space, are easy to realize, how to define the local CFT operator corresponding to a matter field? Let's use the asymptotic expansion of an AdS field $\Theta(x,z)$ near the AdS boundary $z=\epsilon$ $(\epsilon\to 0)$ to this end[6]:

$$\Theta(x,z)=\mathcal{J}(x)z^{\Delta_-}\left(1+\ldots\right)+\mathcal{B}(x)z^{\Delta_+}\left(1+\ldots\right)\,. \tag{2}$$

$\Delta_\pm$ in (2) are the scaling dimensions of the field. They can be found from the expansion of the corresponding AdS field equation of motion near the boundary $z=\epsilon$ (see, e.g., [19] for details). Clearly, the determining

[4] The same concerns, e.g., computations with Feynman diagrams. The diagrams is a fiction, giving the recipe of computing the amplitudes.

[5] The AdS/CMT correspondence also includes holographic hydrodynamics, researches in QCD and quark-gluon plasma, (super)conductor/insulator quantum phase transitions, strange metals and more (see, e.g., a comprehensive review [14], and Refs therein).

[6] Here I use the AdS coordinate system, in which the AdS boundary is at $z=0$; the AdS metric is $ds^2_{AdS}=z^{-2}(\eta_{\mu\nu}dx^\mu dx^\nu+dz^2)$, x^μ are the coordinates of the flat d-dimensional boundary (see [18], [19] for details).

relations for Δ are different for different fields. For scalars one gets $\Delta(\Delta - d) = m^2L^2$, where m and L are, respectively, the mass of the field and the AdS space characteristic length. For a vector field in AdS one gets $\Delta(\Delta - d + 2) = m^2L^2$. Then, $\Delta_\pm$ in (2) are the highest and the lowest roots of the Δ determining relation. Other terms of (2), hidden in dots, are regular on the boundary $z = 0$ terms.

For any AdS space, masses of matter fields in AdS have to be bounded from below, to have well-defined unitary QFT in AdS. Such a restriction is known as the Breitenlohner-Freedman (BF) bound [20], which guarantees the stability of AdS space under perturbations of fields[7]

$$m^2L^2 \geq -\frac{d^2}{4}\,, \tag{3}$$

and the BF bound leads to the following inequality on the scale parameter $\Delta_- \leq 0$. Therefore, the limit $z \to 0$ is not well defined in (2) for a massive scalar field. Adding the appropriate boundary counterterm to the AdS scalar field action removes the divergency, turning the action to the following form

$$S_{AdS} \sim \lim_{\epsilon\to 0} \int_{z=\epsilon} [Dx]\ (d - 2\Delta_-)\, \mathcal{J}(x)\mathcal{B}(x) + \text{regular terms}\,. \tag{4}$$

Now, it's the GKPW celebrated rule time. Following [15], [16], [17], the main rule of the AdS/CFT correspondence is

$$\langle \exp\left(i \int d^dx\, \mathcal{J}(x)\mathcal{O}(x)\right)\rangle_{QFT} = \exp\left(-iS_{bulk}\left[\Theta(x,z)_{|_{z=0}} \to \mathcal{J}(x)\right]\right)\,, \tag{5}$$

according to which the regularized boundary value of the AdS matter field acts like a source to the local CFT operator. Comparing (5) to (4), it is easy to identify $\mathcal{J}(x)$ with the source, and $\mathcal{B}(x)$ with the v.e.v. of the CFT operator $\mathcal{O}(x)$, since the standard QFT manipulations result in

$$\langle \mathcal{O}(x)\rangle = \frac{\delta}{\delta \mathcal{J}(x)} \left(\int d^dx\, \mathcal{J}(x)\mathcal{O}(x)\right)|_{\mathcal{J}=0}\,. \tag{6}$$

Next subtle point is to define the local CFT operators for AdS gauge fields. They are massless, hence $\Delta_- = 0$ for Maxwell and graviton fields. Their boundary values at $z = 0$ coincide with the sources $\mathcal{J}(x)$. Then the symmetry arguments can be used to identify the local CFT operator $\mathcal{O}_m$, corresponding to the gauge boson A_m, with the conserved current J_m; similarly, the local CFT operator $\mathcal{O}_{mn}$ of the graviton field g_{mn} is identified with the energy-momentum tensor T_{mn}. Looking ahead, the local CFT operator of the AdS scalar field, $\mathcal{O}(x) = \Phi(x)$, will play the role of the order parameter in the simplest model of Holographic Superconductivity.

2.2 Main ingredients to build Holographic Superconductor

Let's turn to the construction of a Holographic Supeconductor. Modelling HSC one needs [11]:

- Gravity with matter in AdS, and dual gauge CFT on the flat boundary;
- Non-extremal (charged) AdS Black Hole;
- Interacting with gravity and other gauge fields charged scalar (vector/tensor) with a big enough charge.

(7)

Implementation of (7) results in modeling the phase transition, at some critical temperature T_c, with forming the energy gap. The charged scalar (possibly vector/tensor) field is the BH "hair", which condenses at the boundary. This condensate models the Cooper pairs in HSC.

This is a general scheme. But what are the things behind? How does it work?

Now, the first point in the HSC building instruction (7) does not seem so magic: We are trying to describe a theory at the strong coupling constant by use of the AdS/CFT machinery. But the second point of (7) contains something new. So, we need to understand the role of Black Holes (BHs) in the HSC picture.

It is well known, after Hawking, fact that Black Holes are not black. They can radiate, and its radiation can be measured in thermal units. In other words, Black Holes are warm (or even hot), until they will be evaporated, or will reach a stable extremal limit with zero Hawking temperature. This is the fate of all BHs, unless they live in a space with a compact boundary. The latter is realized only for one case of constant curvature manifolds: For Anti-de-Sitter space. The fate of AdS BHs is more optimistic; even some of them may be transformed into "eternal" BHs. Such transformation becomes possible due to condensation and evaporation of the emitted particles with further absorption by the BH, establishing the thermodynamic equilibrium in the end, see Fig. 1.[8] But it means, that the boundary has the same temperature as the AdS bulk, and this temperature is the

[7] Roughly, one may neglect the back-reaction of fields on the AdS geometry when the BF bound is satisfied. But such a backreaction has to be taken into account once the BF bound is violated.

[8] This picture is very close to the Earth's water cycle: The amount of water on the Earth did not change since the dinosaurs epoch. The Earth's atmosphere plays the role of the compact boundary.

Hawking temperature of the AdS-BH. Therefore, the first role of BHs in forming the HSC is to set non-zero temperature in the boundary field theory.

Another role of the AdS-BHs in the story is more subtle: Some of the emitted particles may condense on the boundary. They will not evaporate, and will form the condensate of the corresponding BHs "hairs". To realize a simple scenario with non-trivial scalar hair, which will be responsible for the phase transition to the superconducting state, one should find a black hole that has the scalar hair at low temperatures, but has not the hair at high temperatures. This is a non-trivial task. However, it was shown [21] that, for a real scalar field Ψ with arbitrary potential $V(\Psi)$, neutral AdS black holes have the scalar hair iff AdS is unstable. Gubser [22] argued that a charged scalar field around a charged black hole would have the desired property. It's because of the scalar effective potential in the background of the AdS charged BH (the Maxwell field is chosen to be $A_m = (A_t, 0, 0, \ldots, 0)$)

$$V_{eff.}(\Psi) = \sqrt{-g}\left[m^2 + A_t g^{tt} A_t\right]\Psi^2\,. \tag{8}$$

Since $g^{tt} < 0$ for AdS space, the effective mass of the scalar field decreases; there is a chance to form a non-trivial scalar hair (see below). Once formed, the scalar hair condensate plays the role of the "Cooper pairs" condensate, if, of course, it remains stable.

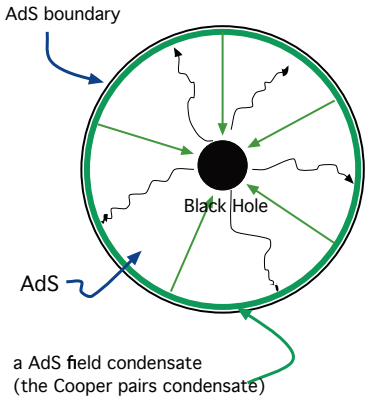

Figure 1. Thermal equilibrium in AdS-Black-Hole space.

Finally, the realization of the third point of (7), on a big enough charge of the BH hair, makes possible to focus on the much simple probe limit, neglecting the back-reaction of the AdS matter fields on the AdS-Black Hole background.

Now, how it looks in details. The proposed in [11] Lagrangian is

$$\frac{\mathcal{L}}{\sqrt{-g}} = \frac{1}{2k^2}\left(R + \frac{6}{L^2}\right) - \frac{1}{4e^2}F_{mn}F^{mn} - \frac{1}{e^2}\left(|\nabla\Psi - iA\Psi|^2 + m^2\Psi^2 + V(|\Psi|)\right), \tag{9}$$

and it describes the interacting system of AdS_4 gravity with Maxwell and charged scalar fields. In the probe limit $e^2 \gg k^2$, and with $V(|\Psi|) \sim |\Psi|^4$, the system is reduced to that of the Ginzburg-Landau (GL) phenomenological theory. But it turns out that for our purposes it is enough to consider trivial potential $V(|\Psi|) = 0$; the phase transition occurs even with this choice.

The gravity part of (9) supports the Reissner-Nordstrom (RN) charged BH solution, geometry of which is, in general, defined by[9]

$$ds^2 = \left[-f(r)dt^2 + g(r)dr^2 + r^2(dx^2 + dy^2)\right], \qquad (r = L/z)\,, \tag{10}$$

$$A = \gamma h(r)dt \quad \rightsquigarrow \quad A_m = (\gamma h(r), 0, 0, 0).$$

The unitarity requirement restricts the effective mass of the scalar field $(m^2 - 2\gamma^2)/6$ to the BF bound value (recall, $m^2_{BF}L^2 = -d^2/4$ for AdS_{d+1}), but near-horizon the AdS-RN BH has the geometry of $AdS_2 \times R_2$, so the effective mass of the scalar field, in $\Psi = \Psi(r)$ ansatz, can be chosen below the AdS_2 BF bound

$$(m^2 - 2\gamma^2) < -\frac{3}{2}\,. \tag{11}$$

This choice provides the instability in deep inside of the AdS space, with forming the scalar hair of the AdS-RN Black Hole. At the same time, the effective mass may satisfy the AdS_4 BF bound

$$\frac{(m^2 - 2\gamma^2)}{6} \geq -\frac{9}{4}\,. \tag{12}$$

[9] Here I use other AdS coordinates, related to the previous ones via $x^\mu \to x^\mu$, $r = L/z$.

Thus, the stable scalar hair condensate is formed on the boundary. Rising the BH temperature results in increasing the effective mass of the scalar field, so at some critical value T_c the AdS_2 geometry becomes stable near the horizon, and the boundary condensate of the BH scalar hair collapses. It corresponds to the phase transition from superconducting to normal state.

2.3 Phase transition

The above mentioned scenario does work even in the background of the neutral planar AdS Black Hole [11], with the geometry

$$ds^2 = -f(r)dt^2 + \frac{dr^2}{f(r)} + r^2(dx^2+dy^2), \qquad f(r) = \frac{r^2}{L^2} - \frac{M}{r}, \quad (r = L/z) \tag{13}$$

and the Hawking temperature

$$T = (3M^{1/3})/(4\pi L^{4/3})\,. \tag{14}$$

In the probe limit, the Lagrangian (9) is reduced to

$$\frac{\mathcal{L}}{\sqrt{-g}} = -\frac{1}{4e^2}F_{mn}F^{mn} - \frac{1}{e^2}\left(|\nabla\Psi - iA\Psi|^2 + m^2\Psi^2 + V(|\Psi|)\right), \tag{15}$$

the interacting fields propagate on the background (13). Equations of motion, coming from (15),

$$(\nabla_m - iA_m)(\nabla^m - iA^m)\Psi - \frac{1}{2}\frac{\Psi}{|\Psi|}(2m^2|\Psi| + V'(|\Psi|)) = 0,$$

$$\nabla^m F_{mn} = i\left[\Psi^*(\nabla_n - iA_n)\Psi - \Psi(\nabla_n + iA_n)\Psi^*\right], \tag{16}$$

set up the system of coupled partial differential equations, which has to be solved. The ansatz of [11] is

$$A_m = (\phi(r), 0, 0, 0), \qquad \Psi = \psi(r), \qquad V(|\Psi|) = 0\,. \tag{17}$$

The resulting system of nonlinear equations (the phase of the scalar field can be fixed to be a constant, so one may consider the real scalar ψ)

$$\psi'' + \left(\frac{f'}{f} + \frac{2}{r}\right)\psi' + \frac{\phi^2}{f^2}\psi - \frac{m^2}{f}\psi = 0,$$

$$\psi'' + \frac{2}{r}\psi' - \frac{2\psi^2}{f}\phi = 0\,, \tag{18}$$

will be numerically solved. But having the non-trivial boundary, we need to supply the system (18) with the correct Boundary Conditions (BCs).

Near the boundary, according to the general expansion (2), the massless vector field is expanded as

$$A_t(r\to\infty) = A_t^{(0)} + \frac{A_t^{(1)}}{r} + \dots \tag{19}$$

The finite part of (19) has to be associated with the source of the local boundary operator. Another part of (19) corresponds to the conserved current. Having it in mind, the $A_t^{(1)}$ part of the near boundary expansion is equated with the temporal component of the current J_m, i.e. with the electric charge density ρ. The finite part of the expansion (19) corresponds to the chemical potential of the electric charge density μ. Therefore, near the boundary, the Maxwell field BC is

$$\phi(r\to\infty) = \mu - \frac{\rho}{r} + \dots \tag{20}$$

The choice of the sign in (20) is fixed from the requirement of smooth behaviour of the Maxwell field near the horizon, $\phi(r_H) = 0$. As usual, the horizon position r_H is determined from vanishing the BH red shift factor $f(r)$ (cf. (13)) on the horizon, $f(r_H) = 0$. Clearly, $\rho = \mu r_H$.

Concerning the BC for the charged scalar field, to get the simple falloff in the asymptote of the scalar field at $r\to\infty$, the authors of [11] fixed its mass to the nearest to the AdS_4 BF bound integer value, $m^2L^2 = -2$. Then, the near boundary expansion of ψ becomes

$$\psi(r\to\infty) = \frac{\psi^{(1)}}{r} + \frac{\psi^{(2)}}{r^2} + \dots\,, \tag{21}$$

so if one chooses $\psi^{(1)} = 0$, then $\langle\mathcal{O}_2\rangle_\psi = \sqrt{2}\psi^{(2)}$ and viceversa. In what follows we will focus on $\psi^{(1)} = 0$ case, hence

$$\psi(r\to\infty) = \frac{\psi^{(2)}}{r^2} + \dots\,. \tag{22}$$

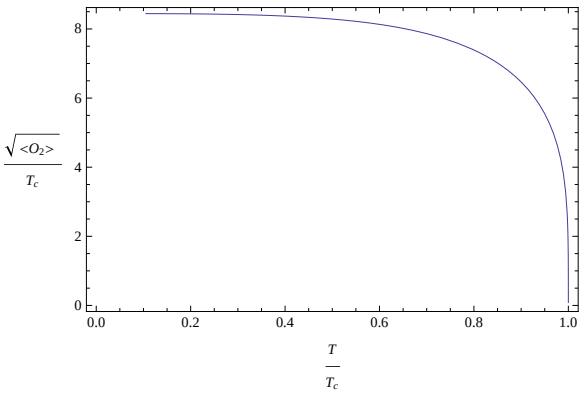

Figure 2. The second order phase transition in the s-wave 3D HSC.

Numerical solution of (16) at the fixed ansatz for AdS fields (17), and at the fixed BCs (20), (22) leads to a phase transition at a critical temperature T_c, see Fig. 2. Note that the critical exponent of the phase transition coincides with that of the GL theory: The results of numerical calculations[10] on the plot Fig. 2 is well approximated with

$$\langle \mathcal{O}_2 \rangle_\psi / T_c^2 \sim (1 - T/T_c)^{1/2}, \quad T \to T_c \,. \tag{23}$$

Also note that $\langle \mathcal{O}_2 \rangle_\psi / T_c \approx 8.3$ at $T \to 0$, and the condensation occurs at $T_c \approx 0.118\sqrt{\rho}$.

2.4 Conductivity

Having established the behavior of the order parameter $\langle \mathcal{O}_2 \rangle_\psi$ with typical characteristics of the 2nd order phase transition, let's turn to the conductivity issue. Optical conductivity can be computed by adding small perturbations to the transverse components of Maxwell field. The simplest choice is [11]

$$\delta A = A_x(r) e^{-i\omega t} dx \quad \rightsquigarrow \quad \delta A_m = (0, A_x(r) e^{-i\omega t}, 0, 0) \,, \tag{24}$$

that leads to the linearized Maxwell equation

$$A_x''(r) + \frac{f'}{f} A_x'(r) + \left(\frac{\omega^2}{f^2} - \frac{2\psi^2}{f} \right) A_x(r) = 0 \,. \tag{25}$$

Specifying the near the horizon BC (no outgoing radiation at the horizon)

$$A_x(r \to r_H) \sim f(r) e^{-i\omega/4r_H} \,, \tag{26}$$

and the near the boundary expansion

$$A_x(r \to \infty) = A_x^{(0)}(r) + \frac{A_x^{(1)}(r)}{r} + \ldots, \tag{27}$$

which, in accordance to general expansion (2), sets $A_x = A_x^{(0)}$ and $\langle J_x \rangle = A_x^{(1)}$, one may solve eq. (25) numerically (see footnote 9 for the code source). Then, the conductivity value comes from the Ohm's law in the Kirchhoff reformulation[11]

$$\sigma = \frac{\langle J_x \rangle}{E_x} = -\frac{\langle J_x \rangle}{\partial_0 A_x} = \frac{\langle J_x \rangle}{i\omega A_x} = -i \frac{A_x^{(1)}}{\omega A_x^{(0)}} \,. \tag{28}$$

Results of numerical simulations are presented on two plots, Fig. 3-4.

According to the results in Fig. 4, the lowest value of the imaginary part of σ can be found near $\omega/T_c \approx 8$. It turns out that a robust feature, that holds in AdS_4 s-wave superconductors for all scalar condensate scalings $\Delta \geq \Delta_{BF}$, is that [24]

$$\frac{\omega}{T_c} \approx 8 \pm 8\% \,. \tag{29}$$

Measurements of this ratio in the real High-T superconductors give roughly this value [25].

[10] One can freely get the "C.P. Herzog's Mathematica notebook for ArXiv:0803.3295" with code and results of numerical simulations by means of any search engine - Google, Yahoo, etc.

[11] The same result follows from the Kubo's formula of the linear response theory

$$\sigma = -\lim_{\omega \to 0} \frac{\Im G^R(\omega)}{\omega}$$

with the current-current retarded Green function $G^R(\omega)$ [23].

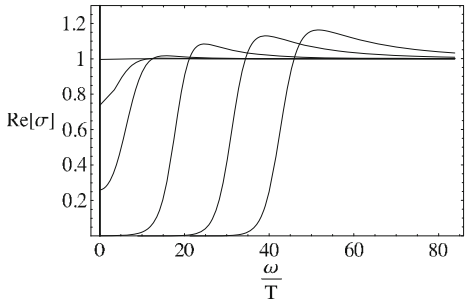

Figure 3. A gap formation in the real part of the conductivity under lowering temperature below the T_c. Taken from [11].

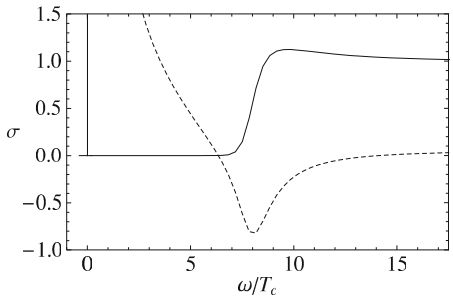

Figure 4. The low temperature limit of the optical conductivity. The solid line is the real part, the dashed line is the imaginary part. Taken from [24].

3 Summary

To summarize, the simple AdS/CFT setup of [11] leads to the second order phase transition from normal to superconducting state, with forming the energy gap. Critical exponent near the phase transition point coincides with that of the BCS theory, the gap is formed in the similar way. These results initiate the CMP community people to ask:"The HSC approach reproduced the known results of the BCS, so what? What the difference between the HSC approach and the standard BCS mechanism then?" At first site, qualitatively, the HSC picture looks very close to the results of the BCS theory. It is very expected, since the simplest model of the HSC [11] deals with s-wave superconductivity; the BCS theory deals with this case too. But quantitatively, there are principle differences between two approaches. The universal relation of the BCS theory, corresponding to (29), is $\omega/T_c \sim 3.5$. This value is twice less than the true experimental value, obtained, say, for cuprates. Mechanisms of forming the bosonic-type condensate, triggering the phase transition, are also different for both approaches. In the BCS theory it comes from the fermions pairing due to the electron-phonon interaction; on the HSC side the condensate forms by means of bosonic fields. Inclusion of fermions into the AdS/CMT setup leads to new objects - "strange metals" [26], [27], whose properties are defined by a holographic non-Fermi liquid. The strange metal state shows a "local quantum criticality", the property which has been experimentally discovered in the late of 80th (see, e.g., [28], [29] for review).

Could we believe in HSC results, having just one coincidence with experimental data as (29)? Could it be an accident? Critics from authors of [30] is appreciated in this respect, and initiates searching for new, may be more powerful arguments in favor of the "strange, but magic" relation between String theory and Condensed Matter Physics.

4 Epilogue

Since the discovery in 2008, the HSC approach has been extended to studies of Holography in disordered systems (like glasses, insulators, semiconductors) (see, e.g., [31]), to non-static and non-equilibrium dynamics within the HSC [32], [33], to the HSC models in periodic potentials, modeling the lattice [34], and to dissipative non-linear dynamics in Holography, which may be considered as first steps to chaos [35]. The list of achievements in the AdS/CMT during the last five years is more comprehensive of course, so there is the strong believe that one day the famous phase diagrams of cuprates, Fig. 5, becomes tractable and clear on the theory side.

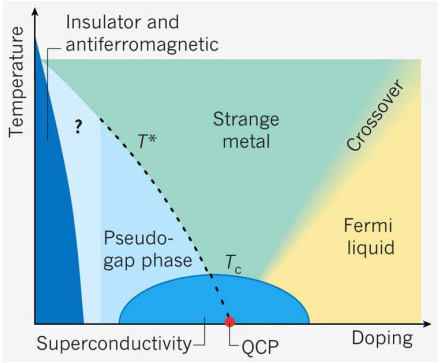

Figure 5. Phase diagram of cuprates.

Acknowledgements. I am thankful to Organizers of the NPQCD'13 School-Seminar for kind hospitality in Dnipropetrovsk and for creating the warm atmosphere during the Meeting. Discussions with V.V. Skalozub and A.N. Tarasov were very useful to me. I am also grateful to people in Kharkov, Moscow and Dubna for their questions and comments during my presentations of the related matters. Questions and comments from V.N. Melnikov, V.D. Ivashchuk, K.A. Bronnikov, E.A. Ivanov, S.A. Fedoruk, Yu.L. Bolotin and O.B. Zaslavsky were helpful in understanding the AdS part of the story. I am really indebted to the CMP community people - I.V. Krive, L.A. Pastur, V.A. Shklovsky, E.A. Kochetov - for their interest to new ideas coming from Strings, critics, comments, and for explaining to me subtle points of modern approaches to HTS and other CMP problems. Partial support from Joint DFFD-RFFR Grant # F53.2/012 is also acknowledged.

References

[1] J.G. Bednorz and K.A. Mueller, Zeit. Phys. B **64**, 189 (1986).
[2] P. Monthoux, A.V. Balatsky and D. Pines Physical Review B **46**, 14803 (1992).
[3] S. Chakravarthy *et al.*, Science **261**, 337 (1993).
[4] K. Le Hur and T.M. Rice, Ann. Phys. **324**, 1452 (2009) [arXiv:0812.1581[cond-mat.supr-con]].
[5] J.P. Carbotte, Rev. Mod. Phys. **62**, 1027 (1990);
E.G. Maksimov, M.L. Kulic and O.V. Dolgov, *Bosonic Spectral Function and The Electron-Phonon Interaction in HTSC Cuprates*, arXiv:1001.4859[cond-mat.supr-con];
A.S. Alexandrov, J. Phys.: Conf. Ser. **286**, 012012 (2011).
[6] K. Byczuk *et al.*, Europhys. Lett. **67**, 1011 (2004);
R.M. Lutchyn and J.H. Skrabacz, Phys. Rev. B **88**, 024511 (2013) [arXiv:1302.0289 [cond-mat.supr-con]].
[7] V. Aji, A. Shekhter and C. Varma, Phys. Rev. B **81**, 064515 (2010); V. Aji, A. Shekhter and C. Varma, arXiv:0807.3741[cond-mat.supr-con].
[8] J.R. Kirtley *et al.* Nature Physics **2**, 190 (2006).
[9] P.W. Anderson, Science **235**, 1196 (1987).
[10] J. Zaanen *et al.* Nature Physics **2**, 138 (2006).
[11] S.A. Hartnoll, C.P. Herzog and G.T. Horowitz, Phys. Rev. Lett. **101**, 031601 (2008) [arXiv:0803.3295[hep-th]];
S.A. Hartnoll, C.P. Herzog and G.T. Horowitz, JHEP **0812**, 015 (2008) [arXiv:0810.1563[hep-th]]
[12] *From Gravity to Thermal Gauge Theories: The AdS/CFT Correspondence*, (E. Papantonopoulos Ed., Lecture Notes in Physics **828**, Berlin Heidelberg, Springer-Verlag, 2011).
[13] A. Leggett, Nature Physics **2**, 134 (2006).
[14] J. Zaanen, Y.W. Sun, Y. Liu and K. Schalm, *The AdS/CMT manual for plumbers and electricians*, may be found at: http://solvayinstitutes.be/events/doctoral/J.Zaanen_Notes.pdf
[15] J.M. Maldacena, Adv. Theor. Math. Phys. **2**, 231 (1998) [hep-th/9711200].
[16] S.S. Gubser, I.R. Klebanov and A.M. Polyakov, Phys. Lett. B **428**, 105 (1998) [hep-th/9802109].
[17] E. Witten, Adv. Theor. Math. Phys. **2**, 253 (1998) [hep-th/9802150].
[18] O. Aharony *et al.*, Phys. Rept. **323**, 183 (2000) [hep-th/9905111].
[19] J. McGreevy, *Holographic duality with a view toward many-body physics*, arXiv:0909.0518 [hep-th].
[20] P. Breitenlohner and D.Z. Freedman, Phys. Lett. B **115**, 197 (1982).
[21] T. Hertog, Phys. Rev. D **74**, 084008 (2006) [gr-qc/0608075].
[22] S.S. Gubser, Phys. Rev. D **78**, 065034 (2008) [arXiv:0801.2977[hep-th]].
[23] D.T.Son and A.O.Starinets JHEP **0209**, 042 (2002) [hep-th/0205051].
[24] G.T. Horowitz and M.M. Roberts, Phys. Rev. D **78**, 126008 (2008) [arXiv:0810.1077[hep-th]].
[25] K.K. Gomes *et al.*, Nature **447**, 569 (2007).
[26] H. Liu, J. McGreevy and D. Vegh, Phys. Rev. D **83**, 065029 (2011) [arXiv:0903.2477[hep-th]].
[27] T. Faulkner *et al.*, *From black holes to strange metals*, arXiv:1003.1728[hep-th].
[28] S. Sachdev and B. Keimer, *Quantum criticality*, arXiv:1102.4628[cond-mat.srt-el.].
[29] S. Sachdev, *Quantum Phase Transitions*, (2nd Edition, Cambridge University Press, 2011).
[30] J. Erlich and Z. Wang, *Model Sensitivity in Holographic Superconductors and their Deconstructed Cousins*, arXiv:1306.3515[hep-ph].
[31] S. Ryu, T. Takayanagi and T. Ugajin, *Holographic Conductivity in Disordered Systems*, arXiv:1103.6068 [hep-th].
[32] X. Gao *et al.*, *Non-Equilibrium Field Dynamics of an Honest Holographic Superconductor*, arXiv:1204.3103[hep-th].
[33] X. Gao *et al.*, *Lack of thermalization in holographic superconductivity*, arXiv:1212.1049[hep-th].
[34] G. T. Horowitz and J.E. Santos, *General Relativity and the Cuprates*, arXiv:1302.6586[hep-th].
[35] P. Basu and A. Ghosh, *Dissipative Nonlinear Dynamics in Holography*, arXiv:1304.6349[hep-th].

Section Talks

Proceedings of the International School-seminar
"New Physics and Quantum Chromodynamics at External Conditions", pp. 74 – 77,
May 22-24, 2013, Dnipropetrovsk, Ukraine

AMPLIFICATION OF Z' SIGNALS IN $e^+e^- \to \mu^+\mu^-$ PROCESS

A. V. Gulov[a], Ya. S. Moroz[b]

Dnipropetrovsk National University, Dnipropetrovsk, Ukraine

One-parameter sign-definite observable with the best value-to-uncertainty ratio is proposed to estimate possible signals of the Abelian Z' boson in $e^+e^- \to \mu^+\mu^-$ process. It is applied to LEP data on differential cross-sections in order to update previous estimates of Z' couplings.

1 Introduction

Electron-positron colliders provide possibility of precise measurements in high-energy physics. The history of LEP experiments showed that lepton processes can be sensitive to off-shell signals of physics beyond the standard model (SM). Unfortunately, the LEP statistics was not rich enough to detect clearly some signals of new heavy particles.

The special observables were designed to select probable signals of the Abelian Z' boson in various LEP processes [1,2]. In particular, a one-parameter sign-definite observable was constructed as a generalized forward-backward cross-section of $e^+e^- \to \mu^+\mu^-$ process, and a hint of Z' boson was found at one standard deviation. However, the latest LHC experiments allow to conclude that the maximum likelihood values of Z' couplings from Ref. [1] seem to be overestimated. In the present investigation, the most powerful observables for Z' boson in $e^+e^- \to \mu^+\mu^-$ are proposed. So, it is possible to revise the LEP data by means of the new approach.

Let us describe briefly main checkpoints of the present investigation. We use common phenomenological parameterization of Z' couplings with SM fermions as well as the model-independent relations between the Z' couplings [3]. The optimal one-parameter observables are constructed as the cross-sections integrated over the scattering angle with proper weight functions maximizing the value-to-uncertainty ratio for the observable. Then, we fit LEP data using the observables in order to estimate Z' coupling.

2 The low-energy phenomenology of the Abelian Z' boson

The Abelian Z' boson [4–6] is usually described by its couplings to vector and axial-vector currents. In general, there is also the mixing between Z and Z' bosons. The corresponding Lagrangian is

$$\begin{aligned}\mathcal{L}_{\bar{f}fZ} &= \frac{1}{2} Z_\mu \bar{f}\gamma^\mu \left[(v_{fZ}^{\rm SM} + \gamma^5 a_{fZ}^{\rm SM})\cos\theta_0 + (v_f + \gamma^5 a_f)\sin\theta_0\right] f,\\ \mathcal{L}_{\bar{f}fZ'} &= \frac{1}{2} Z'_\mu \bar{f}\gamma^\mu \left[(v_f + \gamma^5 a_f)\cos\theta_0 - (v_{fZ}^{\rm SM} + \gamma^5 a_{fZ}^{\rm SM})\sin\theta_0\right] f,\end{aligned} \tag{1}$$

where we omit effective interactions inspired by loop corrections and next-to-leading order terms in inverse heavy mass scales.

Not all the coupling constants in (1) are independent, if we assume the Abelian Z' boson associated with an effective U(1) gauge symmetry at low energies. If we consider the single neutral vector boson with the mass of order TeVs, the following relations arise [3]

$$v_{f[T_3=1/2]} = v_{f[T_3=-1/2]} - 2a, \qquad a_{f[T_3=-1/2]} = -a_{f[T_3=1/2]} = a, \qquad \theta_0 = -a\frac{\sin(2\theta_W)}{\sqrt{4\pi\alpha_{\rm em}}}\left(\frac{m_Z}{m_{Z'}}\right)^2, \tag{2}$$

where T_3 is the third component of the weak isospin, and the fermions are taken from the same SM doublet. The relations can be motivated by general theoretical reasons (gauge symmetry, renormalizability at energies of the Z' decoupling) which are described in details in Ref. [3]. Let us note that the relations (3) cover a wide set of popular Z' models. In this regard, they can be called model-independent.

Considering the cross-sections at energies below the Z' mass, it is convenient to use couplings

$$\bar{a}_f = \frac{m_Z}{\sqrt{4\pi} m_{Z'}} a_f, \quad \bar{v}_f = \frac{m_Z}{\sqrt{4\pi} m_{Z'}} v_f. \tag{3}$$

e-mail: [a]gulov@dsu.dp.ua, [b]yaroslav.moroz91@gmail.com

The virtual Z' boson state contributes to the differential cross-section of $e^+e^- \to \mu^+\mu^-$ process. In the lowest order in the inverse Z' mass the cross-section deviates from its SM value as

$$\frac{d\sigma}{dz} - \frac{d\sigma^{\rm SM}}{dz} = F_1(\sqrt{s},z)\bar{a}^2 + F_2(\sqrt{s},z)\bar{a}\bar{v}_e + F_3(\sqrt{s},z)\bar{a}\bar{v}_\mu + F_4(\sqrt{s},z)\bar{v}_e\bar{v}_\mu + \ldots, \tag{4}$$

where $z = \cos\theta$ is the cosine of the scattering angle and dots stand for higher corrections in the inverse Z' mass. Factors F_i arise from the interference between the SM scattering amplitude and the Z' exchange amplitude. They have to be computed numerically taking into account both the tree-level contribution and loop corrections.

Being measured in experiments, the cross-section (4) allows to estimate the Z' couplings $\bar{a}$, $\bar{v}_e$, and $\bar{v}_\mu$. A non-zero value of some coupling mentioned can be called the Z' signal.

Minimal number of unknown parameters is preferable in fitting data. Therefore, one-parameter observable is the most prominent from the statistical point of view. Moreover, sign-definite observable is more informative, since it can also reject the hypothesis, whereas sign-indefinite one can only accept the signal. These properties are especially important in case of statistics which is not rich enough to detect clear signals at high confidence levels. Fortunately, the cross-section (4) contains one sign-definite term with $\bar{a}^2$. If we could select this term in the cross-section, we would obtain a powerful observable to detect Z' signals in experiments. In case of lepton universality the term with $\bar{v}_e\bar{v}_\mu$ also becomes sign-definite.

It is also worth to note that factors $F_{2,3}$ are small with respect to $F_{1,4}$. Their contributions to the cross-section are about 1%, and their existence does not affect the key ideas of the present investigation. So, the Z' signal in $e^+e^- \to \mu^+\mu^-$ can be discussed as two-parametric.

3 The observables

The differential cross-section (4) contains two leading terms at $\bar{a}^2$ and $\bar{v}_e\bar{v}_\mu$. The corresponding factors $F_i(\sqrt{s},z)$ are the functions of energy and scattering angle. We can use angular integration in order to suppress one factor comparing to another. Actually, this means that we will construct some integrated cross-section with specific properties.

In general, integrated cross-sections are well known in the literature. The most popular integration schemes are based on bin summation with equal weights but opposite signs. As examples, we can mention the total cross-section, the forward-backward cross-section, the center-edge cross-section, etc. However, the equal weight of bins is just a possible option. The most general integration scheme can be described by weight function $p(z)$:

$$\sigma = \int\limits_{-1}^{1} dz\, p\,(z) \left(\frac{d\sigma}{dz} - \frac{d\sigma^{\rm SM}}{dz}\right). \tag{5}$$

In these notations, the popular mentioned cross-sections correspond to step-like weight functions. The observables used in previous analysis of LEP data are also based on step-like weight functions.

The statistical uncertainty of the observable (5) can be estimated taking into account that the actual number of events in bin is distributed under the Poisson distribution. This means the variance of events in a bin coincides the average number of events. Then, the variance of the observable is:

$$(\delta\sigma)^2 = \mathcal{L}^{-2}(\delta N)^2 = \mathcal{L}^{-2}\sum p^2 dN = \mathcal{L}^{-1}\int dz\, p^2(z)\,\frac{d\sigma}{dz}, \tag{6}$$

where $\mathcal{L}$ is the integrated luminosity of the experiment. In general, the differential cross-section under the integral contains both the contributions from the SM and Z' boson. However, the deviations from the SM are considered to be small. Therefore, in order to simplify calculations we can substitute the cross-section by its SM part. As a result, the uncertainty of the observable reads

$$\delta\sigma \simeq \sqrt{\mathcal{L}^{-1}\int\limits_{-1}^{1} dz\, p^2(z)\frac{d\sigma^{\rm SM}}{dz}}. \tag{7}$$

Let us consider the observable which amplifies the Z' signal as much as possible. This aim can be reached by maximizing the value-to-uncertainty (signal-to-uncertainty) ratio

$$\mathrm{abs}\left(\frac{\sigma}{\delta\sigma}\right) = \mathrm{abs}\left(\frac{\int\limits_{-1}^{1} p(z)\left(\frac{d\sigma}{dz} - \frac{d\sigma^{\rm SM}}{dz}\right)dz}{\sqrt{\mathcal{L}^{-1}\int\limits_{-1}^{1} p^2(z)\frac{d\sigma}{dz}\,dz}}\right) \to \max, \tag{8}$$

where the weight function is assumed to be varied in the optimization procedure.

In fact, the optimization (8) has to be performed under additional constraints. First of all, the normalization of the weight function must be taken into account, since (8) is evidently invariant under the rescaling of the weight function. We choose the normalization

$$\int\limits_{-1}^{1} dz\, p^2\,(z) = 1. \tag{9}$$

Second, the weight function is chosen to suppress all the factors in the differential cross-section (4) except for either F_1 or F_4. The most general scheme takes into account both the contributions of leading factors $F_{1,4}$ and small factors $F_{2,3}$ in the differential cross-section (4). In order to select the factor F_1 we can minimize the cumulative relative contribution of the other factors:

$$\frac{\sum\limits_{i=2}^{4} \mathrm{abs}\left(\int\limits_{-1}^{1} dz\, p\,(z)\, F_i\,(\sqrt{s}, z)\right)}{\sum\limits_{i=1}^{4} \mathrm{abs}\left(\int\limits_{-1}^{1} dz\, p\,(z)\, F_i\,(\sqrt{s}, z)\right)} \to \min. \tag{10}$$

The factor F_4 is selected in a similar way using $F_{1,2,3}$ in the nominator, but we will not consider this case in the present investigation. Eq. (10) does not specify a unique weight function, it defines a subspace in the Hilbert space of $p(z)$. It is clearly seen from the fact that (10) does not change when a function orthogonal to $F_{1,2,3,4}$ is added to $p(z)$.

The optimization (8) with the constraints (9) and (10) has to determine uniquely the weight function $p(z)$ for the most amplified Z' signal in the considered process. These calculations require choosing some basis in the Hilbert space of weight functions.

The most natural basis takes into account the kinematics of $e^+e^- \to \mu^+\mu^-$ process. Due to the absence of the flavor-changing neutral currents, there is no virtual bosons in the t-channel. Moreover, all the leptons can be considered as massless. This leads to the well-known two-polynomial structure of all the factors in the differential cross-sections:

$$F_i(\sqrt{s}, z) = a_i(\sqrt{s})p_1(z) + b_i(\sqrt{s})p_2(z), \tag{11}$$

where $p_1 \sim z$, $p_2 \sim (1 + z^2)$. In this regard, it is convenient to use orthogonal polynomials as a basis in the Hilbert space of weight functions. We define orthogonal normalized polynomials in the standard way,

$$\int\limits_{-1}^{1} dz\, p_i(z)p_j(z) = \begin{cases} 1, & i = j, \\ 0, & i \neq j, \end{cases} \tag{12}$$

The full set of polynomials can be reconstructed starting from p_1 and p_2 and increasing the largest power of the polynomial:

$$\begin{aligned}
&p_1 = \sqrt{\frac{3}{2}}z, \quad p_2 = \frac{1}{2}\sqrt{\frac{15}{14}}(z^2+1), \quad p_3 = \sqrt{\frac{3}{14}}\left(5z^2-2\right), \quad p_4 = \frac{1}{2}\sqrt{\frac{7}{2}}\left(5z^3-3z\right), \\
&p_5 = \frac{3}{8\sqrt{2}}\left(35z^4-30z^2+3\right), \quad p_6 = \frac{1}{8}\sqrt{\frac{11}{2}}\left(63z^5-70z^3+15z\right), \\
&p_7 = \frac{5}{16}\sqrt{\frac{13}{2}}\left(-\frac{231}{5}z^6+63z^4-21z^2+1\right), \quad p_8 = -\frac{1}{16}\sqrt{\frac{15}{2}}\left(429z^7-693z^5+315z^3-35z\right), \ \ldots
\end{aligned} \tag{13}$$

Weight function $p(z)$ can be expanded by p_i:

$$p(z) = \sum_{i=1}^{\infty} c_i p_i(z). \tag{14}$$

Then, the normalization condition (9) becomes

$$\sum_{i=1}^{\infty} c_i^2 = 1. \tag{15}$$

Since the Z' contributions to the cross-section are described by two polynomials $p_{1,2}$, Eq. (10) defines a fixed direction in the functional subspace based on $p_{1,2}$, namely, the ratio:

$$k = c_2/c_1. \tag{16}$$

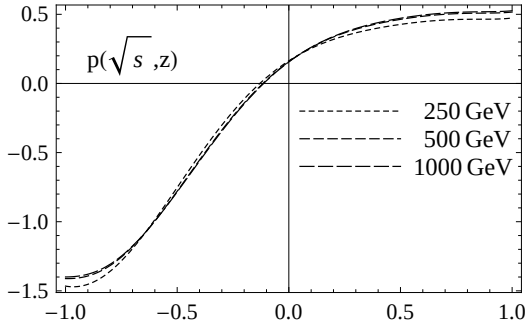

Figure 1. The optimal weight functions to select $\bar{a}^2$ for ILC energies.

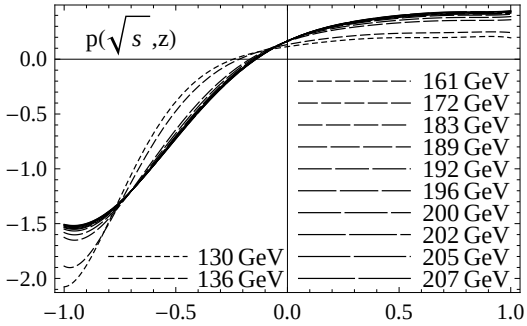

Figure 2. The optimal weight functions to select $\bar{a}^2$ for LEP energies.

The numerical analysis shows that the corresponding relative weight of F_1 or F_4 is 0.98. Thus, we can estimate the systematic error of the variable as 2%.

The normalization condition (15) determines one of the coefficients through the others. For instance,

$$c_1 = \sqrt{\frac{1 - c_3^2 - c_4^2 - \dots}{1 + k^2}}. \tag{17}$$

Thus, two coefficients c_1, c_2 are explicitly expressed by the other coefficients. As a result, $c_3, c_4, \dots$ are to be varied to maximize the signal-to-uncertainty ratio. The obtained values give the weight function (14). Using eight polynomials from the basis, we find the relative accuracy of weight functions to be less than 1% at all the considered energies, which is below the systematic theoretical error of the observables. In Figs. 1, 2 we plot the optimal weight functions for both the LEP and ILC energies.

4 Data fit

LEP data fit is performed in the standard way using χ^2 function to combine different scattering energies together. First, we calculate both the mean values and the statistical uncertainties of the observable for $\bar{a}^2$ at different energies taking data on differential cross-sections published by the LEP Collaborations [7–9]. Dividing the values by a known numeric factor, we compute the experimental estimate of $\bar{a}^2$. In this way we obtain 21 data points for each type of observables. After that, we combine all the data points altogether by means of the standard χ^2 technique obtaining the mean value and the uncertainty of the Z couplings:

$$\bar{a}^2 = (1.4369 \pm 4.8614) \times 10^{-5}.$$

Let us discuss the obtained results. First of all, the uncertainty of $\bar{a}^2$ is close to the uncertainty within the indirect measurement of the axial-vector coupling by the total cross-sections and forward-backward asymmetries [1]. However, we use less data points, since the differential cross-sections were not published for some LEP energies depending on the collaboration. This reflects the fact that the new observables are more statistically powerful with respect to the observables used in [1].

Second, the mean value of $\bar{a}^2$ decreases comparing to the indirect estimates [1]. This is in accordance with the latest constraints from the LHC showing that this coupling should be about 10^{-6} rather than 10^{-5}.

Finally, the new observables for searching for Z' signals in $e^+e^- \to \mu^+\mu^-$ process show they can be useful in data fitting. They have good perspectives in future experiments at lepton colliders such as the ILC.

References

[1] A. V. Gulov and V. V. Skalozub, Int. J. Mod. Phys. A **25**, 5787 (2010) [1009.2320].
[2] A. V. Gulov and V. V. Skalozub, Phys. Rev. D **61**, 055007 (2000) [hep-ph/9906213].
[3] A. V. Gulov and V. V. Skalozub, Eur. Phys. J. C **17**, 685 (2000) [hep-ph/0004038].
[4] A. Leike, Phys. Rep. **317**, 143 (1999) [hep-ph/9805494].
[5] P. Langacker, Rev.Mod.Phys. **81**, 1199 (2009) [0801.1345].
[6] T. G. Rizzo, (2006) [hep-ph/0610104].
[7] G. Abbiendi *at al.* (OPAL Collaboration), Eur. Phys. J. C. **33**, 173 (2004) [hep-ex/0309053].
[8] J. Abdallah *at al.* (DELPHI Collaboration), Eur. Phys. J. C. **45**, 589 (2006) [hep-ex/0512012].
[9] S. Schael *at al.* (ALEPH Collaboration), Eur. Phys. J. C. **49**, 411 (2007) [hep-ex/0609051].

Proceedings of the International School-seminar
"New Physics and Quantum Chromodynamics at External Conditions", pp. 78 – 81,
May 22-24, 2013, Dnipropetrovsk, Ukraine

BIMODALITY AS A SIGNAL OF THE NUCLEAR LIQUID-GAS PHASE TRANSITION

V. V. Sagun[a], A. I. Ivanytskyi[b], D. R. Oliinychenko[c], K. A. Bugaev[d]

Bogolyubov Institute for Theoretical Physics, Kiev, Ukraine

Here we present an explicit counterexample to a bimodality concept as the unique signal of first order phase transition. Using an exact solution of the simplified version of the statistical multifragmentation model we demonstrate that the bimodal distributions can naturally appear in infinite system without a phase transition in the regions of the negative values of the surface tension coefficient. Also we propose a new parameterization for the compressible nuclear liquid which is consistent with the L. van Hove axioms of statistical mechanics. As a result the proposed model does not lead to the irregular behavior of the isotherms in the mixed phase region which is typical for mean-field models. Peculiarly, the suggested approach to account for the nuclear liquid compressibility automatically leads to an appearance of an additional state that in many respects resembles the physical antinuclear matter.

1 Introduction

At the present time the bimodality is often considered as a signal of the first order PT in finite systems. The authors of such schemes [1, 2] identify each local maximum of the bimodal distribution with a pure phase. Such an idea goes back to T. Hill book [3]. Hill justified this assumption on bimodality by stating that due to the fact that an interface between two pure phases 'costs' some additional energy, the probability of their coexisting in a finite system is less than for each of pure phases [3]. It was found [4], however, that such an assumption can be valid for infinite systems only. In order to demonstrate that Hill assumption can be incorrect even in thermodynamic limit, here we present a clear counterexample by considering an exact analytical solution of the constrained statistical multifragmentation model (CSMM) in thermodynamic limit which leads to the bimodal fragment size distributions inside of the cross-over region. For this purpose we consider a more realistic equation of state for the liquid phase which, in contrast to the original SMM formulation [5], is a compressible one [6]. The second important element of the present model is a more realistic parameterization of the temperature dependent surface tension based on an exact analytical solution of the partition function of surface deformations [7].

1.1 CSMM with compressible nuclear liquid in thermodynamic limit

The general solution of the CSMM partition function formulated in the grand canonical variables of volume V, temperature T and baryonic chemical potential μ is given by [8]

$$\mathcal{Z}(V,T,\mu) \;=\; \sum_{\{\lambda_n\}} e^{\lambda_n V}\Big[1-\tfrac{\partial\mathcal{F}(V,\lambda_n)}{\partial\lambda_n}\Big]^{-1}, \tag{1}$$

where the set of λ_n $(n=0,1,2,3,..)$ are all the complex roots of the equation

$$\lambda_n \;=\; \mathcal{F}(V,\lambda_n)\,, \tag{2}$$

ordered as $Re(\lambda_n) > Re(\lambda_{n+1})$ and $Im(\lambda_0)=0$. The function $\mathcal{F}(V,\lambda)$ is defined as

$$\mathcal{F}(V,\lambda) = \left(\frac{mT}{2\pi}\right)^{\frac{3}{2}} z_1 \exp\left\{\frac{\mu-\lambda Tb}{T}\right\} + \sum_{k=2}^{K(V)} \phi_k(T)\exp\left\{\frac{(p_l(T,\mu)-\lambda T)bk}{T}\right\}. \tag{3}$$

Here $m \simeq 940$ MeV is a nucleon mass, $z_1 = 4$ is an internal partition (the degeneracy factor) of nucleons, $b = 1/\rho_0$ is the eigen volume of one nucleon in a vacuum ($\rho_0 \simeq 0.17$ fm^3 is the normal nuclear density at $T=0$ and zero pressure). The reduced distribution function of the k-nucleon fragment in (3) is defined as

$$\phi_{k>1}(T) \equiv \left(\frac{mT}{2\pi}\right)^{\frac{3}{2}} k^{-\tau}\,\exp\left[-\frac{\sigma(T)\,k^{\varsigma}}{T}\right], \tag{4}$$

e-mail: [a]v_sagun@ukr.net, [b]a_iv_@ukr.net, [c]dimafopf@gmail.com, [d]bugaev@th.physik.uni-frankfurt.de

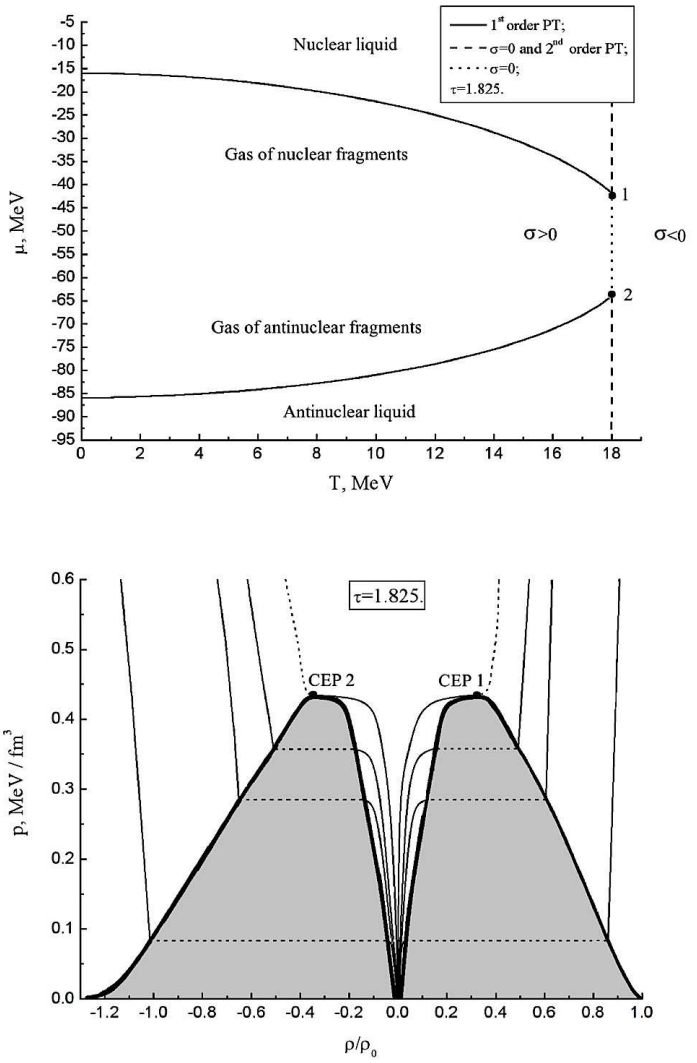

Figure 1. Upper panel: The phase diagrams in $T-\mu$ plane. Along the solid curves there are first order PTs.The vertical dashed lines show the second order PT and the black circles correspond to the tricritical endpoints marked by the digits 1 (nuclear matter) and 2 (antinuclear matter). A cross-over occurs along the dotted vertical line of the vanishing surface tension coefficient. **Lower panel:** The phase diagrams in $\rho-p$ plane. The grey areas show the mixed phases of the first order PTs. The isotherms are shown for $T = 11, 16, 17, 18$ MeV from bottom to top. Negative density values correspond to an 'antimatter'.

where $\tau \simeq 1.825$ is the Fisher topological exponent and $\sigma(T)$ is the T-dependent surface tension coefficient. Usually, the constant, parameterizing the dimension of surface in terms of the volume is $\varsigma = \frac{2}{3}$.

In (3) the exponentials $\exp(-\lambda bk)$ $(k = 1, 2, 3, ...)$ appear due to the hard-core repulsion between the nuclear fragments [8], while $p_l(T, \mu)$ is the pressure of the liquid phase. Here we consider the thermodynamic limit only, i.e. for $V \to \infty$ we have $K(V) \to \infty$. Then the treatment of the model is essentially simplified, since Eq. (2) can have only two kinds of solutions [8], either the gaseous pole $p_g(T, \mu) = T\lambda_0(T, \mu)$ for $\mathcal{F}(V, \lambda_0 - 0) < \infty$ or the liquid essential singularity $p_l(T, \mu) = T\lambda_0(T, \mu)$ for $\mathcal{F}(V, \lambda_0 - 0) \to \infty$. The mathematical reason why only the rightmost solution $\lambda_0(T, \mu) = \max\{Re(\lambda_n)\}$ of Eq. (2) defines the system pressure is evident from Eq. (1): in the limit $V \to \infty$ all the solutions of (2) other than the rightmost one are exponentially suppressed.

In the thermodynamic limit the model has a PT, when there occurs a change of the rightmost solution type, i.e. when the gaseous pole is changed by the liquid essential singularity or vice versa. The PT line $\mu = \mu_c(T)$ is a solution of the equation of 'colliding singularities' $p_g(T, \mu) = p_l(T, \mu)$, which is just the Gibbs criterion of phase equilibrium. The properties of a PT are defined only by the liquid phase pressure $p_l(T, \mu)$ and by the temperature dependence of surface tension $\sigma(T)$.

In order to consider the compressible nuclear liquid in [6] we suggested the following parameterization of its

pressure

$$p_l = \frac{W(T) + \mu + a_2(\mu - \mu_0)^2 + a_4(\mu - \mu_0)^4}{b} \,. \tag{5}$$

Here $W(T) = W_0 + \frac{T^2}{W_0}$ denotes the usual temperature dependent binding energy per nucleon with $W_0 = 16$ MeV [5] and the constants $\mu_0 = -W_0$, $a_2 \simeq 1.233 \cdot 10^{-2}$ MeV^{-1} and $a_4 \simeq 4.099 \cdot 10^{-7}$ MeV^{-3}. These constants are fixed in order to reproduce the properties of normal nuclear matter, i.e. at vanishing temperature $T = 0$ and normal nuclear density $\rho = \rho_0$ the liquid pressure must be zero.

In addition to the new parameterization of the free energy of the k-nucleon fragment (3) we consider a more general parameterization of the surface tension coefficient

$$\sigma(T) = \sigma_0 \left| \frac{T_{cep} - T}{T_{cep}} \right|^{\zeta} \mathrm{sign}(T_{cep} - T) \,, \tag{6}$$

with $\zeta = const \geq 1$, $T_{cep} = 18$ MeV and $\sigma_0 = 18$ MeV the SMM. In contrast to the Fisher droplet model [9] and the usual SMM, the CSMM surface tension (6) is negative above the critical temperature T_{cep}. An extended discussion on the validity of such a parameterization can be found in [6]. The resulting phase diagrams of the present model in different variables are shown in Fig. 1.

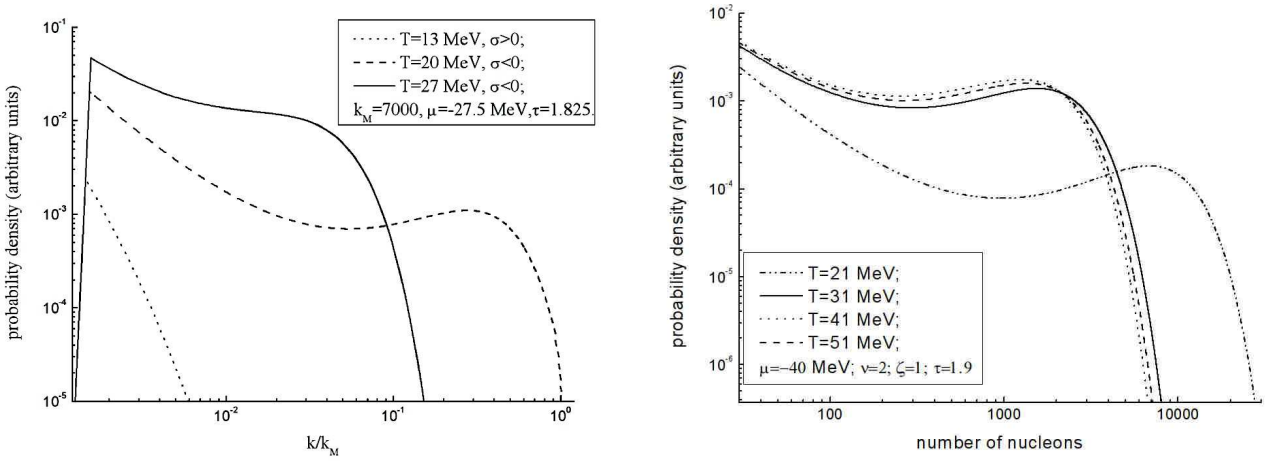

Figure 2. Left panel: Fragment size distribution of the model is shown for a fixed baryonic chemical potential $\mu = -27.5$ MeV and three values of the temperature T. **Right panel:** Same as in the left panel, but for a fixed baryonic chemical potential and different temperatures located at the region of negative values of the surface tension coefficient and $\nu = 2$.

In order to elucidate the role of the negative surface tension coefficient we study the fragment size distribution in two regions of the phase diagram. To demonstrate the pitfalls of the bimodal concept of Refs. [1–3] we compare the gaseous phase fragment size distribution with that one in the supercritical temperature region, where there is no PT by construction. As one can see from Fig. 2 in the gaseous phase, even at the boundary with the mixed phase, the size distribution is a monotonically decreasing function of the number of nucleons in a fragment k. However, for the supercritical temperatures one finds the typical bimodal fragment distribution for a variety of temperatures and chemical potentials as one can see from Fig. 2.

A sharp peak at low k values reflects a fast increase of the probability density of dimers compared to the monomers (nucleons), since the intermediate fragment sizes do not have the binding free energy and the surface free energy and, hence, the monomers are significantly suppressed in this region of thermodynamic parameters. On the other hand it is clear that the tail of fragment distributions in Fig. 2 decreases due to the dominance of the bulk free energy and, hence, the whole structure at intermediate fragment sizes is due a competition between the surface free energy and two other contributions into the fragment free energy, i.e. the bulk one and the Fisher one. It was also found that with temperature increasing the minimum and maximum of the distribution function grow wider and shallower and they shift towards the smaller number of nucleons in a fragment (see the right panel of Fig. 2).

1.2 Conclusions

In the present work we showed that the bimodal distributions can naturally appear in an infinite system without a PT. Our analysis of the fragment size distributions in the region of negative surface tension coefficient shows

that these distributions have a saddle-like shape. Such a behavior closely resembles the fragment size distribution observed in dynamical simulations of nuclear multifragmentation [10]. The compressible nuclear liquid pressure parametrization which generates the tricritical endpoint at the one third of the normal nuclear density is worked out.

References

[1] Ph. Chomaz and F. Gulminelli, Preprint GANIL-02-19, (2002).
[2] F. Gulminelli, Nucl. Phys. A **791**, 165, (2007).
[3] T. L. Hill, *Thermodynamics of small systems* Dover, New York, 1994.
[4] K. A. Bugaev, Phys. Part. Nucl. **38** 447, (2007); arXiv:nucl-th/0511031.
[5] K. A. Bugaev, M. I. Gorenstein, I. N. Mishustin and W. Greiner, Phys. Rev. C **62**, 044320, 2000; arXiv:nucl-th/0007062; Phys. Lett. B **498**, 144, 2001; arXiv:nucl-th/0103075.
[6] K. A. Bugaev, A. I. Ivanytskyi, V. V. Sagun and D. R. Oliinychenko, Phys. Part. Nucl. Lett. **10**, 832 (2013); arXiv:1306.2481 [nucl-th].
[7] K. A. Bugaev, L. Phair and J. B. Elliott, Phys. Rev. E **72**, 047106 (2005); arXiv:nucl-th/0406034.
[8] K. A. Bugaev, Acta. Phys. Polon. B **36**, 3083, (2005) and reference therein.
[9] M. E. Fisher, Physics **3**, 255, (1967).
[10] X. Campi, H. Krivine E. Plagnol and N. Sator, Phys. Rev. C **67**, 044610, (2003).

Proceedings of the International School-seminar
"New Physics and Quantum Chromodynamics at External Conditions", pp. 82 – 85,
May 22-24, 2013, Dnipropetrovsk, Ukraine

NON-ABELIAN COLOR FIELDS FROM RELATIVISTIC COLOR CHARGE CONFIGURATIONS IN THE CLASSICAL LIMIT

W. Cassing[†], V. V. Goloviznin[‡], S. V. Molodtsov[a,⋆,•], A. M. Snigirev[◇], V. D. Toneev[⋆], V. Voronyuk[‡,⋆], G. M. Zinovjev[b,‡]

[†]Institute for Theoretical Physics, University of Giessen, Germany
[‡]Bogolyubov Institute for Theoretical Physics, National Academy of Sciences of Ukraine, Kiev, UKRAINE
[⋆]Joint Institute for Nuclear Research, Dubna, Moscow region, RUSSIA
[•]Institute of Theoretical and Experimental Physics, Moscow, RUSSIA
[◇]Skobeltsyn Institute of Nuclear Physics, Lomonosov Moscow State University, Moscow, Russia

We study the dynamics of color fields generated by simple configurations of relativistic particles with Abelian and non-Abelian ($SU(2)$) charges in the classical limit. We find that chromodynamic (non-Abelian) systems generally show Coulomb-like features by analogy with electrodynamics. A peculiar feature in the non-Abelian case is the additional strength of the chromoelectric and chromomagnetic fields caused by the contribution of changing the color charge. The presence of this non-Abelian additional term in the chromoelectric and chromomagnetic fields creates a "color charge glow". This situation is especially relevant to the very initial phase of ultra-relativistic heavy-ion collisions, where the initial partonic state is governed by high (non-equilibrium) parton densities and strong local color fluctuations.

Our present study is motivated by recent investigations of peripheral ultra-relativistic heavy-ion collisions at the RHIC and the LHC, for which a large electric charge eZ of the colliding nuclei leads to the generation of intense electric and magnetic fields during the passage time of the charged 'spectators', as discussed in Ref. [1]. It is speculated that a very strong electromagnetic field - of short duration essentially in the pre-equilibrium phase - might have an important impact on particle production [2,3]. Fortunately, a large theoretical (phenomenological) activity combined with enthusiasm in studying the chiral magnetic effect (CME) and, in general, strongly interacting matter in magnetic fields in recent years [4] is balanced by a careful analysis of the corresponding RHIC and LHC experimental data [5] on the charge separation dependence of azimuthal correlations and, in particular, correlations with respect to the reaction plane. Actually, the measurements of the ALICE Collaboration [6] of the pion angular correlations are consistent with the qualitative expectations from the chiral magnetic effect. However, these results are also consistent with local charge conservation in combination with a large elliptic flow v_2. Such a classical field dynamics calls for a transport formulation and the development of an extended transport code for ultra-relativistic collision processes, including the color dynamics of the gluon fields.

In order to proceed resolving this task we develop an practical approximation for configurations of two SU(2)-color group charges which are moving along a straight line towards each other. The classical character of the non-Abelian field means, as usual, that the field operators are replaced by their average values for the quantum state, and the off-diagonal elements are neglected. Quarks are treated as classical point-like massive particles possessing a color charge. Recalling briefly the results from classical electrodynamics we have the field of a point-like charge propagating along the trajectory $\mathbf{r}(\mathbf{t})$ is described by the (retarded) Liénard-Wiechert potential at the observation point $\mathbf{r_0}$ [7]

$$\varphi = \frac{1}{4\pi}\left[\frac{e}{R-\mathbf{vR}}\right]_{t'}, \quad \mathbf{A} = \frac{\mathbf{1}}{\mathbf{4\pi}}\left[\frac{\mathbf{e\,v}}{\mathbf{R-vR}}\right]_{\mathbf{t'}}. \tag{1}$$

Here we stick to the standard system of units with speed of light $c = 1$, with dimensionless electrodynamic e and non-Abelian g charges, i.e., have the proper factors of $\hbar c$ to keep the proper dimensions of magnitudes. Then characteristic distances in the problem are of an order of 1 fm and the potentials and field strengths are measured in units of m_π and m_π^2, respectively, where m_π is the π-meson rest mass. In Eq. (1), φ is the 0'th component of the potential and $\mathbf{A}$ is its vector component, $\mathbf{v}$ is the particle velocity at some retarded time t' which is determined by the distance between the observation point and the particle $R = |\mathbf{R}|$ and $\mathbf{R} = \mathbf{r_0} - \mathbf{r}(\mathbf{t'})$ is the radius-vector from the charge position to the observation point $\mathbf{r_0}$. The retarded and laboratory time t

e-mail: [a]Serguei.Molodtsov@cern.ch, [b]Gennady.Zinovjev@cern.ch

are related by $R = t - t'$. The electric and magnetic fields then are given by

$$\begin{aligned} \mathbf{E} &= -\frac{\partial \mathbf{A}}{\partial t} - \nabla\varphi = \frac{\mathbf{1}}{\mathbf{4\pi}} \left[\frac{\mathbf{e}}{\mathbf{R^2}} \frac{\mathbf{(1-v^2)(n-v)}}{\mathbf{(1-vn)^3}} + \frac{\mathbf{e}}{\mathbf{R}} \frac{\mathbf{n\times(n-v)\times\dot{v}}}{\mathbf{(1-vn)^3}} \right]_{\mathbf{t'}} , \\ \mathbf{H} &= \nabla \times \mathbf{A} = \frac{\mathbf{1}}{\mathbf{4\pi}} \left[-\frac{\mathbf{e}}{\mathbf{R^2}} \frac{\mathbf{n\times v}}{\mathbf{(1-vn)^3}} (\mathbf{1-v^2+\dot{v}R}) - \frac{\mathbf{e}}{\mathbf{R}} \mathbf{n\times\dot{v}} \right]_{\mathbf{t'}} = \mathbf{n\times E} . \end{aligned} \tag{2}$$

In SU(2)-color group QCD Lagrangian has the form $\mathcal{L} = -\widetilde{G}^{\mu\nu}\widetilde{G}_{\mu\nu}/4 - \widetilde{j}^{\mu}\widetilde{A}_{\mu}$, where the color vector $\widetilde{A}_{\mu} = (A^1_{\mu}, A^2_{\mu}, A^3_{\mu})$ represents a triplet of the Yang-Mills fields of different colors ("isospin"), $\widetilde{j}^{\mu}$ is the current density of external color sources and $\widetilde{G}_{\mu\nu} = \partial_{\mu}\widetilde{A}_{\nu} - \partial_{\nu}\widetilde{A}_{\mu} + g\widetilde{A}_{\mu} \times \widetilde{A}_{\nu}$ is the gluon field tensor with the covariant derivative acting as $\widetilde{D^{\mu}f} = \partial^{\mu}\widetilde{f} + g\widetilde{A}^{\mu} \times \widetilde{f}$. The product sign $\times$ corresponds to the vector product in the color space. The classical equations of motion, as known, then read $\widetilde{D^{\mu}G_{\mu\nu}} = \widetilde{j}_{\nu}$. The most significant difference between these equations and the electrodynamic equations is the compatibility conditions of the system $\widetilde{D^{\mu}j_{\mu}} = 0$, that generally implies that the color vector charge is not conserved in a sense similar to electrodynamics. In the non-Abelian case we cannot benefit from an analysis of the general Yang-Mills solutions but one can construct approximate solutions with properties similar to the solutions of electrodynamics. Here we focus on the analysis of some simple examples important for practical applications treating the relativistic color objects propagating along a straight line. As an approximate solution, we consider a superposition of the Liénard-Wiechert potentials in which the vector of the particle color charge can change in time and should be taken at the retarded time. In this context the compatibility condition for a point-like charge becomes $\dot{\widetilde{C}} = g \left[\widetilde{\varphi}(t,\mathbf{r}) - \mathbf{v}\ \widetilde{\mathbf{A}}(t,\mathbf{r})\right] \times \widetilde{C}$. From these equations it is easy to see that the modulus of the color charge vector remains constant. In the following we take the color charge as a unit vector and specify the magnitude of the charge to be given by the coupling constant g ($\alpha_g = g^2/(4\pi) = 0.3$), thus taking the coupling strength out as an independent factor. The consideration of the non-Abelian charge as a function of time leads to the generation of additional terms in the expressions for the chromoelectric and chromomagnetic fields of color point-like charges

$$\begin{aligned} \widetilde{\mathbf{E}} &= \frac{1}{4\pi} \left[\frac{\widetilde{C}}{R^2} \frac{\mathbf{(1-v^2)(n-v)}}{\mathbf{(1-vn)^3}} + \frac{\widetilde{C}}{R} \frac{\mathbf{n\times(n-v)\times\dot{v}}}{\mathbf{(1-vn)^3}} + \frac{\widetilde{D}}{R} \frac{\mathbf{n-v}}{\mathbf{(1-vn)^2}} \right]_{t'} , \\ \widetilde{\mathbf{H}} &= \frac{1}{4\pi} \left[-\frac{\widetilde{C}}{R^2} \frac{\mathbf{n\times v}}{\mathbf{(1-vn)^3}} (\mathbf{1-v^2+\dot{v}R}) - \frac{\widetilde{\mathbf{C}}}{\mathbf{R}} \mathbf{n\times\dot{v}} - \frac{\widetilde{\mathbf{D}}}{\mathbf{R}} \frac{\mathbf{n\times v}}{\mathbf{(1-vn)^2}} \right]_{t'} = \mathbf{n\times\widetilde{E}} . \end{aligned} \tag{3}$$

These additional terms formally look like radiation terms. It can be demonstrated that the solutions of the Yang–Mills equations are automatically correct with accuracy of order g, in reality g^3, see [8,9], if the compatibility conditions are satisfied up to this order. Now let us consider the field of two color charges $\widetilde{P}$, $\widetilde{Q}$ moving along the z-axis towards each other with velocities v and $-w$, respectively. If their encounter is supposed to take place at time $t = 0$, their coordinates in the laboratory system are given as $z_1 = vt, z_2 = -wt$. Obviously, when the particles are far from each other their interaction can be assumed weak and their charges remain constant with high accuracy. Adapting the typical scale of non-Abelian (strong) interactions of about 1 fm we assume that the interaction is switched on just at this distance (scale) denoted as D. Obviously, this generates the characteristic time scale in the problem. Then the first "milestone" appears when the particles enter the interaction area, i.e. $T = -D/(v + w)$. The second time instant of importance is t'_1 when a signal of the appearance of charge $\widetilde{Q}_T$ at the distance of 1 fm reaches the first particle (with the color charge $\widetilde{P}$). Similarly for the second particle, the time when the charge $\widetilde{P}_T$ comes at the same distance is denoted by t'_2, where $\widetilde{P}_T$, $\widetilde{Q}_T$ are the color charges before entering the zone of interaction, i.e. before the time T, $t'_1 = \frac{1-w}{1+v}\ T$, $t'_2 = \frac{1-v}{1+w}\ T$. These expressions are easily extracted from the scheme in Fig. 1 by writing out the relations for the arrival of the "light" signals and charges at the points of interest. In the figure, these events take the form of the corresponding triangles. Just at these times the color charges start to rotate with respect to their constant color vector that is the vector peculiar to the partner charge before it entered the interaction area. This regime is going on up to the time $t'' = \frac{1-w}{1+v}\frac{1-v}{1+w}\ T$, which is the same for both particles. It is also the time necessary for a signal to reach the partner providing information on the beginning of rotation starting from its asymptotic charge value $\widetilde{P}_T$, ($\widetilde{Q}_T$). The velocity of a relativistic particle is determined by the relation $v = \left(1 - \frac{m^2}{\mathcal{E}^2}\right)^{1/2} \simeq 1 - \frac{m^2}{2\,\mathcal{E}^2}$, where m is the particle mass and $\mathcal{E}$ its energy. It allows us to estimate the order of magnitude for the characteristic time in the problem as $t' \sim \frac{m^2}{\mathcal{E}^2}\ T$, $t'' \sim \frac{m^4}{\mathcal{E}^4}\ T$. The collision energies of present heavy-ions facilities (RHIC and LHC) allow us to estimate the corresponding factors as $\mathcal{E}/m \sim 10$–10^2 and more. Another interesting scale appear in dipole configuration as distance δ between the dipole charges and we assume it to be of the order of the interquark distance in the nucleon; i.e. around $\delta = 1$ fm. Then in the laboratory system the dipole size (due

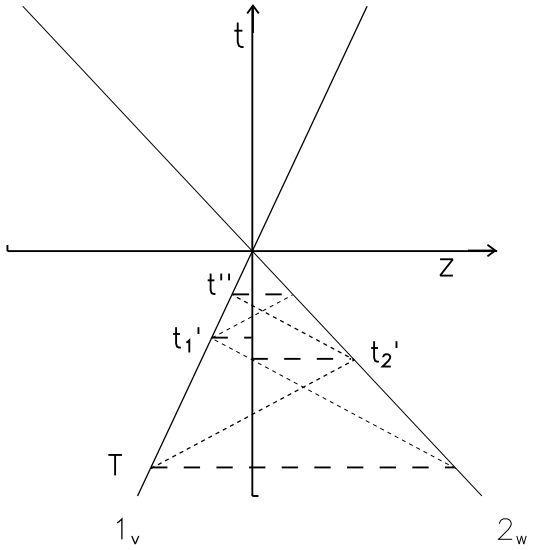

Figure 1. The time scheme for the meeting of two color particles. The solid lines are the particle trajectories, the dashed lines show projections on the time axis, the dotted lines are the light signals. Notations for the parameters T, $D = 1 \sim$ fm, t'_1, t'' are given in the text.

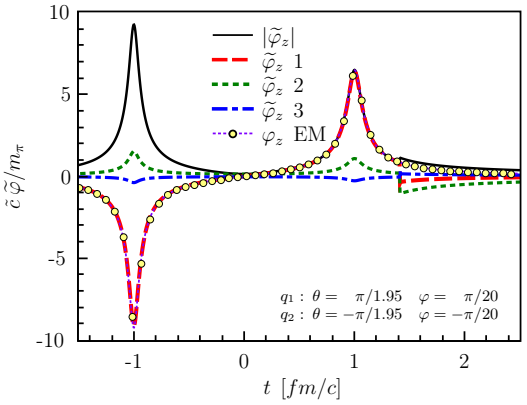

Figure 2. Time evolution of three color components for the scalar $\widetilde{\phi}$ for two oppositely directed charges in color space as a function of time is given by the dashed lines. The solid line shows the absolute value of the isovector potential $|\widetilde{\phi}|$. The electrodynamic potential with charges $\pm e$ corresponding to the coupling constant $\alpha_e = 0.3$ is displayed by open circles.

to Lorentz contraction) will be $\Delta = \delta\ (1 - v^2)^{1/2} \sim \delta\ \frac{m}{\mathcal{E}}$. Let us denote the time corresponding to this scale as $t_3 \sim m/\mathcal{E}$. Thus, for the relativistic problem of interest we obtain the following time hierarchy of interaction stages $t'' \ll t' \ll t_3 \ll T$. Due to the chosen geometry of the problem an approximate solution of the Yang-Mills equations for two color charges can be represented as the following superposition: $\widetilde{\varphi} = [\varphi_1 \widetilde{P}]_{t'} + [\varphi_2 \widetilde{Q}]_{t'}$, $\widetilde{A}_z = v\ [\varphi_1 \widetilde{P}]_{t'} - w\ [\varphi_2 \widetilde{Q}]_{t'}$. The scalar potentials can be specified as $\varphi_1 = \varphi_2 = \frac{1}{4\pi}\ \frac{g}{z_2 - z_1}$. Also, taking into account the form of the vector potential, we arrive at the following expression for the compatibility conditions:

$$\dot{\widetilde{P}} = \alpha_g\ \frac{1 + v\ w}{|z_1 - z_2|}\ \widetilde{Q}(t - t^{**}_{12}) \times \widetilde{P}\ , \quad \dot{\widetilde{Q}} = \alpha_g\ \frac{1 + v\ w}{|z_1 - z_2|}\ \widetilde{P}(t - t^{*}_{21}) \times \widetilde{Q}\ . \tag{4}$$

Details of derivation can be found in [10] As an example, let us consider the field created by two relativistic particles moving with velocities: $v = 1 - 2{\cdot}10^{-2}$ and $|w| = 1 - 1{\cdot}10^{-2}$. The energy-mass ratio for the first particle is $\mathcal{E}/m \simeq 16$, and for the second particle is $\mathcal{E}/m \simeq 22$. Let us take the coordinates of the observation point $\mathbf{r}_0$ as $x = 2$, $y = 0$, $z = 1$ (fm). For comparison, we consider also the field created by particles with electric charge $\pm e$ of the same interaction strength as the color charges ($e^2/(4\pi) = g^2/(4\pi) = 0.3$) moving with the same velocities. The potentials for the scalar $\widetilde{\varphi}$ field of color particles is presented in Fig. 2 where the initial angles

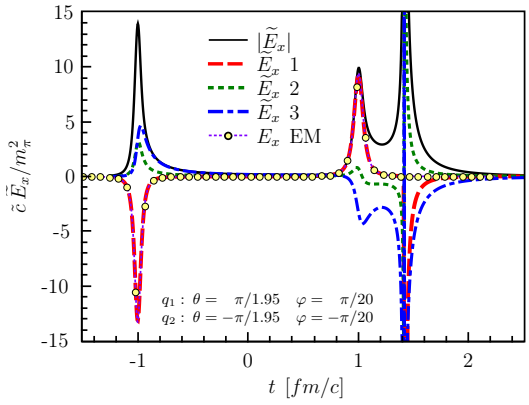

Figure 3. Three color components of the chromoelectric $\widetilde{E}$ field strength for two moving color charges of the opposite signs as a function of time (see the text).

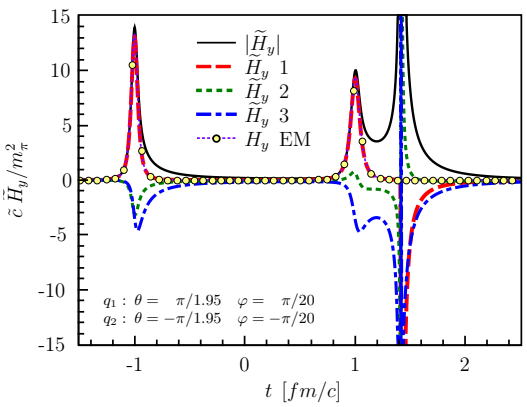

Figure 4. Three color components of the chromomagnetic $\widetilde{H}$ field strength for the same problem as in Fig. 3.

in the color space are determined as $\theta = \pi/1.95$, $\phi = \pi/20$ for the first particle and $\theta = -\pi/1.95$, $\phi = -\pi/20$ for the second one. In this case the color charge of the first particle, for example, will be $\widetilde{P} = (P_1, P_2, P_3)$, with $P_1 = \sin\theta\cos\phi$, $P_2 = \sin\theta\sin\phi$, $P_3 = \cos\theta$. This configuration of color charges $\widetilde{P}$, $\widetilde{Q}$ corresponds to almost oppositely directed charges at the initial stage. The dashed lines in this figure show the three color components of the scalar potential. The open circles are plotted for the potentials corresponding to the enhanced electrodynamic coupling. The modulus of the scalar $|\widetilde{\varphi}|$ is displayed by the solid lines in Fig. 2. According to the choice of the geometry, we see that the first maximum corresponds to the passage of the first particle at the closest distance to the observation point and then the second maximum is the corresponding passage of the second charge. Both bumps are located symmetrically with respect to the point $t = 0$. For the selected configuration of color charges, one of the components of the potentials, shown by the dashed lines, dominates and almost coincides with the appropriate modulus of vectors in the color space (solid line). The meeting point is located at a distance of $R = (x^2 + z^2)^{1/2} = \sqrt{5} \sim 2.24$ from the observation point. It is seen that there is a noticeable difference between the scalar potential as compared to the electrodynamic case (open circles) at the appropriate time when a signal on a meeting of the particles has arrived. The time dependence of the strength components of the chromoelectric $\widetilde{E}_x$ and chromomagnetic $\widetilde{H}_y$ fields is shown in Fig. 3, 4 by the three dashed lines; the solid lines correspond to the modulus of the chromofields $|\widetilde{E}_x|$ and $|\widetilde{H}_y|$; the open circles show the electrodynamic vector field corresponding to charges $\pm e$ and coupling constant $\alpha_e = 0.3$. We have cut the singular peaks at some threshold and thus the lines look somewhat irregular. The E_x and H_y components are dominating. In both cases two maxima (minima) caused by passing the color charges in the vicinity of the observation point are clearly visible. Note that here the color field strength is plotted in dimensionless units where $\widetilde{C}$ is the color charge of the appropriate field component and m_π is the pion mass. The charge velocities considered roughly correspond to the RHIC energy where the maximal electromagnetic field eH_y/m_π^2 reaches a few units [1]. This value is essentially smaller than those in the color charge case (see Fig. 3). It is seen that for the color charge configuration considered the chromoelectric and chromomagnetic field are quite similar to the field in the case of enhanced electrodynamics. Some difference in the hight of the first two maxima are caused by different velocities of color charges. A significant difference at the third maximum is due to the arrival of a signal from the meeting point of particles to the observation point, where there is a noticeable additional contribution of chromoelectric and chromomagnetic fields associated with the temporal change of the particle color charges. This "color glow" effect is not an artifact of the approximation made but results from the pure non-abelian term proportional to $\widetilde{D}$. The longitudinal component is strongly suppressed, as it should be due to relativistic effects, but the signal from the meeting point of the particles leads to almost equal contributions. In a similar manner the collision of a color charge and color dipole as well as of two color dipoles were considered. Such configurations are just the elementary basic examples in ultra-relativistic heavy-ion collisions in the existing phenomenological models. More results can be found in [10].

Acknowledgements. We are grateful to the meeting organizers and personally Professor V. Skalozub for a hospitality and excellent conditions for efficient work.

References

[1] V. Voronyuk, V.D. Toneev, W. Cassing, E.L. Bratkovskaya, V.P. Konchakovski, S.A. Voloshin, Phys. Rev. **C83**, 054911 (2011) [arXiv: 1103.4239].

[2] K. Tuchin, arXiv:1301.0099.

[3] J. Bloczynski, X.-G. Huang, X. Zhang, and J. Liao, Phys. Lett. B **718**, 1529 (2013) [arXiv:1209.6594].

[4] D.E. Kharzeev, K. Landsteiner, A. Schmidt and Ho-Ung Yee, Introduction to Lect. Notes Phys. "Strongly interacting matter in magnetic fields" (Springer), edited by D. Kharzeev, K. Landsteiner, A. Schmitt, H.-U. Yee, arXiv:1211.6245 [hep- ph].

[5] S. Voloshin, arXiv:1211.5680 [nucl-ex].

[6] B. Abelev *et al.* [ALICE Collaboration],

[7] L. D. Landau and E. M. Lifshitz, The Classical Theory of Fields, Fourth English Edition, Course of Theoretical Physics Volume 2, Butterworth/Heinmann, 1994.
Yu. P. Terletsky, Yu. P. Rybakov, Electrodynamics, Ed.-in "High School" , Moscow, 1990.

[8] I.B. Khriplovich, JETF **74**, 37 (1978).

[9] V.V. Goloviznin, S.V. Molodtsov and A.M. Snigirev, Yad. Fiz. **56**, 123 (1993).

[10] W. Cassing, V. V. Goloviznin, S. V. Molodtsov, A. M. Snigirev, V. D. Toneev, V. Voronyuk, G. M. Zinovjev, arXiv:hep-ph/13021313.

Proceedings of the International School-seminar
"New Physics and Quantum Chromodynamics at External Conditions", pp. 86 – 89,
May 22-24, 2013, Dnipropetrovsk, Ukraine

QUANTUM LIQUIDS RESULTED FROM THE MODELS WITH FOUR-FERMION INTERACTION

S. V. Molodtsov[a,†,‡], G. M. Zinovjev[b,◇]

[†]Joint Institute for Nuclear Research, Dubna, Moscow region, RUSSIA
[‡]Institute of Theoretical and Experimental Physics, Moscow, RUSSIA
[◇]Bogolyubov Institute for Theoretical Physics, National Academy of Sciences of Ukraine, Kiev, UKRAINE

A (nearly) perfect liquid discovered in the experiments with ultrarelativistic heavy ion collisions is investigated by studying the quark ensembles with four-fermion interaction as a fundamental theoretical approach. The comparative analysis of several quantum liquid models is performed and it results in the conclusion that the presence of gas—liquid phase transition is their characteristic feature.

Huge amount of data on relativistic heavy ion collisions obtained recently (perceptibly before the LHC began operating) in various experiments (first of all, at RHIC), were well understood and described in terms of concepts based on the equations of relativistic hydrodynamics. In particular, nearly ideal hydrodynamics, supplemented as needed by a variety of hadronic cascade models so as to correctly take into account a hadronic stage of the collision, quite successfully predicted an appearance of the radial and elliptic flows, their dependence on the mass, centrality, beam energy, and transverse momentum (though restricted in the magnitude), clearly indicating at the same time that the expanding liquid exhibits sufficiently specific transport properties. It is very much close to the ideal one, since the ratio η/s of its shear viscosity coefficient η to the density entropy s turned out to be a small quantity.

In the present work some aspects of thermodynamical description of the quark ensemble with four-fermion interaction (generated as it is believed by strong stochastic gluon fields), with the Hamiltonian density

$$\mathcal{H} = -\bar{q}\ (i\gamma\nabla + m)\ q - j^a_\mu \int d\mathbf{y}\ \langle A^a_\mu A'^b_\nu \rangle\ j'^b_\nu\ , \tag{1}$$

where $j^a_\mu = \bar{q} t^a \gamma_\mu q$ is the quark current, with corresponding quark operators q, $\bar{q}$, taken in spatial point $\mathbf{x}$ (the variables with prime corresponds to the $\mathbf{y}$ point), m is the current quark mass, $t^a = \lambda^a/2$ is the color gauge group $SU(N_c)$ generators, $\mu, \nu = 0, 1, 2, 3$. We take the gluon field correlator $\langle A^a_\mu A'^b_\nu \rangle$ in simple singlet in color form, with contact in time interaction (without retarding) $\langle A^a_\mu A'^b_\nu \rangle = G\ \delta^{ab}\ \delta_{\mu\nu}\ F(\mathbf{x}-\mathbf{y})$, (we do not include corresponding delta-function on time in this formula). This simple correlation function is a fragment of corresponding ordered exponent and besides the four-fermion interaction accompanied infinite number of multifermion vertices arises. The mentioned above effective interactions appear in natural way by the coarse-grained description of the system with exploiting the corresponding averaging procedure, and having in mind that vacuum gluon field changed stochastically far enough (for example, in the form of instanton liquid, see [1]). The formfactor $F(\mathbf{x})$ is interpreted in a simple way as an interaction 'potential' of point-like particles. The correlation function itself looks, formally, like a gauge noninvariant object. Nevertheless, there exists an effective way to significantly compensate for this shortcoming, if all similar 'potentials' are looked through, in some sense. For example, this set will be wide enough, if it will turn out to be possible to confront two limits opposite in physics, starting from the form factor with a delta-like function in the coordinate space (the Nambu–Jona-Lasinio (NJL) model [2], the correlation length in this case is finite since the regularization is done) and ending up with a delta-like function in the momentum space (it is clear that in this case the correlation length tends to infinity) analogous to that is well known in condensed matter physics, and named as the Keldysh model (KKB) [3].

It is believed that at sufficiently large interaction the ground state of the system transforms from a trivial vacuum $|0\rangle$ (the vacuum of free Hamiltonian) to the mixed state (with quark–anti-quark pairs with the opposite momenta and vacuum quantum numbers), which is presented as the Bogolyubov trial function $|\sigma\rangle = \mathcal{T}|0\rangle$, $\mathcal{T} = \prod_{p,s} \exp[\varphi_p\ (a^+_{p,s} b^+_{-p,s} + a_{p,s} b_{-p,s})]$. Here a^+, a b^+, b are the quarks creation and annihilation operators, $a|0\rangle = 0$, $b|0\rangle = 0$. The dressing transformation $\mathcal{T}$ transmutes the quark operators to the creation and annihilation operators of quasiparticles $A = \mathcal{T}\ a\ \mathcal{T}^\dagger$, $B^+ = \mathcal{T}\ b^+ \mathcal{T}^\dagger$. The thermodynamic properties of a quark ensemble are known to be determined by solving the following problem. It is required to find such a statistical operator $\xi = e^{-\beta\ \hat{H}_{\rm app}}/Z_0$, $Z_0 = {\rm Tr}\ \{e^{-\beta\ \hat{H}_{\rm app}}\}$ that at fixed mean charge $\overline{Q}_0 = {\rm Tr}\{\xi\ Q_0\} = V\ \gamma\ \int d\widetilde{\mathbf{p}}\ (n - \bar{n})$, $(Q_0 = \bar{q}\gamma^0 q)$,

e-mail: [a]Serguei.Molodtsov@cern.ch, [b]Gennady.Zinovjev@cern.ch

and fixed mean entropy $\overline{S} = -\mathrm{Tr}\{\xi\ S\} = -V\ \gamma\ \int d\widetilde{\mathbf{p}}\ [n\ln n + (1-n)\ln(1-n) + \bar{n}\ln\bar{n} + (1-\bar{n})\ln(1-n)]$, $(S = -\ln\xi)$, the mean energy of the quark ensemble $E = \mathrm{Tr}\{\xi\ H\}$, $(H = \int d\mathbf{x}\ \mathcal{H})$ would be minimal. In other words we are interested in the minimum of the following functional $\Omega = E - \mu\ \overline{Q}_0 - T\ \overline{S}$ where μ and T denote the Lagrangian multiplier for the chemical potential of the quark/baryon charge (which is in phenomenological considerations usually taken to be three times larger than the baryon one) and the temperature $(\beta = T^{-1})$,respectively. V is the volume the system is enclosed in $d\widetilde{\mathbf{p}} = d\mathbf{p}/(2\pi)^3$, $\gamma = 2N_c$ (in the case of several quark flavors $\gamma = 2N_cN_f$, where N_f is the flavor number), $n = \mathrm{Tr}\{\xi A^+A\}$, $\bar{n} = \mathrm{Tr}\{\xi B^+B\}$ are the components of the corresponding density matrix. We restrict ourselves by considering the Bogolyubov–Hartree–Fock approximation. The average specific energy per quark $w = E/(V\gamma)$ results in $w = \int d\widetilde{\mathbf{p}}\ p_0 - \int d\widetilde{\mathbf{p}}\ (1-n-\bar{n})\ p_0\ \cos\theta - \frac{1}{2}\ \int d\widetilde{\mathbf{p}}\ (1-n-\bar{n})\sin(\theta-\theta_m)\ M(\mathbf{p})$, where $M(\mathbf{p}) = 2G\int d\widetilde{\mathbf{q}}\ (1-n'-\bar{n}')\ \sin(\theta'-\theta'_m)\ F(\mathbf{p}+\mathbf{q})$, $\theta = 2\varphi$, $p_0 = (\mathbf{p}^2+m^2)^{1/2}$, the primed variables, hereinafter correspond to the integration over momentum $\mathbf{q}$. The auxiliary angle θ_m is determined from the relation $\sin\theta_m = m/p_0$. The first term is introduced in view of normalizing such that the energy of ground state is zero when an interaction is switched off. For delta-like potential in coordinate space (the NJL model) the expression for w diverges and to obtain the reasonable results the upper limit cutoff in the momentum integration Λ is introduced being one of the tuning model parameters along with the coupling constant G and current quark mass m. Below we use one of the standard sets of the parameters for the NJL model: $\Lambda = 631$ MeV, $G\Lambda^2/(2\pi^2) \approx 1.3$, $m = 5.5$ MeV, whereas the KKB model parameters are chosen in such a way that for the same quark current masses the dynamical quark ones in both NJL and KKB models coincide at vanishing quark momentum. Using the properties of extremals the functional w can be transformed to the form (see [4])

$$w = \int d\widetilde{\mathbf{p}}\ p_0 - \int d\widetilde{\mathbf{p}}\ (1-n-\bar{n})\ P_0 + \frac{1}{4G}\ \int d\widetilde{\mathbf{p}}d\widetilde{\mathbf{q}}\ \ F(\mathbf{p}+\mathbf{q})\ \widetilde{M}(\mathbf{p})\widetilde{M}(\mathbf{q})\ , \tag{2}$$

where $P_0 = [\mathbf{p}^2 + M_q^2(\mathbf{p})]^{1/2}$ is the energy of quark quasiparticle with the dynamical quark mass $M_q(\mathbf{p}) = m + M(\mathbf{p}) = m + \int d\widetilde{\mathbf{q}}\ F(\mathbf{p}+\mathbf{q})\ \widetilde{M}(\mathbf{q})$. Below we omit often the arguments of corresponding functions for the mass and quasiparticle energy. Varying the functional (2) with respect to the density of induced quasiparticle mass $\widetilde{M}$ (in such a form it is convenient to take variational derivatives) we obtain the equation for dynamical quark mass as $M_q(\mathbf{p}) = m + 2G\int d\widetilde{\mathbf{q}}\ (1-n'-\bar{n}')\ \frac{M'_q}{P'_0}\ F(\mathbf{p}+\mathbf{q})$, which corresponds exactly to the mean field approximation. In particular, under normal conditions $(T=0,\ \mu=0)$ the dynamical quark mass in the NJL model is $M_q \sim 340$ MeV, whereas the dynamical quark mass of the KKB model is determined by the following equation $M(\mathbf{p}) = 2G\ M_q(\mathbf{p})/P_0$. In practice, it is convenient to use an inverse function $p(M_q)$. In particular, in the chiral limit $M_q = (4G^2 - \mathbf{p}^2)^{1/2}$, at $|\mathbf{p}| < 2G$, and $M_q = 0$ when $|\mathbf{p}| > 2G$. In this case the quark states with momenta $|\mathbf{p}| < 2G$ are degenerate in energy $P_0 = 2G$. The goal that we pursued while passing from the expression for specific energy w to the form (2) was to derive such a form that would easily be recognized as an energy functional of the Landau Fermi-liquid theory [5]. Some aspects of this theory turn out to be interesting and useful to apply so as to be able to compare the results obtained in the NJL and KKB models. Thus, the second term in (2) describes the contributions coming from quark and antiquark quasiparticles with occupation numbers n and $\bar{n}$ respectively. The unity in the expression $1-n'-\bar{n}'$ corresponds to the vacuum fluctuations of quarks and antiquarks (separately, each of their modes gives 1/2). The last term in (2) is due to the interaction of quasiparticles. The presence of contributions coming from antiparticles and relativistic form of the dynamics are those features which distinguish quark ensembles we study from the Fermi-liquids considered in condensed matter physics. The first variation of the functional (2) with respect to the particle (antiparticle) density leads as it should be to the energy of a quasiparticle: $\frac{\delta w}{\delta n} = P_0$. Consider first the case of zero temperature and discuss some aspects of filling up the Fermi sphere by quarks. Let us assume that the momentum distribution of quarks (antiquarks) is determined by the following expressions taken at the limit $\beta \to 0$: $n = \left[e^{\beta(P_0-\mu)}+1\right]^{-1}$, $\bar{n} = \left[e^{\beta(P_0+\mu)}+1\right]^{-1}$, that is by the Fermi step function: $n = 1$, at $P_0 \le \mu$ and $n = 0$ when $P_0 > \mu$. It is clear that for antiquarks $\bar{n} = 0$. The quark density is determined by using the Fermi momentum: $\rho = \gamma P_{\mathrm{F}}^3(6\pi^2)$, $\rho = Q_0/V$, with the quark chemical potential coinciding with the quasiparticle energy on the Fermi surface $\mu = [P_{\mathrm{F}}^2 + M_q^2(P_{\mathrm{F}})]^{1/2}$. The group velocity of quasiparticles on the Fermi surface $v_f = \partial P_0/\partial\mathbf{p}|_{|\mathbf{p}|=P_{\mathrm{F}}}$, the density of states on the Fermi surface N_f, $N_{\mathrm{F}} = \gamma\int d\widetilde{\mathbf{p}}\ \delta(P_0-\mu) = \frac{\gamma}{2\pi^2}P_{\mathrm{F}}P_{\mathrm{F}}^0\ (1+F_0)^{-1}$, where $F_0 = \frac{M_q}{P_{\mathrm{F}}}\frac{dM_q}{dP_{\mathrm{F}}}$, $P_{\mathrm{F}}^0 = P_0|_{\mathbf{p}=P_{\mathrm{F}}}$, $N_{\mathrm{F}} = d\rho/d\mu$ was compared for considered models, details can be found in [6]. In an ideal gas, the interaction term in the functional (2) vanishes causing the derivative of the quark dynamical mass in the Fermi momentum to turn to zero: $dM_q/dP_{\mathrm{F}} = 0$. Let us define the density of states of an ideal gas as $\widetilde{N}_{\mathrm{F}} = \gamma/(2\ \pi^2)P_{\mathrm{F}}P_{\mathrm{F}}^0$, the, the following relation can be derived: $N_{\mathrm{F}} = \widetilde{N}_{\mathrm{F}}\,(1+F_0)^{-1}$. Another important characteristic is a compression coefficient $K = 9\rho\ \frac{d\mu}{d\rho} = 3\ \frac{P_{\mathrm{F}}^2}{\mu}\left(1+F_0\right)$. The data for the NJL and KKB models demonstrate that they are consistent with specific values obtained for nuclear medium [6]. In principle, these models admit a wide variety of state equations including sufficiently restrictive ones. The first sound velocity

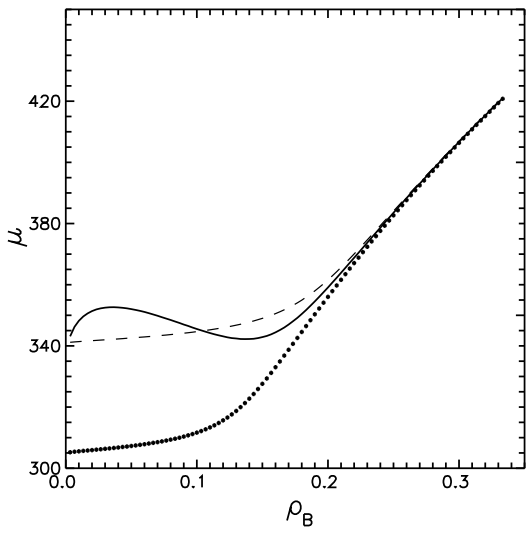

Figure 1. Chemical potential in MeV. For the NJL model it is seen that there is a region of occupied states almost degenerate with the vacuum chemical potential. Similarly, the chemical potential of occupied states in the KKB model differs from that in vacuum by a small quantity proportional to the quark current mass.

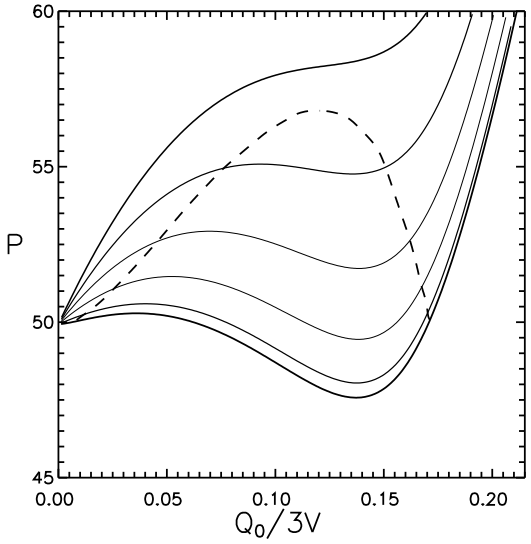

Figure 2. The ensemble pressure P (MeV/fm^3) is shown as a function of charge density $\mathcal{Q}_0$ at temperatures $T = 0$ MeV, ... , $T = 50$ MeV with spacing $T = 10$ MeV. The lowest curve corresponds to zero temperature. The dashed curve shows the boundary of phase transition liquid–gas, see the text.

could be obtained from the relation $C_1^2 = \frac{K}{9\ \mu} = \frac{v_{\rm F}^2}{3}\left(1 + F_0\right)$. When baryon densities are somewhat higher than that of normal nuclear matter, the sound velocity tends to its asymptotic value $C_1 = 1/\sqrt{3}$, which is a natural manifestation of the chiral invariance restoration. If the sound velocity of an ideal Fermi-gas $\widetilde{C}_1^2 = v_{\rm F}^2/3$ is introduced in a way similar to the $\widetilde{N}_{\rm F}$ definition, then it can be demonstrated that the flow coming through the Fermi sphere of quasiparticles of (imaginary) ideal Fermi-gas and interacting Fermi-liquid coincide (that is, there basically is a relativistic analogue of the Luttinger theorem [7]) $N_{\rm F}\ C_1^2 = \widetilde{N}_{\rm F}\ \widetilde{C}_1^2$. The thermal conductivity at constant volume and low temperatures $C_{\rm V} = \frac{1}{3}\ \pi^2 N_{\rm F}\ T$ with the slope (the factor $\frac{1}{3}\pi^2 N_{\rm F}$, $N_{\rm F} = d\rho/d\mu$) would be very informative if measured [6]. Yet another important characteristic of a Fermi-liquid is defined by a second variational derivative, which in the case of the functional (2) has only a scalar component: $f_0 = \frac{\delta^2 w}{\delta n^2} = \frac{M_q}{P_0}\frac{\delta M_q}{\delta n}$. For a Fermi-liquid at zero temperature, in particular, we have $f_0 = \frac{2\pi^2}{\gamma P_{\rm F}\ P_{\rm F}^0}\frac{M_q}{P_{\rm F}}\frac{dM_q}{dP_{\rm F}}$. For example, in the NJL model $\frac{M_q}{P_{\rm F}}\frac{dM_q}{dP_{\rm F}} = -\frac{P_{\rm F}}{P_{\rm F}^0}\frac{1}{I + \pi^2 m/(GM_q^3)}$, $I = \ln\frac{\Lambda + P_\Lambda^0}{P_{\rm F} + P_{\rm F}^0} - \frac{\Lambda}{P_\Lambda^0} + \frac{P_{\rm F}}{P_{\rm F}^0}$, where $P_\Lambda^0 = P_0|_{|\mathbf{p}|=\Lambda}$. In the KKB model $\frac{M_q}{P_{\rm F}}\frac{dM_q}{dP_{\rm F}} = -\frac{M\ M_q^2}{M_q^3 + mP_{\rm F}^3}$. In particular, in the chiral limit, when $m = 0$, we have $(M_q/P_{\rm F})(dM_q/dP_{\rm F}) = -1$. The collective oscillation modes of a Fermi-liquid, the so-called zero sound (the collisionless mode) are found by using the parameter $F_0 = \widetilde{N}_{\rm F}\ f_0 = \frac{M_q}{P_{\rm F}}\frac{dM_q}{dP_{\rm F}}$. In particular, in the KKB model $F_0 = -\frac{MM_q^2}{MM_q^2 + (P_{\rm F}^0)^2 m} \geq -1$.

Turn now to the chemical potential of quasiparticles presented in Fig. 1. From the data for the NJL model it is seen that there is a region of occupied states almost degenerate with respect to the chemical potential, with the vacuum chemical potential of a quasiparticle that quite naturally corresponds to the vanishing Fermi momentum. Similarly, the chemical potential of occupied states in the KKB model differs from that in vacuum by a small quantity proportional to the quark current mass: $\frac{d\mu}{d\rho} = \frac{\mu}{\rho}\frac{v_{\rm F}^2}{3}\left(1 + \frac{M_q}{P_{\rm F}}\frac{dM_q}{dP_{\rm F}}\right) \sim m$. In the chiral limit, all the states with momentum $|\mathbf{p}| < 2G$ are degenerate with respect to the chemical potential. $M_q = (4G^2 - \mathbf{p}^2)^{1/2}$, $P_0 = 2G$, when $P_{\rm F} < |\mathbf{p}| < 2G$, $M_q = 0$, $P_0 = |\mathbf{p}|$ if $|\mathbf{p}| < P_{\rm F}$, and $|\mathbf{p}| > 2G$. Such a behavior of the chemical potential is a consequence of a rapid decrease of the dynamical quark mass with increasing Fermi momentum.

It comes about that the pressure of some occupied states degenerate in the chemical potential almost coincides with that of vacuum (the pressure of a dilute Fermi-gas) ($T = 0$) $P = -\frac{dE}{dV} = -\mathcal{E} + \mu\ \rho$, where $\mathcal{E} = E/V$ is the specific energy. In the KKB model, the energy (and, hence, the pressure) of ensemble is a discontinuous functional of the quark current mass (see [1]). By virtue of the singular pressure of ensemble in the KKB model, it appears sensible to consider the relative pressure of quark ensemble in comparison with a (formally infinite) vacuum value. The pressure derivative in the ensemble density has the form: $dP/d\rho = \rho\ d\mu/d\rho$. Therefore one can conclude that in the chiral limit the occupied states with momenta $|\mathbf{p}| < 2G$, are observed to also

degenerate in the KKB model with respect to the pressure ($\mathcal{E} = 2G\rho$, $\mu = 2G$). Beyond the chiral limit, the deviations are proportional to the quark current mass. Now, determine some thermodynamic properties of a system and consider first the pressure of quark ensemble in a more detail: $P = -\frac{dE}{dV}$. By definition, the volume derivative should be taken at the constant mean entropy, $d\bar{S}/dV = 0$. Treating this condition, one can, for example, extract the volume derivative of the chemical potential $d\mu/dV$. However, this approach cannot be considered as acceptable because the mean charge $\bar{Q}_0$ might change. There is only one possibility to satisfy both conditions, namely, to introduce two independent chemical potentials for quarks and antiquarks. For the quark chemical potential we use a symbol μ introduced earlier, whereas the antiquark chemical potential is taken opposite in charge and denoted as $\bar{\mu}$. Here we are only interested in a special situation when $\bar{\mu} = \mu$. Manipulating the conditions of constant mean entropy and of mean charge conservation for the pressure we have $P = -\frac{E}{V} + \frac{\bar{S}\ T}{V} + \frac{\bar{Q}_0\ \mu}{V}$. We see that the thermodynamic potential Ω satisfies the thermodynamic identity $\Omega = -PV = E - \mu\ \overline{Q}_0 - T\ \overline{S}$, as it does. Fig.2 shows the ensemble pressure P in MeV/fm^3 as a function of the charge density $\mathcal{Q}_0/3V$ for various temperatures. A lower curve is obtained at zero temperature. Next curves following upwards correspond to temperatures $T = 10$ MeV, $T = 50$ MeV (an upper curve) with a step $T = 10$ MeV. Let us also remember that, for the NJL model, the pressure of vacuum was estimated in [1] to be 40 to 50 MeV/fm^3, consistent with those obtained in the bag model. It was also demonstrated that there is a region of instability within a certain interval of the Fermi momenta generated by the anomalous behavior of the pressure $dP/dn < 0$ (see also [8]). The equilibrium points obtained are shown in Fig. 2 by a dashed curve. The points at which a dashed curve intersects with isotherm give a boundary for a gas-liquid phase transition. The respective line $P = \text{const}$ cuts off nonequilibrium and unstable fragments of isotherm and describes a mixed phase. For the tuning parameters, the critical temperature turns out to be equal to $T_c \approx 46$ MeV with a critical charge density $\bar{Q}_0 \approx 0.12$ charge/fm^3. In [4] it was shown that if the quark chemical potential is defined as energy necessary to add (remove) one quasiparticle, $\mu = dE/dN$, then the chemical potential in vacuum coincides with the quark dynamical mass. Therefore, it seems to be reasonable to consider a QCD phase diagram by starting from this value of the chemical potential, though formally it can be taken to be smaller than the quark dynamical mass. In particular, by taking the chemical potential to be zero, we exactly reproduce a standard one picture. The results obtained allowed to conjecture that the phase transition of (partial) restoration of the chiral invariance can already be realized in nature as a mixed phase of physical vacuum and baryonic matter.

Acknowledgements. We are grateful to the meeting organizers and personally V.V. Skalozub for a hospitality and excellent conditions for efficient work.

References

[1] G. M. Zinovjev and S. V. Molodtsov, Theor. Mat. Phys. **160** (2009) 444;
S. V. Molodtsov and G. M. Zinovjev, Phys. Rev. **D80** (2009) 076001;
S. V. Molodtsov, A. N. Sissakian and G. M. Zinovjev, Europhys. Lett. **87** (2009) 61001.

[2] Y. Nambu and G. Jona-Lasinio, Phys. Rev. **122** (1961) 345.

[3] M. V. Sadovskii, Diagrammatics, World Scientific, Singapore, 2006.
L. V. Keldysh, Doctor thesis, FIAN, (1965);
E. V. Kane, Phys. Rev. **131** (1963) 79;
V. L. Bonch-Bruevich, in 'Physics of solid states', VINITI, Moscow, 1965.

[4] S. V. Molodtsov and G. M. Zinovjev, Europhys. Lett. **93** (2011) 11001;
S. V. Molodtsov and G. M. Zinovjev, Phys. Rev. **D84** (2011) 036011;
G. M. Zinovjev and S. V. Molodtsov, Yad. Phys. **75** (2012) 262.

[5] L. D. Landau, JETP **30** (1956) 1058; **32** (1957) 59;
D. Pines and Ph. Nozieres, Theory of Quantum Liquids, W. A. Benjamin, New York, 1966;
Ph. Nozieres, Theory of Interacting Fermi Systems, Westview Press, Boulder, 1997;
A. J. Leggett, Quantum Liquids, Oxford University Press, Oxford, 2006.

[6] S.V. Molodtsov, G.M. Zinovjev, arXiv:1307.0686.

[7] J. M. Luttinger and J. C. Ward, Phys. Rev. **118** (1960) 1417;
J. M. Luttinger, Phys. Rev. **119** (1960) 1153.

[8] H. Tezuka, Phys. Rev. **C22** (1980) 2585; **C24** (1981) 288;
G. Baym and S. A. Chin, Nucl. Phys. **A262** (1976) 537;
T. Matsui, Nucl. Phys. **A370** (1981) 369.

Proceedings of the International School-seminar
"New Physics and Quantum Chromodynamics at External Conditions", pp. 90 – 93,
May 22-24, 2013, Dnipropetrovsk, Ukraine

$2D$ $O(3)$ SIGMA MODEL WITH θ-TERM: CONSTRUCTION OF A POSITIVE BOLTZMANN WEIGHT

O. Borisenko[1,a], V. Kushnir[1,b], B. Allés[2,c], A. Papa[3,d], C. Torrero[4,e]

[1]N.N.Bogolyubov Institute for Theoretical Physics, Kiev, Ukraine
[2]INFN Sezione di Pisa, Pisa, Italy
[3]Dipartimento di Fisica, Università della Calabria and INFN Gruppo Collegato di Cosenza, Cosenza, Italy
[4]Dipartimento di Fisica e Scienze della Terra and INFN Sezione di Parma, Parma, Italy

The continuum limit of the dual formulation of the two-dimensional lattice $SU(N)$ principal chiral model is constructed. The continuum action is in general complex and appears to be a functional of an (N^2-1)-component non-compact scalar field. As an application of this construction we establish a relation between the dual of the $SU(2)$ principal chiral model and the $O(3)$ non-linear sigma model with a θ-term in the continuum limit. This relation is exact when the radial part of the scalar dual field is taken to be a constant. Therefore, the dual formulation of the lattice $SU(2)$ model with constant radial part can be regarded as a non-perturbative regularization of the $O(3)$ model with θ term. Furthermore, under certain conditions one could construct a positive definite dual Boltzmann weight. This property enables us to prospect Monte Carlo simulations of $O(3)$ with a θ term at *real* values of θ.

1 Introduction

In this paper we discuss the continuum limit of the dual formulation of the two-dimensional ($2D$) $SU(N)$ principal chiral model. Our chief interest relies on the fact that upon certain condition on the dual field, the resultant model for $N=2$ turns out to be a valid discretization of the $2D$ $O(3)$ non-linear sigma model with a θ term.

While at $\theta=0$ the $O(3)$ model is integrable [1] with a spectrum exhibiting a massive triplet of scalars [2,3], the physics of this model gets notoriously enriched when the topological parameter θ is switched on. At $\theta=\pi$ it has been argued that the theory is massless (Haldane conjecture) [4–10]. Then, as θ gets lower starting from $\theta=\pi$, the spectrum develops a massive singlet along with the previously mentioned triplet with masses $m_S(\theta)$ and $m_T(\theta)$ respectively. In particular these masses are proportional to $(\pi-\theta)^{\frac{2}{3}}$ for values of θ that are close to π from below [11]. It has been shown, [12–15], that $m_S(\theta)$ is permanently larger than $m_T(\theta)$. Since at $\theta=0$ the spectrum is exclusively composed by the triplet, it has been conjectured that at some critical value $0<\theta_c<\pi$ the mass $m_S(\theta_c)$ becomes exactly twice $m_T(\theta_c)$ in such a way that for any $\theta<\theta_c$ the singlet copiously decays into states belonging to the triplet. Finally, as $\theta\to 0$ the value of $m_S(\theta)$ should diverge, thus leaving the theory without θ bereft of the singlet state.

Monte Carlo simulations on the lattice are a unique tool to probe the physical properties of any statistical model. For the case at hand, numerical computer simulations could greatly help in clarifying the particle content and the θ-dependence of their masses. However, a straightforward attempt to simulate the model by discretizing its action is doomed to failure because the topological θ-term is pure imaginary. Only at $\theta=0$ the problem completely disappears. This is a heavy drawback as importance sampling, which lies at the root of the Monte Carlo process, applies only as long as Boltzmann weights are strictly positive. Thus, one could only simulate the model at imaginary values of θ when the Boltzmann weight becomes positive. In [16] the Haldane conjecture has been verified by extrapolating the mass derived at imaginary values of θ towards the real θ-axis.

The $2D$ $O(3)$ non-linear sigma model with a non-zero θ term is not the only theory afflicted by the above problem. Also QCD at finite quark density cannot be directly simulated because the chemical potential is pure imaginary. None of the known methods provides information about the singlet state and the θ dependence of its mass. Therefore, new simulation algorithms able to examine the model well within the region of real finite θ would be very welcome. In this contribution we derive a non-perturbative regularization for the $2D$ $O(3)$ non-linear sigma model with θ term. This regularization enables us to construct a positive Boltzmann weight which, thus, can be used for Monte Carlo simulations of the model.

We shall work on a $2D$ lattice $\Lambda\in Z^2$ with lattice spacing a and a linear extension L. Periodic boundary conditions are imposed in both directions. Let us define three partition functions:

e-mail: [a]oleg@bitp.kiev.ua, [b]vkushnir@bitp.kiev.ua, [c]alles@df.unipi.it, [d]papa@cs.infn.it, [e]christian.torrero@fis.unipr.it

1. Partition function of the lattice $SU(N)$ principal chiral model in the link formulation [17–19]

$$Z_{SU(N)} \;=\; \int \prod_l dV(l) \exp\left[\beta \sum_l \mathrm{Tr} V(l)\right] \prod_x \left[\sum_r d(r)\chi_r(V_x)\right] \;, \tag{1}$$

where $V(l)$ is the $SU(N)$ matrix associated to the link l, $d(r)$ is the dimension of the representation r and $\chi_r(V_x)$ is the character of the r-th representation. The matrix V_x is defined as

$$V_x \;=\; V(l_1)V(l_2)V^\dagger(l_3)V^\dagger(l_4) \;=\; \exp[i\lambda_k\, \omega_k(x)] \;. \tag{2}$$

Here, l_i are 4 links attached to the site x. The expression $\sum_r d(r)\chi_r(V_x)$ is the $SU(N)$ delta-function which introduces the constraint $V_x = 1$ on the link matrices (local Bianchi identity).

2. We shall use also the following partition function

$$Z(\beta, R) \;=\; \int \prod_l dV(l) \exp\left[\beta \sum_l \mathrm{Tr} V(l)\right] \prod_x \frac{\sin R\;\omega(x)}{\sin \omega(x)} \;. \tag{3}$$

Here, $\omega(x) = (\sum_{k=1}^3 \omega_k^2(x))^{\frac{1}{2}}$ and $\omega_k(x)$ are the angles parameterizing the $SU(2)$ matrix in (2). R is an arbitrary real number. If $R = 2r + 1$ with r taking integer and half-integer values then the expression under the product over x in the last formula is an $SU(2)$ character and the partition function (3) can be regarded as being obtained from (1) by fixing all representations to some constant. Since delta-function is not present, we refer to the model (3) as unconstrained $SU(2)$ model.

3. The partition function of the $O(3)$ non-linear sigma model with a θ-term in the continuum is given by

$$Z_{O(3)} \;=\; \int \prod_{k=1}^3 D\sigma_k(x) \;\exp\left[-\frac{1}{2}\beta_{O(3)} \int d^2x (\partial_\mu \sigma_k(x))^2 + i\theta S_q\right] \;. \tag{4}$$

The integration is performed with the constraint $\sum_{k=1}^3 \sigma_k^2(x) = 1$. The θ-term or topological action S_q reads

$$S_q \;=\; \int \frac{d^2x}{8\pi}\; \epsilon^{\mu\nu}\epsilon^{knm}(\partial_\mu\sigma_k)(\partial_\nu\sigma_n)\sigma_m \;. \tag{5}$$

Below we address the following problems:

- construction of the continuum limit of the $SU(N)$ principal chiral model in the link formulation (1);
- as an application of this construction we establish an exact relation between the $O(3)$ non-linear sigma model with a θ-term and the continuum limit of the unconstrained $SU(2)$ model;
- derivation of a positive definite Boltzmann weight.

2 Continuum limit of the $SU(N)$ principal chiral model

The construction of the continuum limit of the $SU(N)$ principal chiral model (1) uses essentially one basic fact: when $\beta \to \infty$ all link matrices perform only small fluctuations around the unit matrix (for a thorough discussion of this property, see [18]; for a rigorous proof, see [20]). More precisely, any configuration of the link matrix for which $\omega_k(l) > \mathcal{O}(1/\sqrt{\beta})$ is exponentially suppressed and becomes singular in the continuum limit. On smooth configurations the Bianchi constraint $V_x = 1$ can only be satisfied when $\omega_k(x) = 0$ for all $k = 1, \ldots, N^2 - 1$. Therefore, the $SU(N)$ delta-function can be replaced by the Dirac delta-functions

$$\sum_r d(r)\chi_r(V_x) \;\longrightarrow\; \prod_{k=1}^{N^2-1} \int_{-\infty}^{\infty} e^{i\alpha_k(x)\omega_k(x)}\; d\alpha_k(x) \;. \tag{6}$$

Then, the continuum limit for smooth configurations can be constructed in the standard way:

1. introduce dimensionful vector potentials $\omega_k(l) = aA_k(l)$ and expand the action and angles $\omega_k(x)$ in powers of the lattice spacing a;
2. replace the $SU(N)$ invariant measure by a flat measure and extend the integration region over potentials $A_k(l)$ to the non-compact region $A_k(l) \in [-\infty, \infty]$;
3. in the limit $a \to 0$ finite differences are replaced by derivatives and sums by integrals.

Neglecting terms which vanish in the limit $a \to 0$ one gets a Gaussian integral over vector fields $A_k(l)$. Integration over $A_k(l)$ produces a local continuum theory for the dual scalar potentials $\alpha_k(x)$ which can be written as

$$Z_{SU(N)} \;=\; \int_{-\infty}^{\infty} \; e^{-S_{\rm eff}} \; \prod_{k=1}^{N^2-1} \; d\alpha_k(x) \; . \tag{7}$$

The effective continuum action reads

$$S_{\rm eff} \;=\; \frac{1}{4} \int d^2x \;\; (\partial_\mu \alpha_k(x)) \;\; M^{kn}_{\mu\nu} \;\; (\partial_\nu \alpha_n(x)) - \frac{1}{2} \int d^2x \;\;\; \ln {\rm Det} M \; , \tag{8}$$

where the inverse of the matrix M is given by

$$\left[M^{kn}_{\mu\nu} \right]^{-1} \;=\; \beta \; \delta_{\mu\nu} \; \delta_{kn} \;\; - \;\; i \epsilon^{\mu\nu} \; f^{knm} \; \alpha_m(x) \; . \tag{9}$$

Here we turn our attention to the specific model with $N = 2$. In this case $f^{knm} = \epsilon^{knm}$ and both ${\rm Det} M$ and the matrix M can be easily deduced. Let us make the change of variables $\alpha_k(x) = R(x) \; \sigma_k(x)$, $\sum_{k=1}^{3} \sigma_k^2(x) = 1$. By substituting the last formulas into (7) we get for the continuum limit of the $SU(2)$ principal chiral model

$$Z_{SU(2)} = \int_0^\infty \; \prod_x \; \frac{R^2(x) dR(x)}{\beta \left(\beta^2 + R^2(x) \right)} \; \int \; \prod_x \left[\delta(1 - \sum_{k=1}^{3} \sigma_k^2(x)) \prod_{k=1}^{3} \; d\sigma_k(x) \right] \exp \left[- \int \; d^2x \; \mathcal{L}(R(x), \sigma_k(x)) \right] , \tag{10}$$

$$\mathcal{L}(R(x), \sigma_k(x)) \;\equiv\; \frac{1}{4} \;\; (\partial_\mu [R(x) \sigma_k(x)]) \;\; M^{kn}_{\mu\nu} \;\; (\partial_\nu [R(x) \sigma_n(x)]) \;\; , \tag{11}$$

$$M^{kn}_{\mu\nu} \;=\; \frac{1}{\beta^2 + R^2(x)} \;\; \left[\delta_{\mu\nu} \left(\beta \delta_{kn} + \frac{R^2(x)}{\beta} \sigma_k(x) \sigma_n(x) \right) + i R(x) \; \epsilon^{\mu\nu} \; \epsilon^{knm} \; \alpha_m(x) \right] \; . \tag{12}$$

Consider the $SU(2)$ model obtained above on a constant configuration $R(x) = R = {\rm const}$. Noting that $\sum_k \sigma_k(x) \partial_\mu \sigma_k(x) = 0$, one can see that the Lagrangian (11) becomes that of the $O(3)$ sigma model with a θ term. Moreover, this constant radial part R of the dual field $\alpha_k(x)$ can be identified with the parameter R introduced in the unconstrained $SU(2)$ model (3). Indeed, up to terms of order $\mathcal{O}(a^4)$ which vanish in the continuum limit, the factor $\sin R\omega / \sin \omega$ in (3) can be represented as

$$\frac{\sin R\omega}{\sin \omega} \;\approx\; R \frac{\sin R\omega}{R\omega} \;=\; R \; \int \; \delta \left(1 - \sum_{k=1}^{3} \sigma_k^2 \right) \prod_{k=1}^{3} \; d\sigma_k \; e^{i R \omega_k \sigma_k} \; . \tag{13}$$

Using the above calculations for the $SU(2)$ principal chiral model and formula (13) we can easily compute the continuum limit of the unconstrained $SU(2)$ model obtaining the following relation between partition functions

$$Z_{O(3)} \;=\; \left[C(\beta, R) \right]^{L^2} \;\; Z(\beta, R) \; , \tag{14}$$

valid in the continuum limit. The relation between the couplings in both models can be read off from the Lagrangian (11) by taking $R(x) = R$ and comparing it with the Lagrangian of the $O(3)$ model. We have for the direct relation

$$\beta_{O(3)} = \frac{\beta}{2} \;\; \frac{R^2}{R^2 + \beta^2} \; , \; \theta = 2\pi R \;\; \frac{R^2}{R^2 + \beta^2} \; . \tag{15}$$

3 Positive Boltzmann weight

As is seen from (14), the unconstrained $SU(2)$ model does provide a lattice non-perturbative regularization for the $O(3)$ model with real θ. Its Boltzmann weight is real but not necessarily positive. Here we re-write the model in a form such that the Boltzmann weight becomes positive definite. To do that let us consider the following expansion into $SU(2)$ characters

$$\frac{\sin R\omega}{\sin \omega} \;=\; \sum_r \; A_r(R) \; \chi_r(\omega) \; , \tag{16}$$

where the sum runs over all non-negative integers and half-integers and the coefficients $A_r(R)$ of the expansion are given by

$$A_r(R) \;=\; \{ \, \delta_{\, r,s} \, , \; \text{if } \; R = 2s+1, s = 0, 1/2, 1, ... \frac{2 \sin \pi R}{\pi} \;\; \frac{(-1)^{(2r+1)} (2r+1)}{R^2 - (2r+1)^2}, \; \text{otherwise} \; . \tag{17}$$

Then, the partition function (3) appears as

$$Z(\beta,R) \;=\; \sum_{\{r(x)\}} \prod_x \; A_{r(x)}(R)\; \tilde{Z}(\beta,R;[r(x)]) \;, \tag{18}$$

$$\tilde{Z}(\beta,R;[r(x)]) \;=\; \int \prod_l dV(l) \exp\left[\beta \sum_l \mathrm{Tr} V(l)\right] \prod_x \; \chi_{r(x)}(V_x) \;. \tag{19}$$

Note that if R were integer then $Z(\beta,R) = \tilde{Z}(\beta,R;[r(x)])$.

Expressing V_x as a product of link matrices (2) the $SU(2)$ characters turn out to be a sum over magnetic numbers. This yields the partition function

$$\tilde{Z}(\beta,R;[r(x)]) \;=\; \prod_x \left[\sum_{\{m_i(x)=-r(x)\}}^{r(x)} \right] \prod_l Q_0(l) \;, \tag{20}$$

$$Q_0(l) \;=\; \int dV e^{\beta \mathrm{Tr} V} \; V_{r(x)}^{m_i(x)\;\; m_{i+1}(x)} \; V_{r(x+e_n)}^{\dagger\; m_j(x+e_n)\;\; m_{j+1}(x+e_n)} \;, \tag{21}$$

where $V_r^{m\;\; m'}$ indicates the m,m' matrix element of an $SU(2)$ matrix in representation r. There are 4 magnetic numbers $m_i(x)$ $(i=1,2,3,4)$ per lattice site x. The result of the invariant integration can be expanded into a Clebsch-Gordan (CG) series as (up to a sign factor which cancels after multiplication over links)

$$Q_0(l) \;=\; \sum_{J,k} \frac{C_J(\beta)}{2J+1} C^{J\;\; k}_{r(x)\;\; m_i(x)\;\; r(x+e_n)\;\; -m_{j+1}(x+e_n)} \; C^{J\;\; k}_{r(x)\;\; m_{i+1}(x)\;\; r(x+e_n)\;\; -m_j(x+e_n)} \;, \tag{22}$$

with coefficients $C_J(\beta)$ given by

$$C_J(\beta) \;=\; \frac{2J+1}{\beta} I_{2J+1}(2\beta) \;, \tag{23}$$

where $I_{2J+1}(2\beta)$ is the modified Bessel function of first kind. Formulas (18), (20) and (22) define our representation for the partition function of the unconstrained $SU(2)$ model. The new Boltzmann weight, $Q_0(l)$, appears to be always positive on all allowed configurations of the magnetic numbers $m_i(x)$ and representations $r(x)$.

4 Summary

In this paper we have calculated the continuum limit of the dual representation of the $2D$ $SU(N)$ principal chiral model. As an application we have derived a new lattice regularization for the $O(3)$ non-linear sigma model with the θ term. The major advantage of our regularization is that it can be written in a form with strictly positive Boltzmann weight. This opens a possibility for numerical simulations of the model at real values of θ and, therefore for attacking the problems listed in the Introduction from first principles. The work in this direction is now in progress.

References

[1] A. B. Zamolodchikov, Annals of Physics, **120** (1979) 253.
[2] P. Hasenfratz, M. Maggiore, F. Niedermayer, Phys. Lett. **B245** (1990) 522.
[3] B. Allés, A. Buonanno, G. Cella, Nucl. Phys. **B500** (1997) 513.
[4] I. Affleck, Phys. Rev. Lett. **66** (1991) 2429.
[5] I. Affleck, F. D. M. Haldane, Phys. Rev. **B36** (1977) 5291.
[6] R. Shankar, N. Read, Nucl. Phys. **B336** (1990) 457.
[7] W. Bietenholz, A. Pochinsky, U.-J. Wiese, Phys. Rev. Lett. **75** (1995) 4524.
[8] V. Azcoiti, G. Di Carlo, A. Galante, Phys. Rev. Lett. **98** (2007) 257203.
[9] F. D. M. Haldane, Phys. Lett. **A93** (1983) 464.
[10] F. D. M. Haldane, Phys. Rev. Lett. **50** (1983) 1153.
[11] I. Affleck, D. Gepner, H. J. Schulz, T. Ziman, J. Phys. A: Math. Gen. **22** (1989) 511.
[12] G. Delfino, G. Mussardo, P. Simonetti, Nucl. Phys. **B473** (1996) 469.
[13] D. Controzzi, G. Mussardo, Phys. Rev. Lett. **92** (2004) 021601.
[14] D. Controzzi, G. Mussardo, Phys. Lett. **B617** (2005) 133.
[15] L. Campos-Venuti et al., J. Stat. Mech. **0504** (2005) L02004.
[16] B. Allés, A. Papa, Phys. Rev. **D77** (2008) 056008.
[17] G. Batrouni, M.B. Halpern, Phys. Rev. **D30** (1984) 1775.
[18] O. Borisenko, V. Kushnir, A. Velytsky, Phys. Rev. **D62** (2000) 025013.
[19] O. Borisenko, V. Kushnir, Nucl. Phys. **B730** (2005) 103.
[20] J. Bricmont, J.-R. Fontaine, J. Stat. Phys. **26** (1981) 745.

Proceedings of the International School-seminar
"New Physics and Quantum Chromodynamics at External Conditions", pp. 94 – 97,
May 22-24, 2013, Dnipropetrovsk, Ukraine

PLAQUETTE FORMULATION AT FINITE TEMPERATURE AND RELATED PROBLEMS

S. Voloshyn[a]

Bogolyubov Institute for Theoretical Physics, Kiev, Ukraine

We develop an analytical approach for studying plaquette formulation on the periodic lattice using the variant of plaquette formulation that has been developed in our previous papers. In addition, we include dynamical fermions in the plaquette formulation. We also discuss some technical problems appearing in this formulation.

1 Introduction

Investigation of the finite temperature phase structure of the LGT has a long history. In the end of 70's Polyakov and Susskind discovered a phase of quark liberation [1], [2] in $U(1)$ and $SU(2)$ $4D$ model. Investigation of $3D$-case started in [3]. Still, establishing full phase structure of theory remains of great importance. It is known that dual and plaquette formulations are powerful tools in investigation of the phase structure. So far, we do not have yet an adequate plaquette formulation for finite temperaments models. Technically the problem appears when we try to fix a full axial gauge on the periodic lattice.

In this article we undertake an attempt to develop plaquette formulation for finite temperature gauge theories. In previous paper we constructed such formulation for $T = 0$ case, i.e. for non-periodic lattice [4]. Let us remind main steps in transformations leading to the plaquette formulation. As a first step, we introduce the plaquette matrix as

$$V_p \ = \ U_n(x)U_m(x+e_n)U_n^\dagger(x+e_m)U_m^\dagger(x) \ , \tag{1}$$

and make a change of variables assigning plaquette matrices in a spacial way to certain lattice vertices. As a second step, using a plaquette delta function we build Bianchi identities on each cube and fix full axial gauge. As a third step, we integrate out all link degrees of freedom.

2 Gauge fixing on the periodic lattice

Consider now a periodic lattice. We impose the following boundary conditions in t-direction ($1 \le t \le N_t$):

$$U_n(x,1) = U_n(x,N_t+e_0) \ . \tag{2}$$

and try to fix a full axial gauge. Let us perform a change of variables

$$U_1(x,t) \to U_1(x,t) = \prod_{\tau=t-1}^{1} U_0^\dagger(x,y,\tau)T^\dagger(x,y)U_1(x,y,t)T(x+e_1,y)\prod_{\tau=1}^{t-1}U_0(x+e_1,y,\tau) \tag{3}$$

$$U_2(x,t) \to U_2(x,t) = \prod_{\tau=t-1}^{1} U_0^\dagger(x,y,\tau)T^\dagger(x,y)U_2(x,y,t)T(x,y+e_2)\prod_{\tau=1}^{t-1}U_0(x,y+e_2,\tau) \tag{4}$$

$$\overline{\psi}(x,t) \to \overline{\psi}(x,t) = \overline{\psi}(x,y,t)T(x,y)\prod_{\tau=1}^{t-1}U_0(x,y,\tau) \tag{5}$$

where we have denoted

$$T(x,y) = \prod_{x'=1}^{x-1}U_1(x',1,1)\prod_{y'=1}^{y-1}U_2(x,y',1) \tag{6}$$

with additional condition for $U_2(x,t)$

$$U_1(x,t): \ T(x,y) = I \ for \ t=1, y=1 \ , \tag{7}$$

$$U_2(x,t): \ T(x,y) = I \ for \ t=1 \ . \tag{8}$$

e-mail: [a]voloshyn@bitp.kiev.ua

We think this change of variables enables us to fix a full tree for all links (beside the one belonged to timelike plaquettes between $t = N_t$ and $t = 1$ plane)

$$U_3(x, y, t) = U_2(x, y, 1) = U_1(x, 1, 1) = I \tag{9}$$

On the periodic lattice this change of variables leads to some anomaly timelike plaquettes (between $t = N_t$ and $t = 1$ plane)

$$\begin{aligned} V_{01}(x, y, N_t) = U_0^\dagger(x, y, N_t)U_1(x, y, N_t)U_0(x + e_1, y, N_t)U_1^\dagger(x, y, 1) = \\ W^\dagger(x, y)T^\dagger(x, y)U_1(x, y, N_t)T(x + e_1, y)W(x + e_1, y)T^\dagger(x + e_1, y)U_1^\dagger(x, y, 1)T(x, y) \end{aligned} \tag{10}$$

but for a peculiar case $y = 1$ we get

$$\begin{aligned} V_{01}(x, 1, N_t) = W^\dagger(x, 1)T^\dagger(x, 1)U_1(x, 1, N_t)T(x + e_1, 1)W(x + e_1, 1)U_1^\dagger(x, 1, 1) = \\ W^\dagger(x, 1)T^\dagger(x, 1)U_1(x, 1, N_t)T(x + e_1, 1)W(x + e_1, 1)W^\dagger(x + e_1, 1)T(x, 1) \end{aligned} \tag{11}$$

and

$$\begin{aligned} V_{02}(x, y, N_t) = U_0^\dagger(x, y, N_t)U_2(x, y, N_t)U_0(x, y + e_2, N_t)U_2^\dagger(x, y, 1) = \\ W^\dagger(x, y)T^\dagger(x, y)U_2(x, y, N_t)T(x, y + e_2)W(x, y + e_2)U_2^\dagger(x, y, 1) = \\ W^\dagger(x, y)T^\dagger(x, y)U_2(x, y, N_t)T(x, y + e_2)W(x, y + e_2)T^\dagger(x, y + e_2)T(x, y) \end{aligned} \tag{12}$$

where we introduced Polyalov lines as

$$W(x, y) = \prod_{\tau=1}^{N_t} U_0(x, y, \tau) \ . \tag{13}$$

All spacelike plaquettes in this plane are not modified (the same as for non-periodic lattice).

In this place we have a contribution T that consists from product of the links. From first view we could without difficulties kill this contribution with help of shift

$$W(x, y) \to W(x, y) = T^\dagger(x, y)W(x, y)T(x, y) \ . \tag{14}$$

But as we see further on without T we cannot get a correct effective theory in $SU(2)$ case. It remains unclear why it is impossible to get rid of this strange contribution?

Note, that the gauge fixing procedure and the procedure described above are freely interchangeable. After gauge fixing one can easily obtain expressions for link variables in terms of plaquettes. We start from the plane $t = N_t$ and going to $t = 1$ integrating out all link variables plane by plane as we did in [4].

As we already know the expressions for link variables will depend on the position of a link relatively to the vertex A or B. As example, consider a line containing vertices B in t direction, x, y being fixed and let one of the vertices B have the coordinates $B = (x, y, t)$. Then one finds for the link $l = (x, y, t; n_2)$

$$U_2(x, y, t) = \prod_{t'=z-1}^{1} V_{02}(x, y, t') \ , \tag{15}$$

while for the link $l = (x, y - e_2, t; n_2)$

$$U_2(x, y - e_2, t) = \prod_{t'=1}^{z-1} V_{02}(x, y - e_2, t') \ , \tag{16}$$

where V_{02} is the plaquette matrix from the (yt)-plane. Similar expressions one obtains for all links entering in or coming out in n_1 direction. The same rules apply for lines containing vertices A. Using these expressions one can easily integrate out all link variables. Clearly, the presence of the fermion determinant cannot change the integration procedure. For space between $t = N_t$ and $t = 1$ plane we have just global constraints instead of the Bianchi constraint.

The model becomes

$$\begin{aligned} Z = \int \prod_p DV_p \prod_{x\in 2D} \int DW_x \int DT_x \ \exp\left[\beta_t \sum_{p_t} \mathrm{Re\ Tr} V_{p_t} + \beta_s \sum_{p_s} \mathrm{Re\ Tr} V_{p_s}\right] \\ \times \exp\left\{\sum_{f=1}^{N_f} \mathrm{Tr} \ln A_f(x, x'; U_l)\right\} \prod_{c\neq c_0} J(V_c) \prod_{n=1,2} \prod_{x\in 2D} H_n(V_p; W_x, W_{x+e_n}; T(x)) \ , \end{aligned} \tag{17}$$

where V_c is given in our previous work [4], c_0 is a slice of cubes between $t = 1$ and N_t and for $U_0(x, y, N_t) = W(x, y)$ for other U_l we have expressions like (15)-(16).

Beside Bianchi identities we have a global constraint (all for links V_l originated from the vertex A or B)

$$H_1 = \delta[T(x,y)W^\dagger(x,y)T^\dagger(x,y)\prod_{t'=N_t}^{1} V_{01}(x,y,t')\prod_{y'=y-1}^{1} V_{12}(x,y',1)$$
$$T(x+e_1,y)W(x+e_1,y)T^\dagger(x+e_1,y)\prod_{y'=1}^{y-1} V_{12}^\dagger(x,y',1)] \tag{18}$$

for peculiar case $y = 1$ we get

$$H_1 = \delta[T(x,y)W^\dagger(x,1)T^\dagger(x,y)\prod_{t'=N_t}^{1} V_{01}(x,1,t')T(x+e_1,y)W(x+e_1,1)T^\dagger(x+e_1,y)] \tag{19}$$

and

$$H_2 = \delta[T(x,y)W^\dagger(x,y)T^\dagger(x,y)\prod_{t'=N_t}^{1} V_{02}(x,y,t')T(x,y+e_2)W(x,y+e_2)T^\dagger(x,y+e_2)] \tag{20}$$

Analogous expressions we could write for links V_l entering to the vertices A or B.

3 Particular cases

3.1 $U(1)$

First we need to see that we have on each cube full Bianchi identity. To get pure theory for the plaquette variables we need to integrate out all Polyakov loops. However for the Polyakov loop that live on the two-dimensional lattice in $x - y$ plane we have nothing but link delta function for the two Polyakov loops in neighbor sites and product of all plaquette matrices bounded by them

$$H_n(x,y) = \delta[W^\dagger(x,y)\prod_{t'=1}^{N_t} V_{0n}(x,y,t')W(x,y+e_n)] \ , \tag{21}$$

where we put $V_{0n}(x) = e^{i\omega_{0n}(x)}$. We could form a "plaquette" delta function in $x - y$ plane using all link delta-functions in n_1-direction (beside one line). We start from $y = 1$ line. In chosen link delta function we substitute other three and get the expression

$$\delta[\omega(x,y)] = \delta[\sum_{t'=1}^{N_t}(\omega_{01}(x,y,t') + \omega_{02}(x+e_1,y,t') - \omega_{01}(x,y+e_2,t') - \omega_{02}(x,y,t'))] \tag{22}$$

on each plaquette in $x - y$ plane. After substituting in this delta other deltas in t direction that lie "under" or "on top" we get "top" and "bottom" plaquette for this non-typical cubes that lie between $t = 1$ and $t = N_t$. So we get the full set of Bianchi identity on the periodic lattice. We see that delta is direct consequences of Bianchi deltas on other cubes and "global constrains" $H_n(V_{p_s}; W_x, W_{x+e_n}; T(x))$.

After this we integrate out all $W(x, y)$ beginning from the line $x = 1$ and killing at once all deltas in y-direction and residual in x in line $y = N_y$. After all we will get standard plaquette formulation with standard Bianchi identity on each cube (notice, that Polyakov loops also drops out from deltas on cubes between $t = 1$ and N_t). On the dual lattice (with all usual transformation) we have

$$Z = \int \prod_l d\omega_l \ \exp\left[\beta_s \sum_{l_t} \cos\omega(l_t) + \beta_t \sum_{l_s} \cos\omega(l_s)\right] \prod_x \sum_{r_x=-\infty}^{\infty} e^{ir_x\omega_x} \ , \tag{23}$$

where

$$\omega_x = \omega_1(x) + \omega_2(x) + \omega_3(x) - \omega_1(x-e_1) - \omega_2(x-e_2) - \omega_3(x-e_3). \tag{24}$$

Another interesting case is to get an effective theory for Polyakov loop only. Integrating out all plaquette degrees of freedom is possible only in the strong coupling approximation. In the limit of $\beta_s = 0$ we could

integrate out all space-like plaquettes and again get constraint on the plaquettes in one $x-y$ plane (22). We find (where we put $W_x = e^{i\phi_x}$)

$$Z = \prod_{n=1,2}\prod_{x\in 2D}\sum_{r_l=-\infty}^{\infty}\int\prod_{x\in 2D}\frac{d\phi_x}{2\pi}\int\prod_{l_s}\frac{d\omega_{l_s}}{2\pi}\exp\left[\beta_t\sum_{l_s}\cos\omega(l_s)\right]$$
$$\times\exp\left[-i\sum_{n=1,2}\sum_{x\in 2D}[r_l(\phi(x)-\phi(x+e_n)-\sum_{t=0}^{N_t}\omega_n(x,y,t)]\right]$$
$$=\int\prod_{x\in 2D}\frac{d\phi_x}{2\pi}\sum_{r_l=-\infty}^{\infty}\prod_{x\in 2D,n=1,2}I^{N_t}_{r_l}(\beta_t)\exp\left[-ir_l\sum_{z=0}^{N_t}(\phi(x)-\phi(x+e_n))\right]\ . \tag{25}$$

3.2 $SU(2)$

Proving equivalence of "global constraints" and missing Bianchi identity of c_0-slices is less trivial thing in non-abelian cases. Firstly, as in $U(1)$ case we construct from "link" deltas H_n "plaquette" ones. After simple transformation we get full missing Bianchi identity

$$\delta[V_x^{B_1A}] = \delta[V^\dagger_{p_3}V_{p_2}V^\dagger_{p_1}U_{l_4}U_{l_3}TWT^\dagger V_{p_5}V_{p_6}V^\dagger_{p_4}TW^\dagger T^\dagger U^\dagger_{l_3}U^\dagger_{l_4}]\ , \tag{26}$$

Finally, we could drop out "global constraints" and replace it with Bianchi identity on c_0 slices. In non-abelian case we could not integrate out all Polyakov loops because of high complicated structure, mostly because of Polyakov loops entering in Bianchi identity.

In limit of $\beta_s = 0$ we could integrate out all plaquettes and get an effective theory for Polyakov loops only. Just like in abelian case integrating out space-like plaquettes (beside lying in $t = 1$ plane) beginning from plane $t = N_t$ we kill all Bianchi deltas. As usually we expand all in series of group characters. Then we integrate out consequently V_{p_t}, V_{12} and in the last turn T_x

$$Z = \int\prod_p DV_p\prod_{x\in 2D}\int DW_x\int DT_x\ \exp\left[\beta_t\sum_{p_t}\mathrm{Re\ Tr}V_{p_t}\right]\prod_{n=1,2}\prod_{x\in 2D}H_n(V_p;W_x,W_{x+e_n};T(x))$$
$$=\int\prod_{x\in 2D}DW_x\sum_{r_l=0,1/2,1,\ldots}\prod_{x\in 2D,n=1,2}I^{N_t}_{2r_l+1}(2\beta_t)\ d_{r_l}\chi_{r_l}(W_x)\chi_{r_l}(W_{x+n})\ , \tag{27}$$

This expressions coincides with known result [1], [2].

4 Conclusion

Up to this time plaquette formulation on the periodic lattice for non-abelian case has not been fully investigated. Complicated situation with fixation of a gauge for periodic boundary condition is mentioned in [6]. In this work we try to fill this gap in our knowledge. Main result of this paper is formula for partition function of plaquette formulation on periodic lattice (17). One of the big technical problem is to find correctly continuum limit for Bianchi identity. Presence of Polyakov lines in slice c_0 complicates the procedure, because Polyakov lines even in continuum are not concentrated around trivial configurations $W_x \approx I$. This investigation create background for extending our monopole approximation [5] to non-zero temperature and also to check Svetitsky-Yaffe conjecture [7] for important $SU(2)$ case.

Acknowledgements. Authour thank O. Borisenko for stimulating discussions. This work was supported by a common project between Slovak and Ukrainian Academy of Sciences.

References

[1] A. Polyakov, Thermal properties of gauge fields and quark liberation, Phys. Lett. B **72**, 477 (1978).
[2] L. Susskind, Phys. Rev. D **20**, 2610 (1979).
[3] N. Parga, Phys. Let. B **107**, 442 (1981).
[4] O. Borisenko, S. Voloshin, M. Faber, Field strength formulation, lattice Bianchi identities and perturbation theory for non-Abelian models, Nuclear Physics B **816** [FS], 399 (2009).
[5] O. Borisenko, S. Voloshyn, J. Boháčik, Monopoles in the plaquette formulation of the $3D$ $SU(2)$ lattice gauge model, Mod. Phys. Lett. A, Vol. 26, No. 25 (2011) pp. 1853-1867, [arXiv:1106.0293v1].
[6] G. Batrouni, M.B. Halpern, Phys.Rev. D **30**, 1782 (1984).
[7] B. Svetitsky, L. Yaffe, Nucl. Phys. B **210**, Issue 4, 423-447 (1982).

Proceedings of the International School-seminar
"New Physics and Quantum Chromodynamics at External Conditions", pp. 98 – 102,
May 22-24, 2013, Dnipropetrovsk, Ukraine

A HIGH STATISTICS STUDY OF THE BETA-FUNCTION IN THE $SU(2)$ LATTICE THERMODYNAMICS

S. S. Antropov[a], O. A. Mogilevsky[b], V. V. Skalozub[c]

Oles Honchar Dnipropetrovsk National University, Dnipropetrovsk, Ukraine;
Bogolyubov Institute for Theoretical Physics of the National Academy of Sciences of Ukraine, Kiev, Ukraine

The beta-function is investigated on the lattice in $SU(2)$ gluodynamics. It is determined within a scaling hypothesis while a lattice size fixed to be taken into account. The functions calculated are compared with the ones obtained in the continuum limit. Graphics processing units (GPU) are used as a computing platform that allows gathering a huge amount of statistical data. Numerous beta-functions are analyzed for various lattices. The coincidence of the lattice beta-function and the analytical expression in the region of the phase transition is shown. New method for estimating a critical coupling value is proposed.

1 Introduction

The beta-function is one of the main objects in quantum field theory. It defines scaling properties of the theory in different regions of dynamic variables. It is defined as

$$\beta_f(g_\mu) = \mu^2 \frac{\partial \overline{g}(\mu^2)}{\partial(\mu^2)}, \tag{1}$$

where $\beta_f(g_\mu)$ – beta-function, $g_\mu \equiv \overline{g}(\mu^2)$ – effective coupling constant, μ – normalizing momentum.

For the case of the Monte-Carlo (MC) calculations in $SU(N)$ lattice gluodynamics the beta-function has the form

$$\beta_f(g) = -a\frac{dg}{da}, \tag{2}$$

where a replaces the parameter μ^2, a - is lattice spacing. Lattice spacing is a free parameter of the theory. In particular, calculation of $\beta_f(g)$ is one of the ways to define a.

In analytical approach, the beta-function described by an expansion as power series of coupling constant. In the cases of quantum chromodynamics or $SU(N)$ lattice gluodynamics, a non-perturbative beta-function attracts the most interest.

In the paper of one of the authors [6] a new special method was developed. Namely, the effects connected with the final sizes of a lattice were taken into account, and scaling near the critical point of $SU(N)$ lattice gauge theories has been considered without attempt to reach a continuum limit.

The goal of the present paper is the detailed investigation and development of this approach. In $SU(2)$ gluodinamics, we calculate the beta-functions on different lattices and compare their values with those obtained in a continuum limit.

2 Analytical expression

The beta-function describes the dependence of the lattice spacing a on a coupling constant g

$$\beta_f(g) = -a\frac{dg}{da}. \tag{3}$$

Our calculations are based on the special form of the definition of the beta-function [6]. Let us consider a transformation

$$a \to a' = ba = (1 + \Delta b)a. \tag{4}$$

Under this transformation the definition (3) becomes

$$-a\frac{dg}{da} = -\lim_{b\to 1}\left(a\frac{g(ba) - g(a)}{ba - a}\right) = -\lim_{b\to 1}\frac{dg}{db} = \beta_f(g). \tag{5}$$

e-mail: [a]santrop_2@yahoo.com, [b]mogilevsky.oleg@gmail.com, [c]skalozubv@daad-alumni.de

The singular part of the free energy density can be described by the universal finite-size scaling function [9]

$$f(t,h,N_\sigma,N_\tau)=\left(\frac{N_\sigma}{N_\tau}\right)^{-3}Q_f\left(g_t\left(\frac{N_\sigma}{N_\tau}\right)^{1/\nu},g_h\left(\frac{N_\sigma}{N_\tau}\right)^{\frac{\beta+\gamma}{\nu}}\right), \tag{6}$$

where β,γ,ν are the critical indexes of the theory. Due to the finite size scaling hypothesis, these indexes coincide with the critical indexes of 3-d Ising model. The scaling function Q_f depends on the reduced temperature $t=\frac{T-T_c}{T_c}$ and the external field strength h through thermal and magnetic scaling fields

$$\begin{aligned} g_t &= c_t t(1+b_t t), \\ g_h &= c_h h(1+b_h t) \end{aligned} \tag{7}$$

with non-universal coefficients c_t, c_h, b_t, b_h still carrying a possible N_τ.

The existence of the scaling function Q [7], [8] allows developing a procedure to renormalize the coupling constant g^{-2} by using two different lattice sizes N_σ, N_τ and N'_σ, N'_τ (N_σ - number of lattice nods in spatial directions, N_τ - number of lattice nods in time direction). Let us fix $\frac{N'_\tau}{N_\tau}=\frac{N'_\sigma}{N_\sigma}=b$ and make a scale transformation

$$\begin{aligned} a &\to a'=ba, \\ N_\sigma &\to N'_\sigma=\frac{N_\sigma}{b}, \\ N_\tau &\to N'_\tau=\frac{N_\tau}{b}. \end{aligned} \tag{8}$$

Then the phenomenological renormalization is defined by the following equation

$$Q(g^{-2},N_\sigma,N_\tau)=Q\left((g')^{-2},\frac{N_\sigma}{b},\frac{N_\tau}{b}\right). \tag{9}$$

It means that the scaling function Q remains unchanged if the lattice size is rescaled by a factor b and the inverse coupling g^{-2} is shifted to $(g')^{-2}$ simultaneously. Taking the derivative with respect to the scale parameter b of the both sides of (9) and using (5) we obtain the expression

$$a\frac{dg^{-2}}{da}=\frac{\frac{\partial Q(g^{-2},N_\sigma,N_\tau)}{\partial lnN_\sigma}+\frac{\partial Q(g^{-2},N_\sigma,N_\tau)}{\partial lnN_\tau}}{\frac{\partial Q(g^{-2},N_\sigma,N_\tau)}{\partial g^{-2}}}. \tag{10}$$

Fourth derivative of f in h taken at $h=0$ and divided by $\chi^2(\frac{N_\sigma}{N_\tau})^3$ is called the Binder cumulant [10]

$$g_4=\left.\frac{\frac{\partial^4 f}{\partial h^4}}{\chi^2(\frac{N_\sigma}{N_\tau})^3}\right|_{h=0}. \tag{11}$$

It identically coincides with the scale function [10]

$$g_4=Q_{g_4}\left(g_t\left(\frac{N_\sigma}{N_\tau}\right)^{\frac{1}{\nu}}\right). \tag{12}$$

Binder cumulant g_4 is calculated through the Polyakov loops on a lattice [10]

$$g_4=\frac{\langle P^4\rangle}{\langle P^2\rangle^2}-3. \tag{13}$$

We get the expression for the beta-function

$$a\frac{dg^{-2}}{da}=\frac{\frac{\partial g_4}{\partial lnN_\sigma}+\frac{\partial g_4}{\partial lnN_\tau}}{\frac{\partial g_4}{\partial g^{-2}}}=\frac{1}{4}\frac{\frac{\partial g_4}{\partial lnN_\sigma}+\frac{\partial g_4}{\partial lnN_\tau}}{\frac{\partial g_4}{\partial \beta}}. \tag{14}$$

3 Lattice observables

Let us calculate beta function using (14). As the lattice size is discrete, it is necessary to replace the derivatives in (14) by the finite differences which are calculated on lattices with the closest N_σ, N_τ (and corresponding $g_4(N_\sigma, N_\tau)$):

$$\begin{aligned} \frac{\partial g_4(\beta, N_\sigma, N_\tau)}{\partial ln N_\sigma} &\to \frac{g_4(\beta, N'_\sigma, N_\tau) - g_4(\beta, N_\sigma, N_\tau)}{ln(\beta, N'_\sigma/N_\sigma)}, \\ \frac{\partial g_4(\beta, N_\sigma, N_\tau)}{\partial ln N_\tau} &\to \frac{g_4(\beta, N_\sigma, N'_\tau) - g_4(\beta, N_\sigma, N_\tau)}{ln(\beta, N'_\tau/N_\tau)}. \end{aligned} \tag{15}$$

Such replacement,

$$\frac{\partial g_4}{\partial \beta} \to \frac{\Delta g_4}{\Delta \beta}, \tag{16}$$

leads to huge computing errors. Near the phase transition area, the dispersion is increased and the substitution (16) becomes not reasonable. For different lattices investigated, the amount of data near the critical region varies from 120 up to 600 points, but the error for (16) remains large.

If we know g_4 in an analytical form, it is possible to calculate $\frac{\partial g_4}{\partial \beta}$ straightforwardly. However, the result of g_4 calculations is a set of points. To reveal a functional dependence on this sequence, it is necessary to apply some fitting procedure. For this procedure we chose the step functions, since the critical area of g_4 is a step-like (see Tab. 1).

Table 1. Tested fitting curves

Function	*Parameters*
$A_1 + \frac{A_2 - A_1}{1+10^{(\beta_0-\beta)*p}}$	A_1, A_2, β_0, p
$\frac{A_1 - A_2}{1+(\frac{\beta}{\beta_0})^p} + A_2$	A_1, A_2, β_0, p
$\frac{A_1 - A_2}{1+e^{(\beta-\beta_0)/p}} + A_2$	A_1, A_2, β_0, p

Our the best fits (see Fig. 1, Tab. 2) are reached for the function

$$g_4 = A1 + (A2 - A1)/(1 + 10^{(\beta_0-\beta)*p}), \tag{17}$$

where $A1, A2, \beta_0, p$ - fitting parameters.

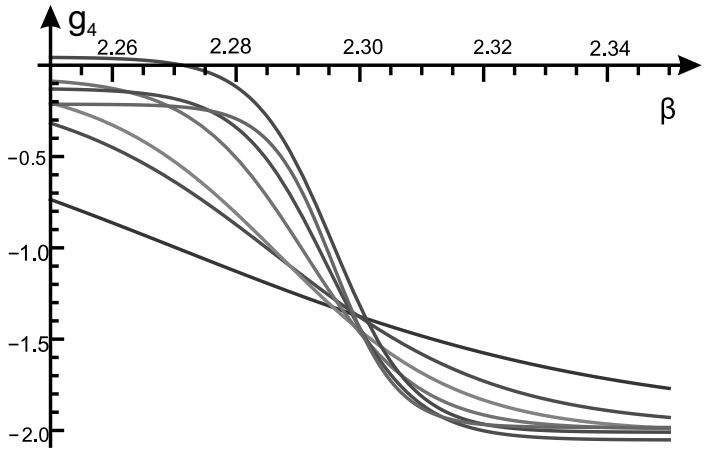

Figure 1. Binder cumulants. Cumulants are received on lattices with $N_\tau = 4$, and N_σ = 8, 12, 16, 24, 28, 32. The higher number of nods in the lattice corresponds with the sharper step. All curves intersect each other in a local area and as it comes from the theory these curves should intersect in one point (the critical point).

In Tab. 2 best fits for number of lattices are represented. We have analyzed up to 600 points for some lattices and have reached small values (down to 10^{-3}) of χ^2 function.

Table 2. Fitting of Binder cumulants by $A_1 + \frac{A_2 - A_1}{1+10^{(\beta_0-\beta)*p}}$

	Parameters						Fitting range	
Lattice	χ^2	A_1	A_2	β_0	p	**Number of points**	β_{min}	β_{max}
$N_\tau = 4, N_\sigma = 8$	0.009	-1.953	-0.0523	2.2705	-12	126	1.7	2.95
$N_\tau = 4, N_\sigma = 8$	0.012	-1.957	-0.0507	2.2747	-11	26	1.7	2.95
$N_\tau = 4, N_\sigma = 12$	0.025	-1.98	-0.1	$2,286$	-24	253	1.7	2.95
$N_\tau = 4, N_\sigma = 12$	0.011	-2	-0.04	$2,289$	-16	26	1.7	2.95
$N_\tau = 4, N_\sigma = 16$	0.029	-2.01	-0.066	2.287	-30.1	236	1.7	2.95
$N_\tau = 4, N_\sigma = 16$	0.013	-1.99	-0.05	2.292	-30.9	26	1.7	2.95
$N_\tau = 4, N_\sigma = 20$	0.055	-2	-0.065	2.291	-48	246	1.7	2.95
$N_\tau = 4, N_\sigma = 24$	0.1	-2.0098	0.044	2.296	-68	126	1.7	2.95
$N_\tau = 4, N_\sigma = 24$	0.006	-2.001	0.061	2.291	-27	26	1.7	2.95
$N_\tau = 4, N_\sigma = 28$	0.089	-2.05	-0.13	2.29	-62	626	1.7	2.95
$N_\tau = 4, N_\sigma = 28$	0.012	-1.99	$-8 \cdot 10^{-5}$	2.28	-21	26	1.7	2.95
$N_\tau = 4, N_\sigma = 32$	0.12	-1.984	-0.2	2.3	-84	626	1.7	2.95
$N_\tau = 4, N_\sigma = 32$	0.01	-1.988	0.014	2.27	-28	26	1.7	2.95
$N_\tau = 4, N_\sigma = 36$	0.19	-2	-0.27	2.3	-105	600	2.28	2.31
$N_\tau = 16, N_\sigma = 20$	0.094	-1.17	-0.017	2.68	-7	126	1.7	2.95
$N_\tau = 16, N_\sigma = 24$	0.054	-1.7	0.04	2.75	-6	26	1.7	2.95
$N_\tau = 16, N_\sigma = 28$	0.021	-1.6	-0.017	2.67	-17	26	1.7	2.95
$N_\tau = 16, N_\sigma = 32$	0.021	-1.7	0.03	2.69	-23	126	1.7	2.95

Now we turn to an interesting features of these fits. Parameters of the curve, which based on 600 data points, are nearly the same as parameters (especially β_0) of the curve, which based on 25 data points. The parameter β_0 coincides (to within 2 up to 3 digits) with an inverse critical coupling constant for a corresponding lattice (see Tab. 3, ref. [9], [12]).

Table 3. Values of the inverse coupling constant

N_τ	2	4	6	8
β_c	1.875	2.301	2.422	2.508

It is common to use linear fits for finding of critical point on the lattice. Because of the dispersion in critical region these fits need a lot of data to be performed. Using both listed above properties one can estimate the inverse critical coupling using just few points. For more precise calculations one can use function (17) with data, which are from above and below critical region. Dispersion for these data is much less than for data, which are near critical area, so one need much less statistics than usually.

The expression for the beta-function in lattice variables reads:

$$\beta_f(\beta) = \frac{1}{\beta^{3/2}} \cdot \frac{\frac{g_4(\beta,N'_\sigma,N_\tau)-g_4(\beta,N_\sigma,N_\tau)}{ln(N'_\sigma/N_\sigma)} + \frac{g_4(\beta,N_\sigma,N'_\tau)-g_4(\beta,N_\sigma,N_\tau)}{ln(N'_\tau/N_\tau)}}{\frac{\partial g_4(\beta,N_\sigma,N_\tau)}{\partial\beta}}. \tag{18}$$

It will be used below.

4 Calculation of the beta-function

We chose the heat-bath as working algorithm in MC procedure. We use standard form of Wilson action of the $SU(2)$ lattice gauge theory. In the MC simulations, we use the hypercubic lattice $L_t \times L_s^3$ with hypertorus geometry.

We use the General Purpose computation on Graphics Processing Units (GPGPU) technology allowing studying large lattices on personal computers. Performance analysis indicates that the GPU-based MC simulation program shows better speed-up factors for big lattices in comparing with the CPU-based one. For the majority lattice geometries the GPU vs. CPU (single-thread CPU execution) speed-up factor is above 50 and for some lattice sizes could overcome the factor 100.

The plots of dependencies of the beta-function on the inverse coupling constant are shown below.

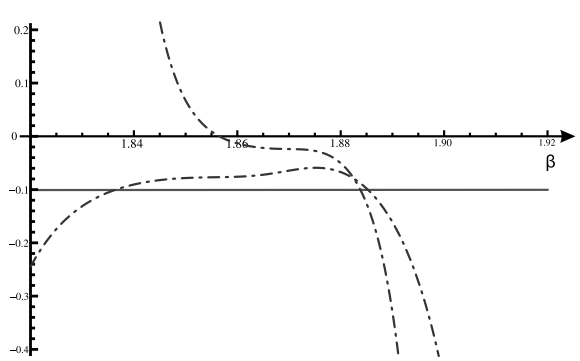

Figure 2. The solid line represents the beta-function in asymptotic expansion. Dashed lines with a point - the beta-functions (18), $N_\tau = 2$, $N_\sigma = 8, 16, 20$, $\Delta N_\tau = N'_\tau - N_\tau = 2$, $\Delta N_\sigma = N'_\sigma - N_\sigma = 4$.

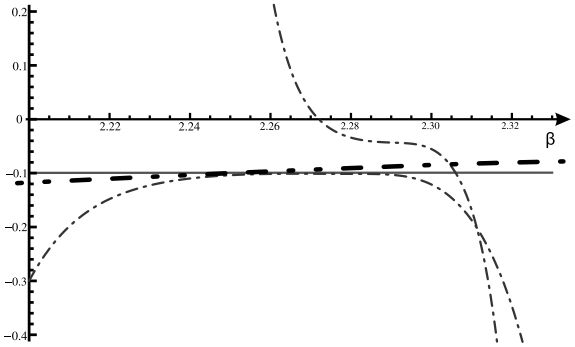

Figure 3. Same as above. Dashed lines with a point - the beta-functions (18), $N_\tau = 4$, $N_\sigma = 12, 20$, $\Delta N_\tau = N'_\tau - N_\tau = 2$, $\Delta N_\sigma = N'_\sigma - N_\sigma = 4$. The Dashed line with two points - the beta-function is received in ref. [1].

Standard deviation of the function (18) is smallest near critical point. It comes from analysis of Binder cumulants. Cumulants decrease linearly in the critical area and change little above and belove that area. Therefore $\frac{\partial g_4(\beta,N_\sigma,N_\tau)}{\partial\beta}$ in the bottom of (18) comes to 0 and leads (18) to infinity. Beta-function values which are calculated near critical point are in good agreement with known results [1].

5 Conclusions

We have performed high-statistics calculations of the beta-function in $SU(2)$ lattice gluodynamics. These calculations became possible due to technology of GPU calculations.

The key point for our investigations is definition (5) [6]. It gives a possibility to analyze a finite size of the lattice.

We have constructed and analyzed the lattice beta-functions for a wide range of different lattices.

Values of all beta-functions in critical region are the same for different functions. In particular, the values of the beta-functions (18) in critical region are almost the same as the values obtained in ref. [1]. The fast method of determination of the inverse critical constant on a lattice based on the formula (17) is proposed.

References

[1] J. Engels, F. Karsch and K. Redlich, Nucl. Phys. B **435**, 295 (1995) [hep-lat/9408009].
[2] R. Sommer, Nucl. Phys. B **411**, 839 (1994) [hep-lat/9310022].
[3] Y. Aoki, Z. Fodor, S. D. Katz and K. K. Szabo, Phys. Lett. B **643**, 46 (2006) [hep-lat/0609068].
[4] Y. Aoki, S. Borsanyi, S. Durr, Z. Fodor, S. D. Katz, S. Krieg and K. K. Szabo, JHEP **0906**, 088 (2009) [arXiv:0903.4155 [hep-lat]].
[5] J. B. Kogut, Rev. Mod. Phys. **55**, 775 (1983).
[6] O. Mogilevsky, Ukr.J.Phys. Vol.51 8, 820-823 (2006).
[7] M. N. Barber, Phase Transitions and Critical Phenomena Vol. 8, ed. C. Domb and J. Lebowitz, Academic Press (1981).
[8] V. Privman, Finite-Size Scaling and Numerical Simulations of Statistical Systems, World Scientific Publishing Co. (1990).
[9] J. Fingberg, U. M. Heller and F. Karsch, Nucl. Phys. B **392**, 493 (1993) [hep-lat/9208012].
[10] K. Binder, Phys. Rev. Lett. **47**, 693 (1981).
[11] V. Demchik and A. Strelchenko, arXiv:0903.3053 [hep-lat].
[12] A. Velytsky, Int. J. Mod. Phys. C **19**, 1079 (2008) [arXiv:0711.0748 [hep-lat]].
[13] K. Binder, Z. Phys. B **43**, 119 (1981).
[14] K. Binder and E. Luijten, Phys. Rept. **344**, 179 (2001).

Proceedings of the International School-seminar
"New Physics and Quantum Chromodynamics at External Conditions", pp. 103 – 106,
May 22-24, 2013, Dnipropetrovsk, Ukraine

STUDY OF THE PHASE STRUCTURE OF $2D$ $Z(N)$ MODELS USING APPROXIMATE RENORMALIZATION GROUP.

O. A. Borisenko[a], V. O. Chelnokov[b], V. A. Kushnir[c]

Bogolyubov Institute for Theoretical Physics, Kiev, Ukraine

We propose a modification of the Migdal-Kadanoff renormalization group for lattice spin and gauge models. Our technique is based on the exact calculation of the partition and correlation functions on a finite width lattice strip and the preservation of the mass gap on each decimation step. The method is applied for studying two-dimensional Z(N) spin models. A perfect agreement with exact results (whenever available) is found.

1 Introduction

The Migdal-Kadanoff (MK) renormalization group (RG) [1,2] had a great impact on the development of the real-space RG methods. Despite its conceptual and technical simplicity, for a number of physically interesting systems the MK RG does provide qualitatively correct results which however are not very precise on the quantitative level. This fact has impelled people to look for a modification of the original MK transformations which would result in a better quantitative predictions. Indeed, numerous such modifications have been developed in the past.

One of these modifications is the so-called phenomenological renormalization group (PRG) proposed by Nightingale [3] (see also [4] and references therein). Originally, this approach utilizes the correlation lengths of the partially finite systems. Their scaling relations are then interpreted as the renormalization group transformations. When expressed *via* an eigenvalues of the transfer matrix these expressions lead to the transcendental equations whose solutions approximate the critical temperature(s).

We would also like to mention an approach to the RG transformations based on the cluster decimation approximation (CDA) [5]. The CDA utilizes the same restructuring of the lattice as in the conventional MK RG. The main idea is to preserve the free energy after each decimation step. This can be done approximately by computing exact free energies on small clusters with periodic boundary conditions (BC), e.g. 2×2 and 1×1. The equality of these free energies is used to establish recursion relations (RR) for the effective coupling constant on the 1×1 lattice. Then, this exact RR is used to approximate the *effective* coupling constant on new $L/2 \times L/2$ lattice. On this way one gets a considerable quantitative improvement of the results over the standard MK RG.

We consider a variant of the PRG. As a cluster we take a finite $(width \times length) = (M \times L)$ lattice strip. RR are established in the limit of the infinite length L of the strip. Then the requirement of the preservation of the mass gap in this limit computed from the two-point correlation function in some representation gives a system of RR for all independent couplings of the model. It turns out that this variant results into a dramatic improvement in the quantitative description of the critical region.

In the spirit of CDA and its predecessor, MK RG, an attempt was made to establish RG equations from the "first principle", in this case starting from the direct transfer matrix formalism' based calculations.

2 Construction of RG transformations

To obtain the RG equations we treat our approach as a CDA RG where we take strips of the lattice as clusters. We explain our strategy on an example of two-dimensional generalized Z(N) spin model where partition function is given by

$$Z(\Lambda_0, \{t_k\}) \;=\; \prod_{x \in \Lambda_0} \left(\frac{1}{N} \sum_{s(x)=0}^{N-1} \right) \prod_{l \in \Lambda_0} \left(\sum_{k=0}^{N-1} t_k \, \exp\left[\frac{2\pi i}{N} \, k \, s(l) \right] \right) \;, \qquad (1)$$

where t_k is a coupling constant for representation k, and link variables $s(l)$ are defined as $s(l) = s(x) - s(x + e_n) \pmod N$.

e-mail: [a]oleg@bitp.kiev.ua, [b]chelnokov@bitp.kiev.ua, [c]vkushnir@bigmir.net

Let $\Lambda = (M \times L)$ be a strip of a $2d$ lattice with a width $M \ll L$ fixed and periodic BC in both directions. Define the free energy and the correlation function in the thermodynamic $L \to \infty$ limit as

$$F(M, \{t_k\}) = \log \lambda_0(M, \{t_k\}) = \lim_{L\to\infty} \frac{1}{L} \log Z(M \times L, \{t_k\}) , \quad (2)$$

$$\Gamma_r(M, \{t_k\}; R) = \lim_{L\to\infty} \Gamma_r(M \times L, \{t_k\}; R) . \quad (3)$$

Suppose that $\Gamma_r(M, \{t_k\}; R)$ has the following very general form

$$\Gamma_r(M, \{t_k\}; R) = D_r(M, \{t_k\}, R) \ [B_r(M, \{t_k\})]^R , \quad (4)$$

where the function $B_r(M, \{t_k\})$ describing the exponential decay is parameterized as

$$B_r(M, \{t_k\}) = \frac{\lambda_r(M, \{t_k\})}{\lambda_0(M, \{t_k\})} \quad (5)$$

and the function $D_r(M, \{t_k\}, R)$ has utmost a power-like decay. Functions λ_r can be considered, e.g. as the eigenvalues of the corresponding transfer matrices. Our basic idea is to present the correlation function $\Gamma_r(M, \{t_k\}; R)$ via the correlation function $\Gamma_r(M/2, \{t_k^{(1)}\}; R/2)$, calculated on the strip of the width $M/2$ with new couplings $\{t_k^{(1)}\}$, in the form

$$\Gamma_r(M, \{t_k\}; R) = \frac{D_r(M, \{t_k\}, R)}{D_r(M/2, \{t_k^{(1)}\}, R/2)} \ \Gamma_r(M/2, \{t_k^{(1)}\}; R/2) . \quad (6)$$

Comparing (4) with the last equation one concludes that (6) holds if

$$B_r^2(M, \{t_k\}) = B_r(M/2, \{t_k^{(1)}\}) \quad (7)$$

for all $r = 1, \cdots, N-1$. This system of $N-1$ equations determines new couplings $t_k^{(1)}$ on the lattice strip $(M/2, L/2)$. We use these exact relations to approximate the partition and the correlation functions on Λ_0 as

$$Z(\Lambda_0, \{t_k\}) = \left[\frac{\lambda_0(M, \{t_k\})}{\lambda_0^{(1/2)}(M/2, \{t_k^{(1)}\})}\right]^{L^2/M} Z(\Lambda_1, \{t_k^{(1)}\}) , \quad (8)$$

$$\Gamma_r(\Lambda_0, \{t_k\}; R) = \frac{D_r(M, \{t_k\}, R)}{D_r(M/2, \{t_k^{(1)}\}, R/2)} \ \Gamma_r(\Lambda_1, \{t_k^{(1)}\}; R/2) . \quad (9)$$

Equations (2)-(3) and (8)-(9) define our RG transformations. Renormalized coupling constants are computed from the equation (7). To distinguish this approach from the conventional CDA RG we shall use in what follows the term strip decimation approximation (SDA) RG.

3 Application of SDA RG for $M = 2$

As an example we provide the description of RG transformations for $2d$ $Z(N)$ models taking $M = 2$.

The partition function for the standard Potts model has been calculated exactly on the finite lattice strips for $M = 2, 3, 4$ and for arbitrary N in [6]. To compute the partition function for the general Potts model we proceed as follows.

Summation over original degrees of freedom produces constraints on link variables in each plaquette of the strip and a constraint on the closed loop in the longitudinal direction. Both types of constraints can be implemented via $Z(N)$ invariant delta-function. This introduces local dual variables which can be placed in the centers of original plaquettes and one global variable associated with the closed loop. The resulting one-dimensional model takes the form

$$Z(2 \times L, \{t_k\}) = \frac{1}{N} \sum_{r=0}^{N-1} \sum_{\{k(x)\}=0}^{N-1} \prod_{x=1}^{L} \left[t_{k(x)} \ t_{k(x+e_n)+r} \ \alpha_{k(x)+k(x+e_n)+r}\right] , \quad (10)$$

where

$$\alpha_k = \frac{\sum_{m=0}^{N-1} t_m t_{k-m}}{\sum_{m=0}^{N-1} t_m^2}$$

appears due to periodic BC in the transverse direction. For free BC one would have $\alpha_k = t_k$. It follows from (10) that

$$Z(2 \times L, \{t_k\}) = \frac{1}{N} \sum_{r=0}^{N-1} \sum_{k=0}^{N-1} [\lambda_{k,r}(\{t_k\})]^L . \quad (11)$$

Here, $\lambda_{k,r}(\{t_k\})$ are N eigenvalues of $N \times N$ transfer matrix W

$$W_{k_1 k_2}(r) \;=\; t_{k_1} t_{k_2+r} \alpha_{k_1+k_2+r} \;. \tag{12}$$

One advantage in dealing with the dual form (10) is that one should solve a problem of diagonalizing $N \times N$ matrix rather than $N^2 \times N^2$ matrix. Another advantage is that eigenvalues $\lambda_k (r \neq 0)$ are nothing but eigenvalues of the transfer matrix in the presence of the correlation function (correlation function introduces a global shift in the indices on links which form a path between sites x and $x + R$). Therefore, we do not need, in principle to compute the correlation function separately to establish RR. A general answer for the correlation function is

$$\begin{aligned} \Gamma_j(2 \times L, \{t_k\}; R) &= \frac{Z_j(2 \times L, \{t_k\}; R)}{Z(2 \times L, \{t_k\})} \\ Z_j(2 \times L, \{t_k\}; R) &= \frac{1}{N} \sum_{r=0}^{N-1} \mathrm{Tr}\, [W(r)^{L-R}\, W(r+j)^R] \;. \end{aligned} \tag{13}$$

Let $\lambda_{0,r}(\{t_k\}) \equiv \lambda_r(\{t_k\})$ be maximal eigenvalue for fixed r. It is easy to prove that $\lambda_0(\{t_k\}) > \lambda_r(\{t_k\})$. Then, one finds in the limit $L \to \infty$

$$Z(2 \times L, \{t_k\}) \;\sim\; [\lambda_0(\{t_k\})]^L \;, \tag{14}$$

$$\Gamma_r(2, \{t_k\}; R) \;\sim\; \left[\frac{\lambda_r(\{t_k\})}{\lambda_0(\{t_k\})}\right]^R \;. \tag{15}$$

The correlation function has been calculated up to pre-exponential factor D_r in which we are not interested at the moment. Now, to derive the RR we need the following formula for the correlation function on the lattice with $M = 1$

$$\Gamma_r(1, \{t_k^{(1)}\}; R/2) \;=\; \left[t_r^{(1)}\right]^{R/2} \;. \tag{16}$$

According to Eq.(7) we get the following system of RR

$$t_r^{(1)} \;=\; \left[\frac{\lambda_r(\{t_k\})}{\lambda_0(\{t_k\})}\right]^2 \;. \tag{17}$$

4 Reduction of the matrix size

If we want to compute a full transfer matrix, than even for $M = 2$ we have to deal with $N^2 \times N^2$ matrices. Fortunately, we need only two largest eigenvalues – so if we find a way to "decouple" them into a smaller matrix we do not need to use the entire transfer matrix.

Looking at the eigenvalues of the transfer matrix we notice a number of coinciding eigenvalues. They correspond to eigenvectors that can be transformed one into another by one of the lattice symmetries. We can choose eigenvectors of our matrix so that each of them, when transformed by one of the lattice symmetries, gets multiplied by some phase factor. After having done that, we note that the eigenvector, corresponding to the largest eigenvalue must be symmetric with respect to all the symmetries – so that the behavior of free energy in the model with free boundary conditions (in which only symmetric eigenvalues are preserved in the partition function) would be the same as that of the model with periodic boundary conditions. Additionally, the eigenvector corresponding to the second largest eigenvalue must be symmetric with respect to all the symmetries, except multiplication of all the spins by a constant phase factor (this symmetry is explicitly violated by insertion of the spins at the ends of the correlation function). So we can symmetrize our basis with respect to all these symmetries, reducing our transfer matrix size.

In the following we will consider standard Potts model on a lattice with $M = 2$ in an external field. The symmetries we may use are: shift in the transverse direction, reversal of the chain and changing of all the spins in the chain so that equal spins remain equal and zero spins remain unchanged. It turns out that after we take into account these symmetries the size of the transfer matrix obtained does not depend on N for $N \geq 3$. That means we can obtain renormalization group equations valid for arbitrary N values.

After symmetrization we get 4 base vectors, obtained by symmetrization of states $(00), (01), (11)$ and (12).

Now the reduced 4×4 transfer matrix will define change of the coefficients in state vector $v(\sigma_0, \sigma_1) = a0 + a1(\sigma_0 + ...) + a2(\sigma_0\sigma_1 + ...) + a3(\sigma_0\sigma_1^2 + ...)$ (the expressions in parentheses are symmetrized with respect to the symmetries mentioned before) after the transformation

$$\begin{aligned} v'(z_0, z_1) \;=\; & \sum_{\sigma_0, \sigma_1} (1 - m + Nm\delta_{\sigma_0})(1 - m + Nm\delta_{\sigma_1})(1 - t + Nt\delta_{\sigma_0\sigma_1^{-1}})^2 \\ & (1 - t + Nt\delta_{z_0\sigma_0^{-1}})(1 - t + Nt\delta_{z_1\sigma_1^{-1}}) v(\sigma_0, \sigma_1) \;. \end{aligned} \tag{18}$$

After performing summation we obtain 4×4 transfer matrix A, which becomes block-diagonal with two 2×2 blocks if $h = 0$. For $M = 1$ using similar method we obtain 2×2 matrix that becomes diagonal if $h = 0$. Now we can use our renormalization group, preserving correlation function and magnetization:

$$\begin{aligned} \frac{\lambda_{11}(t',h')}{\lambda_{10}(t',h')} &= \left(\frac{\lambda_{21}(t,h)}{\lambda_{20}(t,h)}\right)^2 , \\ \frac{d\log(q(t')q(h')\lambda_{10}(t',h'))}{dH(h')} &= \frac{d\log(q(t)^4 q(h)^2 \lambda_{20}(t,h))}{2\ dH(h)} , \end{aligned} \tag{19}$$

where $q(t) = e^{-\frac{\beta(t)}{N-1}} \left(N - 1 + e^{\frac{N\beta(t)}{N-1}}\right)/N$ - coefficient taken from the link when going from β-representation to t-representation, and $\beta(t) = \frac{N-1}{N} \ln \frac{1+(N-1)t}{1-t}$ - β value corresponding to t value.

Solving these we can find critical point for any N (though transfer matrix for $N = 2$ has smaller size, our general transfer matrix contains it, and so the general matrix can be used also for $N = 2$).

Expanding the solution around critical point in t and h we obtain critical indices ν and y_h:

$$\begin{aligned} \nu &= \ln 2 / \ln \left.\frac{dt'}{dt}\right|_{crit} , \\ y_h &= \ln \left.\frac{dh'}{dh}\right|_{crit} / \ln 2 . \end{aligned} \tag{20}$$

The results obtained are summarized in Table 1.

N	β_c	ν	y_h	α	β	γ	η
2	0.435657	0.987303	1.788717	0.025394	0.208601	1.557405	0.422567
	0.440687	1	1.875	0	0.125	1.75	0.25
3	0.655143	0.874834	1.749592	0.250332	0.219065	1.311538	0.500815
	0.670035	0.833333	1.866667	0.333333	0.111111	1.444444	0.266667
4	0.799504	0.807699	1.717679	0.384603	0.228030	1.159337	0.564642
	0.823959	0.666666	1.875	0.666666	0.083333	1.166667	0.5
5	0.906325	-	-	-	-	-	-
	0.939487	-	-	-	-	-	-

Table 1. Critical coupling and critical exponents obtained from SDA for several standard Potts Z(N) models; the second row gives exact values

5 Summary and perspectives

SDA RG works surprisingly well both qualitatively and quantitatively for standard and vector Potts models. Increasing the width of the lattice strips used increases the precision of the results. Using the transfer matrix reduction described above we were able to calculate exact eigenvalues for standard Potts model with arbitrary N and $M = 2, 3, 4$, obtaining the same results as quoted in [6]. For the generalized $Z(N)$ Potts models we have obtained exact RG equations for M up to 8 and $N = 2, 3, 4, 5$. The problem of going to wider strips remains open.

Plots of $\lambda_2(t)/\lambda_0(t)$ give precise critical points for standard Potts models and show qualitatively correct phase structure for vector Potts models. The renormalization group for this quantity is still to be built.

The method described can be generalized to $3d$ lattice gauge models, though in that case only $2 \times 2 \times L$ strips give matrices which have tractable size.

References

[1] A.A. Migdal, Zh. Eksp. Teor. Fiz. **69** 1457 (1975); (Sov. Phys.-JETP **42** 743 (1975)).
[2] L.P. Kadanoff, Ann. Phys. **100** 359 (1976).
[3] M.P. Nightingale, Physica **83A** 561 (1976).
[4] M.A. Yurishchev, JETP **91** 332 (2000).
[5] Raymond E. Goldstein, James S. Walker, J.Phys. A: Math.Gen. **18** 1275 (1985).
[6] Jesus Salas, Shu-Chiuan Chang, Robert Shrock, J. Stat. Phys. **107** 1207 (2002).

Proceedings of the International School-seminar
"New Physics and Quantum Chromodynamics at External Conditions", pp. 107 – 110,
May 22-24, 2013, Dnipropetrovsk, Ukraine

SCALAR FIELD POTENTIAL DISTRIBUTION FOR A CLOSED RADIALLY EXPANDING NULL STRING IN PLANE $Z = 0$

A. P. Lelyakov[a], R. A. Babadzhan[b]

Taurida National V.I. Vernadsky University, Simferopol, Crimea, Ukraine

In this article, we have received, the general view of distribution of potential scalar field for "thick" null string radially expanding in plane $z = 0$. Conditions on potential of a scalar field at which, within the limits of compression of a scalar field in one-dimensional object, the stress energy tensor components of a scalar field coincide with components stress energy tensor of the closed null string moving on the same trajectory are found.

1 Introduction

Along with the traditional scenario in the literature discussed string mechanism of generation of density concentrations in the early universe [1], [2]. It is a great interest to study the dynamics of strings in various pseudo-Riemannian spaces dictated by the fact that, firstly, may provide additional information about yourself background gravitational field. The components of the energy-momentum tensor for a null string have the following form [4]:

$$T^{mn}\sqrt{-g} = \gamma \int d\tau d\sigma \; x^m_{,\tau} x^n_{,\tau} \delta^4 \left(x^l - x^l\left(\tau,\sigma\right)\right), \tag{1}$$

where the indices m, n, l take on the values $0, 1, 2, 3$, the functions $x^m = x^m(\tau,\sigma)$ determine the trajectory of a null string, τ and σ are the parameters on the light surface of the null string, $x^m_{,\tau} = \partial x^m/\partial\tau$, $g = |g_{mn}|$, g_{mn} is the metric tensor of the environment, $\gamma = const$.

In the cylindrical system of coordinates

$$x^0 = t, \quad x^1 = \rho, \quad x^2 = \theta, \quad x^3 = z,$$

the functions $x^m(\tau,\sigma)$, that determine the trajectory of a closed null string, radially expanding in a plane $z = 0$, have the following form:

$$t = \tau, \quad \rho = \tau, \quad \theta = \sigma, \quad z = 0, \quad \tau \in (0, +\infty]. \tag{2}$$

Using the symmetry of the trajectory (2), the general expression of the quadratic form, which describes the motion under consideration null string can be presented as

$$dS^2 = e^{2\nu}(dt)^2 - A(d\rho)^2 - B(d\theta)^2 - e^{2\mu}(dz)^2, \tag{3}$$

where ν, μ, A, B depend on the variables t, ρ, z.

Since trajectory (2) must be one of the solutions of the motion equations of a null string, additional restrictions imposed on the metric functions can be obtained, whose fulfillment provides the constancy of a trajectory of the null string specified by (2).

The motion of a null string in the pseudo-Riemannian space is determined by the system of equations [3]:

$$x^m_{,\tau\tau} + \Gamma^m_{pq} x^p_{,\tau} x^q_{,\tau} = 0, \tag{4}$$

$$g_{mn} x^m_{,\tau} x^n_{,\tau} = 0, \quad g_{mn} x^m_{,\tau} x^n_{,\sigma} = 0, \tag{5}$$

where Γ^m_{pq} are the Christoffel symbols. Putting down the first of (5) for (2), one can make sure that it has form $e^{2\nu} - A = 0$. Consequently,

$$e^{2\nu} \equiv A, \tag{6}$$

whereas the rest of equations of system (4), (5) for (2), (3) under condition (6) are reduced to the single equation $\nu_{,t} - \nu_{,\rho} = 0$, which yields

$$\nu = \nu(\eta, z), \tag{7}$$

where $\eta = t - \rho$. Analyzing the system of Einstein equations and using conditions (6), (7), the dependence of functions of the quadratic form (3) can be redefined as

$$B = B(\eta, z), \quad \mu = \mu(\eta, z). \tag{8}$$

e-mail: [a]lelyakov@crimea.edu, [b]kararaja@mail.ru

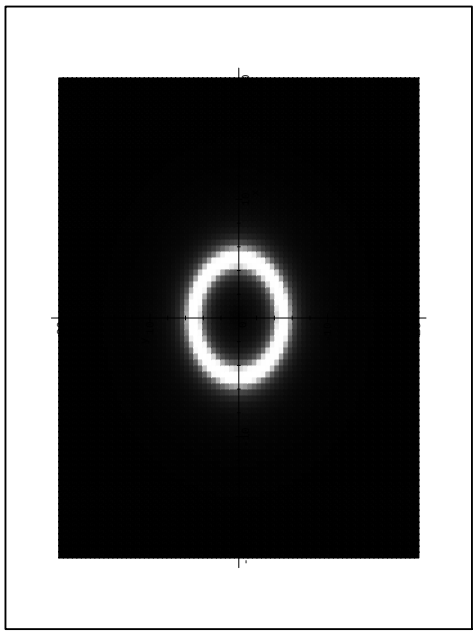

Figure 1. Scalar field potential diastribution specified by (28), (30) with depends on t, at $\epsilon = 0.01$, $\xi = \zeta = 1, 3$, $\gamma = 4$, $\rho \in [0, 20]$, $t = 5$.

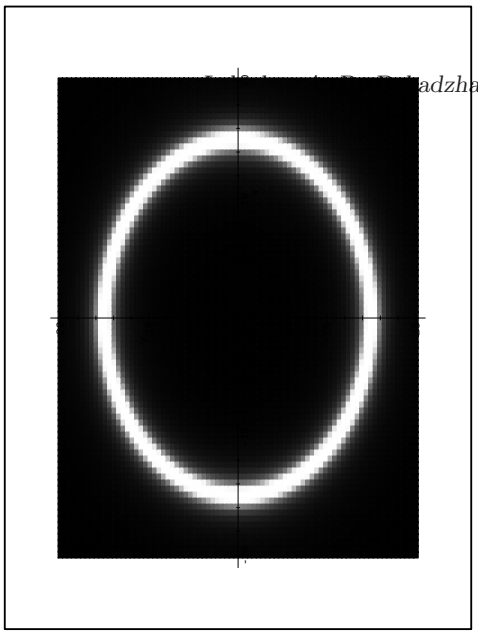

Figure 2. Scalar field potential diastribution specified by (28), (30) with depends on t, at $\epsilon = 0.01$, $\xi = \zeta = 1, 3$, $\gamma = 4$, $\rho \in [0, 20]$, $t = 15$.

In this case, the Einstein system itself is reduced to the equations

$$\frac{B_{,\eta\eta}}{B} + 2\mu_{,\eta\eta} - 2\nu_{,\eta}\left(\frac{B_{,\eta}}{B} + 2\mu_{,\eta}\right) - \frac{1}{2}\left(\frac{B_{,\eta}}{B}\right)^2 + 2\left(\mu_{,\eta}\right)^2 = -2\chi\gamma\frac{e^{2\nu-\mu}}{\sqrt{B}}\delta(\eta)\delta(z) \tag{9}$$

$$\left(\frac{B_{,z}}{B}\right)_{,z} + \frac{1}{2}\left(\frac{B_{,z}}{B}\right)^2 + \frac{B_{,z}}{B}\left(2\nu_{,z} - \mu_{,z}\right) = 0, \tag{10}$$

$$\frac{B_{,\eta z}}{B} + 2\nu_{,\eta z} - \nu_{,z}\left(\frac{B_{,\eta}}{B} + 2\mu_{,\eta}\right) - \frac{1}{2}\frac{B_{,z}}{B}\left(\frac{B_{,\eta}}{B} + 2\mu_{,\eta}\right) = 0, \tag{11}$$

$$2\nu_{,zz} + 4(\nu_{,z})^2 + \nu_{,z}\left(\frac{B_{,z}}{B} - 2\mu_{,z}\right) = 0, \qquad (\nu_{,z})^2 + \nu_{,z}\frac{B_{,z}}{B} = 0. \tag{12}$$

With the use of the obtained conditions (6)-(8), expression (3) can be presented in the form

$$dS^2 = e^{2\nu}\left((dt)^2 - (d\rho)^2\right) - B(d\theta)^2 - e^{2\mu}(dz)^2, \tag{13}$$

where ν, μ, B depend on the variables η, z.

Later, using the result of [5], we consider the components of the zero-string energy-momentum tensor as the limit of a "thick" distribution, in which we choose as a real massless scalar field, because the task at hand, we consider the scalar zero object.

2 System of Einstein for the "thick" problem

The components of the energy-momentum tensor for a real massless scalar field have the form

$$T_{\alpha\beta} = \varphi_{,\alpha}\varphi_{,\beta} - \frac{1}{2}g_{\alpha\beta}L, \tag{14}$$

where $L = g^{\omega\lambda}\varphi_{,\omega}\varphi_{,\lambda}$, $\varphi_{,\alpha} = \partial\varphi/\partial x^{\alpha}$, φ is the scalar field potential, and this indices $\alpha, \beta, \omega, \lambda$ take on the values $0, 1, 2, 3$. To provide the self-consistency of the Einstein equations constructed for (13), (14), we demand that

$$T_{\alpha\beta} = T_{\alpha\beta}(\eta, z) \to \varphi = \varphi(\eta, z). \tag{15}$$

Putting down Eq. (14) for (13), (15), we obtain

$$\begin{aligned} &T_{00} = (\varphi_{,\eta})^2 + \frac{e^{2(\nu-\mu)}}{2}(\varphi_{,z})^2, \quad T_{03} = T_{13} = \varphi_{,\eta}\varphi_{,z}, \quad T_{01} = (\varphi_{,\eta})^2, \\ &T_{11} = (\varphi_{,\eta})^2 - \frac{e^{2(\nu-\mu)}}{2}(\varphi_{,z})^2, \quad T_{22} = -\frac{Be^{-2\mu}}{2}(\varphi_{,z})^2, \quad T_{33} = \frac{1}{2}(\varphi_{,z})^2. \end{aligned} \tag{16}$$

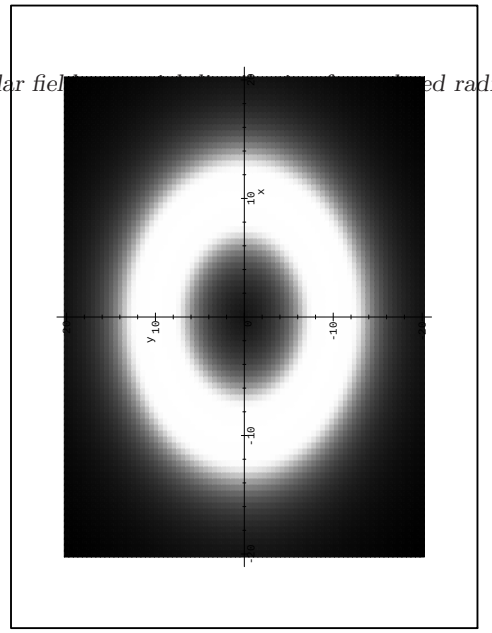

Figure 3. Scalar field potential diastribution specified by (28), (30) with respect to ρ, at $\epsilon = 0.01$, $\zeta = 1, 3$, $\gamma = 4$, $\rho \in [0, 20]$, $t = 10$, $\xi = 0, 2$.

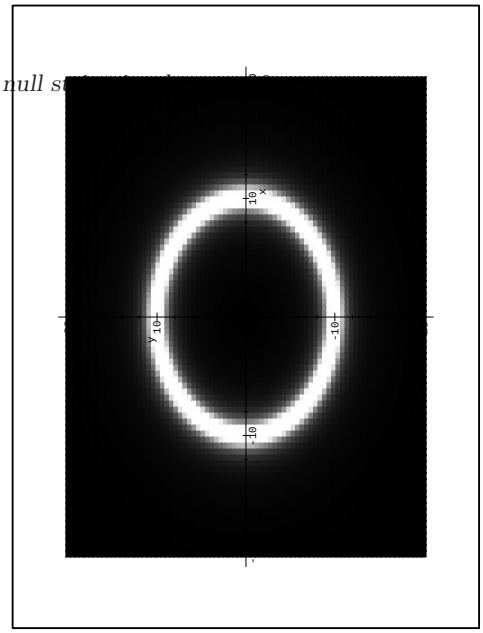

Figure 4. Scalar field potential diastribution specified by (28), (30) with respect to ρ, at $\epsilon = 0.01$, $\zeta = 1, 3$, $\gamma = 4$, $\rho \in [0, 20]$, $t = 10$, $\xi = 0, 6$.

The system of Einstein equations for (13), (16) can be presented as follows

$$\frac{B_{,\eta\eta}}{B} + 2\mu_{,\eta\eta} - 2\nu_{,\eta}\left(\frac{B_{,\eta}}{B} + 2\mu_{,\eta}\right) - \frac{1}{2}\left(\frac{B_{,\eta}}{B}\right)^2 + 2\left(\mu_{,\eta}\right)^2 = -2\chi(\varphi_{,\eta})^2, \tag{17}$$

$$\left(\frac{B_{,z}}{B}\right)_{,z} + \frac{1}{2}\left(\frac{B_{,z}}{B}\right)^2 + \frac{B_{,z}}{B}\left(2\nu_{,z} - \mu_{,z}\right) = 0, \tag{18}$$

$$\frac{B_{,\eta z}}{B} + 2\nu_{,\eta z} - \nu_{,z}\left(\frac{B_{,\eta}}{B} + 2\mu_{,\eta}\right) - \frac{1}{2}\frac{B_{,z}}{B}\left(\frac{B_{,\eta}}{B} + 2\mu_{,\eta}\right) = -2\chi\varphi_{,\eta}\varphi_{,z}, \tag{19}$$

$$2\nu_{,zz} + 4(\nu_{,z})^2 + \nu_{,z}\left(\frac{B_{,z}}{B} - 2\mu_{,z}\right) = 0, \quad (\nu_{,z})^2 + \nu_{,z}\frac{B_{,z}}{B} = \frac{\chi}{2}(\varphi_{,z})^2. \tag{20}$$

Let us consider system (17) - (20) for the distribution of the scalar field already concentrated inside a "thin" ring, with the variables η and z taking values in the interval

$$\eta \in [-\Delta\eta, \Delta\eta]\,, z \in [-\Delta z, \Delta z]\,, \tag{21}$$

where $\Delta\eta$ and Δz are small positive constants that determine the "thickness" of the ring. The space, where such a "thick" null string moves can be conditionally divided into three regions:

- region I, for which

$$z \in (-\infty, -\Delta z) \cup (\Delta z, +\infty)\,, \eta \in (-\infty, +\infty)\,,$$

- region II, for which

$$z \in [-\Delta z, +\Delta z]\,, \eta \in (-\infty, -\Delta\eta) \cup (\Delta\eta, +\infty)\,,$$

- region III, for which

$$\eta \in [-\Delta\eta, \Delta\eta]\,, z \in [-\Delta z, \Delta z]\,.$$

Since the contraction of scalar field into a string mast result in the asymptotic coincidence of system (17) - (20) with the system for a closed null string (9) - (12) we obtain for the regions I, II

$$\varphi \to 0, \quad \varphi_{,z} \to 0, \quad \varphi_{,\eta} \to 0, \tag{22}$$

for the region III, in the general case,

$$\frac{\varphi_{I,II}}{\varphi_{III}} \leq 1, \quad \frac{(\varphi_{,z})_{I,II}}{(\varphi_{,z})_{III}} \leq 1, \quad \frac{(\varphi_{,\eta})_{I,II}}{(\varphi_{,\eta})_{III}} \leq 1, \tag{23}$$

where $\varphi_{I,II}$ are values of the scalar field potential in the regions I, II, φ_{III} are values of the scalar field potential in the regions III (inside the "thin" ring), equality is realized on the boundary.

Comparing the system of Einstein equations for a closed null string (9) - (12) with system (17) - (20), we may conclude that, under the contraction of the scalar field into a stringe of the required configuration, i.e., at $\Delta\eta \to 0$, $\Delta z \to 0$

$$(\varphi_{,z})^2\big|_{z\to 0,\eta\to 0} \to 0, \quad (\varphi_{,\eta})^2\big|_{z\to 0,\eta\to 0} \to \infty, \quad (\varphi_{,z}\varphi_{,\eta})|_{z\to 0,\eta\to 0} \to 0. \tag{24}$$

According to (22), the scalar field potential in region I at any fixed value of $\eta = \eta_0 \in (-\infty, -\Delta\eta) \cup (+\Delta\eta, +\infty)$ and all values of $z \in (-\infty, +\infty)$

$$\varphi(\eta_0, z) \to 0, \tag{25}$$

Considering the scalar field potential distribution at any fixed value of $\eta = \eta_0 \in [-\Delta\eta, \Delta\eta]$ (regions II and III), if $z \in (-\infty, -\Delta z) \cup (\Delta z, +\infty)$ (region II), must be realized

$$\varphi(\eta_0, z) \to 0, \tag{26}$$

whereas, for $z \in [-\Delta z, \Delta z]$ (region III)

$$\frac{\varphi(\eta_0, z)_{III}}{\varphi(\eta_0, z)_{II}} > 1. \tag{27}$$

3 Scalar field potential distribution for a "thick" null string

For the conditions (22)-(27) it is suitable to present the scalar field potential distribution in the form

$$\varphi(\eta, z) = -\ln\left(\alpha(\eta) + \lambda(\eta) f(z)\right), \tag{28}$$

where the functions $\alpha(\eta)$ and $\lambda(\eta) = (1 - \alpha(\eta))\frac{1}{f_0}$, $f_0 = const.$, are symmetric with respect to the inversion of η to $-\eta$. The function $\alpha(\eta) + \lambda(\eta) f(z)$ is bounded

$$0 < \alpha(\eta) + \lambda(\eta) f(z) \leq 1, \tag{29}$$

As an example, the functions $\alpha(\eta)$ and $f(z)$ can be chosen as follows:

$$\alpha(\eta) = \exp\left(-(\epsilon + (\xi\eta)^2)^{-1}\right), \quad f(z) = f_0 \exp\left(-\gamma\left(1 - \exp\left(((\zeta z)^2)^{-1}\right)\right)\right), \tag{30}$$

where the constants ξ and ζ determine the size ("thickness") of the ring, the positive constants ϵ and γ provide the fulfillment of conditions.

Figures 1-4 present different space-time sections (depends on t, ρ) for a closed "thick" null string radially expanding in a plane $z = 0$ in region $\eta \in [-10, 10]$, $z \in [-10, 10]$, for the functions $\alpha(\eta)$, $f(z)$, defined by the equalities (30). Note that in the presented figure 1-4, black shows an area in which $\varphi \to 0$.

From the Figures 1-4 follows that with increasing of the variable t (Fig. 1, 2) radius of the "thick" null string increases (null string extends radially in plane $z = 0$), and with increasing values of the constants ξ, ζ (Fig. 3, 4)) region decreases, where scalar field potential isn't tend to zero. In other words, the "thickness" of the ring, where the scalar field is concentrated, decreases.

References

[1] A. Vilenkin, E.P.S. Shellard *Cosmic strings and other topological defects*, (Cambridge Univ. Press, 1994).
[2] A. D. Linde *Particle physics and inflationary cosmology*, (Harwood, Chur. Switzerland, 1990).
[3] P.J.E. Peebles, *Principles of physical cosmology*, (Prinston University Press, 1994).
[4] S.N. Roshchupkin, A.A. Zheltukhin, Class. Quantum. Grav, **12**, (1995).
[5] A.P. Lelyakov, Ukr. J. Phys. **56**, 3 (2011).

Proceedings of the International School-seminar
"New Physics and Quantum Chromodynamics at External Conditions", pp. 111 – 114,
May 22-24, 2013, Dnipropetrovsk, Ukraine

TARGET MASS CORRECTIONS TO STRUCTURE FUNCTIONS IN NEUTRINO DEEP-INELASTIC SCATTERING

V. I. Lashkevich[1], O. P. Solovtsova[1,2 a]

[1] Gomel State Technical University, Gomel, Belarus
[2] Joint Institute for Nuclear Research, Dubna,Russia

With the improvement of accuracy in the inclusive deep-inelastic scattering experiments, it has become apparent that comparable improvements are needed in the accuracy of the theoretical analysis tools. As well-known, extracting structure functions in the region large values of the Bjorken variable x, it is crucial to correct data by effects associated with the non-zero mass of the target. We investigate this question and demonstrate that target mass corrections to structure functions calculated by using the new approach have a correct spectral property and noticeably differ that the standard Georgi-Politzer method gives, especially for values Q^2 of the order of $1 \div 2$ GeV^2 and large values of the Bjorken variable x.

1 Introduction

Presently the structure functions in deep-inelastic scattering is a well-proved way of probing the internal structure of nucleons and testing the physical theories governing their structure. The cross section of inelastic lepton-hadron scattering in the case of a unpolarized nucleon is determined by the hadron tensor $W_{\mu\nu}$, which is parameterized by the nucleon structure functions F_1, F_2, and F_3. (Other structure functions are proportional to the lepton mass and are therefore negligible for the kinematics of the deep-inelastic region.)

We concentrate here on the unpolarized neutrino-nucleon scattering. Neutrinos interact with matter only via the weak-interactions, which are classified as the neutral-current (NC) and the charged current (CC) interactions. CC interactions are mediated by charged $W^{\pm}$ bosons, while NC interactions are mediated by electrically neutral Z bosons. A CC reaction transforms a neutrino into its corresponding charged lepton, and vice versa. We do not consider the first two structure function F_1 and F_2 in the neutrino-nucleon scattering as these functions are simile to charged lepton deep-inelastic scattering: the electromagnetic current replaced by the corresponding weak current. Therefore, F_1 and F_2 can be easily obtained from our results which have been presented earlier in Ref. [1]. Instead we focus on the structure function F_3 associated to the totally antisymmetric tensor, which arises from the vector/axial-vector interference of the two VA currents.

To analyze the properties of structure functions the operator product expansion (OPE) method is usually used. According to the OPE, the contributions from different quark-gluon operators to hadronic tensor can be ordered according to their twist. For the structure functions this leads to the expansion in inverse powers of Q^2. The first term is the leading twist (LT) contribution which is directly related to the distributions of quarks and gluons inside the nucleon, the parton distribution functions via the factorization theorem as a convolution with coefficient functions. The coefficient functions depend on the process and the type of the structure function but are independent of the target. These functions are computable as power series in α_s. The parton distributions are independent of the process but do depend on the target. The parton distribution functions have non-perturbative origin and cannot be calculated in the perturbative QCD. The twist-4 contributions (higher twist, HT) involve interactions between quarks and gluons and lack simple probabilistic interpretation.

It must be stressed that the OPE expansion was derived in the massless limit. If a finite mass for the nucleon target is considered, the new terms arise: leading to additional power terms of kinematical origin called the target mass corrections (TMC). The TMC play a somewhat special role become larger and larger at low Q^2 and approaching to the kinematic limit as the Bjorken variable x tends to unity. The OPE was first used to study target mass effects by Georgi and Politzer in Ref. [2]. Such an approach for considering TMS became known as the Georgi and Politzer (GP) approach or ξ-scaling method because was formulated through the Nachtmann ξ variable [3]. However, the expressions for the structure functions obtained by using GP method have a difficulty arising from the violation of the spectral condition. It hence became a problem to describe the structure functions as the Bjorken variable x tends to unity. This problem has been widely discussed in the literature ever since its appearance (see, e.g., [4–6]).

As it was shown by Solovtsov [7] that this problem is similar to the problem that appears for an invariant charge in quantum chromodynamics, when the violation of the general principles of the theory, which are

e-mail: [a]olsol07@mail.ru

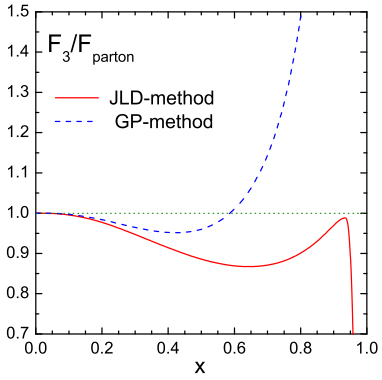

Figure 1. The behavior of the ratio vs x (without QCD corrections).

reflected in the Källén–Lehmann representation, leads to unphysical singularities. A solution of this problem was proposed in the Shirkov-Solovtsov analytic approach [8]. By using the Jost-Lehmann-Dyson (JLD) integral representation [9, 10] it was shown [7] that the natural scaling variable is a new variable s, which leads to the moments $\mathcal{M}_n(Q^2)$ that are analytic functions. In this case, the spectral property for the structure functions is satisfied automatically, and no problem arises in the limit as the Bjorken variable x tends to unity. Note the proof of the JLD representation is based on the most general principles of the theory, such as the covariance, Hermiticity, spectrality, and causality. In the present work we continue the researches begun earlier in Refs. [1] and we extend them on the structure function F_3 in charged-current, measured with high precision in neutrino-nucleon DIS [11]. As in the previous works, we concentrate on effects associated with the non-zero mass of the target including next-to-leading order (NLO) QCD corrections.

2 Threshold problem

To begin let us demonstrate a threshold problem within the GP approach. The structure function F_3 corrected by the TMC reads as follows [2]:

$$F_3(x,Q^2) = \frac{x\,F_3^{(0)}(\xi,Q^2)}{\xi(1+4\varepsilon x^2)} + \frac{2\varepsilon x^2}{\sqrt{(1+4\varepsilon x^2)^3}}\cdot\int\limits_{\xi}^{1}\frac{F_3^{(0)}(y,Q^2)}{y}\cdot dy\,, \tag{1}$$

where the Bjorken variable $x = Q^2/2\nu$, the Nachtmann variable [3] reads

$$\xi = \frac{2\,x}{1+\sqrt{1+4\varepsilon x^2}}\,,\quad \epsilon \equiv \frac{M^2}{Q^2}\,,\quad F_3^0(\xi,Q^2) = \lim_{M\to 0} F_3(x,Q^2)_{x=\xi}\,, \tag{2}$$

M is the nucleon mass. In Fig. 1 we show the behavior of the ratio of F_3 structure function with TMC according to the expression (1) to the parton distribution $F(x) = \sqrt{x}(1-x)^3$ (see Ref. [12]) for the JLD-method (solid line) and the ξ-approach (dashed curve) at the $\varepsilon \equiv M^2/Q^2 = 1/2$. This figure shows that there is a difference in results got by different methods (see Ref. [5] for more details) and within the method based on the JLD representation it is possible to get a correct behavior of the structure function as $x \to 1$.

Accounting the NLO QCD corrections, we use the following expressions for the proton and the neutron structure functions (see, e.g., Refs. [13, 14]):

$$\begin{aligned}
F_3^{\nu p}(x,Q^2) &= (\delta(1-x) + a_s(Q^2)\cdot C_3^1(x))\otimes q^{\nu p}(x,Q^2)\,,\\
F_3^{\bar\nu p}(x,Q^2) &= (\delta(1-x) + a_s(Q^2)\cdot C_3^1(x))\otimes q^{\bar\nu p}(x,Q^2)\,,\\
F_3^{\nu n}(x,Q^2) &= (\delta(1-x) + a_s(Q^2)\cdot C_3^1(x))\otimes q^{\nu n}(x,Q^2)\,,\\
F_3^{\bar\nu n}(x,Q^2) &= (\delta(1-x) + a_s(Q^2)\cdot C_3^1(x))\otimes q^{\bar\nu n}(x,Q^2)\,,
\end{aligned} \tag{3}$$

where $a_s(Q^{2)}) = \alpha_s(Q^2)/4\pi$ and the splitting function reads as

$$C_3^1(x) = \frac{4}{3}\left\{4\left[\frac{\ln(1-x)}{1-x}\right]_+ - 3\left[\frac{1}{1-x}\right]_+ - (9+\frac{2\pi^2}{3})\cdot\delta(1-x)\right\} - \frac{4}{3}\left\{2(1+x)\cdot\ln\frac{1-x}{x} + 4\cdot\frac{\ln x}{1-x} - 4 - 2x\right\}.$$

The convolution of functions means

$$a(x) \otimes f(x) = \int\limits_x^1 a(x/y) \cdot \frac{f(y)}{y} dy \,,\; a(x)_+ \otimes f(x) = \int\limits_x^1 a(x/y) \cdot \left[f(y) - \frac{x}{y} \cdot f(x) \right] \cdot \frac{dy}{y} - f(x) \cdot \int\limits_0^x C(y) dy.$$

As target mass corrections most essential at small $Q^2 < 1 \div 2$ GeV^2, we consider only the light quarks:

$$q^{\nu p}(x,Q^2) = 2 \cdot \left\{ d(x,Q^2) \cdot \cos^2\theta_c - \bar{u}(x,Q^2) + s(x,Q^2) \cdot \sin^2\theta_c \right\},$$
$$q^{\bar{\nu} p}(x,Q^2) = 2 \cdot \left\{ -\bar{d}(x,Q^2) \cdot \cos^2\theta_c + u(x,Q^2) - s(x,Q^2) \cdot \sin^2\theta_c \right\},$$
$$q^{\nu n}(x,Q^2) = 2 \cdot \left\{ u(x,Q^2) \cdot \cos^2\theta_c - \bar{d}(x,Q^2) + \bar{s}(x,Q^2) \cdot \sin^2\theta_c \right\},$$
$$q^{\bar{\nu} n}(x,Q^2) = 2 \cdot \left\{ -u(x,Q^2) \cdot \cos^2\theta_c + d(x,Q^2) - \bar{s}(x,Q^2) \cdot \sin^2\theta_c \right\},$$

where u, d, s / $\bar{u}, \bar{d}, \bar{s}$ are quark/anti-quark distributions, and θ_c is the usual Cabibbo angle. In our calculations we use quark/anti-quark distributions from Ref. [15], where was also fixed NLO value of the QCD parameter $\Lambda_{\rm QCD} = 0.248$ GeV. Note we have tested quark distributions given by other groups, e.g., the MRST/MSTW [16] and have found that no significant difference in behaviour in the region of $x > 0.2$ for which become essential the target mass corrections.

3 New approach

The method suggested by Solovtsov [7] is based on the JLD representation and gives a new scaling variable, $s = x\sqrt{(1+4\varepsilon)/(1+4\varepsilon x^2)}$, the moments on which become analytical functions. It has been shown, that for any physical structure function from the JLD representation follows

$$W(x,Q^2) = \int_0^1 d\beta\, \theta[f(\beta;x,\varepsilon)]\, H_0(\beta)\,, \tag{4}$$

where $H_0(\beta) = -dF(\beta)/d\beta$, $f(\beta;x,\varepsilon) = \dfrac{\beta}{s}\sqrt{1+4\varepsilon} - 1 - 2\varepsilon(1-\sqrt{1-\beta^2})$. One can find the roots of the equation $f(\beta;x,\varepsilon) = 0$. If $x > \tilde{x} \equiv 1/\sqrt{1+4\varepsilon^2}$, there are the two roots

$$\beta_\pm = \frac{x\sqrt{1+4\varepsilon x^2}}{1+4\varepsilon x^2+4\varepsilon^2 x^2} \times \left(1 + 2\varepsilon \pm 2\varepsilon \sqrt{\frac{1-x^2}{1+4\varepsilon x^2}} \right),$$

if $x < \tilde{x}$, then there is one root β_-.

According to the method the function $W(x,Q^2)$ for any physical structure function is expressed via the corresponding parton distribution $F(x)$ as follows

$$W(x,Q^2) = \begin{cases} F(\beta_-) - F(1)\,, & 0 \le x < \tilde{x}\,, \\ F(\beta_-) - F(\beta_+)\,, & \tilde{x} \le x \le 1\,, \end{cases} \tag{5}$$

where $\tilde{x} = 1/(\sqrt{1+4\varepsilon^2})$. The spectral property of the function $W(x,Q^2)$ (that it vanishes as $x \to 1$) and its continuity for $x = \tilde{x}$ follow because $\beta_-(x=1) = \beta_+(x=1)$ and $\beta_+(\tilde{x}) = 1$.

The results of calculations for the average neutrino and anti-neutrino structure function $xF_3^p(x,Q^2) = [F_3^{\nu p}(x,Q^2) + F_3^{\bar{\nu}p}(x,Q^2)])/2$ are presented in Figs. 2 and 3 which show the behavior of the proton structure function xF_3^p as a function of x for $Q^2 = 1$ GeV^2 and $Q^2 = 3$ GeV^2. The solid line corresponds to our result obtained by using the Solovtsov's approach, the dashed curve reflects the result obtained by standard GP method [2], the dotted line corresponds to the behavior without target mass corrections [15]. It should be mentioned that the integral of over all x of the $F_3^p(x,Q^2)$ structure function gives the Gross–Llewellyn Smith sum [17]. As may be seen from Fig. 2 for this sum rule, the target mass corrections will give a noticeable contribution.

4 Conclusion

We have reported a new result of including the target mass corrections to the structure function F_3 in neutrino nucleon deep inelastic scattering. We observed that at low $Q^2 \sim 1 \div 2$ GeV^2 the target mass corrections to structure function F_3 calculated by using new method (S-method) noticeably differ from the standard Georgi-Polizer method result. It is necessary to emphasize that the inclusion of target mass corrections in the fits of deep-inelastic scattering data is important [18, 19] as reduces everywhere the magnitude of the HT terms needed to describe the data [20]. We believe that the new method including target mass effects will be useful in extracting the magnitude of the structure functions from the experimental data.

Acknowledgements. We are grateful to the organizers of the "NPQCD-2013" for their warm hospitality, the support, and the interesting scientific program. interest in this work and helpful discussions. This research was partly supported by the RFBR grant 11-01-00182 and the BelRFFR-JINR grant F12D-002.

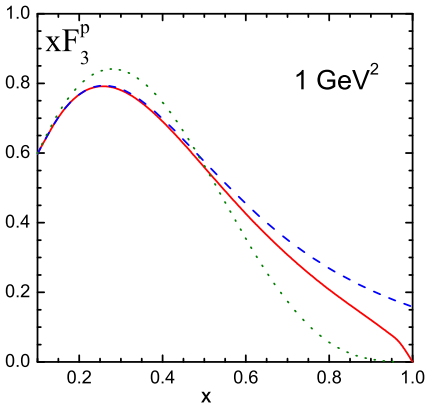

Figure 2. The function xF_3^p vs x at Q^2=1 GeV^2.

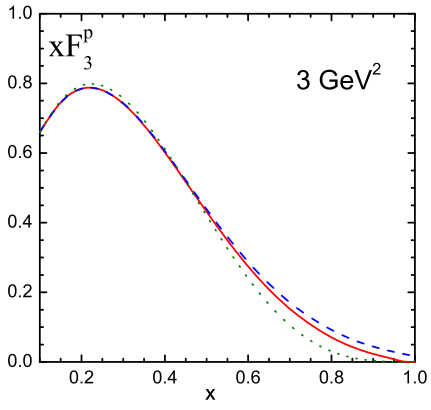

Figure 3. The function xF_3^p vs x at Q^2=3 GeV^2.

References

[1] V.I. Lashkevich and O.P. Solovtsova, Nonlin. Phenom. Complex Syst. **14**, 184 (2011); *Proc. of XVIII Annual Seminar "NPCS'2011"*, 230 (2011).
[2] H. Georgi and H.D. Politser, Phys. Rev. D **14**, 1829 (1976).
[3] O. Nachtmann, Nucl. Phys. B **63**, 237 (1973).
[4] W. Melnitchouk, R. Ent, and C. Keppel, Phys. Rep. **406**, 127 (2005); I. Schienbein *et al.*, J. Phys. G. **35**, 053101 (2008).
[5] V.I. Lashkevich and O.P. Solovtsova, Teor. Mat. Fiz. **160**, 471 (2009); Nonlin. Phenom. Complex Syst. **13**, 286 (2010).
[6] A. Accardi *et al.*, Phys. Rev. D **81**, 034016 (2010).
[7] I.L. Solovtsov, Part. Nucl. Lett. **101**, 10 (2000).
[8] D.V. Shirkov and I.L. Solovtsov, Phys. Rev. Lett. **79**, 1209 (1997).
[9] R. Jost and H. Lehmann, Nuov. Cim. **5**, 1598 (1957).
[10] F.J. Dyson, Phys. Rev. **110**, 1460 (1958).
[11] J. Beringer *et al.*, Particle Data Group, Phys. Rev. D **86**, 010001 (2012).
[12] A.L. Kataev, G. Parente, and A.V. Sidorov, Phys. Part. Nucl. **34**, 43 (2003).
[13] A. De Rújula, H. Georgi, and H.D. Politzer, Annals of Phys. **103**, 315 (1977).
[14] S. Kretzer and M.H. Reno, Phys. Rev. D **69**, 034002 (2004).
[15] M. Glück, E. Reya, and A. Vong, Z. Phys. C **7**, 433 (1995); Eur. Phys. J. C **5**, 461 (1998).
[16] A.D. Martin, R.G. Roberts, W.J. Stirling, and R.S. Thorne, Eur. Phys. J. C **16**, 117 (2000); A.D. Martin, W.J. Stirling, R.S. Thorne, and G. Watt, Eur. Phys. J. C **63**, 189 (2009).
[17] D.J Gross and C.H. Llewellyn Smith, Nucl. Phys. B **14**, 337 (1969).
[18] M. Virchaux and A. Milsztajn, Phys. Lett. B **274**, 221 (1992).
[19] S. Alekhin, J. Blümlein, S. Klein, and S. Moch, Phys. Rev. D **81**, 014032 (2009).
[20] J. Blümlein, Prog. Part. Nucl. Phys. **69**, 28 (2013).

Proceedings of the International School-seminar
"New Physics and Quantum Chromodynamics at External Conditions", pp. 115 – 119,
May 22-24, 2013, Dnipropetrovsk, Ukraine

EXTRACTING $P\Lambda$ SCATTERING LENGTHS FROM HEAVY ION COLLISIONS

V. M. Shapoval[a], B. Erazmus[b], R. Lednicky[c], and Yu. M. Sinyukov[d]

[a,d] Bogolyubov Institute for Theoretical Physics, Kyiv, Ukraine
[b] European Organization for Nuclear Research (CERN), Geneva, Switzerland
[b] SUBATECH, Ecole des Mines de Nantes, Université de Nantes, CNRS-IN2P3, Nantes, France
[c] Joint Institute for Nuclear Research, Dubna, 141 980, Russia

The $p-\Lambda\oplus\bar{p}-\bar{\Lambda}$ and $\bar{p}-\Lambda\oplus p-\bar{\Lambda}$ correlation functions for 10% most central Au+Au collisions at top RHIC energy $\sqrt{s_{NN}}=200$ GeV are modeled with Lednický and Lyuboshitz analytical formula using the source radii extracted from the hydrokinetic model (HKM) simulations. For the baryon-antibaryon case the corresponding spin-averaged strong interaction scattering length is obtained by fitting the STAR correlation function. In contrast to the experimental results, where extracted $p\bar{\Lambda}$ source radius value was found ~ 2 times smaller, than the corresponding $p\Lambda$ one, the calculations in HKM show both $p\Lambda$ and $p\bar{\Lambda}$ effective source radii to be quite close, as expected from theoretical considerations. To obtain the satisfactory fit to the measured baryon-antibaryon correlation function at this large source radius value, the modified analytical approximation to the correlation function, effectively accounting for the residual correlations, is utilized.

1 Introduction

The heavy ion collision experiments provide a good possibility for a study of the baryon-baryon strong interactions using the Final State Interaction (FSI) correlation technique [1–3]. The latter is based on the analysis of the momentum correlations caused by the final state interaction between corresponding baryons produced in the collision. This activity is especially interesting in view of the ongoing nuclear collision experiments at the LHC, which produce great amounts of various particles, including exotic multi-strange, charmed and beauty ones. It allows one to study the fundamental interactions between different hadron species, even among such particle pairs, which are difficult to produce sufficiently in other experiments. The extraction of this information makes it possible to check the correctness of hadron-hadron strong interaction models, constrain corresponding interaction potentials, and also improve existing cascade models (like UrQMD) by including into them the information about still unknown baryon-antibaryon annihilation cross-sections.

In the paper [4] the experimental $p\Lambda$ and $p\bar{\Lambda}$ correlation functions were fitted with Lednický and Lyuboshitz analytical model [1] that allowed to extract scattering length characterizing the two-particle strong interaction. However, apart from the interaction characteristics, the analytical approximation to the correlation function depends also on the source spatial structure, described in terms of emission source function, being the time-integrated relative distance distribution in the pair rest frame. This fact complicates a study of the particle interaction, as it increases the number of free parameters which enter the fit formula.

To simplify this study, one could calculate the corresponding source functions in realistic models of the collision process, which are known to describe well the experimental observables. The hydrokinetic model [5–7] provides successful simultaneous description of a wide class of bulk observables in the heavy ion collision experiments at RHIC and LHC [8]. Moreover, it reproduces well [9] the pion and kaon source functions for semi-central Au+Au collisions at the top RHIC energy [10], including the specific non-Gaussian tails observed in the pair momentum and beam direction projections of the experimental source function. In this talk we present the results of fitting the experimental data from [4] within the analytical model [1] where the Gaussian parametrization for the emission source function is utilized, and the corresponding Gaussian radii are extracted from the HKM model simulations.

2 Models description

The STAR collaboration studied [4] baryon-baryon $p-\Lambda\oplus\bar{p}-\bar{\Lambda}$ and baryon-antibaryon $p-\bar{\Lambda}\oplus\bar{p}-\Lambda$ correlation functions in 10% most central RHIC Au+Au collisions at $\sqrt{s_{NN}}=200$ GeV. Protons & antiprotons in transverse momentum range $0.4<p_T<1.1$ GeV/c with the rapidity $|y|<0.5$, and lambdas & antilambdas with $0.3<p_T<2.0$ GeV/c and $|y|<1.5$ were selected for the analysis.

e-mail: [a]shapoval@bitp.kiev.ua, [b]barbara.erazmus@cern.ch, [c]lednicky@fzu.cz, [d]sinyukov@bitp.kiev.ua

The experimental correlation function is constructed as the ratio of the distribution of particle momentum in the pair rest frame, k^*, in the same events to the analogous distribution in mixed events. Then the measured correlation function C_{meas} is corrected for the pair purity, defined as the fraction of correctly identified primary particle pairs among all the selected ones, to give the corrected function C_{corr}

$$C_{corr}(k^*) = \frac{C_{meas}(k^*) - 1}{\text{Pair Purity}} + 1. \tag{1}$$

The estimated mean pair purity in the experiment is $\lambda = 17.5 \pm 2.5\%$.

To fit the experimental correlation function the Lednický and Lyuboshitz analytical model [1] is used, which connects the two-particle correlation function $C(k^*)$ with the particle emission source size r_0 and the strong interaction scattering amplitude $f(k^*)$. In the equal-time approximation, valid on condition $|t_1^* - t_2^*| \ll m_{2,1}r^{*2}$ for $\text{sign}(t_1^* - t_2^*) = \pm 1$ respectively, the correlation function can be calculated as a square of the wave function $\Psi^S_{-\mathbf{k}^*}$, representing the stationary solution of the scattering problem with the opposite sign of the vector $\mathbf{k}^*$, averaged over the total spin S and the distribution of the relative distances $S(\mathbf{r}^*)$:

$$C(k^*) = \left\langle \left| \Psi^S_{-\mathbf{k}^*}(\mathbf{r}^*) \right|^2 \right\rangle. \tag{2}$$

In typical nuclear collisions the source radius can be considered much larger than the range of the strong interaction potential, so $\Psi^S_{-\mathbf{k}^*}$ at small k^* can be approximated by the s-wave solution in the outer region:

$$\Psi^S_{-\mathbf{k}^*}(\mathbf{r}^*) = e^{-i\mathbf{k}^*\cdot\mathbf{r}^*} + \frac{f^S(k^*)}{r^*} e^{ik^*\cdot r^*}. \tag{3}$$

The effective range approximation for the s-wave scattering amplitude is utilized

$$f^S(k^*) = \left(\frac{1}{f_0^S} + \frac{1}{2} d_0^S k^{*2} - ik^* \right)^{-1}, \tag{4}$$

where f_0^S is the scattering length and d_0^S is the effective radius for a given total spin $S = 1$ or $S = 0$.

The particles are assumed to be emitted unpolarized (i.e. with the polarization $P = 0$), so that the fraction of pairs in the singlet state $\rho_0 = 1/4(1 - P^2) = 1/4$, and in the triplet state $\rho_1 = 1/4(3 + P^2) = 3/4$. The pair separation distribution (source function) $S(\mathbf{r}^*) = d^3N/d^3r^*$ is assumed to be Gaussian one

$$d^3N/d^3r^* \propto e^{-\frac{\mathbf{r}^{*2}}{4r_0^2}}, \tag{5}$$

where r_0 is considered as the effective radius of the source.

Under such assumptions the correlation function can be calculated analytically [1]:

$$C(k^*) = 1 + \sum_S \rho_S \left[\frac{1}{2} \left| \frac{f^S(k^*)}{r_0} \right|^2 \left(1 - \frac{d_0^S}{2\sqrt{\pi} r_0} \right) + \frac{2\Re f^S(k^*)}{\sqrt{\pi} r_0} F_1(2k^* r_0) - \frac{\Im f^S(k^*)}{r_0} F_2(2k^* r_0) \right], \tag{6}$$

where $F_1(z) = \int_0^z dx e^{x^2 - z^2}/z$ and $F_2(z) = (1 - e^{-z^2})/z$. The term $-\frac{d_0^S}{2\sqrt{\pi} r_0}$ in this expression corresponds to the correction accounting for deviation of $\Psi^S_{-\mathbf{k}^*}$ from the true wave function inside the range of the strong interaction potential. So, the model has a quite large number of parameters, being the scattering lengths f_0^S, which may be complex in general case, the effective radii d_0^S and the source radius r_0. Although in principle all of them can be determined from the measured data, in each concrete situation the number of free parameters can be reduced by making certain reasonable assumptions about the values of some of them.

In our study the source radius r_0 is extracted from the Gaussian fit to the source functions calculated in hybrid HKM model. The simulation of the full process of evolution of the system formed in nuclear or particle collision in hHKM consists of two stages. The first one is hydrodynamical expansion of thermally and chemically equilibrated matter described within ideal hydrodynamics approximation with the lattice-QCD inspired equation of state [11] (corrected for small but nonzero chemical potentials), which is matched with the hadron-resonance gas in chemical equilibrium via cross-over type transition. The second stage consists in gradual system decoupling after loosing chemical and thermal equilibrium. It can be described either within hydrokinetic approach with switching to UrQMD cascade at some space-like hypersurface situated behind the hadronization one, or with sudden switch to UrQMD cascade at the hadronization hypersurface. In current

study we choose the second variant of switching to cascade, basing on [8], where the comparison of one- and two-particle spectra, calculated at both types of matching hydro and cascade stages for RHIC and LHC energies, showed a fairly small difference between them.

The model provides particle distribution functions $\frac{d^6N}{d^3xd^3p}$ at the chosen switching hypersurface. Using the Monte-Carlo procedure, one generates particle momenta and coordinates according to these distributions, which serve as the input for the UrQMD hadronic cascade.

To perform a specific calculation one should specify the initial conditions for the hydrodynamics stage attributed to the starting proper time τ_0. These conditions are the initial energy density (or entropy) profile $\epsilon(\mathbf{r})$ and the initial rapidity profile (initial flow) $y(\mathbf{r})$. Here we suppose longitudinal boost-invariance and use $\epsilon(\mathbf{r}_T)$ corresponding to the MC-Glauber model calculated with GLISSANDO code [12]. The maximal energy density ϵ_0 is chosen to reproduce the experimental mean charged particle multiplicity, and the initial flow is supposed to be $y_T = \alpha\frac{r_T}{R^2(\phi)}$, with $\alpha = 0.45$ fm for top RHIC energy. Thus, model has only two free parameters ϵ_0 and α. We start hydrodynamics at $\tau_0 = 0.1$ fm/c and work in mid-rapidity region. Sudden switch from hydrodynamics to UrQMD is performed at the isotherm $T = 165$ MeV. The hadron distribution functions (for each hadron sort i) at the switching hypersurface σ_{sw} are calculated according to the Cooper-Frye formula

$$p_0\frac{d^3N_i}{p_T dp_T d\phi_p dy} = \int_{\sigma_{sw}} p^\mu d\sigma_\mu f_i^{eq}(p\cdot u(x), T(x), \mu_i(x)). \tag{7}$$

The source functions $S(\mathbf{r}^*)$ are calculated as

$$S(\mathbf{r}^*) = \frac{\sum_{i\neq j}\delta_\Delta(\mathbf{r}^* - \mathbf{r}_i^* + \mathbf{r}_j^*)}{\sum_{i\neq j} 1}. \tag{8}$$

Here $\mathbf{r}_i^*$ and $\mathbf{r}_j^*$ are the particles space positions, and $\mathbf{r}^*$ is the particle separation in the pair rest frame, $\delta_\Delta(x) = 1$ if $|x| < \Delta p/2$ and 0 otherwise, Δp is the size of the histogram bin.

3 Results and discussion

The $p\Lambda$ source function projections calculated in HKM together with the corresponding Gaussian fits are presented in Fig. 1. Here the out-side-long coordinate system is used, where the *out* axis is directed along the pair total momentum, the *long* direction coincides with the beam axis, and the *side* axis is perpendicular to the latter two ones. One can notice that non-Gaussian power-law tails, observed in pion source function [10], are also present in $p\Lambda$ case. They are partially related with the averaging over a wide p_T interval.

In Fig. 2 we present experimental $p-\Lambda\oplus\bar{p}-\bar{\Lambda}$ and $\bar{p}-\Lambda\oplus p-\bar{\Lambda}$ correlation functions, measured by STAR collaboration in 10% most central Au+Au collisions at top RHIC energy $\sqrt{s_{NN}} = 200$ GeV together with the fits performed within Lednický and Lyuboshitz analytical model.

For baryon-baryon case (Fig. 2, a) the scattering lengths f_0^S and effective radii d_0^S values are taken from [13] ($f_0^s = 2.88$ fm, $f_0^t = 1.66$ fm, $d_0^s = 2.92$ fm, $d_0^t = 3.78$ fm), leaving only one parameter r_0 free in the STAR fit [4] (red curve) and making all the parameters fixed in our own fit (blue curve), where r_0 value is taken from the HKM simulations. One can see that our fitting curve describes the data well. The experimental and HKM source radius values are $r_0^{exp} = 3.09 \pm 0.30^{+0.17}_{-0.25} \pm 0.2$ fm and $r_0^{\mathrm{HKM}} = 3.637 \pm 0.001$ fm respectively.

As for the baryon-antibaryon case (Fig. 2, b), the corresponding scattering lengths were measured in the STAR experiment for the first time, being included into the fit as free parameters. To reduce the number of free parameters both singlet and triplet scattering amplitudes are assumed to be equal, $f^s = f^t = f$ (approximately corresponding to the spin-averaged scattering length), and both effective radii are set to zero $d_0^s = d_0^t = 0$. The scattering length is assumed to have positive imaginary part $\Im f > 0$ describing the contribution of annihilation channels and leading to a wide dip in the correlation function at intermediate k^*-values. Thus, the model has three free parameters $\Re f$, $\Im f$ and r_0 in [4] and two free parameters $\Re f$, $\Im f$ in our fit. The STAR has obtained the following parameter values: $\Re f = -2.03 \pm 0.96^{+1.37}_{-0.12}$ fm, $\Im f = 1.01 \pm 0.92^{+2.43}_{-1.11}$ fm, $r_0 = 1.50 \pm 0.05^{+0.10}_{-0.12} \pm 0.3$ fm (red curve). One can see that experimental $p\bar{\Lambda}$ source radius value is ~ 2 times smaller than the $p\Lambda$ one, although there is no apparent physical reason for such a difference. Both radii can be expected to have similar values, and the HKM source radius for the baryon-antibaryon case $r_0^{\mathrm{HKM}} = 3.621 \pm 0.001$ fm is expectedly close to the corresponding baryon-baryon one. But at this source radius value the fitting curve (blue) is too narrow to describe the data points. Still, we think that the real baryon-antibaryon source size is close to the baryon-baryon one, and the apparent difference between them is caused by some additional effect.

The possible reason for the small fitted baryon-antibaryon source radius could be the influence of residual correlations and imperfection of purity correction. Constructing the experimental correlation function one usually supposes that only the pairs composed of two primary particles are correlated, and the rest of the pairs, which include secondary or misidentified particles, are supposed to be uncorrelated. However, the correlation can exist between two parents of secondary particles or between the parent of secondary particle and the primary

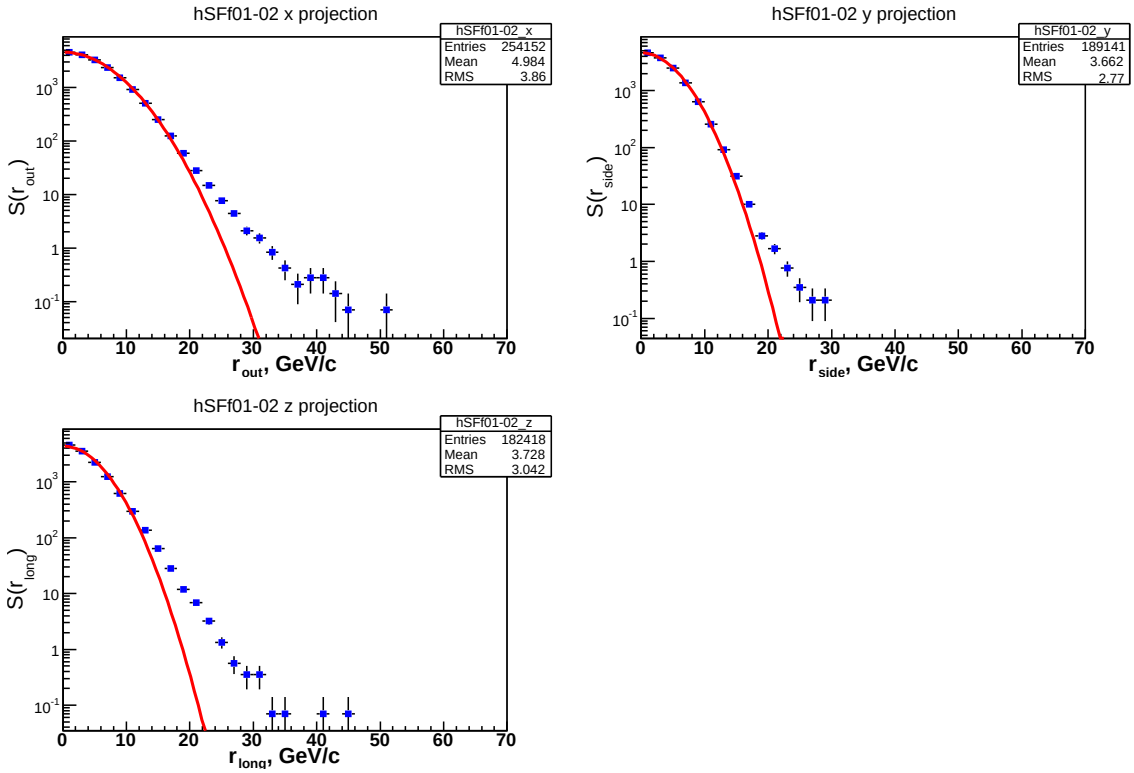

Figure 1. The $p\Lambda$ source function projections calculated in HKM (blue markers) and the Gaussian fits to them (red lines). The simulations correspond to Au+Au collision STAR experiment at RHIC top energy [4], $c = 0 - 10\%$.

one. In case, when the secondary particle carries most of the momentum of its parent, such a particle can be "residually" correlated with another particle (or its daughter), which was correlated with its parent. The interactions in most of such pairs are unknown, so at the moment there is no possibility to reliably refine the constructed experimental correlation function from the effect of residual correlations. However, one can try to account for the residual correlations at least phenomenologically in analytical model used for fitting of the correlation function.

In case when the measured correlation function is not corrected for purity, the fitted uncorrected correlation function is expressed through the true one in (6) similar to (1):

$$C_{uncorr}(k^*) = \lambda C(k^*) + (1 - \lambda), \tag{9}$$

where λ is the pair purity. The first term in this formula corresponds to the pairs of correlated (primary only) particles, and the second one represents the contribution of the uncorrelated pairs, where one or both particles are secondary (or misidentified) ones. Taking into account that the effect of baryon-antibaryon residual correlations is dominated by the effect of annihilation dip in parent correlations and that this dip is essentially widen in residual correlations, it can be effectively described by a factor $(1 - \beta e^{-4k^{*2}R^2})$ multiplying the second term in (9):

$$C(k^*) = \lambda C(k^*) + (1 - \lambda)(1 - \beta e^{-4k^{*2}R^2}), \tag{10}$$

thus introducing two new parameters $\beta > 0$ and $R \ll r_0$.

In Fig. 3 one can see the result of fitting the experimental $\bar{p} - \Lambda \oplus p - \bar{\Lambda}$ correlation function not corrected for purity (the data are taken from [14]) using the analytical expressions (10) and (6). The source radius was fixed at the value obtained from HKM simulations, $r_0^{\rm HKM} = 3.621 \pm 0.001$ fm, and five parameters, λ, $\Re f$, $\Im f$, β, and R were left to vary freely. The extracted parameter values are the following: $\lambda = 0.23 \pm 0.17$, $\Re f = 0.41 \pm 1.05$ fm, $\Im f = 1.50 \pm 1.93$ fm, $\beta = 0.035 \pm 0.004$, and $R = 0.49 \pm 0.05$ fm. The obtained fitting curve describes the data quite well, and the extracted spin-averaged scattering length qualitatively agrees with the one obtained in [4].

Acknowledgements. The research was carried out within the scope of the EUREA: European Ultra Relativistic Energies Agreement (European Research Group: "Heavy ions at ultrarelativistic energies") and is supported by the National Academy of Sciences of Ukraine (Agreement F4-2013) and by the State Fund for Fundamental Researches of Ukraine (Agreement F33/24-2013).

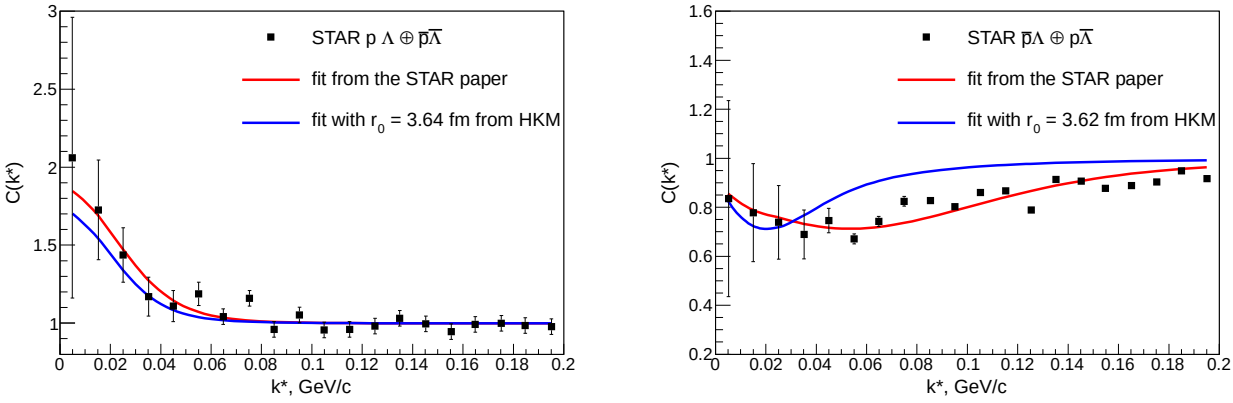

a b

Figure 2. a) The $p-\Lambda\oplus\bar{p}-\bar{\Lambda}$ correlation function measured by STAR (black markers), the corresponding fit from the STAR paper [4] within the Lednický and Lyuboshitz analytical model [1] (red line) and our fit within the same model with the source radius r_0 extracted from the HKM calculations (blue line); b) The same as in a) for the $\bar{p}-\Lambda\oplus p-\bar{\Lambda}$ correlation function.

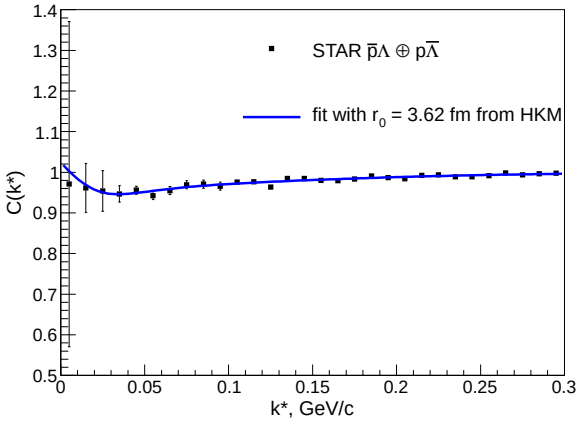

Figure 3. The purity uncorrected $\bar{p}-\Lambda\oplus p-\bar{\Lambda}$ correlation function measured by STAR [14] (black markers) and our fit according to (10) and (6) (blue line), with the account for the residual correlations. The source radius r_0 was fixed at a value extracted from the HKM calculations.

References

[1] R. Lednický, V. L. Lyuboshitz, Yad. Fiz. **35**, 1316 (1982); Proc. CORINNE 90, Nantes, France, 1990 (ed. D. Ardouin, World Sci., 1990) p. 42.
[2] L. Nemenov, Yad. Fiz. **41**, 980 (1985); V.L. Lyuboshitz, Yad. Fiz. **48**, 1501 (1988) (Sov. J. Nucl. Phys. **48**, 956 (1988)).
[3] Yu.M. Sinyukov, R. Lednický, S.V. Akkelin, J. Pluta, and B. Erazmus, Phys. Lett. B **432**, 248 (1998).
[4] J. Adams *et. al.* (STAR), Phys. Rev. C, **74**, 064906 (2006).
[5] Yu.M. Sinyukov, S.V. Akkelin, and Y. Hama, Phys. Rev. Lett. **89**, 052301 (2002).
[6] S.V. Akkelin, Y. Hama, Iu.A. Karpenko, Yu.M. Sinyukov. Phys. Rev. C **78**, 034906, (2008).
[7] Iu.A. Karpenko, Yu.M. Sinyukov. Phys. Rev. C **81** 054903, (2010).
[8] Iu.A. Karpenko, Yu.M. Sinyukov, K. Werner. Phys. Rev. C **87**, 024914, (2013), arXiv:1204.5351v2 [nucl-th].
[9] V.M. Shapoval, Yu.M. Sinyukov, and Iu.A. Karpenko, arXiv:1308.6272.
[10] S. Afanasiev et al. PHENIX Collaboration, Phys. Rev. Lett. **100**, 232301 (2008).
[11] M. Laine, Y. Schröder, Phys. Rev. D **73**, 085009 (2006).
[12] W. Broniowski, M. Rybczynski, P. Bozek, Comput. Phys. Commun. **180**, 69 (2009).
[13] F. Wang and S. Pratt, Phys. Rev. Lett. 83, 3138 (1999).
[14] G. Renault for the STAR Collaboration, Acta Phys. Hung. A**24**, 131 (2005).

Proceedings of the International School-seminar
"New Physics and Quantum Chromodynamics at External Conditions", pp. 120 – 123,
May 22-24, 2013, Dnipropetrovsk, Ukraine

ESTIMATES FOR THE ABELIAN Z' COUPLINGS FROM THE LHC DATA

A. V. Gulov[a], A. A. Kozhushko[b]

Dnipropetrovsk National University, Dnipropetrovsk, Ukraine

We investigate the Drell-Yan process with the intermediate heavy Z' boson. We use a general approach to the Abelian Z' with the renormalization-group relations between the Z' couplings in order to reduce the number of unknown Z' parameters. In a proposed estimation strategy we derive the LHC-driven constraints for the Z' couplings to lepton and quark vector currents. To do this, we calculate the Z'-related contribution in the narrow-width approximation and compare the obtained values to the experimental data presented by the ATLAS collaboration. Our method allows to estimate the values of Z' couplings to the u and d quarks and to final-state leptons.

1 Introduction

Searching for new particles beyond the Standard Model (SM) is an important part of experiments at the LHC. Among the scenarios of new physics a heavy neutral vector boson (Z' boson) is one of the most promising intermediate states to be detected in hadron scattering processes in the annihilation channel. This particle resides in popular grand unification theories (GUTs) and other models with extended gauge sector (see Refs. [1–3] for review). Considering a couple of Z' models, current experiments constrain its mass to be no less than 2-3 TeV [4, 5].

In general, to accurately describe the Z' contribution to the Drell-Yan process, we have to consider scattering amplitudes with intermediate virtual states. This allows to derive few-parametric observables suitable for data fitting [6, 7]. But if the resonance is estimated to be narrow, then one can describe it in a more simple way by a small number of Z' production and decay characteristics. the Z' mass, the production cross-section, and the total and partial decay widths. Being quite simple, such a scheme at the same time could give estimations of Z' couplings to the SM fields based on the current experimental data.

It is possible to calculate effects of Z' boson in details for each specific GUT model. Such model-dependent estimates are widely presented in the literature [8, 9]. Some set of popular E_6-based models and left-right models is usually considered in this approach. However, probing the set one can still miss the actual Z' model. Therefore, it is useful to complement the model-dependent Z' searches by some kind of model-independent analysis.

Lots of the usually considered models belong to the models with the so-called Abelian Z' boson. The Abelian Z' is usually understood as an effective additional $U(1)$ gauge state at energies of order of several TeVs, which obtains its heavy mass beyond the scope of the SM. Such kind of Z' boson is characterized by specific relations between its couplings to SM particles. The relations were derived in Refs. [10, 11].

In our present investigation we use the relations for the Abelian Z' couplings to estimate the Abelian Z' production in the Drell-Yan process. We compare the obtained cross section to the current LHC bounds. This allows us to constrain Z' couplings. It also shows how far the LHC will potentially advance the Z' searches compared to the LEP.

2 Z' parameterization

In the present paper we use the following effective Lagrangian to describe Z' couplings to the axial-vector and vector fermion currents:

$$\begin{aligned}\mathcal{L}_{Z\bar{f}f} &= \frac{1}{2} Z_\mu \bar{f}\gamma^\mu \left[(v_{fZ}^{\mathrm{SM}} + \gamma^5 a_{fZ}^{\mathrm{SM}})\cos\theta_0 + (v_f + \gamma^5 a_f)\sin\theta_0\right] f, \\ \mathcal{L}_{Z'\bar{f}f} &= \frac{1}{2} Z'_\mu \bar{f}\gamma^\mu \left[(v_f + \gamma^5 a_f)\cos\theta_0 - (v_{fZ}^{\mathrm{SM}} + \gamma^5 a_{fZ}^{\mathrm{SM}})\sin\theta_0\right] f, \end{aligned} \quad (1)$$

where f is an arbitrary SM fermion state; a_f and v_f are the Z' couplings to the axial-vector and vector fermion currents; θ_0 is the Z–Z' mixing angle; v_{fZ}^{SM}, a_{fZ}^{SM} are the SM couplings of the Z-boson. The commonly considered Z' gauge coupling $\tilde{g}$ is included into a_f and v_f.

e-mail: [a]alexey.gulov@gmail.com, [b]a.kozhushko@yandex.ru

This popular parameterization follows from a number of natural conditions. First of all, the Z' interactions of renormalizable types are expected to be dominant. Also, the SM gauge group $\mathrm{SU}(2)_L \times \mathrm{U}(1)_Y$ is considered as a subgroup of the GUT group. In this case, a product of the SM subgroup generators is a linear combination of these generators. Consequently, all the structure constants that connect the two SM gauge bosons with Z' have to be zero, and at the tree-level Z' interactions to the SM gauge fields are possible due to a Z–Z' mixing only.

To calculate the Z' contribution to the Drell-Yan process, we also need to parameterize the Z' interactions with the SM scalar and vector fields. The explicit Lagrangian describing Z' couplings to all the SM fields can be found in Ref. [12].

The parameters a_f, v_f, and θ_0 could be obtained from experimental data. If the model is unknown, all of them are potentially arbitrary numbers. If one assumes that the underlying extended model is renormalizable, then, as was shown in Refs. [10, 11], there is a relation between these parameters:

$$v_f - a_f = v_{f^*} - a_{f^*}, \qquad a_f = T_{3f}\tilde{g}\tilde{Y}_\phi. \tag{2}$$

Here, f and f^* are the components of the $SU(2)_L$ fermion doublet ($l^* = \nu_l, \nu^* = l, q_u^* = q_d$, and $q_d^* = q_u$), T_{3f} is the third component of weak isospin, and $\tilde{g}\tilde{Y}_\phi$ determines Z' couplings to the SM scalar fields and the Z–Z' mixing angle θ_0 in (1) (see Ref. [12] for details).

Let us note that the couplings of the Abelian Z' to the axial-vector fermion currents are described by a universal absolute value. Therefore we introduce the notation

$$a = a_d = a_{e^-} = -a_u = -a_\nu, \quad v_{f_d} = v_{f_u} + 2a. \tag{3}$$

In total, the Z' interactions with the SM particles can be parameterized by seven independent couplings: a, v_u, v_c, v_t, v_e, v_μ, v_τ. From Eq. (2) it follows, that this value a is proportional to the Z' coupling to scalar fields. The Z–Z' mixing angle θ_0 is also determined by the axial-vector coupling:

$$\theta_0 \approx -2a\frac{\sin\theta_W \cos\theta_W}{\sqrt{4\pi\alpha_{\mathrm{em}}}}\frac{m_Z^2}{m_{Z'}^2}. \tag{4}$$

For further calculations we use $\alpha_{\mathrm{em}} = 1/128.9$, $\sin^2\theta_W = 0.2304$.

In Ref. [13] the limits on Z' couplings from the LEP I and LEP II data were obtained. One can interpret those limits as some hints of Z' boson at 1-2σ CL. Namely, the couplings a and v_e show non-zero maximum-likelihood (ML) values. In our estimates we use the value

$$a_{\mathrm{ML}}^2/m_{Z'}^2 = 1.97 \times 10^{-2}\ \mathrm{TeV}^{-2}. \tag{5}$$

The electron vector coupling v_e is constrained at 95% CL:

$$6.07 \times 10^{-2}\ \mathrm{TeV}^{-2} < v_e^2/m_{Z'}^2 < 2.56 \times 10^{-1}\ \mathrm{TeV}^{-2}. \tag{6}$$

These constraints seem to be less stable, so we will use them only to compare our final results avoiding taking them into account in calculations.

There are no significant constraints on the other Z' coupling constants from the existing data.

3 Z' production at the LHC

At the LHC Z' bosons are expected to be produced in proton-proton collisions: $pp \to Z'$. At the parton level this process is described by the Z' production in the quark-antiquark pair annihilation, $q\bar{q} \to Z'$. The cross-section of the $pp \to Z'$ process is obtained by integrating the partonic cross-section $\sigma_{q\bar{q}\to Z'}$ with the parton distribution functions (PDFs):

$$\sigma_{AB} = \sum_{q,\bar{q}} \int_0^1 dx_q \int_0^1 dx_{\bar{q}}\, f_{q,A}(x_q, \mu_R, \mu_F) f_{\bar{q},B}(x_{\bar{q}}, \mu_R, \mu_F) \times \sigma_{q\bar{q}\to Z'}(m_{Z'}, x_q k_A, x_{\bar{q}} k_B), \tag{7}$$

where A, B mark the interacting hadrons (protons in our case) with the four-momenta k_A, k_B; $f_{q,A}$ is the parton distribution function for the parton q in the hadron A with the momentum fraction x_q at the renormalization scale μ_R and factorization scale μ_F. We use the parton distribution functions provided by the MSTW PDF package [14].

The production cross-section includes quadratic combinations of the Z' couplings to quarks,

$$\sigma_{AB} = a^2\sigma_{a^2} + av_u\sigma_{av_u} + v_u^2\sigma_{v_u^2} + av_c\sigma_{av_c} + v_c^2\sigma_{v_c^2} + av_t\sigma_{av_t} + v_t^2\sigma_{v_t^2}. \tag{8}$$

Here we took into account relations (3). The factors σ on the right side of the previous equation depend on $m_{Z'}$ and the beam energy. At energies above 2 TeV the factors σ_{av_c}, $\sigma_{v_c^2}$, σ_{av_t}, and $\sigma_{v_t^2}$ amount to less than 1% of each of the factors σ_{a^2}, σ_{av_u}, and $\sigma_{v_u^2}$, and therefore we neglect their contributions.

We take into account the 90% CL uncertainty intervals for the parton distributions provided in the MSTW PDF package, and also the uncertainties that arise from the renormalization and factorization scales variation: $\mu_R = \mu_F = \mu$, $m_{Z'}/2 \le \mu \le 2m_{Z'}$.

Both the Z' production cross section and the uncertainties are calculated in the leading order in α_S. The next-to-next-to-leading order cross section together with the corresponding uncertainties is obtained using the NNLO K-factor for the Drell-Yan process calculated in the Standard model. It is calculated using the FEWZ software [15]. The K-factor increases monotonically from 1.28 ± 0.08 to 1.30 ± 0.06, as $m_{Z'}$ varies from 2 TeV to 3 TeV.

Finally, the production cross-section reads:

$$\begin{aligned} \sigma_{pp\to Z'} &= a^2\sigma_{a^2} + av_u\sigma_{av_u} + v_u^2\sigma_{v_u^2} \pm \Delta\sigma^{\text{pdf+scale}}, \\ \Delta\sigma^{\text{pdf+scale}} &= a^2\Delta\sigma_{a^2}^{\text{pdf+scale}} + av_u\Delta\sigma_{av_u}^{\text{pdf+scale}} + v_u^2\Delta\sigma_{v_u^2}^{\text{pdf+scale}}. \end{aligned} \quad (9)$$

The Z' decay width $\Gamma_{Z'}$ is calculated using the optical theorem at the one-loop level.

4 Estimation Scheme

The main Z' decay channels considered by ATLAS and CMS are dielectronic and dimuonic channels. The couplings that enter the corresponding cross sections are a, v_u, and v_e for the $pp \to Z' \to e^+e^-$ case and a, v_u, and v_μ for the $pp \to Z' \to \mu^+\mu^-$ case. Since v_μ was not constrained by the LEP data, we are going to study only the dielectron final state. This allows us to estimate how the LHC data limits the Z' couplings compared to the LEP results.

Let us present our estimation scheme. Since there is a maximum-likelihood value for a^2 from LEP, $a^2_{\text{ML}}/m^2_{Z'} = 1.97 \times 10^{-2}$ TeV^{-2}, we can consider it as our "optimistic" estimate. There is a "pessimistic" estimate with $a^2 = 0$ for weakly-coupled Z'. To obtain a kind of an arbitrary estimate, we also consider $a^2 = a^2_{\text{ML}}/4$. Replacing the axial-vector coupling by these three estimates in the $pp \to Z' \to e^+e^-$ cross section, we can investigate possible v_e and v_u values taking onto account the LHC results on direct searches for Z' resonances [4, 5].

We investigate how the currently available LHC data constrains the values of v_e and v_u. Both the ATLAS [4] and CMS [5] results indicate that the lower bounds for the Z' mass lie between 2 TeV and 3 TeV. Therefore, we shall derive our constraints for those two values.

We compare this cross section to the experimental upper bounds presented in Refs. [4] and [5] for pp collisions at $\sqrt{S} = 8$ TeV. At the considered Z' mass values it is always possible to choose such v_f ($f \neq e^-, u$) values, that correspond to the upper bound of the Z' decay width $\Gamma^2_{Z'}/m^2_{Z'} \le 0.01$. Therefore, both for $m_{Z'} = 2$ TeV and $m_{Z'} = 3$ TeV we set $\Gamma_{Z'}$ to 0.1 $m_{Z'}$. This will allow us to obtain widest possible intervals for v_e and v_u.

5 Results and Discussion

The constraints are shown in Fig. 1 on the v_u-vs-v_e planes. We present the areas of v_u and v_e values for which the NWA is applicable. For the "optimistic" estimation we use two possible values for the axial-vector coupling: $a/m_{Z'} \simeq \pm 0.14$ TeV^{-1}. Also the LEP bounds for v_e are shown for comparison.

The ATLAS collaboration [4] reports upper bounds for $\sigma_{pp\to Z'\to e^+e^-}$ at 1.5×10^{-3} pb for $m_{Z'} = 2$ TeV and 2.5×10^{-3} pb for $m_{Z'} = 3$ TeV. The "optimistic" estimation for σ_{NWA} lies higher than these values, therefore, the LEP maximum-likelihood value $a^2_{\text{ML}}/m^2_{Z'} = 1.97 \times 10^{-2}$ TeV^{-2} is discouraged by the LHC results for $m_{Z'}$ from 2 TeV to 3 TeV. The LEP maximum-likelihood value is consistent with the LHC results for Z' masses below 700 GeV. The region for the "pessimistic" and "intermediate" estimations overlaps with the LHC values, therefore allowing for non-zero upper bounds for the vector couplings. The regions of those are also plotted in Fig. 1. This indicates that the maximum-likelihood LEP value a^2_{ML} is disfavored approximately by one order of magnitude.

Alsowe can see that the LHC may limit the vector couplings to $v_u^2/m^2_{Z'} \le 10^{-2}..10^{-3}$ TeV^{-2}, $v_e^2/m^2_{Z'} \le 10^{-1}..10^{-2}$ TeV^{-2}. It is interesting to calculate the Z–Z' mixing angle value based on our estimations. Current LEP-driven upper limits for θ_0 in different Z' models are of order of 10^{-3} (see Table IV in Ref. [2]). For our "optimistic" estimate Eq. (4) gives 1.6×10^{-3} for the θ_0 value considering $m_{Z'} = 2$ TeV. As it was noted, this value is all but ruled out by the LHC data, so for Ableian Z' models one may expect θ_0 less than (a few)$\times 10^{-4}$.

To obtain more strict bounds, one has to take into account the contributions from the remaining fermions and consider the differential cross-section, rather than working in the narrow-width approximation. Nevertheless, the two presented estimates, being rough, still allow to see, how far it is possible to advance both the direct and indirect Z' searches compared to the LEP results.

This research is presented in more details in Ref. [16].

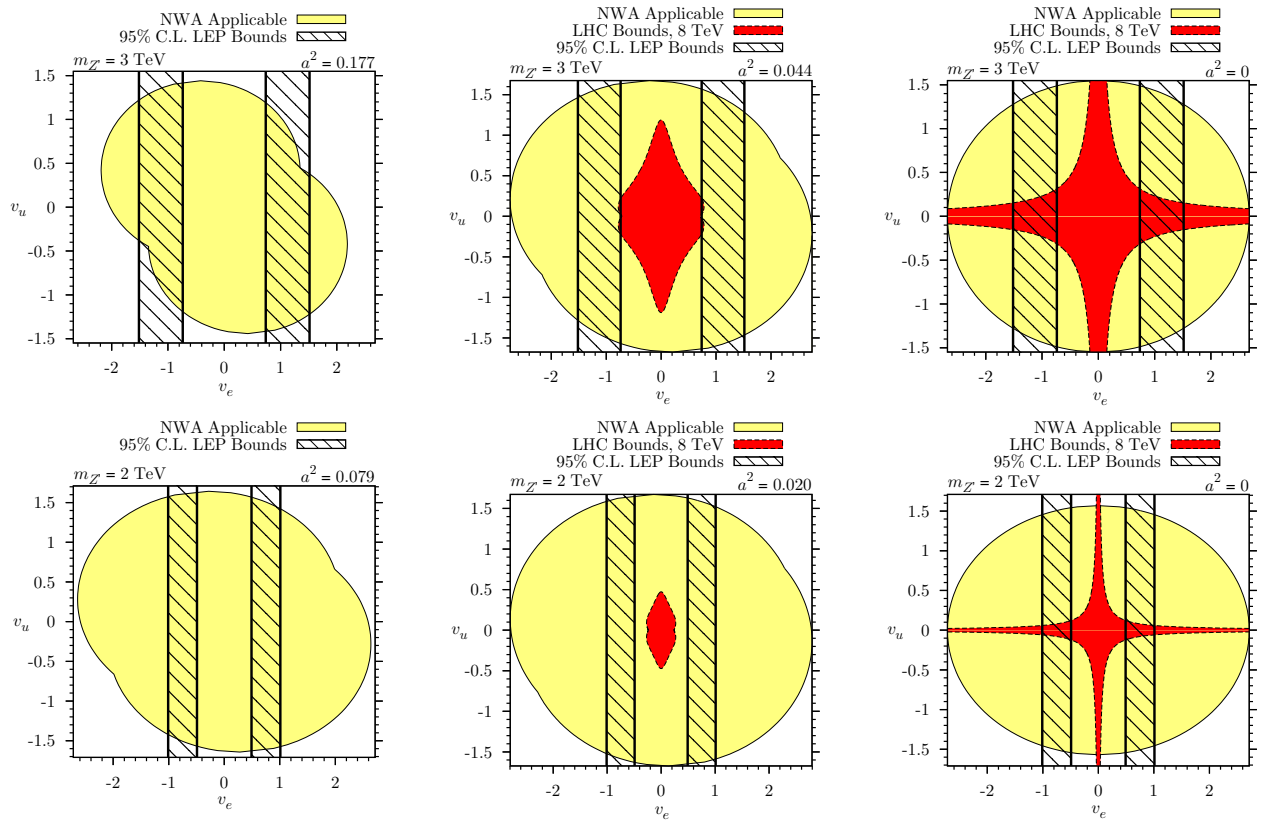

Figure 1. The v_u-vs-v_e planes. First row: $m_{Z'} = 3$ TeV; second row : $m_{Z'} = 2$ TeV. The upper row is for the "optimistic" estimation scheme, the middle row is for the intermediate estimation, and on the plots of the last row the "pessimistic" scheme is presented. The light-gray (yellow) areas represent the coupling values for which the narrow-width approximation is applicable (i.e. $\Gamma_{Z'}/m_{Z'} \leq 0.1$). The hatched areas are for the 95% CL bounds on the v_e coupling (from LEP II data). The dark-gray (red) area represents the v_u and v_e values allowed by the LHC.

References

[1] A. Leike, *Phys. Rep.* **317**, 143 (1999).

[2] P. Langacker, *Rev. Mod. Phys.* **81**, 1199-1228 (2008).

[3] T. Rizzo, e-print hep-ph/0610104.

[4] N. Hod, on behalf of the ATLAS collaboration, e-print arXiv:1303.4287 [hep-ex].

[5] CMS Collaboration, *Phys. Lett. B* **720**, 63 (2013) e-print arXiv:1212.6175 [hep-ex].

[6] P. Osland, A. A. Pankov, N. Paver and A. V. Tsytrinov *Phys. Rev. D* **79**, 115021 (2009).

[7] A. Gulov and A. Kozhushko, e-print arXiv:1209.5022 [hep-ph].

[8] J. Erler, P. Langacker, S. Munir and E. R. Pena, *JHEP* **08**, 017 (2009).

[9] V. V. Andreev and A. A. Pankov, *Phys. Atom. Nucl.* **76**, 753-765 (2013).

[10] A. V. Gulov and V. V. Skalozub, *Eur. Phys. J. C* **17**, 685 (2000).

[11] A. V. Gulov and V. V. Skalozub, *Phys. Rev. D* **61**, 055007 (2000).

[12] A. V. Gulov and A. A. Kozhushko, *Int. J. Mod. Phys. A* **26**, 4083-4100 (2011).

[13] A. V. Gulov and V. V. Skalozub, *Int. J. Mod. Phys. A* **25**, 5787-5815 (2010).

[14] A.D. Martin, W.J. Stirling, R.S. Thorne and G. Watt, *Eur. Phys. J. C* **63**, 189 (2009).

[15] R. Gavin, Y. Li, F. Petriello and S. Quackenbush, *Comput. Phys. Commun.* **182**, 2388-2403 (2011)

[16] A. Gulov and A. Kozhushko, e-print arXiv:1307.2393 [hep-ph].

Proceedings of the International School-seminar
"New Physics and Quantum Chromodynamics at External Conditions", pp. 124 – 126,
May 22-24, 2013, Dnipropetrovsk, Ukraine

TUNNELING OF A WAVE-PACKAGE THROUGH A QUANTUM DIODE

V. V. Skalozub[a], N. A. Ivanov[b]

Dnipropetrovsk National University, Dnipropetrovsk, Ukraine

The modified saddle-point method is applied to describing the tunneling of wave packages through quantum diodes. The S-matrix for a diode structure consisting of the perturbed potential is calculated. The case of a Gaussian incident pulse is considered in detail. The time delay and amplitude of the outgoing wave package are calculated. The dependence of the time delay of the incident pulse momentum and the internal quantum diode characteristics is illustrated.

1 Introduction

Wave package tunneling through an opened quantum system with resonance levels [1, 2] is one of the long-standing problems of nanophysics. It has been already investigated in both analytic and numeric approaches (see, for instance, [3–5] and references therein). The necessity of taking into account numerous proper parameters of the incident pulses and quantum systems simultaneously is the main difficulty here. So, in most studies, various possible cases (wide or narrow resonance levels, wave pulses of different kinds, etc.) were investigated separately. In the series of papers [6–8] a modified quasi-classical method providing a possibility to investigate a general case analytically has been developed. The approach is based on two main ideas: measuring a quantum system in terms of the incident pulse size and using the modified saddle-point method. The quantum systems were described in the S-matrix formalism. These utilities allow, in particular, to introduce dimensionless variables corresponding to arbitrary quantum systems and wave packages. The S-matrix formalism is commonly used in the scattering theory for describing the connection between final states appearing after interaction and states before it. For S-matrix calculation the perturbation theory or methods based on analyticity of matrix elements are usually used. The S-matrix poles are of great importance in tunneling phenomena. They determine the existence of resonance levels in scattering systems. Thus, if the S-matrix of quantum system and the parameters of incident wave pulse are known, it is possible to investigate the tunneling process in all details. For calculating the S-matrix elements, a method based on the solutions of the Lippman-Shwinger equation for a given scattering potential has been developed [9,10]. By splitting the potential into an unperturbed part and a perturbation and finding the Green functions for the first one, it is possible to determine a solution for the case when the complete potential is taken into account. At the next step, one can calculate the R-matrix and find the values of the S-matrix elements using the relation between R- and S- matrixes. This approach is completely formalized and allows to determine an S-matrix for arbitrary potentials of interest. Below we apply this method for calculating the S-matrix for a diode of a special type used in real devices and for determining a time delay for incident Gaussian pulses. Time delays for pulses of other types can be expressed in terms of results obtained for the case under consideration [7]. The existence of potential wells with discreet energy levels is a common feature of quantum dots, double-well diodes, quantum tunneling transistors. Hence, resonance conductivities of these systems are supposed. The time delay determination (for pulse tunneling) in systems of such type is a very important problem [5, 11, 12]. Particularly its solution allows to find out the parameters of either the pulse or the quantum system for which the rate of tunneling becomes maximal. It also gives an opportunity for miniaturization and the increase of productivity of microcircuits with quantum elements.

2 Tunneling through the quantum diode

Let us use the developed approach to calculate an S-matrix for the structure shown in Fig.1. Using the matching conditions, we obtain from it the amplitudes for all the states (we do not include this equation in the main text because it can easily be obtained by using various mathematical packets). The scattering state wave-functions, Green functions and eigenstates matrix for this case are presented in Appendix A. Substituting this equation into solutions to the Lippman-Shwinger equation we find transmission and reflection amplitudes for the perturbed potential. The difference between the wave function of the initial state and the wave function after interaction is expressed in the occurrence of supplementary components. Such components are associated with the existence of the perturbed potential $\Delta V_1(z)$ in the $(z_1; z_4)$ interval and perturbed potential $\Delta V_2(z)$ in

e-mail: [a]skalozubv@daad-alumni.de, [b]na_ivanov@dsu.dp.ua

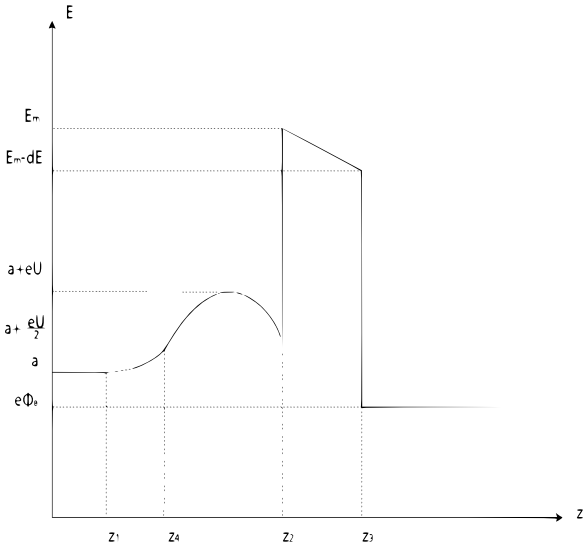

Figure 1. Potential energy of diode

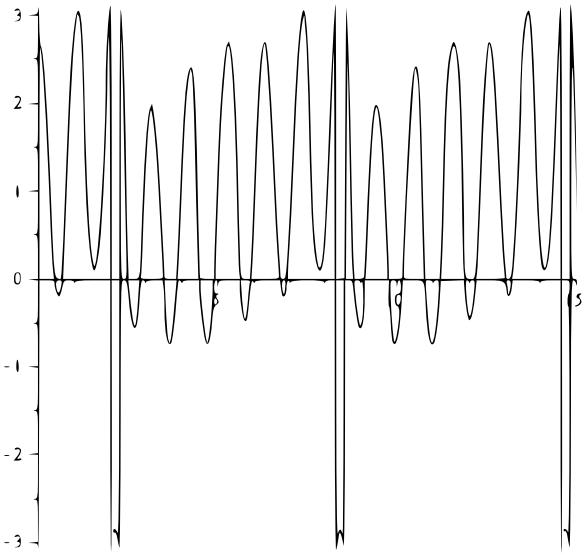

Figure 2. Wave function amplitude for incident pulse momentum having $\Gamma = 1$ and $k_1 = 1; k_2 = 1; k_3 = 2; k_4 = 5; k_5 = 1$

the $(z_4; z_2)$ interval etc. After founding the wave functions for each interval, we can build the eigenstate matrix Ψ. Then we determining the R-matrix,

$$R = \hat{\Psi}' * \hat{\Psi}^{-1}. \tag{1}$$

After that we can obtain the corresponding S-matrix. Now, we apply the above results to investigate the tunneling of the Gaussian wave packet through this diode. The packet is described as

$$\Psi(x) = exp(-\frac{1}{2}a^2(k-k_0)^2), \tag{2}$$

where a is a packet width. We use the known Fourier transform for this function and the following parameterizations

$$q' = \frac{x}{a};\ \tau = \frac{t}{t_a};\ S = a(k-k_0);\ l_j = ak_j;\ \rho_j = a\frac{\Gamma_j}{2};\ l_0 = ak_0. \tag{3}$$

Applying the matching conditions, we find the saddle points. For outgoing wave packet, considering these saddle points, we get the superposition of each result. Then after integration we obtain the outgoing wave function. Now, we find the argument of outgoing wave-package Fig.2. The wave function of the outgoing pulse differs from the incident wave packet by some phase factor. This factor depends on the kinetic energy of the incident pulse, the potential energy of the barrier and time delay. Time delay can be calculated from the equation (see, for instance, [5]),

$$\triangle t = \frac{dArg(\Psi)}{dE}. \tag{4}$$

Hence the advantage of the analytic methods is obvious. Dependencies of the wave function argument and the time delay on the incident pulse momentum are illustrated in Figs. 2-4. We do not include any obviously equation (but it can be simply found by using known mathematical packages). As one can see from Figs. 3-4, for some values of the incident pulse momentum the time delay minimum is observed.This means that wave packet is tunneling the system with a maximal velocity. When the momentum becomes large enough, the time delay takes a definite value which is not changing with the momentum increasing.

3 Results and discussion

In the present paper, we applied a new approach to investigate time-delay for a quantum diode. The wave package tunneling through the realistic used in practice quantum diode is investigated. At first, we found the S-matrix for this structure. We split the potential of the diode in perturbed and unperturbed parts. For the latter one, we found the solutions of the Schrödinger equation and Green's functions. After that, using the Lippman-Shwinger equation, we extended the solution to account for the perturbed part. In this way we calculated the transmission and reflection coefficients. Using these coefficients, we derived the diode S-matrix. It gives a possibility for investigation of the tunneling process. For such type signal the amplitude of the outgoing package is determine. The time delay dependence on the resonance level width, incident pulse momentum

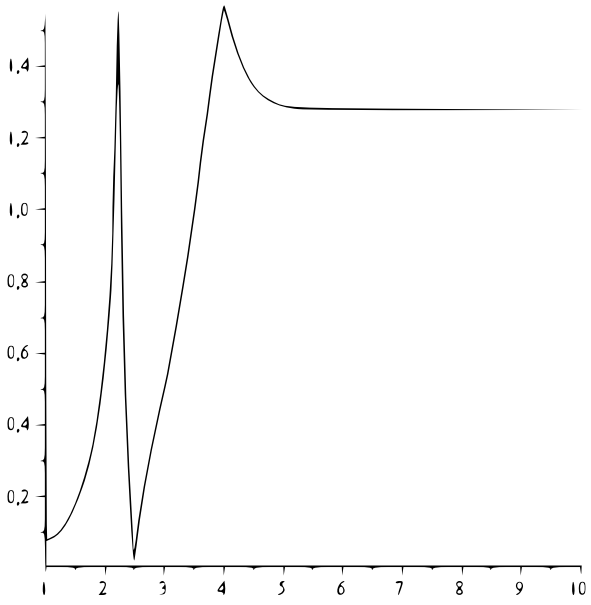

Figure 3. Time delay for incident pulse momentum having $\Gamma = 1$ and $k_1 = 1; k_2 = 1; k_3 = 2; k_4 = 5; k_5 = 1$

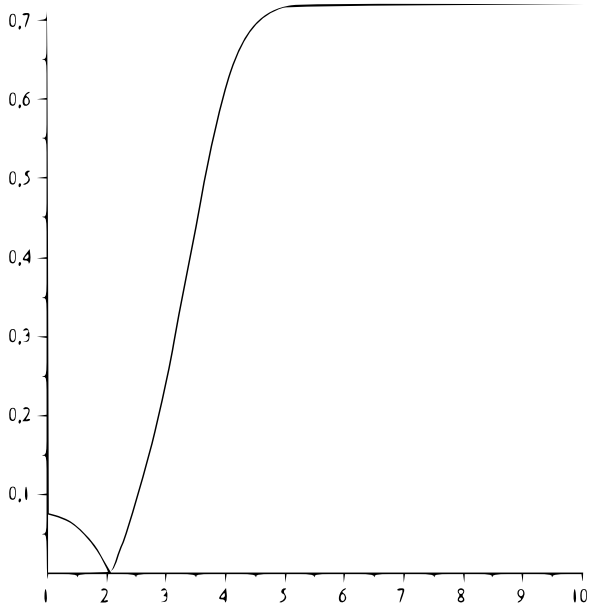

Figure 4. Time delay for incident pulse momentum having $\Gamma = 1$ and $k_1 = 1; k_2 = 3; k_3 = 4; k_4 = 4; k_5 = 1$

and internal diode characteristic is determined and shown in plots. Using the results for the Gaussian packet, one can calculate a time delay for different type signal [7] tunneling through the considered diode. It was shown, in particular, that for some specific values of the system and the pulse parameters the full internal scattering is realized. This means that an outgoing pulse is absent, tunneling does not happen. The observed dependence on the parameters exhibits specific interesting behavior that can obtain applications in practice. As it was noted in Introduction, the problem on the resonant transmission of the general type pulses through quantum systems were not investigated analytically already. The obtained results can find different applications in microelectronics. In particular, due to explicit expressions and their simplicity, it is possible to work out a general mathematical packet allowing to calculate automatically all the parameters of the transmitted pulse for various quantum systems and pulses of interest. Other obvious application is an extension of the approach developed to the case of electromagnetic wave packets and classical resonance systems. These problems we left for the future.

References

[1] W. G. van der Wiel, S. De Franceschi, J. M. Elzerman, T. Fujisawa, S. Tarucha, and L. P. Kouwenhoven, Rev. Mod. Phys. 75 (2002) 17-23.
[2] A. D. Stone and P. A. Lee, Phys. Rev. Lett. 54 (1985) 1196.
[3] Z. T. Jiang and Q. F. Sun, J. Phys. Condens. Matter 19 (2007) 156213.
[4] E.U. Condon, P.M. Morse, Rev. Mod. Phys. 3 (1931) 43-88.
[5] M. Razavy, Quantum Theory of Tunneling, World Scientific, 2003, pp. 351-375.
[6] U.Wulf, V.V.Skalozub and A.Zaharov, Phys.Rev. B.77 (2004) 045318.
[7] N.A.Ivanov, V.V.Skalozub. Propagation of wave packets through resonant quantum systems, Theoretical and mathematical physics, 168 (2011) 1096-1104.
[8] N.A.Ivanov, V.V.Skalozub. Transmission of wave packets through open mesoscopic systems, Problems of Atomic Science and Technology 1 (2012) 292-295.
[9] V. de Alfaro, T.Regge, Potential scattering, University of Turin,Italy, 1965.
[10] P.N. Racec, Ph.D. Thesis, University of Technology Cottbus, 2002.
[11] L. Brillouin, Wave propagation and Group Velocity, Academic Press, New York, 1960.
[12] A.O.Barut, The Theory of the Scattering Matrix, Macmillan, New York, 1967.

Proceedings of the International School-seminar
"New Physics and Quantum Chromodynamics at External Conditions", pp. 127 – 130,
May 22-24, 2013, Dnipropetrovsk, Ukraine

TO KINETICS OF PHOTONS IN EQUILIBRIUM MEDIUM

G.G. Orlovsky[a], A.O. Pevzner[b], A.I. Sokolovsky[c]

Dnipropetrovsk National University, Dnipropetrovsk, Ukraine

The kinetics of photons in equilibrium plasma medium is investigated. For weakly nonuniform states of the photon system kinetic equation for the distribution of photons over energies was obtained. This equation describes the diffusion of photons similar to the known diffusion equation for neutrons in a medium. Some corrections to results obtained by Kompaneets are proposed.

1 Introduction

The study of the kinetics of electromagnetic field in a medium is an actual problem. It has several areas of focus. A number of fundamental problems of the quantum theory of the electromagnetic field continues to be discussed actively. See review [1], which describes the development of the ideas of Landau and Peierls devoted the quantum mechanics of the photon. An important direction of the studies is the radiative transfer theory, in which the problem of the problems of choice of parameters describing the radiation and of consistent accounting characteristics of medium continues to be discussed [2]. Many problems of the electromagnetic field kinetics are considered in quantum optics, which reveal the complexity of the quantum electromagnetic field even at low energies [3].

It is important to conduct mentioned studies in terms of the modern theory of nonequilibrium processes and, in particular, on the basis of the Bogolyubov reduced description of nonequilibrium states (see an overview of the method in [4]). In this direction the work by Akhiezer and Peletminsky [5] stands out, in which the transport equation for photons in equilibrium medium, taking into account the bremsstrahlung, is derived. Also Kompaneets work [6] deserves attention, in which the transport equation for photons in a medium, taking into account the Compton scattering, is discussed.

In this paper, the reduced description of the kinetics of the photon gas in equilibrium plasma is investigated taking into account the Compton scattering and assuming that evolution of the system connected with the bremsstrahlung has been finished.

2 Basic equations of the theory

We assume that bremsstrahlung processes are over, and the system evolution is completely determined by the Compton scattering of photons by electrons of equilibrium rarefied plasma medium. Ion dynamics is neglected. The kinetic equation for the distribution of photons $\mathrm{f}_p(x,t)$ in the medium has the Boltzmann form

$$\frac{\partial \mathrm{f}_p(x,t)}{\partial t} = -c\frac{p_l}{p}\frac{\partial \mathrm{f}_p(x,t)}{\partial x_l} + I_p(\mathrm{f}(x,t)) \tag{1}$$

with the collision integral

$$I_p(\mathrm{f}) = \int d^3p_1 d^3p'_1 d^3p' W(p,p_1;p',p'_1)\left\{\mathrm{f}_{p'}(1+\mathrm{f}_p)w_{p'_1} - \mathrm{f}_p(1+\mathrm{f}_{p'})w_{p_1}\right\}\times$$

$$\times\delta(p+p_1-p'-p'_1)\delta(\varepsilon_p+E_{p_1}-\varepsilon_{p'}-E_{p'_1}) \tag{2}$$

($E_p = p^2/2m$, $\varepsilon_p \equiv cp$ are the energies of the electron and photon). Polarization phenomena are neglected, it is assumed that the distribution function of photons does not depend on polarization indexes and is normalized by the condition

$$\frac{2}{h^3}\int d^3p \mathrm{f}_p(x,t) = n_{ph}(x,t), \tag{3}$$

where $n_{ph}(x,t)$ is the total number density of the photons. Similarly, we assume that the equilibrium distribution function of electrons does not depend on the spin indexes and is given by a Maxwell distribution

$$w_p = \frac{nh^3}{2(2\pi mT)^{3/2}}e^{-E_p/T} \tag{4}$$

e-mail: [a]gleb87@3g.ua, [b]pevzner@ffeks.dnulive.dp.ua, [c]alexsokolovsky@mail.ru

(n is the total number density of the electrons). In this case, $W(p, p_1; p', p'_1)$ can be considered as probability of the scattering process of a photon by an electron per unit of time, summed over the final polarizations and averaged over their initial values.

In the quasi-relativistic approximation energy change of the electrons in collisions can be considered small

$$\delta(\varepsilon_{p'} - \varepsilon_p + E_{p'} - E_p) = \delta(\varepsilon_{p'} - \varepsilon_p) + \delta'(\varepsilon_{p'} - \varepsilon_p)(E_{p'} - E_p) + O(\lambda^2) \tag{5}$$

where a dimensionless small parameter can be estimated by the formula $\lambda \equiv (T/mc^2)^{1/2}$. It takes into account that the characteristic velocity of the electrons, at the considered temperatures, is significantly less than the speed of light. This leads to a corresponding series expansion of the collision integral

$$I_p(\mathrm{f}) = \sum_{s=0}^{\infty} I_{sp}(\mathrm{f}), \qquad I_{sp}(f) \sim \lambda^s,$$

$$I_{sp}(\mathrm{f}) = \int d^3p' \left\{ W_s(p, p')\mathrm{f}_{p'}(1 + \mathrm{f}_p) + (-1)^{s+1} W_s(p', p)\mathrm{f}_p(1 + \mathrm{f}_{p'}) \right\} \delta^{(s)}(\varepsilon_p - \varepsilon_{p'}),$$

$$W_s(p, p') \equiv \frac{1}{s!} \int d^3p_1 d^3p'_1 W(p, p_1; p', p'_1) w_{p'_1} \delta(p + p_1 - p' - p'_1)(E_{p_1} - E_{p'_1})^s \tag{6}$$

where it was taken into account that due to detailed balance relation holds $W(p, p_1; p', p'_1) = W(p', p'_1; p, p_1)$.

Further it is convenient to express momenta of photons through their energy, putting

$$\mathrm{f}_p(x, t)|_{p=n\varepsilon/c} = \mathrm{f}_\varepsilon(n, x, t), \qquad I_p(\mathrm{f})|_{p=n\varepsilon/c} = I_\varepsilon(n, \mathrm{f}), \qquad I_{sp}(\mathrm{f})|_{p=n\varepsilon/c} = I_{s\varepsilon}(n, \mathrm{f}) \tag{7}$$

(n_l is a unit vector). The most simple expression is obtained from (6) for the function

$$I_{0\varepsilon}(n, \mathrm{f}) = \frac{\varepsilon^2}{c^3} \int d\Omega_{n'} \Phi_0(\varepsilon, \varepsilon, nn')\{\mathrm{f}_\varepsilon(n') - \mathrm{f}_\varepsilon(n)\}, \tag{8}$$

where denoted

$$\Phi_s(\varepsilon, \varepsilon', nn') \equiv W_s(p', p)|_{p=\varepsilon n/c,\ p'=\varepsilon' n'/c}. \tag{9}$$

This function has the property

$$\int d\Omega_n I_{0\varepsilon}(n, \mathrm{f}) = 0; \tag{10}$$

hence taking into account (1), (2) the relation

$$\frac{\partial}{\partial t} \int d\Omega_n \mathrm{f}_\varepsilon(n, x, t) = -c \int d\Omega_n n_l \frac{\partial \mathrm{f}_\varepsilon(n, x, t)}{\partial x_l} + \int d\Omega_n \{I_\varepsilon(n, \mathrm{f}(x, t)) - I_{0\varepsilon}(n, \mathrm{f}(x, t))\}$$

is obtained.This formula, due to inequality $\lambda \ll 1$, shows, that value $\int d\Omega_n \mathrm{f}_\varepsilon(n, x, t)$ changes slowly with time in weakly nonuniform states, when

$$\partial^s \mathrm{f}_\varepsilon(n, x, t)/\partial x_{n_1} ... \partial x_{n_s} \sim g^s, \qquad g \ll 1$$

(g the value of the order of the ratio of the mean free path of a photon to the characteristic distance at which the function varies significantly). This result suggests that reduced description of the system is possible by the photon energy distribution $\varphi_\varepsilon(x, t)$. This description is based on the functional hypothesis

$$\mathrm{f}_\varepsilon(n, x, t) \overset{t \gg \tau_0}{\longrightarrow} \mathrm{f}_\varepsilon(n, x, \varphi(t)), \qquad \varphi_\varepsilon(x) \equiv \frac{1}{4\pi} \int d\Omega_n \mathrm{f}_\varepsilon(n, x, \varphi) \tag{11}$$

where τ_0 is characteristic time, depending on the initial state of the system $\mathrm{f}_\varepsilon(\mathrm{n}, \mathrm{x}, 0)$ (functional $\mathrm{f}_\varepsilon(n, x, \varphi)$ does not depend on $\mathrm{f}_\varepsilon(n, x, 0)$). In this situation distribution function $\mathrm{f}_\varepsilon(n, x, \varphi)$ is a functional of the photon distribution $\varphi_\varepsilon(x)$. Functional hypothesis (11) and the equation (1), (2) lead to the following kinetic equation for the function $\varphi_\varepsilon(x, t)$

$$\frac{\partial \varphi_\varepsilon(x, t)}{\partial t} = L_\varepsilon(x, \varphi(t)), \qquad L_\varepsilon(x, \varphi) \equiv \frac{1}{4\pi} \int d\Omega_n \left\{ -cn_l \frac{\partial \mathrm{f}_\varepsilon(n, x, \varphi)}{\partial x_l} + I_\varepsilon(n, \mathrm{f}(x, \varphi)) \right\}. \tag{12}$$

Functional $\mathrm{f}_\varepsilon(n, x, \varphi)$ according to (1), (11), (12) satisfies the equation

$$\int d^3x' d\varepsilon' \frac{\delta \mathrm{f}_\varepsilon(n, x, \varphi)}{\delta \varphi_{\varepsilon'}(x')} L_{\varepsilon'}(x', \varphi) = -cn_l \frac{\partial \mathrm{f}_\varepsilon(n, x, \varphi)}{\partial x_l} + I_\varepsilon(n, \mathrm{f}(x, \varphi)), \tag{13}$$

which should be solved taking into account second formula in (11) as an additional condition.

3 Perturbation theory

The basic equations of the theory should be solved in a double perturbation theory in parameters g and λ. An important role is played by arguments of rotational invariance and based on them relations

$$I_{s\varepsilon}(n,\varphi) = I_{s\varepsilon}(\varphi),$$

$$I_{s\varepsilon}(\varphi) \equiv \int\limits_0^\infty d\varepsilon' \varepsilon'^2 \left[F_s(\varepsilon,\varepsilon')\,\varphi'_\varepsilon\,(1+\varphi_\varepsilon) + (-1)^{s+1} F_s(\varepsilon',\varepsilon)\,\varphi_\varepsilon\,(1+\varphi_{\varepsilon'})\right]\delta^{(n)}(\varepsilon-\varepsilon'),$$

$$F_s(\varepsilon,\varepsilon') \equiv \frac{1}{c^3}\int d\Omega_{n'}\Phi_s(\varepsilon,\varepsilon',nn'), \qquad \Phi_s(\varepsilon,\varepsilon',nn') \equiv W_s(p',p)|_{p=\varepsilon n/c,\ p'=\varepsilon' n'/c}, \tag{14}$$

derived from the definition (6).

The solution of equation (13) is based on expansions of the distribution function $\mathrm{f}_\varepsilon(n,x,\varphi)$ in parameters g and λ

$$\mathrm{f}_\varepsilon(n,x,\varphi) = \mathrm{f}_\varepsilon^{(0)} + \mathrm{f}_\varepsilon^{(1)} + \mathrm{O}(g^2), \qquad \mathrm{f}_\varepsilon^{(m)} = \mathrm{f}_\varepsilon^{(m,0)} + \mathrm{f}_\varepsilon^{(m,1)} + \mathrm{O}(g^m\lambda^2). \tag{15}$$

In the zero approximation in the gradients the distribution function and the right-hand side of equation (12) have the structure

$$\mathrm{f}_\varepsilon^{(0)}(n,x,\varphi) = h_\varepsilon(n,\varphi(x)), \qquad L_\varepsilon^{(0)}(x,\varphi) = M_\varepsilon(\varphi(x)), \tag{16}$$

where $h_\varepsilon(n,\varphi)$, $M_\varepsilon(\varphi)$ are some functions. The integral equation (13) and the second relation (11) in this case give the following equation for $h_\varepsilon(n,\varphi)$ with an additional condition

$$\int d\varepsilon' \frac{\partial h_\varepsilon(n,\varphi)}{\partial\varphi_{\varepsilon'}} M_{\varepsilon'}(\varphi) = I_\varepsilon(n,h(\varphi)), \qquad \varphi_\varepsilon = \frac{1}{4\pi}\int d\Omega_n h_\varepsilon(n,\varphi), \tag{17}$$

where according to (12)

$$M_\varepsilon(\varphi) = \frac{1}{4\pi}\int d\Omega_n I_\varepsilon(n,h(\varphi)). \tag{18}$$

The solution of the equation is sought in the form of a power series λ

$$h_\varepsilon(n,\varphi) = \sum_{0\le s\le\infty} h_{s\varepsilon}(n,\varphi).$$

In the zero approximation in λ according to (10) we have $0 = I_{0\varepsilon}(n,h_0(\varphi))$ and due to (8) $h_{0\varepsilon}(n,\varphi)$ is an arbitrary function of ε. Now the additional condition (17) indicates that $h_{0\varepsilon}(n,\varphi) = \varphi_\varepsilon$. In the next step of the iterative procedure equation (17) gives

$$\frac{1}{4\pi}\int d\Omega_n I_{1\varepsilon}(n,\varphi) = I_{1\varepsilon}(n,\varphi) + I_{0\varepsilon}(n,h_1(\varphi)).$$

Hence, according to (14), we obtain an equation $0 = I_{0\varepsilon}(n,h_1(\varphi))$. As noted above, the solution of this equation $h_{1\varepsilon}(n,\varphi)$ is an arbitrary function of ε, but the additional condition (17) $\int d\Omega_n h_{1\varepsilon}(n,\varphi) = 0$ shows, that $h_{1\varepsilon}(n,\varphi) = 0$. Continuing further iterative procedure, we find that $h_{s\varepsilon}(n,\varphi) = 0$ $(1 \le s < \infty)$, and so in the zero-order approximation in the gradients the result is

$$\mathrm{f}_\varepsilon^{(0)}(n,x,\varphi) = \varphi_\varepsilon(x). \tag{19}$$

At the same time, according to (14), (18), the right side of equation (12) is given by the formula

$$L_\varepsilon^{(0)}(x,\varphi) = \sum_{1\le s\le\infty} I_{s\varepsilon}(\varphi(x)). \tag{20}$$

In other words, in spatially uniform case the right side of the time equation for $\varphi_{\varepsilon_p}(x,t)$ is the result of substitution of this function in the collision integral (2).

Thus, in the zero approximation in the gradients (in other words, in the spatially uniform case) the distribution function of the photon after the transition process duration τ_0 (see (11)) ceases to depend on the direction of the momentum of the photon. This justifies the initial assumptions of [6], where the author is limited to consideration of an isotropic distribution of photons in a spatially uniform case without justification of generality of this view.

We limit calculation in the first order in the gradients to the main contributions of perturbation theory in λ, that is by $\mathrm{f}_\varepsilon^{(1,0)}(n,\varphi)$. To do this, we first note that, according to (10), (12) $L_\varepsilon^{(1,0)}(x,\varphi)=0$. Taking into account (19) the integral equation (13) and the additional condition (11) give the equation for $\mathrm{f}_\varepsilon^{(1,0)}(n,\varphi)$

$$0=-cn_l\frac{\partial\varphi_\varepsilon(x)}{\partial x_l}+I_{0\varepsilon}(n,\mathrm{f}^{(1,0)}),\qquad \int d\Omega_n \mathrm{f}_\varepsilon^{(1,0)}(n,\varphi)=0. \tag{21}$$

Arguments of rotational invariance show that their solution can be sought in the form

$$\mathrm{f}_\varepsilon^{(1,0)}(n,x,\varphi)=a_\varepsilon n_l\frac{\partial\varphi_\varepsilon(x)}{\partial x_l} \tag{22}$$

where a_ε is a function. Taking into account (8) and noting that

$$\frac{\varepsilon^2}{c^3}\int d\Omega_{n'}\Phi_0(\varepsilon,\varepsilon,nn')(n'_l-n_l)=-n_l/\tau_\varepsilon$$

(τ_ε is a function), we obtain

$$\mathrm{f}_\varepsilon^{(1,0)}(n,x,\varphi)=-c\tau_\varepsilon n_l\frac{\partial\varphi_\varepsilon(x)}{\partial x_l}. \tag{23}$$

As a result, formula (12) shows that

$$L_\varepsilon^{(2,0)}(x,\varphi)=\frac{\tau_\varepsilon}{3}\Delta\varphi_\varepsilon(x) \tag{24}$$

Bringing our final results we restrict ourself by calculation of $L_\varepsilon^{(0)}(x,\varphi)$ on the basis of (20) up to the second order in λ. Taking this and contribution (24) into account, we obtain the following kinetic equation for the photon energy distribution function $\varphi_\varepsilon(x,t)$

$$\frac{\partial\varphi_\varepsilon}{\partial t}=\frac{1}{\varepsilon^2}\frac{\partial}{\partial\varepsilon}\left\{\varepsilon^4\left[g_1^{00}(\varepsilon)\varphi_\varepsilon\left(1+\varphi_\varepsilon\right)+g_2^{00}\left(\varepsilon\right)\frac{\partial\varphi_\varepsilon}{\partial\varepsilon}+\left(g_2^{10}(\varepsilon)-g_2^{01}(\varepsilon)\right)\varphi_\varepsilon\left(1+\varphi_\varepsilon\right)\right]\right\}+$$
$$+D(\varepsilon)\Delta\varphi_\varepsilon(x)+O(g^0\lambda^3,g^1\lambda^1,g^2\lambda^1), \tag{25}$$

where denoted

$$g_s^{mn}(\varepsilon)=\partial^{m+n}F_s(\varepsilon,\varepsilon')/\partial\varepsilon^m\partial\varepsilon'^n|_{\varepsilon'=\varepsilon},\qquad D(\varepsilon)^{-1}=\frac{3\varepsilon^2}{c^3}\int d\Omega_{n'}\Phi_0(\varepsilon,\varepsilon,nn')(1-nn'). \tag{26}$$

Equation (25) can be called the photon diffusion equation. It is an analogue of the neutron diffusion equation derived in [4]. The contribution of zero approximation in the gradients in the equation (25) does not coincide with the expression obtained in [6]. This is a consequence of an assumption made in this paper that it should vanish by substitution the Planck distribution $\varphi_\varepsilon\to n_\varepsilon$, $n_\varepsilon\equiv(e^{\varepsilon/T}-1)^{-1}$. However, substitution $\mathrm{f}_p\to n_{\varepsilon_p}$ reduces to zero only full collision integral (2). This property is connected with full δ-function entering (2) and is absent in finite sum of the series (6).

4 Conclusion

The photon kinetics in equilibrium plasma medium was investigated on the basis of the Bogolyubov reduced description method. A starting point of the analysis is a kinetic equation of the Boltzmann type, which takes into account the Compton scattering of photons on electrons of the medium. The kinetic equation for the photon energy distribution was obtained for weakly nonuniform states of the system. It describes the photon diffusion similar to the known neutron diffusion equation. The results was obtained in the quasi-relativistic approximation when energy change of an electron at the collisions is small.

References

[1] Yu.P. Stepanovsky, *On wave mechanics of light quanta and uncertainty relation in quantum electrodynamics* In: *Problems of modern physics*, N.F.Shul'ga - ed.(Kharkov, NSC KhFTI, 2008), P. 317-366 (in Russian).
[2] L.A. Apresyan, Yu.A. Kravtsov, *Theory of radiative transfer: Statistical and wave aspects*, (M., Nauka, 1983), 216 p.(in Russian).
[3] M.O. Scully, M.S. Zubairy, *Quantum optics*, (Cambridge, University Press, 1997), 630 p.
[4] A.I. Akhiezer, S.V. Peletminsky, *Methods of Statistical Physics*, (Oxford: Pergamon Press, 1981).
[5] A.I. Akhiezer, S.V. Peletminsky, *Kinetics of the black radiation*, DAN SSSR **200**, 1317 (1971)(in Russian).
[6] A.S. Kompaneets *On establishing of thermal equilibrium between photons and electrons*, ZhETF **31**, Iss. 5, 876-885 (1956) (in Russian).

Proceedings of the International School-seminar
"New Physics and Quantum Chromodynamics at External Conditions", pp. 131 – 134,
May 22-24, 2013, Dnipropetrovsk, Ukraine

BASIC IDEAS OF THE BOGOLYUBOV REDUCED DESCRIPTION METHOD AND EXACT SOLVABLE MODEL FOR BROWNIAN MOTION

A.I. Sokolovsky [a], Z.Yu. Chelbaevsky [b], S.A. Yanenko [c]

Oles Honchar Dnipropetrovsk National University, Dnipropetrovsk, Ukraine

Projection formalism is applied to an analysis of linear kinetic equation that describes Brownian motion in equilibrium medium and leads to reduced description of diffusion of Brownian particles. With the help of the exact solution of the kinetic equation the main objects of the reduced description method have been calculated. A Markov master equation is derived which is as possible close to the diffusion equation, is valid for all times and at long times obviously leads to usual diffusion equation.

1 Introduction

The Bogolyubov reduced description method is an universal approach to description of nonequilibrium processes. Developed in [1]- [4] projection formulation of the reduced description method justified its basic structures. This approach can be applied also to an analyze of evolution described by a kinetic equation. It is a pity but basic structures of the reduced description method can be calculated usually only in a perturbation theory. Therefore, search for exact solvable models, which allow studying in details forming of the reduced description and calculating all introduced in this approach quantities, is very important. Here as this type model Brownian motion in an equilibrium medium is considered. Exact solution of kinetic equation for this model was given, for example, in [5]. On this basis we calculate the main objects of the reduced description method and derive an exact equation for Brownian particle density. A preliminary version of this investigation was published in [6].

2 Exact solution of the kinetic equation

Evolution of a rarefied gas of Brownian particles in equilibrium fluid is investigated. Its dynamics is described by kinetic equation

$$\partial_t \mathrm{f}_t(x,p) = \mathbf{L}\mathrm{f}_t(x,p); \qquad \mathbf{L} = \mathbf{L}_0 + \mathbf{L}_1, \quad \mathbf{L}_0 = \gamma \frac{\partial}{\partial p_n}\left(\frac{\partial}{\partial p_n} + \frac{p_n}{mT}\right), \quad \mathbf{L}_1 = -\frac{p_n}{m}\frac{\partial}{\partial x_n} \tag{1}$$

where m is mass of a Brownian particle, T is temperature of the fluid, γ is a positive constant. Distribution function of a particle $\mathrm{f}_t(x,p)$ is normalized by condition

$$\int d^3p\, \mathrm{f}_t(x,p) = n_t(x) \tag{2}$$

where $n_t(x)$ is number density of the Brownian particles. It is convenient to find solution of the equation (1) in a form of the Fourier expansion using notations

$$\mathrm{f}_{kt}(p) = \int\limits_V d^3x \mathrm{f}_t(x,p) e^{-i\,k\,x}, \qquad \mathrm{f}_{kt}(q) = \frac{1}{(2\pi)^{3/2}} \int d^3p\, \mathrm{f}_{kt}(p) e^{-i\,p\,q}. \tag{3}$$

As a result solution of the kinetic equation can be written in the form [5]

$$\mathrm{f}_{kt}(q) = D_{kt}(q)\mathrm{f}_{k0}(q\alpha_t + kb\,(\alpha_t - 1)),$$
$$D_{kt}(q) = \chi_{kt}\, e^{a\,b\{2b\,k\,q(\alpha_t-1)^2 + q^2(\alpha_t^2-1)\}}, \qquad \chi_{kt} \equiv e^{a\,b^3k^2(\alpha_t^2 - 4\alpha_t + 3 - 2\lambda\,t)} \tag{4}$$

where notations

$$\alpha_t = e^{-\lambda\,t}, \quad \lambda = \gamma/mT, \quad a = m\gamma/2, \quad b = T/\gamma. \tag{5}$$

are introduced.

Formulas (4), (5) show that after a characteristic time τ_0 state of the system is simplified

$$\tilde{\mathrm{f}}_{kt}(q) \xrightarrow[t \gg \tau_0]{} \tilde{\mathrm{f}}^{as}_{kt}(q), \qquad \tilde{\mathrm{f}}^{as}_{kt}(q) = D^{as}_{kt}(q)\tilde{\mathrm{f}}_{k0}(-kb) \qquad (\tau_0 \equiv \lambda^{-1}) \tag{6}$$

e-mail: [a]alexsokolovsky@mail.ru, [b]zak_tch@rambler.ru, [c]losnazi@mail.ru

where

$$D_{kt}^{as}(q) \equiv \exp\{ab^3k^2(3-2\lambda t)+2ab^2kq-abq^2\}. \tag{7}$$

According (2), (3) number of particles density is given by the formula

$$n_{kt} = (2\pi)^{3/2}\tilde{\mathrm{f}}_{kt}(0) = (2\pi)^{3/2}D_{kt}(0)\tilde{\mathrm{f}}_{k0}(kb(\alpha_t-1)). \tag{8}$$

At long times $t \gg \tau_0$ this value takes the form

$$n_{kt} \xrightarrow[t\gg\tau_0]{} n_{kt}^{as}, \qquad n_{kt}^{as} \equiv (2\pi)^{3/2}D_{kt}^{as}(0)\tilde{\mathrm{f}}_{k0}(-kb). \tag{9}$$

Formulas (6), (7), (9) show that at long times distribution function of Brownian particles depends on time only through their density

$$\tilde{\mathrm{f}}_{kt}^{as}(q) = \frac{1}{(2\pi)^{3/2}}n_{kt}^{as}e^{ab(2bkq-q^2)} \tag{10}$$

Relations (10) have the form of the functional hypothesis which first was proven for the considered model in a more complicated form in [5]. As a result at $t \gg \tau_0$ state of the system is described completely by the density of Brownian particles n_{kt}^{as}. This value according to (7), (9) satisfies the diffusion equation

$$\partial_t n_{kt}^{as} = -Dk^2 n_{kt}^{as} \qquad (D \equiv T^2/\gamma) \tag{11}$$

with coefficient of diffusion D. With account for (7), (9) effective initial condition $n_{k0}^{\mathrm{ef}} \equiv n_{k0}^{as}$ to this equation is given by the formula

$$n_{k0}^{\mathrm{ef}} = (2\pi)^{3/2}\tilde{\mathrm{f}}_{k0}(-bk)e^{3a\,b^3\,k^2}. \tag{12}$$

According to (2), (3) real initial value of the particle density n_{k0} has the form

$$n_{k0} = (2\pi)^{3/2}\tilde{\mathrm{f}}_{k0}(0) \tag{13}$$

and differs from the effective one. It is interesting to note that even for simplest initial distribution function of the system formula (12) gives nontrivial effective value of the density

$$\mathrm{f}_0(x,p) = n_0(x)w(p) \qquad \Longrightarrow \qquad n_{k0}^{\mathrm{ef}} = n_{k0}e^{2ab^3\,k^2}. \tag{14}$$

3 Projection formalism for description of the diffusion

Kinetic equation (1) is a linear one. Therefore, developed in [1]- [4] for investigation of the Liouville equation projection approach can be applied here to (1) for construction of the reduced description on this basis. A problem of this paper consists in investigation of the time evolution of the distribution function f_t and its projection $\mathbf{P}\mathrm{f}_t$ as a reduced description parameter. In the case of diffusion of Brownian particles the projection operator can be chosen in the form

$$\mathbf{P}h(x,p) = w(p)\int d^3p\, h(x,p), \qquad w(p) \equiv \frac{1}{(2\pi mT)^{3/2}}e^{-\frac{p^2}{2mT}}, \qquad \mathbf{L}_0 w(p) = 0 \tag{15}$$

where $h(x,p)$ is an arbitrary function of phase variables. According to (1) this operator has the properties

$$\mathbf{L} = \mathbf{L}_0 + \mathbf{L}_1, \qquad \mathbf{P}\mathbf{L}_0 = \mathbf{L}_0\mathbf{P}, \qquad \mathbf{P}^2 = \mathbf{P}. \tag{16}$$

It can be used for construction of the reduced description of the system in the terms of number density of Brownian particles $n_t(x)$ because according to (2), (16) the formula

$$\mathbf{P}\mathrm{f}_t(x,p) = w(p)n_t(x) \tag{17}$$

is valid.

In the projection formulation of the reduced description method the functional hypothesis has the form

$$\mathrm{f}_t \xrightarrow[t\gg\tau_0]{} \mathrm{f}_t^{as}, \qquad \mathrm{f}_t^{as} = \mathbf{C}\mathbf{P}\cdot\mathbf{P}\mathrm{f}_t^{as} \tag{18}$$

where

$$\mathrm{f}_t^{as} = \mathbf{S}_t^{as}\mathrm{f}_0, \qquad \mathbf{S}_t^{as} = \mathbf{S}_t\sigma \qquad (t \geq 0, \quad \mathrm{f}_0 = \mathrm{f}_{t=0}, \quad \mathbf{S}_t = e^{t\,\mathbf{L}}). \tag{19}$$

Operators $\mathbf{C}$, σ are called the reduced description operator and coarse graining operator respectively. Functional hypothesis (10) shows that namely projection $\mathbf{P}\mathrm{f}_t^{as}$ is the reduced description parameter.

In [1]- [4] a method of master operator was elaborated that was applied for proving of the functional hypothesis and in general to describe transition of a system to the reduced description. The master operator $\mathbf{C}_t$ is defined by the formula

$$\mathbf{S}_t = \mathbf{C}_t\mathbf{P}\mathbf{S}_t + \mathbf{C}_t\mathbf{Q} \qquad (\mathbf{Q} \equiv 1 - \mathbf{P}). \tag{20}$$

For investigation of the reduced description forming it is naturally to use [1]- [4] the master equation

$$\partial_t \mathbf{P}\mathrm{f}_t = \mathbf{M}_t\mathbf{P}\mathrm{f}_t + \mathbf{N}_t\mathbf{Q}\mathrm{f}_0 \qquad (\mathbf{M}_t \equiv \mathbf{PLC}_t\mathbf{P}, \quad \mathbf{N}_t \equiv \mathbf{PLC}_t\mathbf{Q}) \tag{21}$$

and the corresponding representation of the system distribution function

$$\mathrm{f}_t = \mathbf{A}_t\mathbf{P}\mathrm{f}_t + \mathbf{B}_t\mathbf{Q}\mathrm{f}_0 \qquad (\mathbf{A}_t \equiv \mathbf{C}_t\mathbf{P}, \quad \mathbf{B}_t \equiv \mathbf{C}_t\mathbf{Q}), \tag{22}$$

that follow from the definition (20). The second summands on right hand side of formulas (21), (22) take into account influence of initial correlation $\mathbf{Q}\mathrm{f}_0$ on description of a system by parameter $\mathbf{P}\mathrm{f}_t$. Note, that in a projection operator approach a master equation was obtained first by Zwanzig [7] but in non-Markovian form.

According to the above mentioned, the reduced description takes place at

$$\mathbf{C}_t \xrightarrow[t\gg\tau_0]{} \mathbf{C}, \qquad \mathbf{CQ} = 0, \quad \mathbf{PC} = \mathbf{P} \tag{23}$$

that ensures the fulfillment of the conditions

$$\mathbf{M}_t \xrightarrow[t\gg\tau_0]{} \mathbf{M}, \quad \mathbf{N}_t \xrightarrow[t\gg\tau_0]{} 0 \qquad (\mathbf{M} \equiv \mathbf{PLCP}) \tag{24}$$

which make equation (21) a closed one. The described approach of the master operator will be used below.

4 Calculation of the basic objects of the reduced description

To simplify the next consideration it is convenient to use some additional definitions. To each linear operator $\mathbf{A}$ acting in the space of functions of phase variables x, p corresponds operator $\mathbf{A}_k$ acting in space of functions of momentum and defined by the formula

$$\mathbf{A}e^{i\,k\,x}h(p) = e^{i\,k\,x}\mathbf{A}_k h(p). \tag{25}$$

In the considered theory it is convenient to use the Dirac notations to describe transition from p-representation to q-one by definitions

$$\mathbf{A}_k\delta(p-p') = \langle p|\hat{\mathbf{A}}_k|p'\rangle; \qquad \langle q|p\rangle = \frac{1}{(2\pi)^{3/2}}e^{i\,q\,p}, \qquad \int d^3p|p\rangle\langle p| = \hat{1}, \qquad \int d^3q|q\rangle\langle q| = \hat{1}. \tag{26}$$

Here the first formula introduces abstract Dirac operator $\hat{\mathbf{A}}_k$ for each mentioned operator $\mathbf{A}_k$ (the Dirac operators are supplied by the cap). In this approach a state of the Brownian system particles can be described by abstract vector $|k,t\rangle$ defined by the formula

$$\langle p|k,t\rangle = \mathrm{f}_{kt}(p). \tag{27}$$

The abstract Dirac operators act in a set of vectors to which belong vectors $|p\rangle$, $|q\rangle$, $|k,t\rangle$ and so on. In this terms kinetic equation (1) has the form

$$\partial_t|k,t\rangle = \hat{\mathbf{L}}_k|k,t\rangle. \tag{28}$$

The considered kinetic equation is the exact solvable one. Therefore, all mathematical objects introduced by the reduced description method can be calculated exactly. Evolution operator of the system $\hat{\mathbf{S}}_{kt}$ defined by expression (19) is given by formula

$$\langle q|\hat{\mathbf{S}}_{kt}|q'\rangle = D_{kt}(q)\delta\left(q' - [q\alpha_t + bk(\alpha_t - 1)]\right) \tag{29}$$

where the notations from (4) are used. Evolution of the system at $t \gg \tau_0$ ($\tau_0 = \lambda^{-1}$) is described by asymptotic evolution operator that has the form

$$\langle q|\hat{\mathbf{S}}^{as}_{kt}|q'\rangle = D^{as}_{kt}(q)\delta(q' - bk). \tag{30}$$

According to (19) the coarse graining operator $\hat{\sigma}_k$ is defined by the formula

$$\langle q|\hat{\sigma}_k|q'\rangle = D^{as}_{k0}(q)\delta(q' + bk) \qquad (\hat{\sigma}_k \equiv \hat{\mathbf{S}}^{as}_{k0}). \tag{31}$$

By direct calculation taking into account expressions for the necessary matrix elements the identities

$$\hat{\mathbf{S}}^{as}_{kt} = \hat{\mathbf{S}}_{kt}\hat{\sigma}_k, \qquad \hat{\sigma}^2_k = \hat{\sigma}_k, \qquad \hat{\sigma}_k\hat{\mathbf{L}}_k = \hat{\mathbf{L}}_k\hat{\sigma}_k \tag{32}$$

are obtained that were proven in general theory [1]- [4] only on the basis of heuristic arguments.

According to (18) the reduced description operator $\hat{\mathbf{C}}_k$ is given by the formula

$$\langle q|\hat{\mathbf{C}}_k|q'\rangle = \delta(q')e^{ab(2bkq-q^2)} \tag{33}$$

This formula with account for the expression for the projection operator $\langle q|\hat{\mathbf{P}}|q'\rangle = \delta(q')e^{-abq^2}$ allows proving the relations

$$\hat{\mathbf{P}}\hat{\mathbf{C}}_k = \hat{\mathbf{P}}, \qquad \hat{\mathbf{C}}_k\hat{\mathbf{P}} = \hat{\mathbf{C}}_k, \qquad \hat{\sigma}_k = \hat{\mathbf{C}}_k\hat{\sigma}_k; \qquad \hat{\mathbf{C}}_0 = \hat{\mathbf{P}}, \qquad \hat{\sigma}_0 = \hat{\mathbf{P}} \tag{34}$$

that were proven in general theory [1]- [4] only on the basis of heuristic arguments.

For the considered model the master operator $\hat{\mathbf{C}}_{kt}$ defined by relation (20) is calculated in the presented theory too. Its fragments $\hat{\mathbf{A}}_{kt} \equiv \hat{\mathbf{C}}_{kt}\hat{\mathbf{P}}$, $\hat{\mathbf{B}}_{kt} \equiv \hat{\mathbf{C}}_{kt}\hat{\mathbf{Q}}$ are given by the formulas

$$\langle q|\hat{\mathbf{A}}_{kt}|q'\rangle = \delta(q')e^{ab\{2bkq(1-\alpha_t)-q^2\}}; \qquad \langle q|\hat{\mathbf{B}}_{kt}|q'\rangle = \chi_{kt}e^{ab\{2b\,k\,q\,(1-\alpha_t)-q^2\}}\times$$
$$\times\left[\delta(q'-\{kb(\alpha_t-1)+q\alpha_t\}e^{ab\{2b\,kq\,\alpha_t(\alpha_t-1)+q^2\alpha_t^2\}} - \delta(q'-kb(\alpha_t-1))\right]. \tag{35}$$

These operators give the basic representation of the system distribution function (22)

$$\mathrm{f}_{kt} = \mathbf{A}_{kt}\mathbf{P}\mathrm{f}_{kt} + \mathbf{B}_{kt}\mathbf{Q}\mathrm{f}_{k0} \tag{36}$$

that can be used in an analyze of transition of the system to the reduced description.

The master equation (21) in these terms has the form

$$\partial_t\mathbf{P}\mathrm{f}_{kt} = \mathbf{M}_{kt}\mathbf{P}\mathrm{f}_{kt} + \mathbf{N}_{kt}\mathbf{Q}\mathrm{f}_{k0} \qquad (\mathbf{M}_{kt} \equiv \mathbf{P}\mathbf{L}_k\mathbf{A}_{kt}, \quad \mathbf{N}_{kt} = \mathbf{P}\mathbf{L}_{kt}\mathbf{B}_{kt}) \tag{37}$$

and is the closest equation to the equation for the reduced description parameter $\mathbf{P}\mathrm{f}^{as}_{kt}$. The obtained in the present paper expressions for operators $\mathbf{M}_{kt}$, $\mathbf{N}_{kt}$ are

$$\mathbf{M}_{kt} = Dk^2(\alpha_t-1)\mathbf{P}, \qquad \langle p|\hat{\mathbf{N}}_{kt}|p'\rangle = w(p)\alpha_t\chi_{kt}\{Dk^2(1-\alpha_t) - \frac{i}{m}kp'\}e^{i\,b\,kp'(\alpha_t-1)}. \tag{38}$$

As a result the master equation (37) for number density of Brownian particles n_{kt} takes the form

$$\partial_t n_{kt} = Dk^2(\alpha_t-1)n_{kt} + Dk^2\alpha_t(1-\alpha_t)\chi_{kt}\int d^3p'\{\mathrm{f}_{k0}(p') - w(p')n_{k0}\}e^{i\,b\,k\,p'(\alpha_t-1)}. \tag{39}$$

Equation (39) is valid for all times and obviously demonstrates transition of the system to description by usual diffusion equation (according to (4) $\alpha_t = e^{-t/\tau_0}$, $\tau_0 = mT/\gamma$ and function χ_{kt} decays too). This equation is a Markovian one. It is not a closed equation for n_{kt} because it contains information about initial state of the system described by distribution f_{k0} ($\int d^3p\,\mathrm{f}_{kt}(p) = n_{kt}$).

5 Conclusions

The Brownian motion in equilibrium medium described by an exact solvable kinetic equation was investigated. All mathematical objects, that are introduced by the reduced description method in its projection operator formulation, have been calculated. The Markovian diffusion master equation for number density of Brownian particles was derived. This equation is valid for all times and obviously demonstrates behavior of the system at its transition to the reduced description by the diffusion equation. The investigation was simplified by using the Dirac notations in a linear space describing solutions of the kinetic equation.

References

[1] I. Oppenheim, A.I. Sokolovsky, M.Yu. Tseitlin. *On the reduced description of nonequilibrium states of simple fluids*, Physica A **136**, No. 1, P. 1-20 (1986).

[2] A.I. Sokolovsky, *Markovian master equation and the reduced description method*, Dopovidi NANU **6**, P. 91-96 (1998) (in Russian).

[3] A.I. Sokolovsky, *Method of the master operator in the theory of nonequilibrium processes*, Visnyk of Dnipropetrovsk University. Physics. Radio Electronics **4**, 59-63 (1998) (in Russian).

[4] A.I. Sokolovsky, *Projection formulation of the Bogolyubov reduced description method and its application to fluctuation kinetics*, Ukr. J. Phys. **45**, No. 4-5, P.548-553 (2000).

[5] A.I. Akhiezer, S.V. Peletminsky, *Methods of Statistical Physics*, (Oxford, Pergamon Press, 1981), 368 p.

[6] A.I. Sokolovsky, Z.Yu. Chelbaevsky, S.A. Yanenko, *Forming of the reduced description in a model of Brownian motion*, Visnyk of Dnipropetrovsk University. Physics. Radio Electronics **20**, No. 2, 24-30 (2012) (in Russian).

[7] R. Zwanzig, *Ensemble method in the theory of irreversibility*, J.Chem.Phys. **33**, No. 5, 1338-1341 (1960).

Proceedings of the International School-seminar
"New Physics and Quantum Chromodynamics at External Conditions", pp. 135 – 138,
May 22-24, 2013, Dnipropetrovsk, Ukraine

HYDRODYNAMICS OF A COMPLETELY IONIZED PLASMA TAKING INTO ACCOUNT RELAXATION PHENOMENA

V.N. Gorev[a], A.I. Sokolovsky[b]

Dnipropetrovsk National University, Dnipropetrovsk, Ukraine

The hydrodynamics of a completely ionized two-component electron-ion plasma is studied at the end of the components temperature and velocity relaxation on the basis of the Landau kinetic equation and the Chapman-Enskog method. Linearized hydrodynamic equations are built, and the hydrodynamic modes of the system are obtained.

1 Introduction

In his well-known work [1] Landau derived a kinetic equation that adequately describes plasma. He investigated the component temperature relaxation for a space uniform quasi-equilibrium plasma and calculated the corresponding relaxation time. According to his assumption, in this situation the plasma components are described by the Maxwell distribution. From his approach the component velocity relaxation time can also be obtained. The investigation of non-uniform systems can be made on the basis of the Chapman–Enskog method with the usual assumption that all hydrodynamic variables have small gradients [2]. These results are important for investigation of the hydrodynamic modes of the system. The method by which hydrodynamic modes are obtained is rather well-known [3], but the investigation of hydrodynamic modes for plasma on the basis of the Landau equation cannot be found in the literature. Notice that plasma hydrodynamic modes are usually studied on the basis of the Vlasov kinetic equation and plasma oscillations are obtained (see, for example, [4]), but the component temperature and velocity relaxation cannot be described by that equation, because the collision integral is omitted there.

The aim of this work is to find plasma hydrodynamic modes on the basis of the Landau equation with taking into account relaxation processes.

2 Basic equations of the theory

The Landau kinetic equation can be written as follows [1]:

$$\frac{\partial f_{ap}(x,t)}{\partial t} = -\frac{p_{an}}{m_a}\frac{\partial f_{ap}(x,t)}{\partial x_n} + I_{ap}\left(f(x,t)\right), \tag{1}$$

where $f_{ap}(x,t)$ is is the component distribution function (DF) $(a,b,c,... = e,i)$ and I_{ap} is the Landau collision integral

$$I_{ap}(f) = -\frac{\partial}{\partial p_n}\sum_c 2\pi(e_a e_c)^2 L\int\left[f_{ap}\frac{\partial f_{cp'}}{\partial p'_l} - f_{cp'}\frac{\partial f_{ap}}{\partial p_l}\right]D_{nl}\left(\frac{p}{m_a}-\frac{p'}{m_c}\right)d^3p' \tag{2}$$

where

$$D_{nl}(u) \equiv (u^2\delta_{nl} - u_n u_l)/|u|^3. \tag{3}$$

Here e_a is the component charge ($e_e = -e, e_i = ze$; e is the elementary electric charge, z is the ion charge number), L is the Coulomb logarithm.

By definition [2], the component temperature T_a, velocity v_{an}, and particle density n_a can be expressed in the terms of DF

$$n_a = \int f_{ap}d^3p, \quad \pi_{an} = m_a n_a v_{an} = \int f_{ap}p_n d^3p, \quad \varepsilon_a = \frac{3}{2}n_a T_a + \frac{m_a n_a {v_a}^2}{2} = \int f_{ap}\varepsilon_{ap}d^3p, \tag{4}$$

where π_{an}, ε_a are the component momentum and energy densities ($\varepsilon_{ap} \equiv p^2/2m_a$).

We consider the system to be at the end of the temperature and velocity relaxation. It is evident that after the end of this relaxation the temperature T and the velocity v_n of the system are given by the relations

$$\pi_n = \sum_a \pi_{an} = v_n\sum_a m_a n_a, \qquad \varepsilon = \sum_a \varepsilon_a = \frac{3}{2}T\sum_a n_a + \frac{1}{2}v^2\sum_a m_a n_a, \tag{5}$$

e-mail: [a]lordjainor@gmail.com, [b]alexsokolovsky@mail.ru

where π_n and ε are the total momentum and energy densities of the system, respectively.

From (1) and (5) it can be shown that

$$\frac{\partial n_a}{\partial t} = -\frac{1}{m_a}\frac{\partial \pi_{an}}{\partial x_n}, \qquad \frac{\partial \pi_{an}}{\partial t} = -\frac{\partial t_{anl}}{\partial x_l} + R_{an}, \qquad \frac{\partial \varepsilon_a}{\partial t} = -\frac{\partial q_{an}}{\partial x_n} + Q_a, \tag{6}$$

where

$$q_{an} \equiv \int d^3p\ \varepsilon_{ap}\frac{p_n}{m_a}f_{ap}, \qquad t_{aln} \equiv \int d^3p\ p_l\frac{p_n}{m_a}f_{ap} \tag{7}$$

are the component energy and momentum fluxes and

$$Q_a = \int d^3p\ \varepsilon_{ap}I_{ap}\left(f\right), \qquad R_{an} = \int d^3p\ p_nI_{ap}\left(f\right) \tag{8}$$

are the component energy and momentum sources.

Further we consider the system at the end of component temperature and velocity relaxation and introduce small deviations of the electron temperature and velocity from T and υ_n

$$\tau \equiv T_e - T, \qquad u_n \equiv \upsilon_{en} - \upsilon_n, \tag{9}$$

that are estimated by the expressions

$$u \sim \mu\sqrt{T/m_e}, \quad \tau \sim \mu T; \qquad \mu \ll 1. \tag{10}$$

At the hydrodynamic stage of evolution of two-component systems [2] the component particle densities n_a, temperature T, velocity υ_n are the reduced description parameters. Relations (4), (5) and (9) show that the deviations of the ion temperature and velocity from T and υ_n are expressed in terms of τ and u_n. Thus the reduced description parameters of the theory with account for relaxation are $\xi_\alpha(x,t)$

$$n_i(x,t) \equiv \xi_1(x,t),\ n_e(x,t) \equiv \xi_2(x,t),\ \upsilon_n(x,t) \equiv \xi_{2+n}(x,t),\ T(x,t) \equiv \xi_6(x,t),$$

$$u_n(x,t) \equiv \xi_{6+n}(x,t),\ \tau(x,t) \equiv \xi_{10}(x,t). \tag{11}$$

Besides the small parameter of our theory μ, the gradients of the reduced description parameters are additionally small

$$\frac{\partial^s \xi_\alpha}{\partial x_{n_1}...\partial x_{n_s}} \sim g^s, \quad (\alpha = 1,...,6) \qquad \frac{\partial^s \xi_\alpha}{\partial x_{n_1}...\partial x_{n_s}} \sim \mu g^s, \quad (\alpha = 7,...,10) \qquad g \ll 1. \tag{12}$$

3 Linearized hydrodynamic equations and hydrodynamic modes

According to [3], we should build linearized hydrodynamic equations (LHE) for obtaining the hydrodynamic modes of the system. The reduced description parameters are taken in the vicinity of their equilibrium values:

$$n_a = n_a^{eq} + \delta n_a\left(x,t\right), \quad \upsilon_n = \delta\upsilon_n\left(x,t\right), \quad T = T^{eq} + \delta T\left(x,t\right), \quad u_n = \delta u_n\left(\vec{x},t\right), \quad \tau = \delta\tau\left(x,t\right), \tag{13}$$

where the deviations of their values from their equilibrium values are small quantities of the same order (we use the reference frame where $\upsilon_n^{eq} = 0$). The equilibrium values of the reduced description parameters are constant ones and condition of the electro neutrality

$$n_e^{eq} = zn_i^{eq} \tag{14}$$

is true.

To build LHE, we need the contributions to the DF up to the first order in μ and the second order in g. These functions are calculated here by using the Chapman–Enskog method [2], the Sonine polynomial expansion [5], and the results of the Landau approximation [1]. The LHE must be rotationally invariant and, therefore, have the structure

$$\partial_t\delta n_e = (\gamma_{ee}\Delta\delta n_e + \gamma_{ei}\Delta\delta n_i) + \gamma_{e\upsilon}\mathrm{div}\delta\upsilon + \gamma_{eT}\Delta\delta T + \gamma_{eu}\mathrm{div}\delta u + \gamma_{e\tau}\Delta\delta\tau,$$

$$\partial_t\delta n_i = (\gamma_{ie}\Delta\delta n_e + \gamma_{ii}\Delta\delta n_i) + \gamma_{\upsilon}\mathrm{div}\delta\upsilon + \gamma_{iT}\Delta\delta T + \gamma_{u}\mathrm{div}\delta u + \gamma_{i\tau}\Delta\delta\tau,$$

$$\partial_t\delta\upsilon_l = (\beta_e\mathrm{grad}_l\delta n_e + \beta_i\mathrm{grad}_l\delta n_i) + (\eta_\upsilon\Delta\delta\upsilon_l + \tilde{\eta}_\upsilon\mathrm{grad}_l\mathrm{div}\delta\upsilon) + \beta_T\mathrm{grad}_l\delta T + (\eta_u\Delta\delta u_l + \tilde{\eta}_u\mathrm{grad}_l\mathrm{div}\delta u) + \beta_\tau\mathrm{grad}_l\delta\tau,$$

$$\partial_t\delta T = (\alpha_e\Delta\delta n_e + \alpha_i\Delta\delta n_i) + \alpha_\upsilon\mathrm{div}\delta\upsilon + \alpha_T\Delta\delta T + \alpha_u\mathrm{div}\delta u + \alpha_\tau\Delta\delta\tau,$$

$$\partial_t\delta u_l = (\chi_e\mathrm{grad}_l\delta n_e + \chi_i\mathrm{grad}_l\delta n_i) + (\chi_\upsilon\Delta\delta\upsilon_l + \tilde{\chi}_\upsilon\mathrm{grad}_l\mathrm{div}\delta\upsilon) + \chi_T\mathrm{grad}_l\delta T +$$

$$+(-\lambda_u\delta u_l + \chi_u\Delta\delta u_l + \tilde{\chi}_u\mathrm{grad}_l\mathrm{div}\delta u) + \chi_\tau\mathrm{grad}_l\delta\tau,$$

$$\partial_t\delta\tau = (\theta_e\Delta\delta n_e + \theta_i\Delta\delta n_i) + \theta_\upsilon\mathrm{div}\delta\upsilon + \theta_T\Delta\delta T + \theta_u\mathrm{div}\delta u + (-\lambda_\tau\delta\tau + \theta_\tau\Delta\delta\tau). \tag{15}$$

The coefficients appearing in (15) are calculated in a perturbation theory in the small mass ratio $\sigma \equiv \sqrt{m_e/m_i}$. As a result we obtain

$$\alpha_T = \frac{\sqrt{2}+17z}{2z(1+z)(\sqrt{2}+z)}\Lambda + O(\sigma), \qquad \alpha_e = \frac{\sqrt{2}+7z}{2z^2(1+z)(\sqrt{2}+z)}\frac{T}{n_i}\Lambda + O(\sigma), \qquad \alpha_v = -\frac{2T}{3},$$
$$\alpha_\tau = \frac{25}{2(1+z)(4\sqrt{2}+13z)}\Lambda + O(\sigma), \qquad \alpha_u = -\frac{2Tz}{3(1+z)} + O(\sigma^2), \qquad \alpha_i = O(\sigma^2);$$
$$\beta_e = -\frac{T}{n_i m_e}\sigma^2 + O(\sigma^4), \qquad \beta_i = \beta_e, \qquad \beta_T = -\frac{1+z}{m_e}\sigma^2 + O(\sigma^4), \qquad \beta_\tau = 0;$$
$$\gamma_{ie} = O(\sigma^2), \qquad \gamma_{ii} = O(\sigma^4), \qquad \gamma_{iv} = -n_i, \qquad \gamma_{iu} = n_i z\sigma^2, \qquad \gamma_{iT} = O(\sigma^2), \qquad \gamma_{i\tau} = 0,$$
$$\gamma_{ei} = O(\sigma^2), \qquad \gamma_{ev} = -n_i z, \qquad \gamma_{eu} = -n_i z, \qquad \gamma_{e\tau} = 0,$$
$$\gamma_{ee} = \frac{3(4\sqrt{2}+13z)}{16z^2(\sqrt{2}+z)}\Lambda + O(\sigma), \qquad \gamma_{eT} = \frac{3(\sqrt{2}+7z)}{4z(\sqrt{2}+z)}\frac{n_i}{T}\Lambda + O(\sigma);$$
$$\eta_u = O(\sigma^2), \qquad \tilde{\eta}_u = \frac{\eta_u}{3}, \qquad \eta_v = \frac{5}{4\sqrt{2}z^4}\Lambda\sigma + O(\sigma^2), \qquad \tilde{\eta}_v = \frac{\eta_v}{3};$$
$$\chi_e = O(\sigma), \qquad \chi_i = O(\sigma^3), \qquad \chi_v = -\frac{5}{4\sqrt{2}z\left(1+\sqrt{2}z\right)}\Lambda + O(\sigma), \qquad \tilde{\chi}_v = \frac{\chi_v}{3}, \qquad \chi_T = O(\sigma),$$
$$\chi_\tau = -\frac{4(\sqrt{2}+7z)}{4\sqrt{2}+13z}\frac{1}{m_e} + O(\sigma), \qquad \chi_u = \frac{15}{4z(3\sqrt{2}+z)}\Lambda + O(\sigma), \qquad \tilde{\chi}_u = \frac{\chi_u}{3} + O(\sigma);$$
$$\theta_e = \frac{\alpha_e}{z}, \qquad \theta_i = O(\sigma^2), \qquad \theta_v = O(\sigma), \qquad \theta_T = \frac{\alpha_T}{z}, \qquad \theta_\tau = \frac{\alpha_\tau}{z}, \qquad \theta_u = \frac{\alpha_u}{z}. \tag{16}$$

In the considered approximation the relaxation rates in (15) have the form [1,6]

$$\lambda_u = \frac{2^{5/2}}{3}z^2\lambda + O(\sigma), \qquad \lambda_\tau = \frac{2^{7/2}}{3}z^2(z+1)\sigma^2\lambda + O(\sigma^4) \tag{17}$$

where and in (16) the notations

$$\lambda = \frac{n_i e^4 L \pi^{1/2}}{(m_e T^3)^{1/2}}, \qquad \Lambda = \frac{T^{5/2}}{n_i e^4 L\sqrt{2\pi m_e}} \tag{18}$$

are introduced (in (16), (18) superscript eq is omitted in T^{eq}, n_i^{eq}).

To analyze the modes described by hydrodynamic equation (15) one has to make the Fourier transformation of the form

$$\xi_{\alpha k}(t) \equiv \int d^3x \delta\xi_\alpha(x,t)e^{-ikx}, \qquad \delta\xi_\alpha(x,t) = \frac{1}{(2\pi)^3}\int d^3k \xi_{\alpha k}(t)e^{ikx} \tag{19}$$

(we use the periodic boundary conditions) and introduce the longitudinal and transversal parts of vectors u_{nk} and v_{nk}.

$$u_k = k_n u_{nk}/k, \quad u^\perp_{nk} = (\delta_{nl} - k_n k_l/k^2)u_{lk}; \qquad v_k = k_n v_{nk}/k, \quad v^\perp_{nk} = (\delta_{nl} - k_n k_l/k^2)v_{lk}.$$

This lead to the following two disconnected sets of equations

$$\partial_t n_{ek} = -k^2(\gamma_{ee}n_{ek} + \gamma_{ei}n_{ik}) + i\gamma_{ev}kv_k - \gamma_{eT}k^2T_k + i\gamma_{eu}ku_k - \gamma_{e\tau}k^2\tau_k,$$
$$\partial_t n_{ik} = -k^2(\gamma_{ie}n_{ek} + \gamma_{ii}n_{ik}) + i\gamma_{v}kv_k - \gamma_{iT}k^2T_k + i\gamma_{iu}ku_k - \gamma_{i\tau}k^2\tau_k,$$
$$\partial_t v_k = ik(\beta_e n_{ek} + \beta_i n_{ik}) - (\eta_v + \tilde{\eta}_v)k^2v_k + i\beta_T kT_k - (\eta_u + \tilde{\eta}_u)k^2u_k + i\beta_\tau k\tau_k,$$
$$\partial_t T_k = -k^2(\alpha_e n_{ek} + \alpha_i n_{ik}) + i\alpha_v kv_k - \alpha_T k^2T_k + i\alpha_u ku_k - k^2\alpha_\tau\tau_k,$$
$$\partial_t u_k = i(\chi_e k n_{ek} + \chi_i\delta n_{ik}) - (\chi_v + \tilde{\chi}_v)k^2v_k + i\chi_T kT_k - (\lambda_u + \chi_u k^2 + \tilde{\chi}_u k^2)u_k + i\chi_\tau k\tau_k,$$
$$\partial_t \tau_k = -k^2(\theta_e n_{ek} + \theta_i n_{ik}) + i\theta_v kv_k - \theta_T k^2T_k + i\theta_u ku_k - (\lambda_\tau + \theta_\tau k^2)\tau_k; \tag{20}$$
$$\partial_t u^\perp_{nk} = -\chi_v k^2 v^\perp_{nk} - (\lambda_u + \chi_u k^2)u^\perp_{nk}, \qquad \partial_t v^\perp_{nk} = -\eta_v k^2 v^\perp_{nk} - \eta_u k^2 u^\perp_{nk}. \tag{21}$$

Solution of the obtained equations (20), (21) is found in the usual form $\xi_{\alpha k}(t) = c_{\alpha k}e^{\lambda t}$ where $c_{\alpha k}$ are some coefficients. Here λ will be eigenvalue of the matrix $M_{\alpha\alpha'}(k)$ built from the coefficients of equations (20), (21) and satisfies the equation of the form $\det|M(k) - \lambda I| = 0$, where I is the unit matrix. Expressions for λ should

be calculated in a k-power series $\lambda = \lambda_0 + \lambda_1 k + \lambda_2 k^2 + O(k^3)$ and give the dispersion laws for the modes of the considered system. As a result the following eigenvalues

$$\lambda_{1,2} = \pm ikc - D_s k^2 + O(k^3), \qquad c = \sqrt{\frac{2}{3} T\beta_T + \beta_N n_i\,(z+1)} = \sigma\sqrt{\frac{5T}{3m_e}\,(z+1)} + O(\sigma^2),$$

$$D_s = \Lambda\,\frac{5(29z+4\sqrt{2})}{2^5 z(z+\sqrt{2})(z+1)} + O(\sigma);$$

$$\lambda_3 = -D_3 k^2 + O(k^3), \qquad D_3 = \Lambda\,\frac{3}{10(z+\sqrt{2})(z+1)}\left[a(z) + \sqrt{a(z)^2 - b(z)}\right] + O(\sigma);$$

$$\lambda_4 = -D_4 k^2 + O(k^3), \qquad D_4 = \Lambda\,\frac{3}{10(z+\sqrt{2})(z+1)}\left[a(z) - \sqrt{a(z)^2 - b(z)}\right] + O(\sigma);$$

$$\lambda_5 = \lambda_6 = -\eta_v k^2 + O(k^4),$$

$$\lambda_7 = -\lambda_u - D_u k^2 + O(k^3), \qquad D_u = \Lambda\left[\frac{5}{z\left(3\sqrt{2}+z\right)} - \frac{1}{2z^2}\frac{1}{(z+1)}\left(1 + \frac{15z}{4\sqrt{2}+13z}\right)\right] + O(\sigma);$$

$$\lambda_8 = -\lambda_\tau - D_\tau k^2 + O(k^3), \qquad D_\tau = \Lambda\,\frac{4\sqrt{2}+53z}{2z^2(z+1)(4\sqrt{2}+13z)} + O(\sigma);$$

$$\lambda_9 = \lambda_{10} = -\lambda_u - \chi_u k^2 + O(k^4) \tag{22}$$

are obtained with functions $a\,(z)$, $b\,(z)$ defined by

$$a\,(z) = \frac{25}{8} + \frac{5}{16z^2}(4\sqrt{2}+13z), \qquad b\,(z) = \frac{125}{8z^2}(\sqrt{2}+z).$$

Here $\lambda_1 - \lambda_6$ are a generalization of the modes observable in the absence of relaxation; the other modes $\lambda_7 - \lambda_{10}$ are related to the relaxation. λ_1, λ_2 are the sound modes, λ_3, λ_4 are the diffusion and heat modes. Modes $\lambda_{5,6}, \lambda_{9,10}$ are found from equations (21) and describe the evolution of the transversal components of the velocities υ_{nk}, u_{nk}.

4 Conclusions

The hydrodynamics of a two-component completely ionized plasma was studied at the end of the component temperature and velocity relaxation on the basis of the Landau kinetic equation. The hydrodynamic modes (22) of the system were obtained in the small wave vector approximation with additional account for the small electron-to-ion mass ratio. It was shown that six hydrodynamic modes of the system are the standard hydrodynamic modes of a two-component plasma. The other four modes of the system are relaxation ones and they take place due to the component temperature and velocity relaxation.

The results for plasma modes described by the Vlasov kinetic equation (the plasma oscillations) are well-known. The plasma oscillations cannot be investigated in our approach because the Landau equation takes into account only the short-range part of the Coulomb interaction. Its long-range part can be described by a longitudinal electromagnetic field or by the self-consistent Coulomb field (see, for example, [7]). This situation will be discussed by the authors in another paper.

References

[1] L.D. Landau, *Kinetic equation in case of coulomb interaction*, ZhETF **7**, 203-209 (1937)(in Russian).
[2] A.I. Akhiezer, S.V. Peletminsky, *Methods of Statistical Physics*, (Oxford, Pergamon Press, 1981), 368 p.
[3] P. Resibois, M. De Leener, *Classical Kinetic Theory of Fluids*, (New York, Wiley, 1977), 412 p.
[4] R. Balescu *Equilibrium and Non-Equilibrium Statistical Mechanics*, New York, Wiley, 1975, 742 pp.
[5] E.M. Lifshitz, L.P. Pitaevsky, *Physical Kinetics*, (Oxford, Pergamon Press, 1981), 452 p.
[6] A.F. Alexandrov, L.S. Bogdankevich, A.A. Rukhadze, *Fundamentals of plasma electrodynamics* (Moscow, Vysshaya Shkola, 1988), (in Russian).
[7] A.I. Sokolovsky, A.A. Stupka, Z.Yu. Chelbaevsky, *On the Bohm-Pines gauge for system of charged particles*, Proceedings of 2012 International Conference on Mathematical Methods in Electromagnetic Theory (Kharkiv, Ukraine, August 28-30, 2012), Proceedings CD-ROM, ISBN 978-1-4673-4479-1, NCE-1, P. 189-192.

Proceedings of the International School-seminar
"New Physics and Quantum Chromodynamics at External Conditions", pp. 139 – 142,
May 22-24, 2013, Dnipropetrovsk, Ukraine

DISPERSION RELATION FOR WAVES OF CORRELATIONS OF ELECTROMAGNETIC FIELD IN NONEQUILIBRIUM EMITTER MEDIUM

S.F. Lyagushyn[a], A.I. Sokolovsky[b]

Dnipropetrovsk National University, Dnipropetrovsk, Ukraine

Waves of average electromagnetic field and its binary correlations in a medium of two-level emitters are discussed. The concept of correlation waves is analyzed. The dispersion law for the waves of correlations in equilibrium medium has been obtained in terms of parameters of waves of average electromagnetic field. Expressions for weakly non-uniform waves are obtained. Coupled oscillations of electromagnetic field correlations and the nonequilibrium medium as well as a dispersion relation for such waves are considered.

1 Introduction

Conventional approaches in investigations of the Dicke model were based on turning to the dynamics of the emitter subsystem with the elimination of boson variables. On such a way the superradiance occurrence was indicated, but the properties of emitted radiation remained unknown, though they were of interest in view of recent advances in quantum optics. In our paper [1] the joint description of matter and field behavior was implemented in the framework of the Bogolyubov reduced description method. Under the assumption of the weak interaction between the field and emitters, some kind of electrodynamics of continuous media was obtained; the medium consisting of two-level emitters should be considered. The field was described with its average value and binary correlations, the quasiequilibrium medium was supposed. To investigate nonequilibrium processes in the system under study, the concept of normal waves in it proves to be useful. Considering waves and oscillations in the system, we find, besides average field waves, correlation waves, the idea of which has been discussed in the paper [2] with respect to plasma medium. Now such waves of field correlations emerge in the medium of emitters with corresponding material equations and the possibility of detecting them together with the waves in the emitter subsystem is of concern.

2 Basic equations of the theory

The electromagnetic field is described with its average values $B_n(x,t) \equiv \xi_{1n}(x)$, $E_n(x,t) \equiv \xi_{2n}(x,t)$ and binary correlations $(\xi^x_{in}, \xi^{x'}_{i'l})_t$

$$\xi_{in}(x,t) = \mathrm{Sp}\rho(\eta(t))\hat{\xi}_{in}(x), \quad (\xi^x_{in}, \xi^{x'}_{i'l})_t \equiv \frac{1}{2}\mathrm{Sp}\rho(\eta(t))\{\hat{\xi}_{in}(x), \hat{\xi}_{i'l}(x')\} - \xi_{in}(x,t)\xi_{i'l}(x',t), \tag{1}$$

$\hat{\xi}_{1n}(x) \equiv \hat{B}_n(x)$, $\hat{\xi}_{2n}(x) \equiv \hat{E}_n(x)$ stand for magnetic and electric field operators, the motionless two-level emitters are described with the average energy density

$$\varepsilon(x,t) = \mathrm{Sp}\rho(\eta(t))\hat{\varepsilon}(x) \tag{2}$$

$\hat{\varepsilon}(x)$ is an operator of energy density of emitters, $\rho(\eta)$ is a statistical operator of the nonequilibrium state under consideration $\eta(t) \equiv \{\xi_{in}(x,t), (\xi^x_{in}, \xi^{x'}_{i'l})_t, \varepsilon(x,t)\}$.

Average fields satisfy the Maxwell equations

$$\partial_t B_n(x,t) = -c\mathrm{rot}_n E(x,t), \qquad \partial_t E_n(x,t) = c\mathrm{rot}_n B(x,t) - 4\pi J_n(x,t)$$
$$\mathrm{div}B(x,t) = 0, \qquad \mathrm{div}E(x,t) = 4\pi\rho(x,t) \tag{3}$$

$J_n(x,t)$, $\rho(x,t)$ are current and charge densities. The compact form for field equations

$$\partial_t \xi_\mu(t) = i\sum_{\mu'} c_{\mu\mu'}\xi_{\mu'}(t) + J_\mu(t), \tag{4}$$

where the designations $\xi_\mu \equiv \xi_{in}(x)$, $\sum\limits_\mu = \sum\limits_{in}\int d^3x$, $J_\mu \equiv J_{in}(x)$ $(J_{1n}(x) \equiv 0\ ,\ J_{2n}(x) \equiv J_n(x))$ are used. For the current density a material equation of the form

$$J_n(x,t) = \int d^3x'\sigma(x-x', \varepsilon(x,t))E_n(x',t) + c\int d^3x'\tilde{\chi}(x-x', \varepsilon(x,t))Z_n(x',t) \tag{5}$$

e-mail: [a]lyagush@dnu.dp.ua, [b]alexsokolovsky@mail.ru

($Z_n(x) \equiv \mathrm{rot}_n B(x)$) has been obtained. Fourier-components $\sigma_k(\varepsilon)$, $\tilde{\chi}_k(\varepsilon)$ of the kernels $\sigma(x,\varepsilon)$, $\tilde{\chi}(x,\varepsilon)$ are conductivity and magnetic susceptibility of the emitter medium. Such quantities are functions of a vector k_n modulus, they are proportional to emitter energy density ε and do not depend on their quantity density $n(x)$.

The material equation (5) takes into account effects of spatial dispersion and virtually generalizes a standard view of electrodynamics of continuous media to the case of medium non-equilibrium. Usually average current is expressed via the field strength $H_n(x)$ instead of the average field $B_n(x)$. The usual magnetic susceptibility χ_k is included into the formulas $B_{nk} = \mu_k H_{nk}$, $\mu_k = 1 + 4\pi\chi_k$ (μ_k means magnetic permeability) and connected with $\tilde{\chi}_k$ through the relation $\tilde{\chi}_k = \chi_k/(1 + 4\pi\chi_k)$.

A time equation for binary field correlations have been obtained in [1], the equation has a following form in the compact notations

$$\partial_t(\xi_1,\xi_2)_t = i\sum_{1'} c_{11'}(\xi_{1'},\xi_2)_t + i\sum_{2'} c_{22'}(\xi_1,\xi_{2'})_t + (J_1,\xi_2)_t + (\xi_1,J_2)_t, \tag{6}$$

we put $\xi_{\mu_1} \equiv \xi_1$, $\xi_{\mu_{1'}} \equiv \xi_{1'}$, $\sum\limits_1 \equiv \sum\limits_{\mu_1}$ and so on. A material equation to the equation (6) has the form

$$(J_n^x, \xi_{il}^{x'})_t = \int d^3x''\sigma(x-x'',\varepsilon(x,t))(E_n^{x''},\xi_{il}^{x'})_t + c\int d^3x''\tilde{\chi}(x-x'',\varepsilon(x,t))(Z_n^{x''},\xi_{il}^{x'})_t + S_{n,il}(x-x',n(x)) \tag{7}$$

where the last summand does not depend on time and field variables and is proportional to the emitter quantity density $n(x)$.

The similarity of this material equation structure to that of the equation (5) is known as the On-sager principle in the case of equilibrium medium. Comparing the formulas (4) and (5) with formulas (6) and (7) allows formulating it in a rather clear sense in the following way: binary field correlations in the case of equilibrium medium ($\varepsilon(x,t) \to \varepsilon^{eq}$) evolve according to the same law as the average field does. In order to illustrate this idea, we rewrite equations (4), (5), (7) in the form

$$\partial_t\xi_1(t) = i\sum_{1'} c_{11'}\xi_{1'}(t) + J_1(t), \quad J_1 = \sum_{1'}\sigma_{11'}\xi_{1'}; \qquad (J_1,\xi_2)_t = \sum_{1'}\sigma_{11'}(\xi_{1'},\xi_2)_t + S_{12}. \tag{8}$$

The formulas (6) and (8) show that equation solutions for the average field and its binary correlations have the form

$$\xi_1(t) = \sum_{1'} U_{11'}(t)\xi_{1'}(0), \qquad (\xi_1,\xi_2)_t = \sum_{1'2'} U_{11'}(t)U_{22'}(t)(\xi_{1'},\xi_{2'})_0 + \sum_{1'2'}\int\limits_0^t dt' U_{11'}(t')U_{22'}(t')S_{1'2'} \tag{9}$$

where the evolution matrix is defined by the formula

$$\hat{U}(t) = e^{(i\hat{c}+\hat{\sigma})t}. \tag{10}$$

It will be analyzed in details in the next section. An equation for emitter energy density is given by the formula

$$\partial_t\varepsilon(x,t) = (J_n^x, E_n^x)_t + J_n(x,t)E_n(x,t) + R(n(x)) \tag{11}$$

where the last summand determines losses of the emitter system through the dipole radiation ($R(n)$ is proportional to n) [1].

3 Evolution of electromagnetic field in equilibrium medium

Expression (10) for the evolution matrix is a rather formal one. In order to concretize it, we consider the solution of the Cauchy problem for the Maxwell equations in an equilibrium medium. According to the formulas (3), (5) for longitudinal and transversal parts of electric and magnetic fields, they can be written in the form

$$\partial_t E_{nk}^l = -\sigma_k E_{nk}^l, \qquad B_{nk}^l = 0,$$
$$\partial_t B_{nk}^t = -ic\left(k\times E_k^t\right)_n, \qquad \partial_t E_{nk}^t = i\frac{c}{\mu_k}\left(k\times B_k^t\right)_n - 4\pi\sigma_k E_{nk}^t. \tag{12}$$

The 2nd and 3rd equations give the closed equation for E_{nk}^t

$$\partial_t^2 E_{nk}^t + 4\pi\sigma_k\partial_t E_{nk}^t + \frac{\omega_k^2}{\mu_k}E_{nk}^t = 0. \tag{13}$$

Its general solution has the form

$$E_{nk}^t(t) = a_{nk}^t e^{z_{1k}t} + b_{nk}^t e^{z_{2k}t}, \qquad E_{nk}^l(t) = c_{nk}^l e^{-\sigma_k t},$$

$$z_{1k} \equiv i\Omega_k - \gamma_k, \quad z_{2k} \equiv -i\Omega_k - \gamma_k; \quad \Omega_k = \sqrt{\omega_k^2/\mu_k - (2\pi\sigma_k)^2}, \quad \gamma_k = 2\pi\sigma_k, \quad \omega_k = ck \tag{14}$$

where a^t_{nk}, b^t_{nk}, c^l_{nk} are time-independent fields. The 3rd relation in (12) allows finding such an expression for the magnetic field

$$B^t_{nk}(t) = -\frac{ic}{z_{1k}}\left(k \times a^t_k\right)_n e^{z_{1k}\,t} - \frac{ic}{z_{2k}}\left(k \times b^t_k\right)_n e^{z_{2k}\,t}. \tag{15}$$

In this expression integration constant should be set equal to zero, since electromagnetic field should attenuate at $\gamma_k > 0$. Formulas (14) and (15) show that the field under consideration has three modes in an equilibrium medium. Two of them are of wave nature at a real frequency Ω_k. The expression (14) for the transversal electric field gives relations

$$a^t_{nk}e^{z_{1k}\,t} = \frac{z_{1k}}{2i\Omega_k}E^t_{nk}(t) + \frac{c}{2i\Omega_k\mu_k}Z^t_{nk}(t), \qquad b^t_{nk}e^{z_{2k}\,t} = -\frac{z_{2k}}{2i\Omega_k}E^t_{nk}(t) - \frac{c}{2i\Omega_k\mu_k}Z^t_{nk}(t) \tag{16}$$

while taking into account the Maxwell equations (12). These formulas show that fields

$$\zeta^t_{ink}(t) = E^t_{nk}(t) + \frac{c}{z_{ik}\mu_k}Z^t_{nk}(t) \equiv \sum_{i'} R_{in,i'l}(k)\xi_{i'lk}, \qquad \partial_t\zeta^t_{ink}(t) = z_{ik}\zeta^t_{ink}(t) \tag{17}$$

are transversal modes of electromagnetic field in the equilibrium medium. The Cauchy problem solution for electromagnetic field is given by the formulas (14), (15) with taking into account expressions for quantities a^t_{nk}, b^t_{nk}, c^l_{nk} via initial field values $E^t_{nk}(0)$, $B^t_{nk}(0)$ proceeding from the formulas (16)

$$a^t_{nk} = \frac{z_{1k}}{2i\Omega_k}E^t_{nk}(0) + \frac{c}{2i\Omega_k\mu_k}Z^t_{nk}(0), \qquad b^t_{nk} = -\frac{z_{2k}}{2i\Omega_k}E^t_{nk}(0) - \frac{c}{2i\Omega_k\mu_k}Z^t_{nk}(0). \tag{18}$$

Now it is easy to write an expression for elements of the evolution matrix $\hat{U}(t)$ comparing the 1st formula in (9) to the relations (14), (15), (19). We restrict ourselves with the remark that its elements have a structure

$$U^{x,x'}_{in,i'n'}(t) = \frac{1}{V}\sum_k U_{in,i'n'}(k)e^{i\,k(x-x')}, \qquad U_{in,i'n'}(k,t) = A_{in,i'n'}(k)e^{z_{1k}\,t} + B_{in,i'n'}(k)e^{z_{2k}\,t} \tag{19}$$

where $A_{in,i'n'}(k)$, $B_{in,i'n'}(k)$ are known functions.

4 Concept of waves of binary correlations

In the spatially uniform case correlation functions $(\xi^x_{in}, \xi^{x'}_{i'l})_t$ depend only on coordinate difference and their Fourier components $(\xi^k_{in}, \xi^{k'}_{i'l})_t \sim \delta_{k',-k}$. Therefore a spatial nonuniformity of correlations should be related to the dependence of Fourier components $(\xi^{p+k/2}_{in}, \xi^{-p+k/2}_{i'l})_t$ on the vector k_n and this vector should be regarded as a wave one. In other words, field correlation waves should be described with the function deviation from its equilibrium value

$$\delta(\xi^{p+k/2}_{in}, \xi^{-p+k/2}_{i'l})_t = (\xi^{p+k/2}_{in}, \xi^{-p+k/2}_{i'l})_t - (\xi^{p+k/2}_{in}, \xi^{-p+k/2}_{i'l})^{eq}. \tag{20}$$

The easiest way to find a dispersion law for defined in such way correlation waves of the transversal components of electromagnetic field is using the formula (9) that gives

$$\delta(\xi_1, \xi_2)_t = \sum_{1'2'} U_{11'}(t)U_{22'}(t)\delta(\xi_{1'}, \xi_{2'})_0. \tag{21}$$

Substituting the evolution matrix of (19) here, we obtain the wave representation as a sum of modes

$$\delta(\xi^{p+k/2}_{i_1n_1}, \xi^{-p+k/2}_{i_2n_2})_t = \sum_{ii'} F^{ii'}_{i_1n_1,i_2n_2}(k,p)e^{\{z_{i,p+k/2}+z_{i',-p+k/2}\}t} \tag{22}$$

possessing frequencies $z_{p,ii'}(k) = z_{i,p+k/2} + z_{i',-p+k/2}$. Usually one limit oneself with considering weakly nonuniform states where correlations (20) are different from zero only at small wave vector k_n. Herewith the dispersion law for correlation waves has the form:

$$z_{p,ii'}(k): \qquad \pm i(2\Omega_p + \frac{1}{4}k_lk_n\frac{\partial^2\Omega_p}{\partial p_n\partial p_l}) - (2\gamma_p + \frac{1}{4}k_lk_n\frac{\partial^2\gamma_p}{\partial p_n\partial p_l}), \qquad \pm ik_l\frac{\partial\Omega_p}{\partial p_l} - (2\gamma_p + \frac{1}{4}k_lk_n\frac{\partial^2\gamma_p}{\partial p_n\partial p_l}). \tag{23}$$

The possibility of observing such waves depends upon the correlation between vectors p_n, k_n and should be discussed in future.

5 Connected waves of field and emitter medium

Let us consider coupled oscillations of field and medium near the equilibrium regarding the equilibrium average field as equal to zero. Oscillations will be described with Fourier components of deviations of field $\delta\xi_{in}(x,t) = \xi_{in}(x,t)$, medium energy density $\delta\varepsilon(x,t) = \varepsilon(x,t) - \varepsilon^{eq}$, and field correlations from their equilibrium values. It is convenient to use field mode correlations instead of field correlations

$$\mathrm{f}_p^{in,i'l}(k,t) = (\zeta_{in}^{p+k/2}, \zeta_{i'l}^{-p+k/2})_t, \qquad \delta\mathrm{f}_p^{in,i'l}(k,t) = (\zeta_{in}^{p+k/2}, \zeta_{i'l}^{-p+k/2})_t - (\zeta_{in}^{p+k/2}, \zeta_{i'l}^{-p+k/2})^{eq}. \tag{24}$$

It is possible since there is one correspondence between modes and field (see (17)). Note that coupled oscillations of field and a hydrodynamic medium were investigated in the paper [3] where the approximation of small correlation radius has been considered.

The coupled set of equations for the mentioned quantities according to (6) and (7) has the form

$$\partial_t \delta\mathrm{f}_p^{in,i'l}(k,t) = \{z_{i,p+k/2} + z_{i',-p+k/2}\}\delta\mathrm{f}_p^{in,i'l}(k,t) + M_p^{in,i'l}(k)\delta\varepsilon_k(t),$$

$$\partial_t \delta\varepsilon_k(t) = \sum_{ii'} \int d^3p N_p^{in,i'l}(k)\, \delta\mathrm{f}_p^{in,i'l}(k,t) + \nu\delta\varepsilon_k(t) \tag{25}$$

where we have

$$M_p^{in,i'l}(k) = \frac{1}{\varepsilon^{eq}V} \sum_{i_1 i_2 i''} R_{in,i_1 n_1}(p+\frac{k}{2})\sigma_{i_1 n_1, i'' m}(p-\frac{k}{2}, \varepsilon^{eq}) R^{-1}_{i'' m, i_2 n_2}(p-\frac{k}{2})(\zeta_{i_2 n_2}^{p-k/2}, \zeta_{i'l}^{-p+k/2})^{eq} +$$

$$+\frac{1}{\varepsilon^{eq}V} \sum_{i_1 i_2 i''} R_{i'l,i_1 n_1}(-p+\frac{k}{2})\sigma_{i_1 n_1, i'' m}(-p-\frac{k}{2}, \varepsilon^{eq}) R^{-1}_{i'' m, i_2 n_2}(-p-\frac{k}{2})(\zeta_{in}^{p+k/2}, \zeta_{i_2 n_2}^{-p-k/2})^{eq},$$

$$\nu = \frac{1}{\varepsilon^{eq}V(2\pi)^3} \sum_{i_1 i_2 ii'} \int d^3k' \sigma_{in,i'l}(k', \varepsilon^{eq}) R^{-1}_{in,i_1 n_1}(-k') R^{-1}_{i'l,i_2 n_2}(k')(\zeta_{i_2 n_2}^{k'}, \zeta_{i_1 n_1}^{-k'})^{eq},$$

$$N_p^{in,i'l}(k) = \frac{1}{(2\pi)^3} \sum_{i_1 i_2} \sigma_{i_1 n_1, i_2 n_2}(p+\frac{k}{2}, \varepsilon^{eq}) R^{-1}_{i_2 n_2, in}(p+\frac{k}{2}) R^{-1}_{i_1 n_1, i'l}(-p+\frac{k}{2}) \tag{26}$$

($\sigma_{1n,i'l}(k,\varepsilon) \equiv 0$, $\sigma_{2n,2l}(k,\varepsilon) \equiv \sigma_k(\varepsilon)$, $\sigma_{2n,1l}(k,\varepsilon) \equiv ice_{nml}k_m\chi_k(\varepsilon)$). In order to analyze the modes of the set of equations (26), we search for its solution in the form $\delta\mathrm{f}_p^{in,i'l}(k,t) = C_p^{in,i'l}(k)e^{zt}$, $\delta\varepsilon_k(t) = C_k e^{zt}$ resulting in the following dispersion equation

$$z = \nu + \sum_{ii'} \int d^3p \frac{M_p^{in,i'l}(k) N_p^{in,i'l}(k)}{z - z_{i,p+k/2} - z_{i',-p+k/2}}. \tag{27}$$

Our consideration is based on the theory supposing the interaction between field and emitters to be weak (a small parameter λ). Herewith the conductivity, magnetic susceptibility and equilibrium correlation functions are quantities $\sim \lambda^2$, and hence the functions in the numerator of the relation (27) are small. The detailed analysis of the equation (27) with taking into account the smallness of λ, as well as the case of small wave vectors k will be presented subsequently.

6 Conclusions

In the framework of the concept of continuous medium consisting of motionless two-level emitters the theory of normal waves in it are constructed and discussed. Expressions for transversal modes of electromagnetic field in the equilibrium medium and the Cauchy problem solution are obtained with using compact designations for field amplitudes and correlations that are necessary in the scheme of reduced description. In the case of spatial non-uniformity waves of binary correlations can be introduced through considering the deviation of correlations from their equilibrium values. The dispersion law for such waves is obtained using the description of field amplitude evolution. For weakly non-uniform waves the corresponding expressions are presented. Binary correlation modes prove to be connected with energy density oscillations in the subsystem of emitters. For coupled oscillations of field mode correlations and the medium consisting of emitters a dispersion relation emerges in our consideration.

References

[1] S.F. Lyagushyn, A.I. Sokolovsky, *Kinetics of system of emitters and nonequilibrium electromagnetic field*, Physics of Particles and Nuclei **41**, No. 7, 1035-1038 (2010).

[2] A.I. Sokolovsky, A.A. Stupka, *Kinetic theory of electromagnetic processes in equilibrium medium*, Visnyk of Dnipropetrovsk University. Physics. Radio Electronics **10**, 63-70 (2003) (in Russian).

[3] A.I. Sokolovsky, A.A. Stupka, *Electromagnetic field correlations and sound waves*, Problems of Atomic Science and Technology **3(2)**, 335-339 (2007).